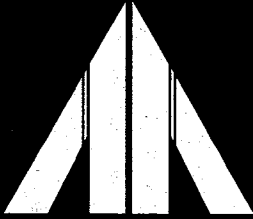


NSF/ENG-85006

R-8222-5603

PB85-196293



SEISMIC RESPONSE CHARACTERISTICS OF MELOLAND ROAD OVERPASS DURING 1979 IMPERIAL VALLEY EARTHQUAKE

by

S.D. Werner
M.B. Levine
J.L. Beck

March 1985

Prepared under

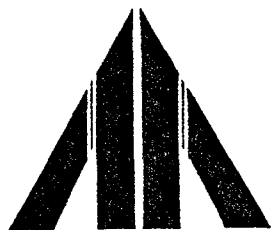
NATIONAL SCIENCE FOUNDATION

Grant No. CEE-8111964

AGBABIAN ASSOCIATES

250 North Nash Street
El Segundo, CA 90245

REPORT DOCUMENTATION PAGE	1. REPORT NO. NSF/ENG-85006	2.	3. Recipient's Accession No. PB85 196293 /AS
4. Title and Subtitle Seismic Response Characteristics of Meloland Road Overpass During 1979 Imperial Valley Earthquake			5. Report Date March 1985
7. Author(s) S.D. Werner, M.B. Levine, and J.L. Beck			6.
9. Performing Organization Name and Address Agbabian Associates 250 North Nash Street El Segundo, CA 90245			8. Performing Organization Rept. No. R-8222-5603
12. Sponsoring Organization Name and Address National Science Foundation Civil and Environmental Division 1800 "G" Street, NW Washington, DC 20550			10. Project/Task/Work Unit No. 8222
15. Supplementary Notes			11. Contract(C) or Grant(G) No. (C) (G) CEE-8111964
16. Abstract (Limit: 200 words) The Meloland Road Overpass (MRO), a two-span reinforced concrete bridge located near El Centro, California, survived very strong shaking during the 1979 Imperial Valley earthquake with virtually no damage. This shaking triggered a total of 26 strong motion accelerometers located on or near the bridge, providing the most extensive array of earthquake response measurements yet obtained for bridges in the United States. This report describes work directed toward using these data to gain insights that can enhance future design, analysis, and instrumentation of bridges in an earthquake environment. The work involved (1) special reprocessing of the original motions measured at the MRO, to correct for recorder stall and nonsynchronization problems that had arisen during the earthquake; (2) formulation of a new methodology for modal identification of structures with any number of support and response measurements; and (3) application of this new methodology to the reprocessed bridge motions, in order to assess the seismic response characteristics of the MRO. This application identified linear models that produced excellent fits to the measured MRO motions, despite the fact that the peak accelerations exceeded 0.50 g. The results also described the relative effects of the bridge's foundation and superstructure elements on its overall seismic response, the level of damping attained in the bridge during the ground shaking, and practical considerations in the analysis of measured motions to interpret bridge response characteristics.			13. Type of Report & Period Covered Final Report 4-18-82 - 3/31/85
17. Document Analysis a. Descriptors Bridges, earthquakes, dynamics, vibrations			14.
b. Identifiers/Open-Ended Terms Meloland Road Overpass, Seismic Response Characteristics, Measured Earthquake Motions, System Identification			
c. COSATI Field/Group			
18. Availability Statement: Release Unlimited	19. Security Class (This Report) Unclassified	21. No. of Pages 264	
	20. Security Class (This Page)	22. Price	



**SEISMIC RESPONSE
CHARACTERISTICS OF
MELOLAND ROAD OVERPASS
DURING 1979 IMPERIAL VALLEY
EARTHQUAKE**

by

**S.D. Werner
M.B. Levine
J.L. Beck**

March 1985

Prepared under

**NATIONAL SCIENCE FOUNDATION
Grant No. CEE-8111964**

**AGBABIAN ASSOCIATES
250 North Nash Street
El Segundo, CA 90245**



ABSTRACT

The Meloland Road Overpass (MRO), a two-span reinforced concrete bridge located near El Centro, California, survived very strong shaking during the 1979 Imperial Valley earthquake with virtually no damage. This shaking triggered a total of 26 strong motion accelerometers located on or near the bridge, providing the most extensive array of earthquake response measurements yet obtained for bridges in the United States. This project has been directed toward using these data to gain insights that can enhance future design, analysis, and instrumentation of bridges in an earthquake environment. The main efforts that comprised the project were (1) special reprocessing of the original motions measured at the MRO, to correct for recorder stall and nonsynchronization problems that had arisen during the earthquake; (2) formulation of a new methodology for modal identification of structures with any number of support and response measurements; and (3) application of this new methodology to the reprocessed bridge motions, in order to assess the seismic response characteristics of the MRO. This application identified linear models that produced excellent fits to the measured MRO motions, despite the fact that the peak accelerations exceeded 0.50 g. The results also described the relative effects of the bridge's foundation and superstructure elements on its overall seismic response, the level of damping attained in the bridge during the ground shaking, and practical considerations in the analysis of measured motions to interpret bridge response characteristics.

1
2
3
4
5
6
7
8
9
10
11
12
13
14
15
16
17
18
19
20
21
22
23
24
25
26
27
28
29
30
31
32
33
34
35
36
37
38
39
40
41
42
43
44
45
46
47
48
49
50
51
52
53
54
55
56
57
58
59
60
61
62
63
64
65
66
67
68
69
70
71
72
73
74
75
76
77
78
79
80
81
82
83
84
85
86
87
88
89
90
91
92
93
94
95
96
97
98
99
100



ACKNOWLEDGEMENTS

This report is one of two prepared under a research project carried out at Agbabian Associates (AA) and funded through a grant by the National Science Foundation (Grant No. CEE-8111964). The support from this grant is gratefully acknowledged.

The principal contributors to the work described in this report were S.D. Werner of AA (project principal investigator), M.B. Levine of the California Institute of Technology (CIT) and former AA staff member (data analysis and system identification calculations), and J.L. Beck of CIT (special consultant and author of the system identification methodology described herein). AA staff members who also contributed to the report were S.F. Masri of the University of Southern California (USC) and part-time AA employee (system identification background and project review), J. Rubottom and P. LaPonza (typists), and E. Harding (illustrator).

In addition to the project staff, other individuals provided significant contributions to particular phases of this research effort. These were M.D. Trifunac and V.W. Lee of USC (redigitization and reprocessing of bridge motions), J.T. Ragsdale and N.A. Kaliakin of the California Division of Mines and Geology (assistance and guidance in data reprocessing efforts), R.M. Coppolino of MacNeal-Schwendler (support of initial system identification efforts), R.T. Scott of CIT (foundation/soil system modeling procedures), and J.H. Gates of the California Department of Transportation (bridge drawings and data interpretation). The contributions of each of these individuals is greatly appreciated.

71
72
73
74
75
76
77
78
79
80
81
82
83
84
85
86
87
88
89
90
91
92
93
94
95
96
97
98
99
100
101
102
103
104
105
106
107
108
109
110
111
112
113
114
115
116
117
118
119
120
121
122
123
124
125
126
127
128
129
130
131
132
133
134
135
136
137
138
139
140
141
142
143
144
145
146
147
148
149
150
151
152
153
154
155
156
157
158
159
160
161
162
163
164
165
166
167
168
169
170
171
172
173
174
175
176
177
178
179
180
181
182
183
184
185
186
187
188
189
190
191
192
193
194
195
196
197
198
199
200



TABLE OF CONTENTS

<u>Chapter</u>		<u>Page</u>
1	INTRODUCTION	1-1
	1.1 Background Information.	1-1
	1.2 Project Objective	1-4
	1.3 Project Scope	1-8
	1.4 Report Organization	1-9
2	STRONG MOTION DATA REPROCESSING.	2-1
	2.1 Strong Motion Instrumentation and Accelerograms	2-1
	2.2 Data Reconstruction at Recorder Stalls. .	2-2
	2.3 Evaluation of Possible Nonsynchronization Effects	2-17
	2.4 Availability and Use of Reprocessed Data.	2-30
3	MODAL IDENTIFICATION METHODOLOGY	3-1
	3.1 Formulation of the Model.	3-1
	3.2 Identification of Model Parameters. . . .	3-9
	3.3 Verification Analysis	3-18
4	SEISMIC RESPONSE CHARACTERISTICS OF MELOLAND ROAD OVERPASS.	4-1
	4.1 Examination of Recorded Motions	4-1
	4.2 Overview of Modal Identification Process.	4-25
	4.3 Case 1 Results.	4-43
	4.4 Case 2 Results.	4-74
5	CONCLUDING COMMENTS.	5-1
	5.1 Summary of Project Results.	5-1
	5.2 Recommendations	5-6
	5.3 Planning of Strong Motion Instrumentation at Major Bridge Structures.	5-9
	REFERENCES	R-1
<u>Appendix</u>		
A	PLOTS AND AVAILABLE DATA TAPES FOR REPROCESSED MOTIONS FROM MELOLAND ROAD OVERPASS	A-1



01
02
03
04
05
06
07
08
09
10
11
12
13
14
15
16
17
18
19
20
21
22
23
24
25
26
27
28
29
30
31
32
33
34
35
36
37
38
39
40
41
42
43
44
45
46
47
48
49
50
51
52
53
54
55
56
57
58
59
60
61
62
63
64
65
66
67
68
69
70
71
72
73
74
75
76
77
78
79
80
81
82
83
84
85
86
87
88
89
90
91
92
93
94
95
96
97
98
99
100



CHAPTER 1

INTRODUCTION

1.1 BACKGROUND INFORMATION

Bridge structures are important components of lifeline systems. They provide the means for overcrossing both man-made and natural obstacles and, as such, represent an important link for transporting people and supplies. The loss of function of bridge structures due to a natural disaster would disrupt this transportation flow, resulting in significant cost, inconvenience, and possibly even loss of life to the surrounding population.


One type of natural disaster that has imparted significant damage to bridges is earthquakes. For example, the 1971 San Fernando, California earthquake caused either complete failure or substantial damage to some 42 bridge structures in the epicentral area, resulting in a total repair cost of more than 15 million dollars (Jennings and Wood, 1971). The 1978 Santa Barbara, California earthquake resulted in considerable damage to four main overpass structures on U.S. Highway 101, the major coastal highway route between northern and southern California, causing a significant disruption of traffic on this busy thoroughfare (Miller and Felszeghy, 1978). During the 1964 Alaska Earthquake, substantial damage was imparted to numerous railroad bridges on the Kenai Peninsula and to numerous highway bridges, particularly on the Seward and Copper River highways (Sturman, 1973a; 1973b). Abroad, some 78 bridge structures were damaged by the 1978 Miyagi-Ken-Okii, Japan earthquake, while during the 1976 Tangshan, China earthquake, 20 highway bridges collapsed or were seriously damaged, and an additional 211 bridges were damaged to a lesser degree (Yanev, 1978; Jennings, 1980). Damage to bridges abroad also occurred during the recent 1982 Utsunomiya-Oki earthquake (Iwasaki and Hagiwara, 1983).

In recognition of the potential consequences of bridge failures or damage due to earthquakes, seismic design provisions



in the United States have been updated and improved in recent years, particularly since the 1971 San Fernando earthquake. For example, the California Department of Transportation (CALTRANS) introduced new seismic design criteria for bridges in California that incorporated results and insights gained from earthquake engineering advances since the 1971 San Fernando earthquake (Gates, 1976; 1979). More recently, the Applied Technology Council has prepared seismic design guidelines for highway bridges throughout the United States (ATC, 1981) that have been adopted as a Guide Specification by the American Association of State Highway and Transportation Officials (AASHTO, 1983). Guidelines for seismic retrofitting of existing bridges have also been developed through the Applied Technology Council (ATC, 1983).

The seismic design provisions for bridges, although markedly enhanced through the years, will continue to evolve as more insight into the behavior of bridges during earthquakes is attained. One key source of such insight has been qualitative observations and interpretations of the seismic behavior of bridges during prior earthquakes (e.g., Iwasaki et al., 1972; Jennings and Wood, 1971; PWRI, 1984). Such qualitative assessments have been supplemented by numerous quantitative research programs that have been both analytical and experimental in nature. Analytical programs have been valuable for improving understanding of how the seismic response of bridges is affected by nonlinear response phenomena, traveling wave effects, skewness, soil/structure interaction, etc. (e.g., Imbsen, 1984; Werner et al., 1979; Tseng and Penzien, 1973; Chen and Penzien, 1979). Various types of experimental programs have also played a key role here. Such programs have entailed dynamic tests of bridge components (e.g., Selna, 1984; Lew, 1984; Park et al., 1984), shake table tests of scale models of bridges (e.g., Godden, 1979); ambient vibration tests of actual bridge structures (e.g., Abdel-Ghaffar et al., 1983; Gates and Smith 1982), and full-scale forced vibration tests of bridges (e.g., Douglas and Norris, 1983; Douglas and Richardson, 1984). Recognition of



the need for further experimental programs that address the seismic behavior of bridges has resulted in initial planning of a national bridge engineering laboratory (Douglas, 1984).

In addition to analysis and testing of bridges, it is clear that strong motion measurements of actual bridge response during earthquakes, when obtained from a well-planned array of instruments and evaluated using established system identification techniques, can provide an important basis for gaining further insight into how bridges respond to seismic excitations. However, although many excellent measurements have been obtained from buildings, it was not until the mid-1970's that a program of strong motion instrumentation of bridges and other transportation structures was first initiated in California. This California program, which has been based on established guidelines for strong motion instrumentation and interpretation of records from highway bridges (Raggett and Rojahn, 1978; Rojahn and Raggett, 1981), has resulted in the instrumentation of five bridges to record earthquake motions (Table 1-1). To date, three of these five bridges have yielded significant data and, aside from the Meloland Road Overpass, strong motion data from only one of these bridges has been systematically evaluated using established system identification procedures (Wilson, 1984). Therefore, the instrumentation and evaluation of strong motion measurements represents a largely untapped resource for gaining significant information on the behavior of bridges during earthquakes. As shown by the results of this project, such measurements can indeed provide unique and valuable information along these lines.



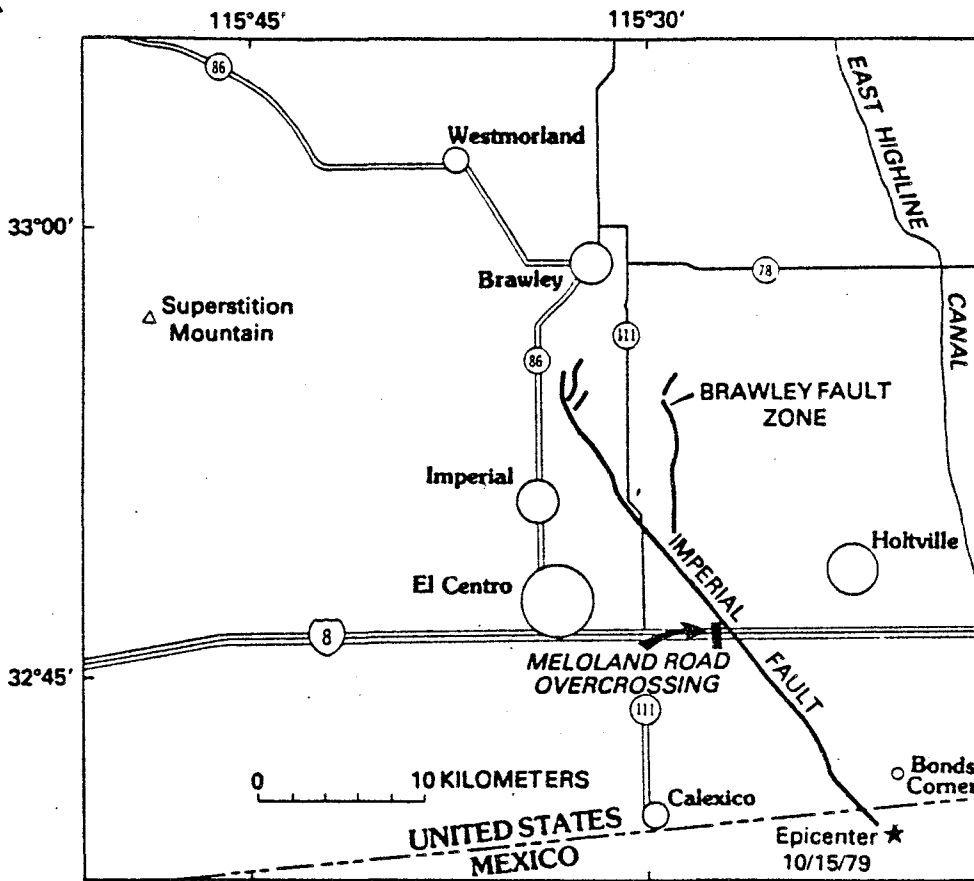
TABLE 1-1. CALIFORNIA BRIDGES WITH STRONG-MOTION INSTRUMENTATION AS OF MAY 1984 (Wilson, 1984)

Bridge Name and Location	Number of Transducers	Recorded Events
10-15E Interchange (San Bernardino)	1	None to date
San Juan Bautista 156/101 Separation (San Benito Co.)	12	8/6/79 - Coyote Lake
Meloland Road Overpass (El Centro)	26	10/15/79 - Imperial Valley 1980-81 - Several small events
101/Painter St. Overcrossing (Rio Dell; Humboldt Co.)	20	11/8/80 - Trinidad Offshore 12/16/82 - Rio Dell 8/24/83 - Cape Mendocino Offshore
Vincent Thomas Suspension Bridge (Los Angeles)	26	None to date

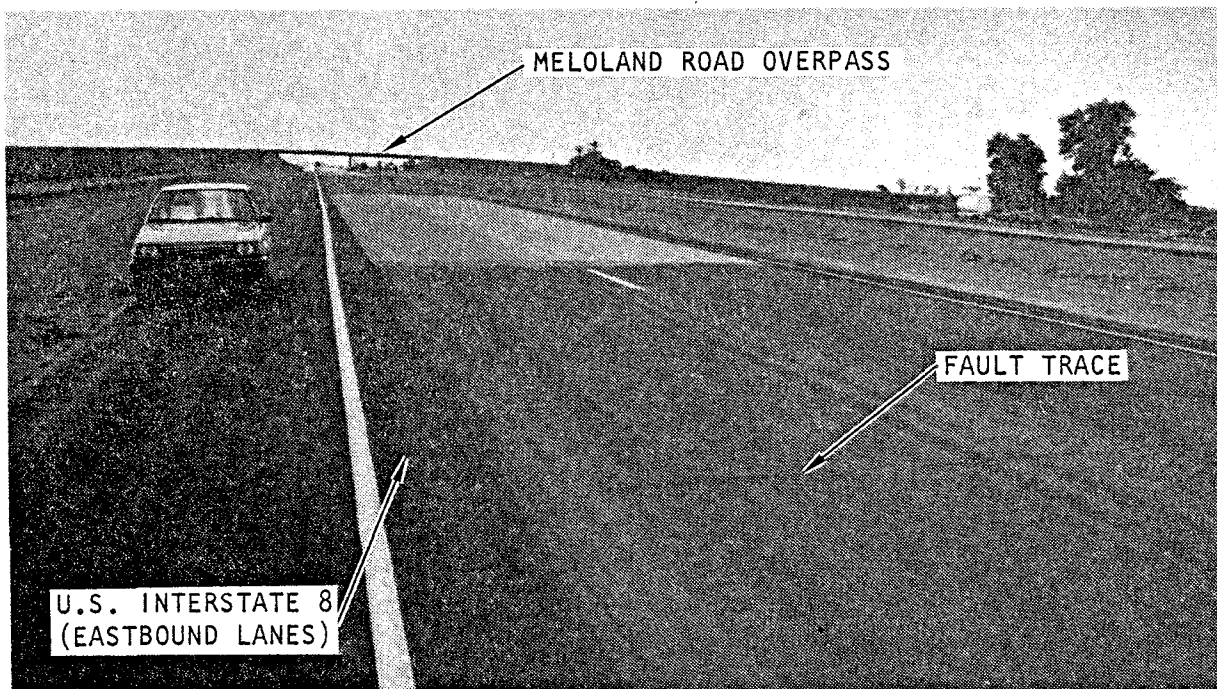
1.2 PROJECT OBJECTIVE

In October 1979, a magnitude 6.4 earthquake occurred along the Imperial fault just south of the United States-Mexico border and caused significant ground shaking throughout Southeastern California and Northcentral Mexico. This event, named the Imperial Valley Earthquake, triggered numerous strong motion accelerometers to provide an extensive set of strong motion measurements, particularly in the near field (Brady, 1980; McJunkin and Ragsdale, 1980; Porcella et al., 1982; and Brune et al., 1982).

Among the accelerograms obtained during this earthquake were those measured by an array of 26 transducers located on or near the Meloland Road Overpass (MRO) - a two-span bridge structure located 0.5 km west of the causative fault (Fig. 1-1).



(a) Map of El Centro area



(b) View looking west from Imperial fault

FIGURE 1-1. BRIDGE LOCATION

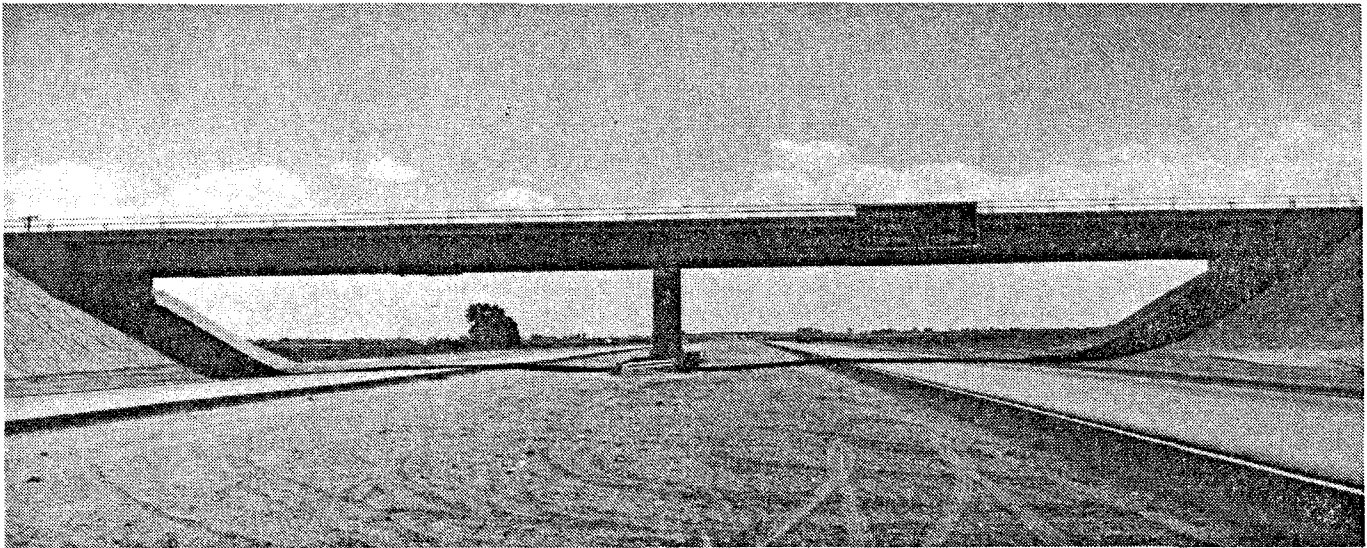


This bridge (Fig. 1-2) consists of a continuous reinforced-concrete three-cell box-girder road deck on open-end diaphragm abutments and a reinforced-concrete single-column pier, all on timber piles. The two spans of the bridge, each 104 ft long, are not skewed and contain no joints or sliding details. The bridge was designed in 1968-69 by the California Department of Transportation (CALTRANS), using 1968 California Division of Highways design criteria (Degenkolb and Jurach, 1980; Rojahn et al., 1982).

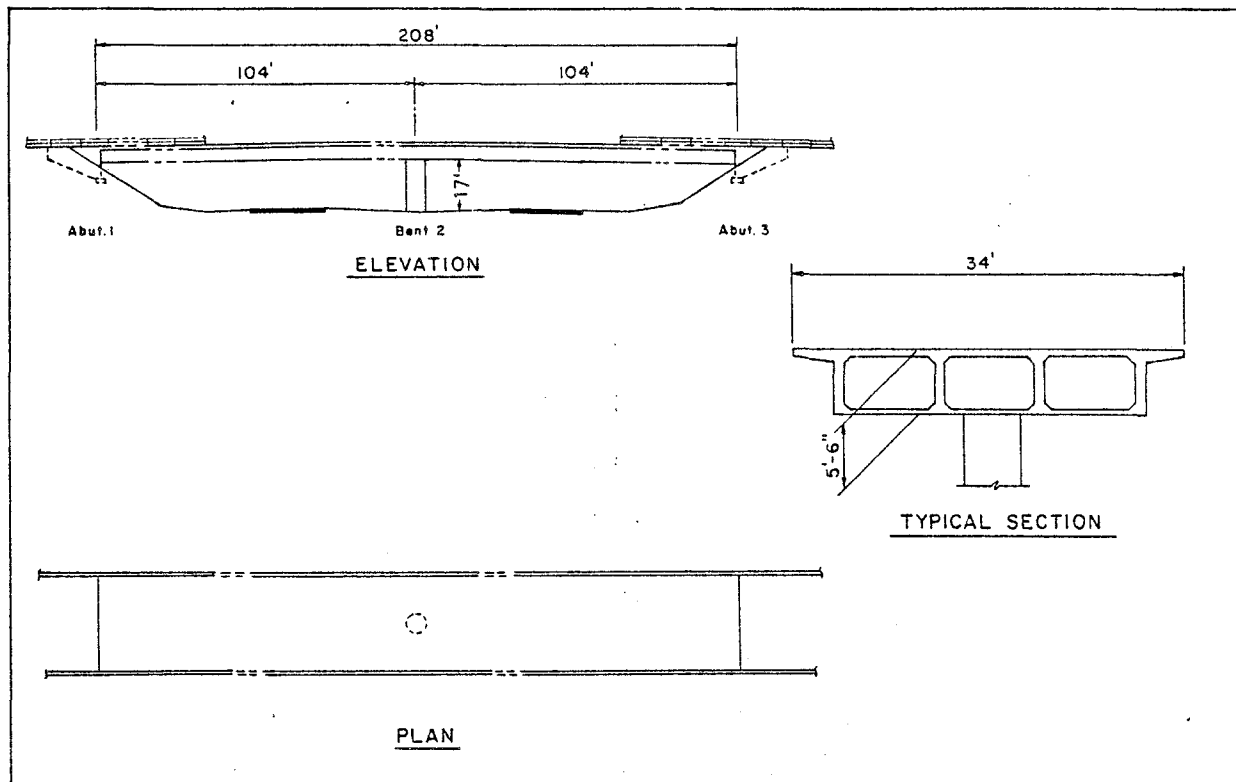
The Imperial Valley earthquake induced very intense shaking at the bridge, with peak horizontal and vertical accelerations along the road deck reaching levels of 0.51 g and 0.50 g, respectively. Despite this, the bridge was virtually undamaged by the shaking, except for some evidence of small relative motion and separation at the abutment/backfill interface (Rojahn et al., 1982). This can be contrasted with the New River bridges, northeast of El Centro, which were located further from the causative fault but nevertheless suffered extensive damage from the Imperial Valley earthquake motions.

The array of measurements obtained at the Meloland Road Overpass during the 1979 Imperial Valley earthquake is significant in that it represents the most extensive set of strong motion data yet obtained for bridges in the United States. Therefore, these data provide a unique opportunity for gaining new insights into how bridges behave during strong earthquakes. In particular, when properly interpreted and analyzed, the data can provide substantial information pertaining to the following key elements of the seismic design, analysis, and instrumentation of bridge structures:

- How do the various elements of a bridge structure (e.g., its abutments, road deck, piers, etc.) participate in its overall dynamic response during a major earthquake?
- What levels of damping can be anticipated for bridge structures subjected to strong seismic excitations?



(a) View looking east



(b) General plan (Gates and Smith, 1982)

FIGURE 1-2. MELOLAND ROAD OVERPASS



- To what degree of accuracy can conventional mathematical modeling procedures serve to analyze the seismic response of bridges?
- How should bridges be instrumented to obtain strong motion data that are sufficient to fully characterize their seismic response?
- What judgment factors and practical considerations exist in the processing of such data, and in the analysis of the data to interpret bridge response characteristics?

This project has been implemented with each of these important issues in mind.

1.3 PROJECT SCOPE

This project is one of several that have been implemented to use the MRO's strong motion measurements as a means of evaluating its seismic response characteristics (e.g., Abdel-Ghaffar and Illiscu, 1982; Lisiecki, 1982; Gates and Smith, 1982; Douglas and Reid, 1982). The present project builds on the insights gained from these past evaluations, through incorporation of the following special and unique features:

- Reprocessed Strong Motion Data. Special data processing procedures have been developed and applied to the original film traces of the accelerograms, in order to correct the traces for recorder stall and nonsynchronization problems that arose during the ground shaking. These procedures produced a consistent and complete set of corrected data from all 26 traces, that are suitable for use in evaluating structural response characteristics.
- System Identification Methodology. A new, state-of-the-art system identification methodology has been developed for evaluating the strong motion data at the MRO. The methodology is unique in that it is directly



applicable to structures with any number of support and structural response measurements. It identifies the complete set of pseudostatic and normal mode parameters necessary to fully characterize the response of the MRO to the earthquake ground shaking.

- Results of MRO Response Evaluation. The above system identification methodology has been applied to the reprocessed strong motion measurements at the MRO in order to (1) identify all of the pseudostatic parameters and significant modes of vibration of the MRO; and (2) use these results to show how each element of the bridge (e.g., abutments, superstructure, torsional vs. translational response components, etc.) has influenced its measured motions. Such applications have been implemented for two different sets of input and response measurements, in order to assess dynamic response characteristics of two alternative subsystems of the bridge. In addition, each application includes a detailed assessment of how the results have been affected by the use of a classical mode model (that neglects nonlinear and complex mode phenomena) and by certain limitations in the array of strong motion instruments deployed at the MRO.

1.4 REPORT ORGANIZATION

The remainder of the report is divided into four main chapters and one appendix. The reprocessing of the MRO's strong motion data is described in Chapter 2 and the new system identification methodology developed under this project is formulated and verified in Chapter 3. Chapter 4, which is the heart of the project, describes our use of the data and methodology developed in Chapters 2 and 3 in order to assess the seismic response characteristics of the MRO. A summary of the results of the project and a discussion of recommended areas for further investigation are provided in Chapter 5. Appendix A provides



time-history and spectrum plots for all of the reprocessed strong motion data at the MRO, and describes how interested parties can obtain these data.



CHAPTER 2

STRONG MOTION DATA REPROCESSING

This chapter describes our reprocessing of the strong motion data measured at the Meloland Road Overpass, in order to: (1) reconstruct motions in the vicinity of periodic recorder stalls that affected the motions measured at 13 of the 26 channels at the bridge; and (2) correct for effects of non-synchronization of the motions from the two recorders due to differences in their start-up characteristics. The chapter first summarizes the instrumentation layout and accelerogram measurements at the bridge, and then describes our data reprocessing efforts.

2.1 STRONG MOTION INSTRUMENTATION AND ACCELEROGRAMS

2.1.1 INSTRUMENTATION

The instrumentation of the Meloland Road Overpass has been described in detail by Rojahn et al. (1982) and is summarized here. This bridge was selected for instrumentation because of its structural characteristics and its close proximity to the Imperial Fault. Instruments were installed at the bridge in November 1978, and are maintained by the California Division of Mines and Geology, Office of Strong Motion Studies.

The instrumentation consists of two 13-channel Kinematics CRA-1 remote-accelerometer central recording systems. It is comprised of FBA-1 (single axis) and FBA-3 (triaxial) accelerometer packages, two 13-channel central recording units interconnected for common timing, and one VS-1 starter. The recorders and starter are located at the ground level next to the base of the central pier. The FBA accelerometers have a natural frequency of about 50 Hz and are designed to measure accelerations up to 1 g over a nominal frequency range of 0 to 50 Hz.



The instrumentation layout is shown in Figure 2-1. The data recorded at the indicated instrument locations provide measurements of the vertical (flexural), transverse (horizontal), and torsional response of the road deck, the translational response at the two abutments and the base of the central pier, the motions in the embankments adjacent to the abutments, and the free field response. Some typical instrument locations are shown in Figure 2-2.

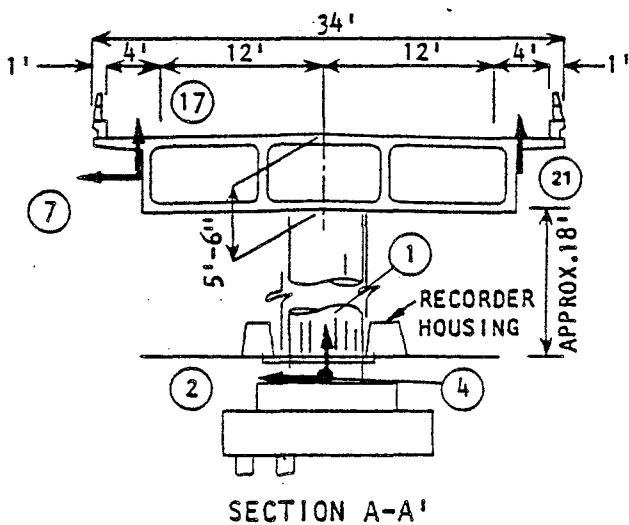
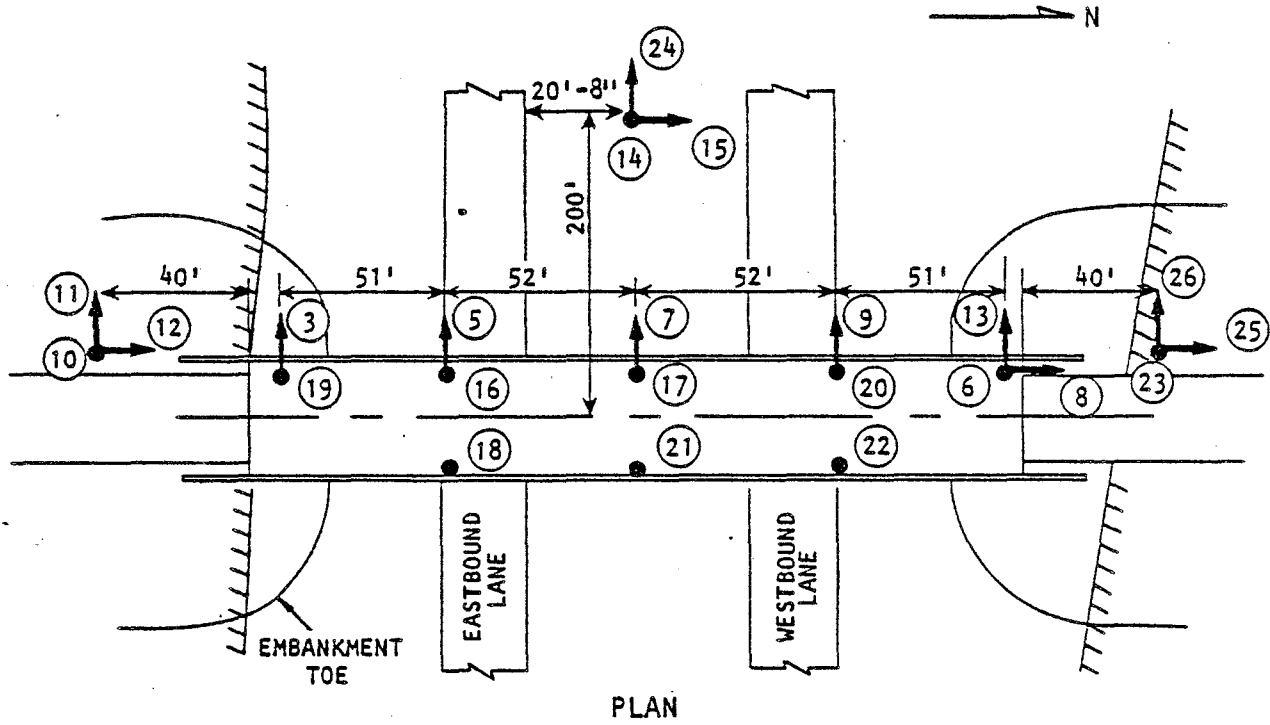
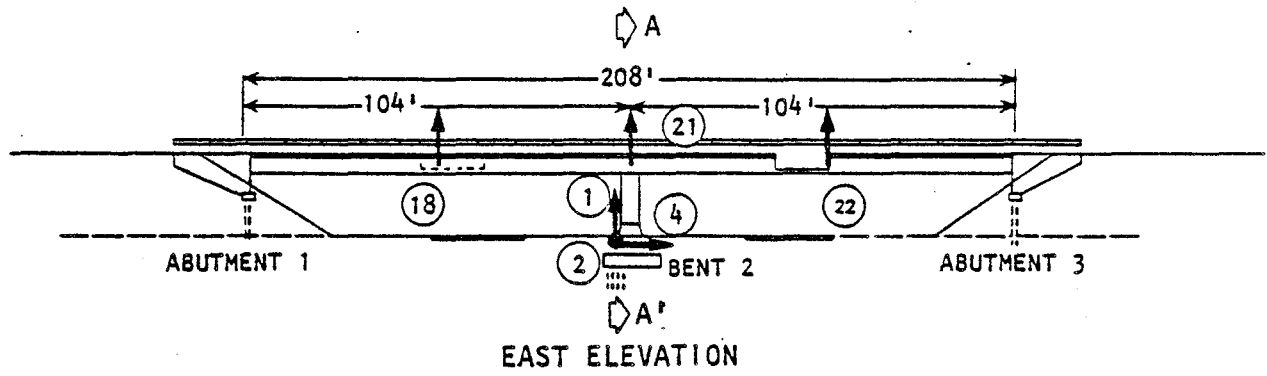
2.1.2 ACCELEROGRAMS

The 26 accelerograms recorded at the Meloland Road Overpass during the 1979 Imperial Valley earthquake are shown in Figure 2-3. This figure shows that, although each of the 13-channel accelerometer systems operated during the earthquake, the records from one system (involving data from Channels 1 to 13) suffered data loss because the recorder film transport stalled periodically during the earthquake. These stalls occurred at approximately 3 sec intervals, and are characterized by a distortion of the acceleration trace and a bulging and shortening of the time trace. Because of these stall effects, special digitization techniques were developed and implemented as part of this project, in order to reconstruct the bridge response in the stalled regions of the trace. These techniques are described in the following section of this chapter. Following this, an additional data reprocessing effort - which has addressed an apparent lack of synchronization of the data from the two recorders - is described.

2.2 DATA RECONSTRUCTION AT RECORDER STALLS

2.2.1 OVERVIEW

The objectives of this data reconstruction effort have been: (1) to reconstruct the motions from Channels 1 to 13 that

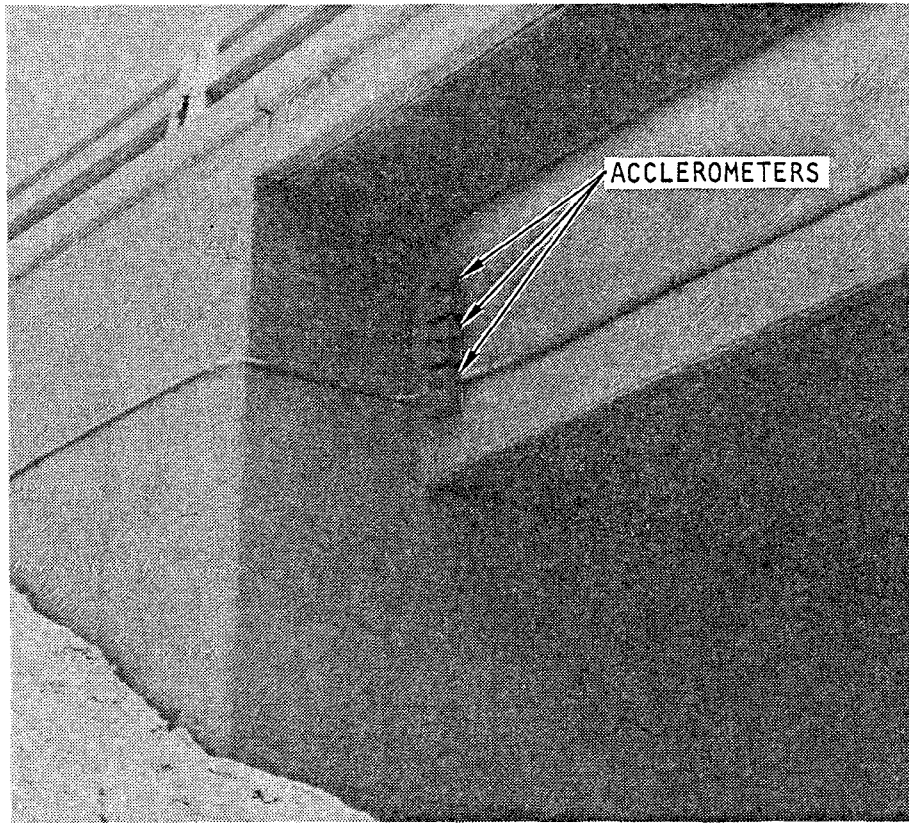


EXPLANATION

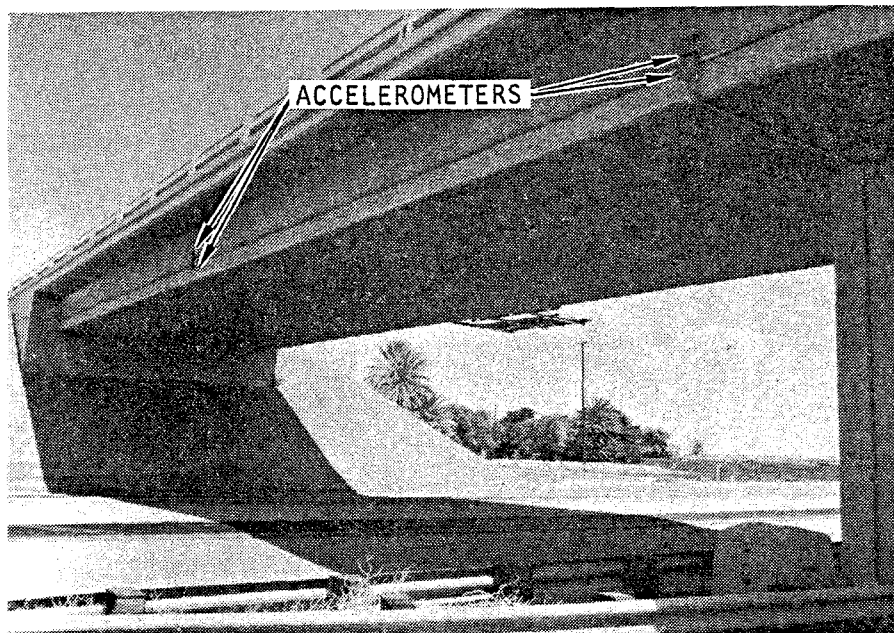
● → FBA accelerometer — Arrow shows direction of acceleration recorded; dot, acceleration in direction perpendicular to plane of figure. Corresponding record-trace number shown in adjacent circle.

Note: Accelerometers 1, 2, and 4 mounted on footing in ground vault; 10-12, 14-15, and 23-26 located in ground vault beneath ground surface; and 3, 5-9, 13, and 16-22 mounted on side of box girder supporting roadway deck.

FIGURE 2-1. STRONG MOTION INSTRUMENTATION LAYOUT AT MELOLAND ROAD OVERPASS (Rojahn et al., 1982)

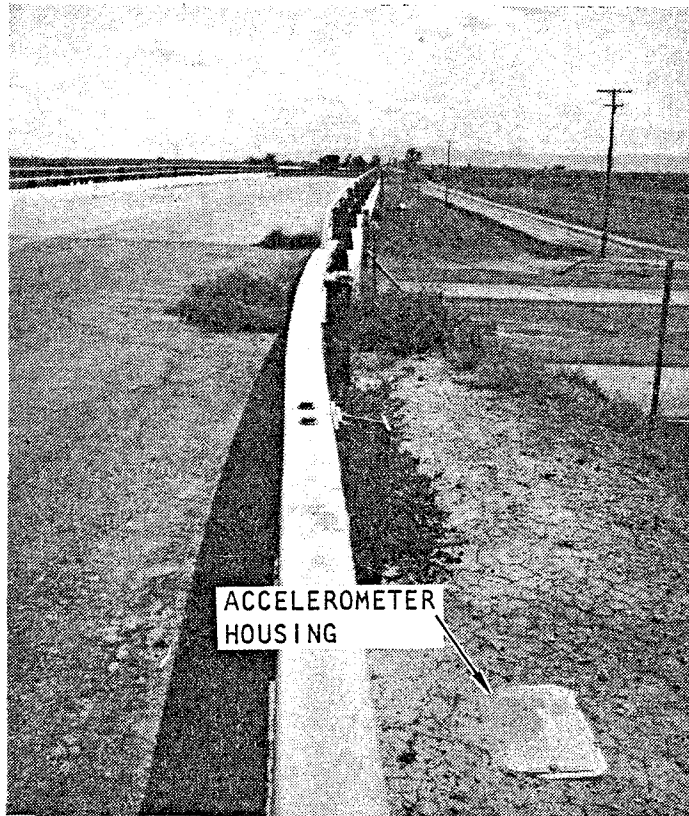


(a) West face of north abutment

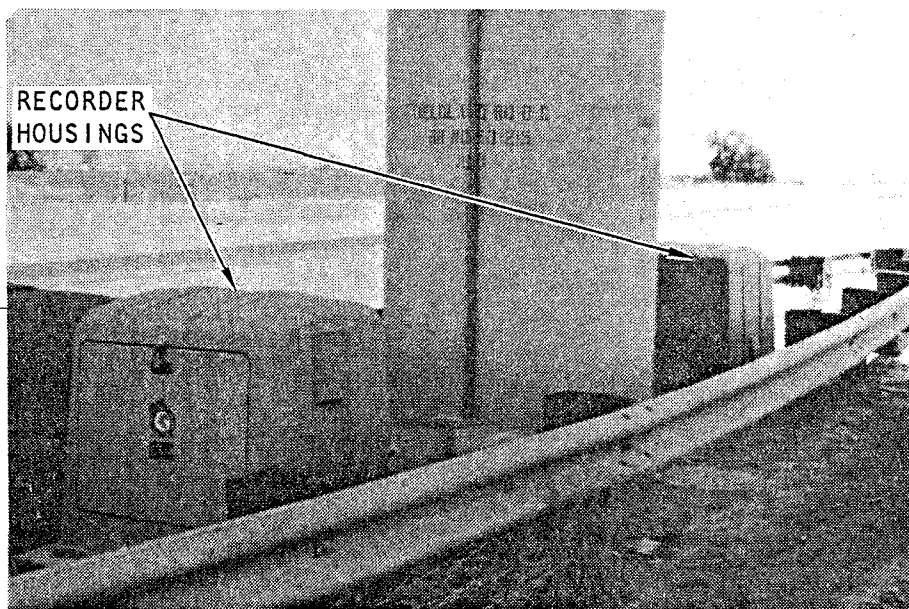


(b) West face of road deck

FIGURE 2-2. STRONG MOTION ACCELEROMETERS AT MELOLAND ROAD OVERPASS



(c) North embankment



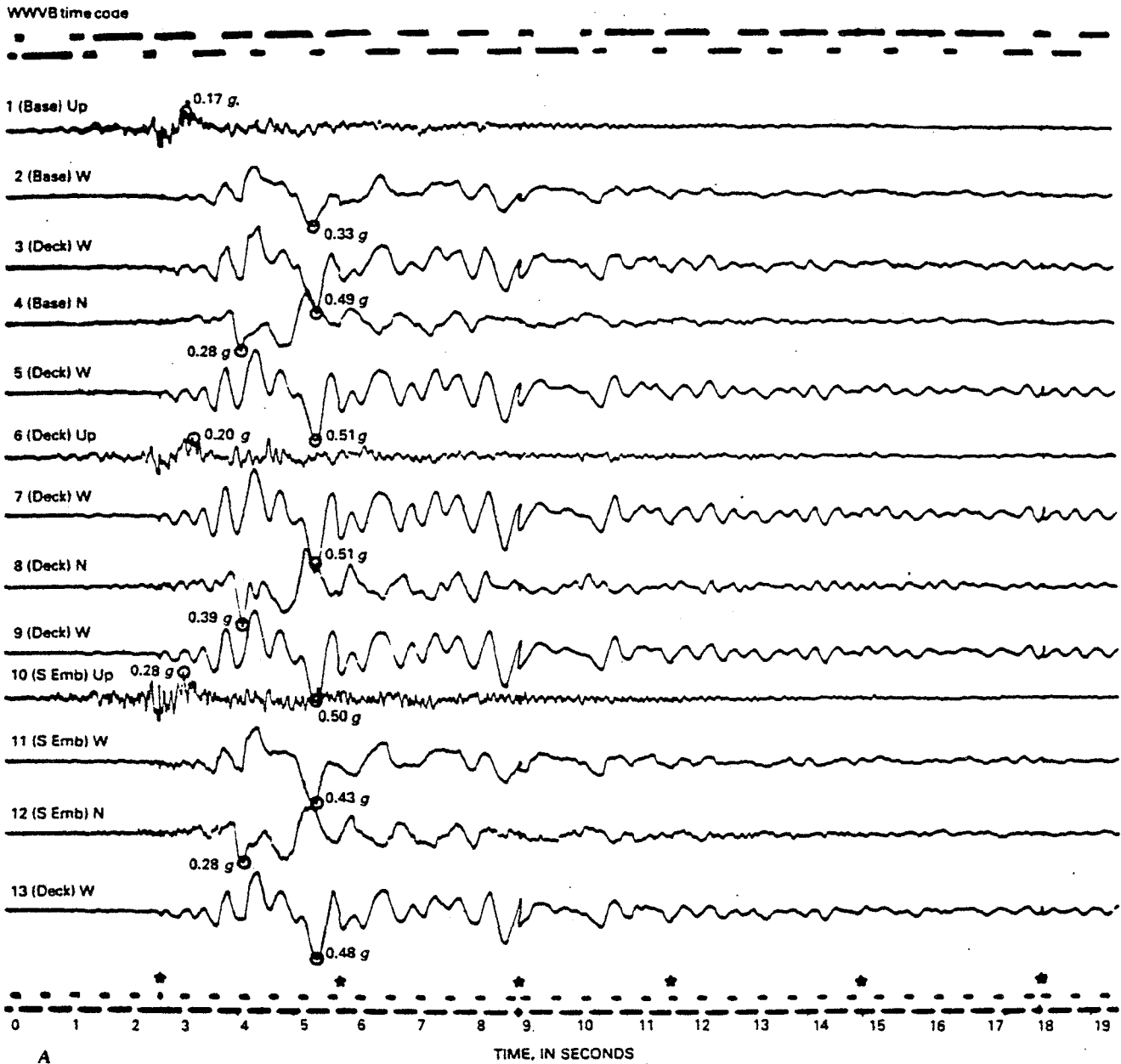
(d) Central recorders

FIGURE 2-2. (CONCLUDED)



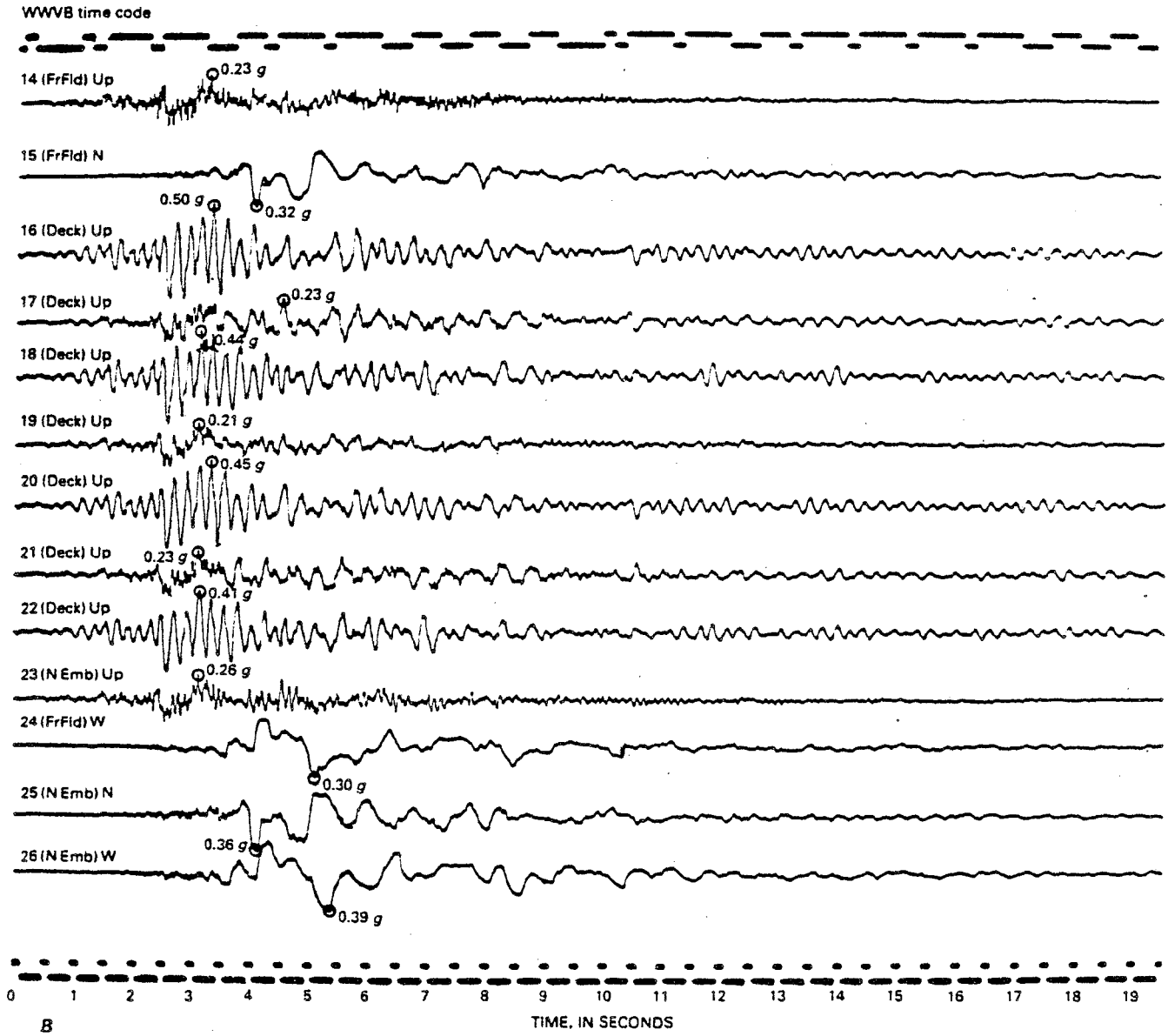
NOTES:

1. Directions in trace identification denote direction of positive acceleration — N (north), W (west), or Up (vertical).
2. Circle denotes peak acceleration for each trace.
3. Asterisks along lower time traces denote approximate times of recorder stalls.



(a) Traces from Channels 1 to 13

FIGURE 2-3. RAW ACCELEROGRAPH TRACES OBTAINED AT MELOLAND ROAD OVERPASS DURING 1979 IMPERIAL VALLEY EARTHQUAKE



(b) Traces from Channels 14 to 26

FIGURE 2-3. (CONCLUDED)



were distorted by the recorder stalls; and (2) to provide consistent data from all 26 channels that can be used simultaneously to evaluate the bridge response characteristics in accordance with the project objectives. The reconstruction of the motions in the vicinity of the recorder stalls and the subsequent routine processing of the reconstructed records was carried out under this project by M.D. Trifunac and V.W. Lee of the University of Southern California (USC). This endeavor was aided by the support and cooperation of personnel from the Office of Strong Motion Studies, California Division of Mines and Geology.

The reconstruction of the data at the recorder stalls used the Automatic Record Digitizing System (ARDS) at USC. This effort involved certain manual operations, together with automatic operations controlled by the ARDS routine software and one additional program developed specifically for this application. Once the data from Channels 1 to 13 was reconstructed, it was then reprocessed using the USC routine data-processing software. Data from Channels 14 to 26 (which were not affected by recorder stalls) were also redigitized and reprocessed so as to assure consistency between records from all channels.

2.2.2 DATA DIGITIZATION

The basic elements of the ARDS facility are indicated schematically in Figure 2-4 and are described in detail by Trifunac and Lee (1979). All digitization operations using these elements are controlled through the existing programs FILM, TRACE, TV, and SCRIBE, and through the special purpose program, MAKGAP, written for application to the Meloland Bridge data. The use of these programs in the reconstruction of motions from Channels 1 to 13 is illustrated in Figure 2-5, and is summarized in the paragraphs that follow. The existing programs were also used in the routine digitization of the traces from Channels 14 to 26.

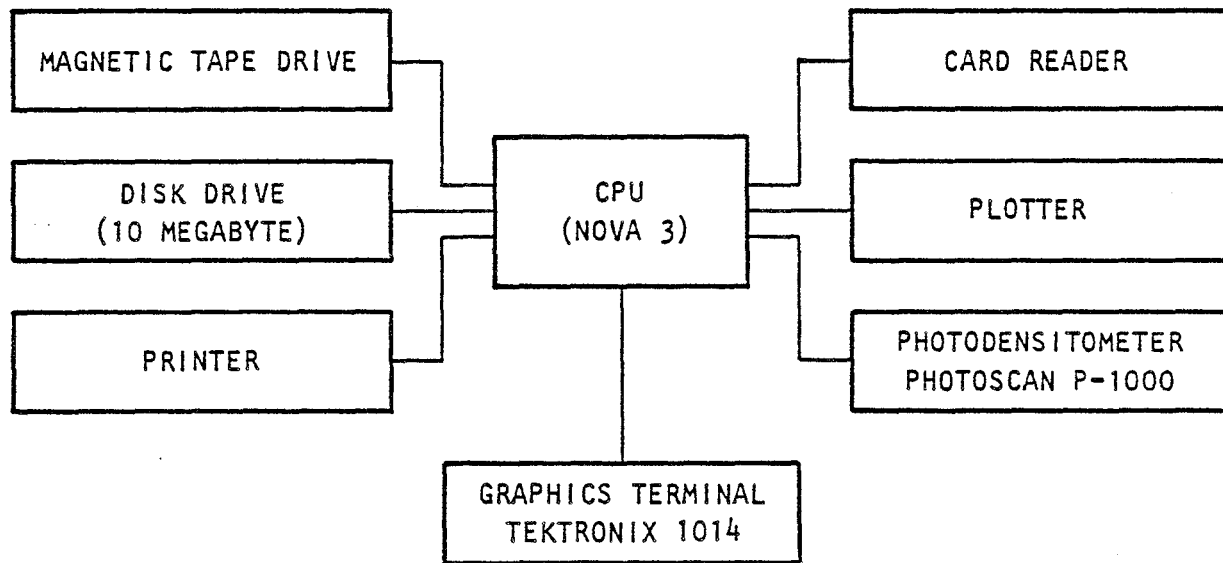


FIGURE 2-4. HARDWARE COMPONENTS OF USC AUTOMATIC ACCELEROGRAPH RECORD DIGITIZING SYSTEM (Trifunac and Lee, 1979)

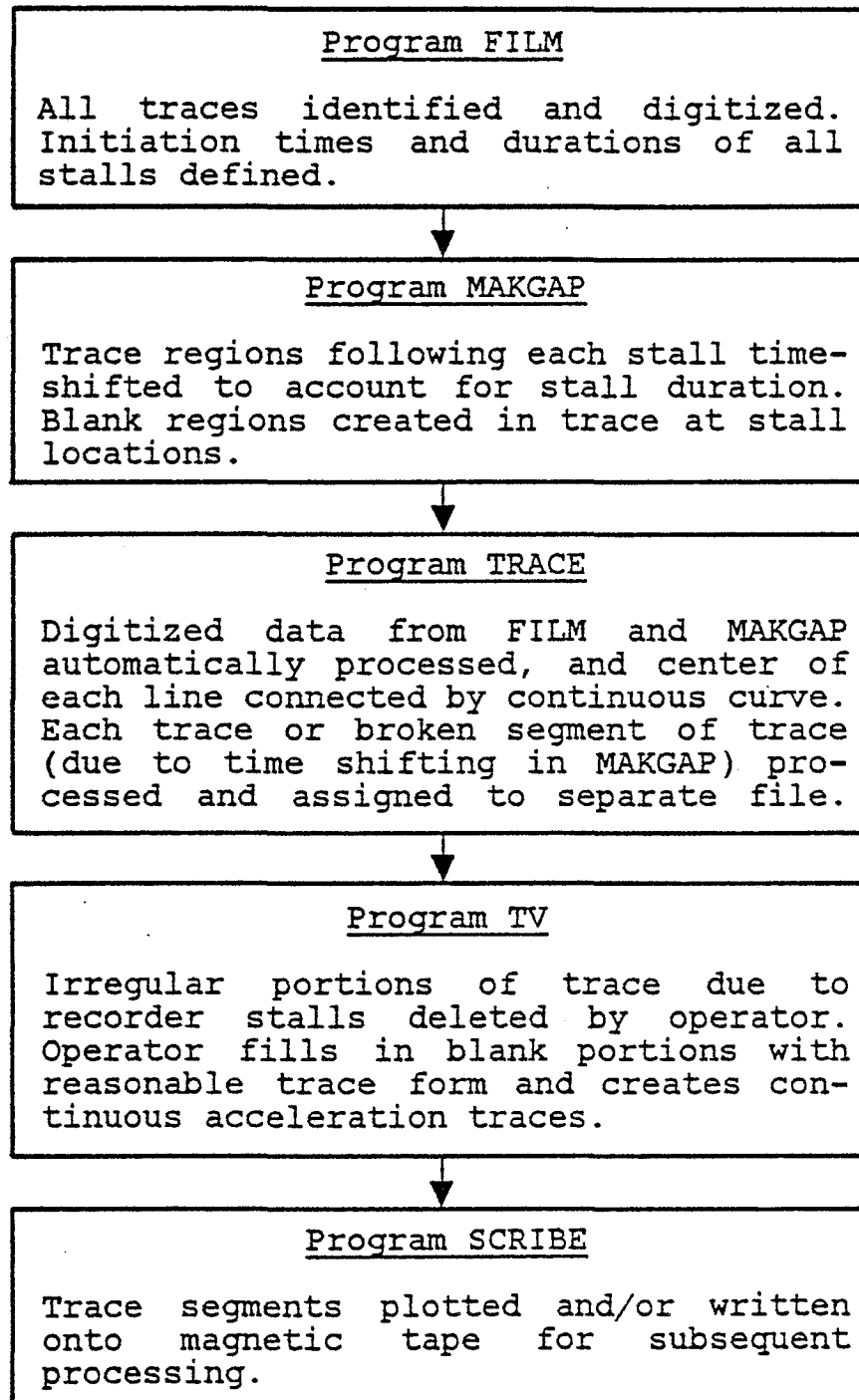
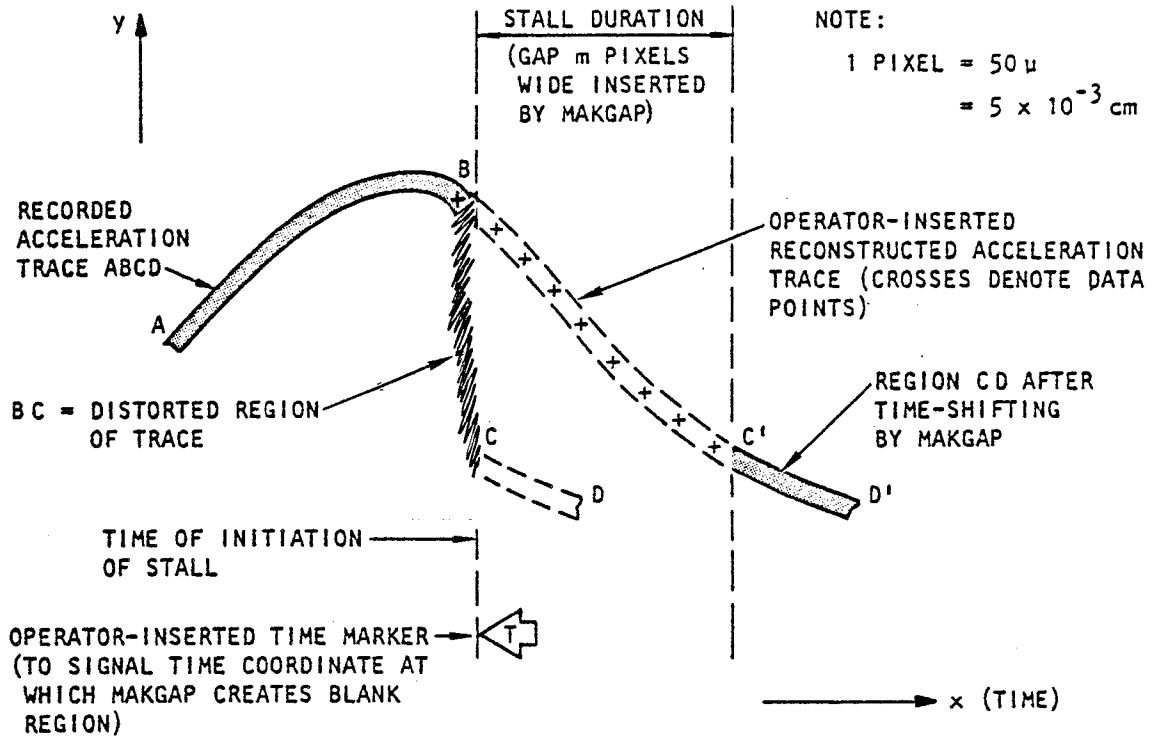


FIGURE 2-5. PROCESS FOR RECONSTRUCTION OF MOTION AT RECORDER STALLS

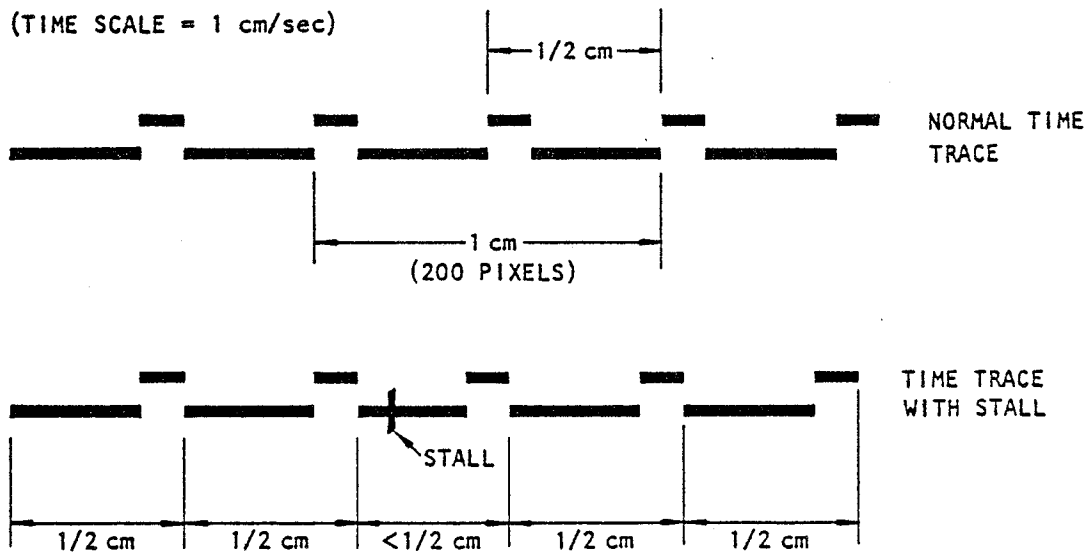
2.2.2.1 Program FILM

The reading of the negative film is performed by the ARDS drum photodensitometer, which is controlled by the program FILM. In this operation, a rotating drum to which the film is attached is scanned by a light source, and light intensities are measured. This scanning operation proceeds along the vertical axis of the film at 1 pixel (50 micron) intervals, and each light intensity reading greater than a chosen threshold level together with its vertical axis coordinate are stored onto a disk file for future use. After each vertical scan is completed, the light source moves 1 pixel to the right (along the horizontal axis of the film) and the above vertical scanning process is repeated.

This automated scanning operation was applied to the Meloland Road Overpass data until a region affected by a recorder stall was encountered; as previously noted, such stall effects were evidenced by a localized distortion of the Channel 1 to 13 acceleration traces displayed on the ARDS graphics terminal, and a discernable bulge in the time trace (Fig. 2-6). When this occurred, the automated digitization process was temporarily halted, and the following manual procedures were conducted by the operator: (1) the distorted region of the film trace was enlarged on the graphics terminal; (2) from careful examination of this distorted region, the estimated time of initiation of the stall was defined by manual insertion of a time-marker at the appropriate pixel location along the time axis of the trace (Fig. 2-6a); and (3) the duration of the stall was obtained by measuring (in pixel units) the amount of shortening of the time trace in the stalled region (Fig. 2-6b). This procedure, repeated for each stall in the Channel 1 to 13 records, resulted in the identification of seven stalls with initiation times approximately 3 sec apart and with durations ranging from 0.04 sec to 0.25 sec (Table 2-1).



(a) Acceleration trace



(b) Normal vs. stalled time trace

FIGURE 2-6. RECONSTRUCTION OF MOTION AT RECORDER STALL

TABLE 2-1. RECORDER STALLS IN TRACES AT CHANNELS 1 TO 13
OF MELOLAND ROAD OVERPASS RECORDS

Stall Number	Initiation Time After Triggering (sec)	Duration of Stall (sec)	Width of Stall (pixels)
1	2.65	0.13	26
2	5.60	0.04	8
3	8.55	0.25	51
4	11.15	0.05	10
5	14.30	0.04	8
6	17.35	0.22	44
7	20.05	0.19	38

2.2.2.2 Program MAKGAP

The second part of this process involved the use of MAKGAP, which is a new program incorporated in the ARDS software to facilitate the reconstruction of the motions that occurred during the recorder stalls. MAKGAP served to correct the time coordinates of each digitized point of the acceleration trace by: (1) reading the data generated by FILM until one of the operator-inserted time-markers denoting the initiation of a stall was encountered; and (2) inserting an appropriate number of blank pixel bands so as to shift the time coordinates of every point beyond the flag, by an amount equal to the total duration of all previous stalls (Fig. 2-8a). This operation was carried out for each stall identified in FILM.

2.2.2.3 Program TRACE

During the third part of this digitization process, the digitized data were automatically analyzed by the program TRACE in the following manner: (1) at each time location, it identified the coordinates of the mid-thickness of each acceleration



trace (whose overall thickness was defined in terms of light intensity readings obtained from the vertical scanning process controlled by FILM); and (2) it defined each continuous trace segment on the film negative and assigned it to a particular file. When the traces were broken due to the gaps created by MAKGAP at each stall occurrence, TRACE assigned a new file number to each trace segment.

2.2.2.4 Program TV

The fourth operation in this digitization process involved editing of the acceleration trace data in the vicinity of the stalls to produce a continuous trace. This operation is illustrated by referring to Figure 2-6a, which shows the original recorded accelerograph trace at a stall as curve ABCD, as well as the gap created by MAKGAP over the duration of the stall. The following steps were involved in the editing process indicated in this figure: (1) the operator deleted segment BC, which is the portion of the trace distorted by the recorder stall; and (2) the operator then inserted points to define a reasonable "corrected trace segment" over the duration of the stall, that connected the undistorted trace segments AB and C'D',* and created a continuous trace ABC'D'. This process was repeated at each of the seven gap locations for all acceleration traces (Channels 1 to 13) and for all fixed and other traces present on the film.

2.2.2.5 Program SCRIBE

In the final operation in this digitization process, the reconstructed accelerograms were plotted and written onto magnetic tape for subsequent data processing.

* Note from Figure 2-6a that segment C'D' corresponds to segment CD of the original acceleration trace, after it was time shifted by MAKGAP to account for the stall duration.



2.2.3 STANDARD DATA PROCESSING

The processing of the data from the Meloland Road Overpass, after correction for the recorder stall effects, was carried out using standard USC software described by Lee and Trifunac (1979). This processing is briefly summarized as follows:

- "Volume 1" Processing. The "Volume 1" processing consists of various smoothing and scaling operations. These operations, however, represent a minimum interference with the basic data, so that the data so obtained may be referred to as "uncorrected."
- "Volume 2" Processing. In this stage of the processing operation, the "Volume 1" data are corrected for instrument frequency response and baseline adjustment, as described by Hudson (1979). This results in "corrected" acceleration, velocity, and displacement histories at each channel (Fig. 2-7a). It is noted that the data from each channel of recorded motion at the Meloland Road Overpass was band-pass filtered over the same frequency range, nominally 1/6 Hz to 25 Hz, so as to maintain consistency when all of the channels of data are used together in the subsequent modal extraction tasks under this project.
- "Volume 3" Processing. In this final data processing stage, Fourier amplitude spectra and response spectra for damping ratios of 0, 2, 5, 10, and 20 percent of critical are obtained (Fig. 2-7b).

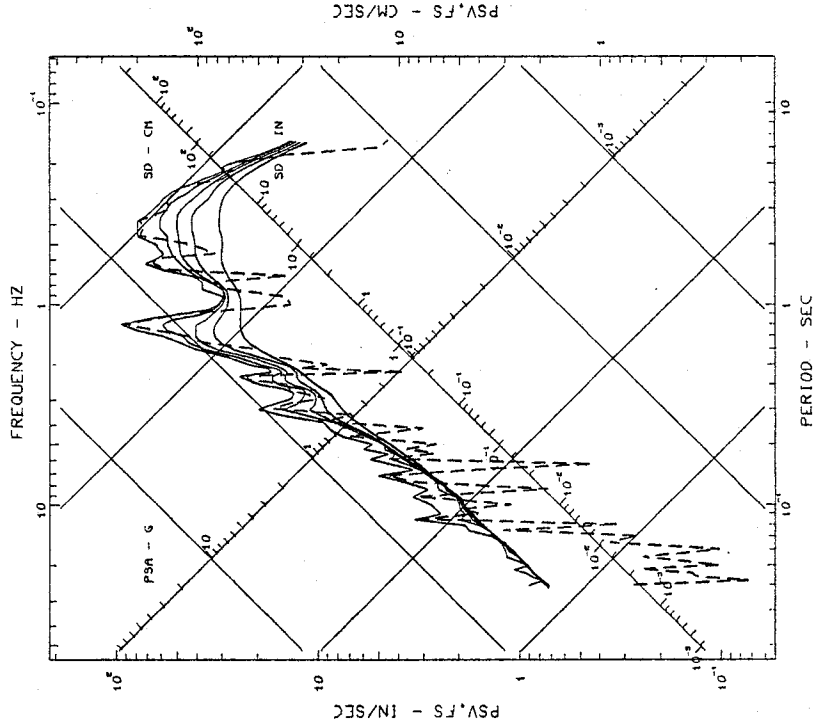
2.2.4 DISCUSSION

The above process for reconstructing the bridge response during the recorder stalls utilizes state-of-the-art digitization hardware and software. Nevertheless, the end results of

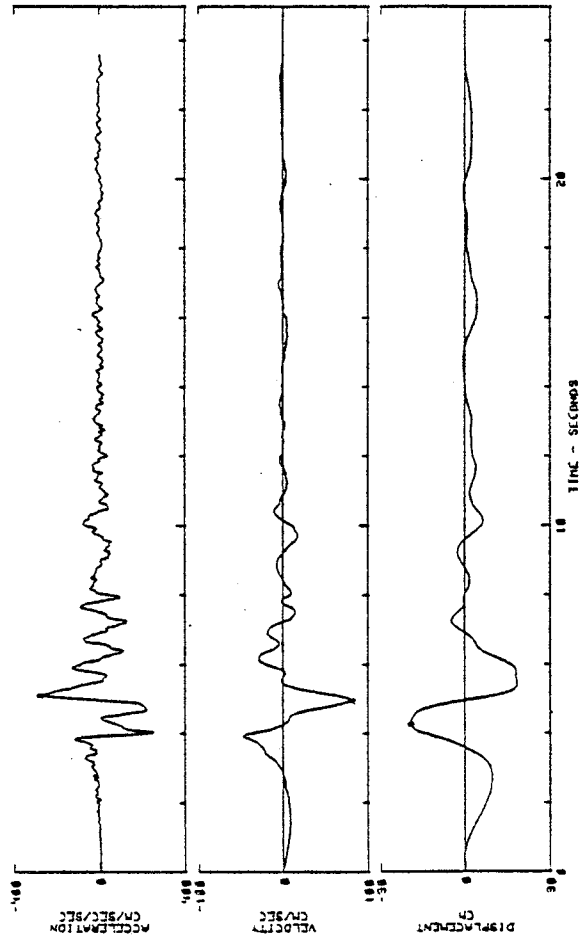


RESPONSE AND FOURIER SPECTRA
 IMPERIAL VALLEY EARTHQUAKE OCT 15, 1979 -1616 PDT
 IIMP201 79.201.0 COMP TR 4
 ROUTE 8/MELOLAND OVERPASS, EL CENTRO, CA
 ACCELEROGRAM IS BAND-PASS FILTERED BETWEEN .145- .165 AND 25.00-27.00 CYC/SEC.
 DAMPING VALUES ARE 0, 2, 5, 10 & 20 % OF CRITICAL.

RESPONSE SPECTRA: PSV, P9A & SD --- FOURIER AMPLITUDE SPECTRUM: FS




IMPERIAL VALLEY EARTHQUAKE OCT 15, 1979 -1616 PDT
 IIMP201 79.201.0 ROUTE 8/MELOLAND OVERPASS, EL CENTRO, CA COMP TR 4
 ACCELEROGRAM IS BAND-PASS FILTERED BETWEEN .145- .165 AND 25.00-27.00 CYC/SEC.
 PEAK VALUES: ACCELERATION = -.201.1 CM/SEC/SEC VELOCITY = 79.9 CM/SEC DISPLACEMENT = -.19.4 CM



(a) "Volume 2" processing - corrected time histories

(b) "Volume 3" processing - Fourier and response spectra

FIGURE 2-7. DATA PROCESSING OF STRONG MOTION DATA FROM MELOLAND ROAD OVERPASS - 1979 IMPERIAL VALLEY EARTHQUAKE



the process are clearly dependent on the judgment of the operator; i.e., different qualified operators may well interpret the bridge motions within the stalls somewhat differently. However, the relatively short duration (less than 0.25 sec*) of most of the stalls and the clearly visible limits of maximum and minimum excursions of recorded acceleration were not difficult to interpret. Furthermore, the acceleration traces in the vicinity of the stalls did not contain significant high frequency components, which also simplified the data reconstruction process. In view of this, errors in the final digitized data, though certainly present, are believed to be small.

2.3 EVALUATION OF POSSIBLE NONSYNCHRONIZATION EFFECTS

2.3.1 GENERAL DISCUSSION

When digitizing a strong motion accelerograph record, the time origin is typically selected to correspond to the start of the light trace of the record. However, when more than one recorder is involved in recording groups of accelerograph records within a structure, the recorders may have slight differences in start-up times of their film transporting mechanisms. These factors together could result in an artificial nonsynchronization of the motions from each recorder, even if the recorders are triggered simultaneously as intended. Furthermore, past experience with other sets of strong motion data has shown that such nonsynchronization effects can lead to problems in data analysis and optimization efforts (McVerry and Beck, 1983).

*From Figure 2-6b, it is apparent that, if the duration of a stall were longer than 1/2 sec, it would not be possible to determine its actual duration, since a multiple of 1/2 sec could always be added without altering the appearance of the recorded time trace. Fortunately, all stalls encountered in the data from Channels 1 to 13 were less than 1/2 sec, as indicated by perusal of the recorded acceleration traces.



In view of this, the final reprocessing operation for the Meloland Road Overpass records was directed toward evaluating the extent of any nonsynchronization effects of the type described above. This evaluation was based on computations of cross correlations between several pairs of Meloland Road Overpass records, in which one member of each pair was from the recorder for Channels 1 to 13 (hereafter referred to as Recorder A) and the other member was from the recorder for Channels 14 to 26 (termed Recorder B). Furthermore, the records that comprise each pair were judiciously selected to correspond to instruments located such that the two records should be well correlated except for recorder nonsynchronization effects. The instrument locations corresponding to the two records in each pair are most typically located on opposite abutments or embankments, and it is recognized that traveling wave effects as well as small errors in the estimates of recorder stalls for the Recorder A data could contribute to any nonsynchronization that is observed. Therefore, in this evaluation, special effort was directed toward separating these latter effects from effects of recorder start-up characteristics.

2.3.2 EVALUATION PROCEDURE

To evaluate recorder nonsynchronization effects on the data at the Meloland Road Overpass, cross-correlation functions were computed for the two records that comprise each pair, according to the following expression (Bendat and Piersol, 1971)

$$R_{xy}(\tau) = \frac{1}{T'_d} \int_0^{T'_d} \ddot{x}(t) \ddot{y}(t + \tau) dt \quad 0 < \tau < T_d \quad (2-1)$$

where

$\ddot{x}(t)$, $\ddot{y}(t + \tau)$ = The accelerograms from Recorders A and B respectively that comprise each pair

$$T'_d = T_d - \tau$$



T_d = The time duration over which $R_{xy}(\tau)$ is calculated

τ = Time shift

The phase time difference between the two accelerograms, τ_0 , was taken as the value of τ at which $R_{xy}(\tau)$ was maximized. In this, τ_0 represents the time by which \ddot{x} (which, in most record pairs, are the motions from Recorder A) lead \ddot{y} (which most typically are the motions from Recorder B).

2.3.3 RESULTS

Cross-correlation calculations were carried out for the eight pairs of records listed in Table 2-2. Results of these calculations are tabulated in Tables 2-2 and 2-3, and are plotted in Figure 2-8. The results show that, for those pairs involving one accelerogram from Recorder A and the other from Recorder B, the overall phase time difference between the two recorders is remarkably consistent. These phase time differences indicate that the motions from Recorder A (for Channels 1 to 13) lead the motions from Recorder B (Channels 14 to 26) by values ranging from 0.05 sec to 0.07 sec, with the most typical value corresponding to 0.06 sec. Further evaluation of these results is provided in the paragraphs that follow, in order to separate recorder nonsynchronization effects from possible effects of traveling waves and any errors in the estimates of recorder stalls when processing the accelerograms from Recorder A.

2.3.3.1 Motions at Top and Bottom of Central Pier

The first pair of records shown in Table 2-2 corresponds to vertical motions at the base and top of the central pier (as obtained from Recorders A and B, respectively). For these motions, the transit time due to P-wave propagation is computed as

$$t_s = \frac{\ell}{V_p}$$



TABLE 2-2. RECORD PAIRS CONSIDERED IN EVALUATION OF RECORDER NONSYNCHRONIZATION EFFECTS

Pair Number	Description	x(t)			y(t+τ)			Phase Time Difference, ¹ sec
		Channel Number	Location	Recorder	Channel Number	Location	Recorder	
1	Vertical motions at top and bottom of central pier	1	Base of central pier	A	Average of Channels 17 and 21	Equivalent vertical translation at top of central pier ²	B	0.05 ³
2	Transverse (east-west) horizontal motions at north and south abutments, both from Recorder A	3	South abutment	A	13	North abutment	A	0.0
3	Vertical motions at north and south abutments (entire record)	6	North abutment	A	19	South abutment	B	0.05 ³
4	Vertical motions at north and south abutments (first 2 sec)							0.06
5	Transverse (east-west) horizontal motions at north and south embankment	11	South embankment	A	26	North embankment	B	0.06
6	Vertical motions at north and south embankment (entire record)	10	South embankment	A	23	North embankment	B	0.06
7	Vertical motions at north and south embankments (first 2 sec)							0.07 ⁴
8	Longitudinal (north-south) motions at north and south embankments	12	South embankment	A	25	North embankment	B	0.06

Notes:

¹Phase time differences are times at which cross-correlation function R_{xy} (Eq. 2-1) is maximized. This corresponds to time at which motions from Recorder A lead those from Recorder B.

²The equivalent vertical translation at the top of the central pier has been obtained as the time-step by time-step average of the accelerograms from Channels 17 and 21. These channels correspond to instruments located on the west and east faces respectively of the road deck, above the central pier. The accelerations from both of these channels were recorded on Recorder B.

³Nearly identical peak values of $R_{xy}(\tau)$ occur at $\tau = 0.04$ sec ($2\Delta t$) and at $\tau = 0.06$ sec ($3\Delta t$) where Δt is the time increment of the processed motions (= 0.02 sec). Therefore, the phase time difference between the vertical motions at the top and bottom of the central pier are estimated to be about 0.05 sec.

⁴Nearly identical peak values of $R_{xy}(\tau)$ occur at $\tau = 0.06$ sec ($3\Delta t$) and $\tau = 0.08$ sec ($4\Delta t$), where, as above, $\Delta t = 0.02$ sec. Therefore the phase time difference between the first 2 sec of the vertical motions of the south and north embankments are estimated to be about 0.07 sec.



TABLE 2-3. PARTIAL TABULATION OF CROSS CORRELATION RESULTS
(BEFORE TIME SHIFT OF CHANNEL 1 TO 13 DATA)

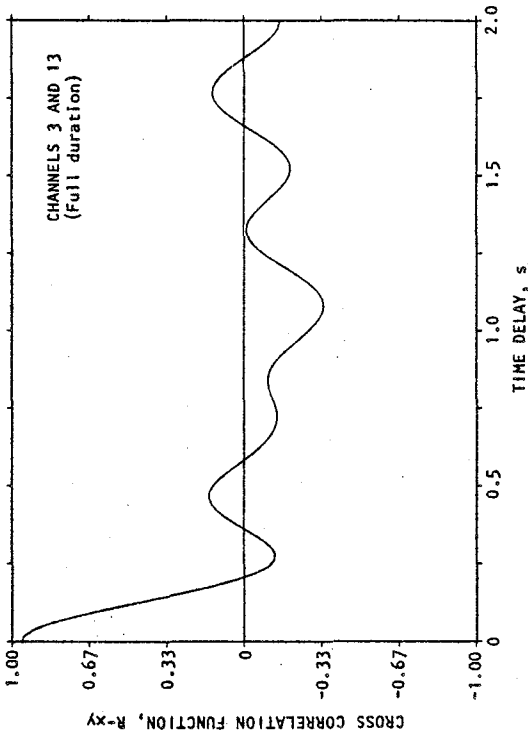
Time Lag, τ (sec)	Cross Correlation Function, R_{xy}			
	Record Pair No. 1 Channels 1 and CL1* Full Duration	Record Pair No. 2 Channels 3 and 13 Full Duration	Record Pair No. 3 Channels 6 and 19 Full Duration	Record Pair No. 4 Channels 6 and 19 2 sec Duration
0.	.41055	.95750	.38936	.23158
.02	.64535	.94817	.55012	.50372
.04	.89936	.90484	.69701	.74723
.06	.88363	.83264	.70995	.85461
.08	.58807	.73788	.56459	.56659
.10	.38061	.62650	.41927	.28307
.12	.32511	.50412	.27769	.04780
.14	.30570	.37659	.17806	-.10109
.16	.29183	.25068	.12799	-.14423
.18	.22377	.13367	.11128	-.14328
.20	.13366	.03267	.10586	-.17990
.22	.10999	-.04667	.09194	-.30848
.24	.14945	-.10109	.07994	-.30997
.26	.19125	-.12990	.04755	-.22207
.28	.21902	-.13510	-.00238	-.14110
.30	.23670	-.12033	-.01998	-.06885
.32	.21764	-.09028	-.01059	-.01733
.34	.16645	-.05005	.02012	.05938
.36	.11487	-.00474	.06168	.13951
.38	.07001	.04090	.05994	.21770
.40	.01623	.08260	.02305	.26482
.42	-.05541	.11665	-.00802	.23082
.44	-.12043	.14013	-.03711	.22653
.46	-.15001	.15112	-.06398	.12346
.48	-.15184	.14907	-.07860	-.06106
.50	-.16391	.13488	-.08863	-.19576
.52	-.18828	.11077	-.09603	-.28106
.54	-.19633	.07956	-.10286	-.28018
.56	-.18893	.04422	-.09772	-.23872
.58	-.19071	.00751	-.10214	-.17729
.60	-.20901	-.02808	-.12158	-.10821
.62	-.20019	-.06048	-.13239	-.72210
.64	-.18202	-.08825	-.14356	.00154
.66	-.17983	-.11058	-.15821	.08077
.68	-.17865	-.12697	-.15979	.13922
.70	-.16601	-.13713	-.14433	.12074
.72	-.13316	-.14087	-.12552	.08663
.74	-.11172	-.13864	-.12174	.07901
.76	-.11791	-.13178	-.13107	.04445
.78	-.15744	-.12240	-.14667	.07479
.80	-.20129	-.11298	-.15057	.06549
.82	-.21561	-.10603	-.12659	.01469
.84	-.20313	-.10364	-.07714	-.04112

*Note: CL1 = average vertical translation from Channels 17 and 21.

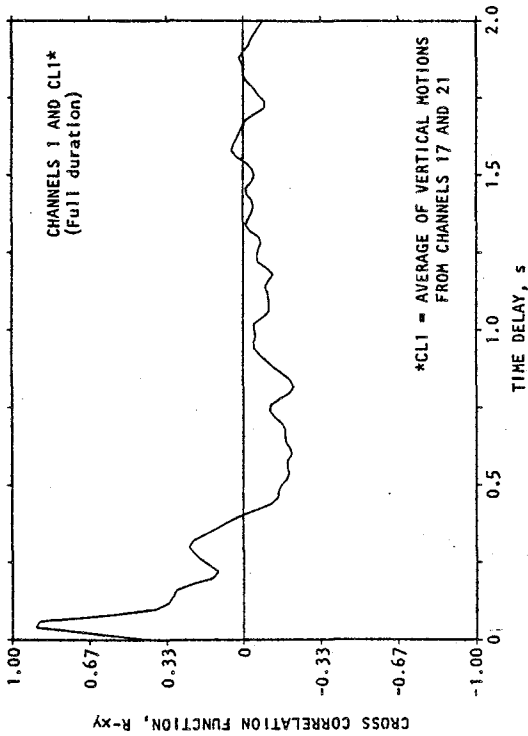


TABLE 2-3. (CONCLUDED)

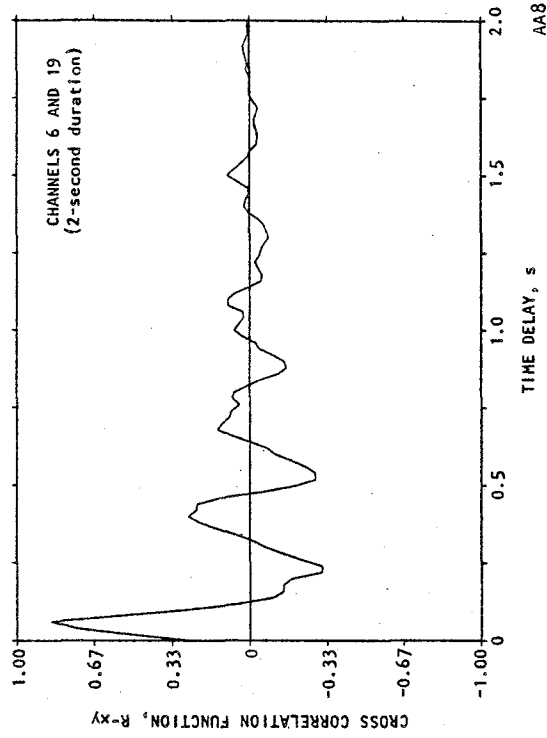
Time Lag, τ (sec)	Cross Correlation Function, R_{xy}			
	Record Pair No. 5 Channels 11 and 26 Full Duration	Record Pair No. 6 Channels 10 and 23 Full Duration	Record Pair No. 7 Channels 10 and 23 2 sec Duration	Record Pair No. 8 Channels 12 and 25 Full Duration
0.	.85079	.14553	-.10492	.75973
.02	.90502	.19640	.09239	.83496
.04	.94464	.39711	.35162	.88094
.06	.96472	.64154	.70323	.89717
.08	.95969	.54721	.69464	.88516
.10	.92928	.25073	.34073	.83975
.12	.87987	.10630	.17934	.76806
.14	.81862	.11040	-.00629	.67815
.16	.74923	.22005	-.23102	.57640
.18	.67281	.29379	-.25552	.47039
.20	.59092	.19840	-.25800	.36535
.22	.50589	.08803	-.16146	.26771
.24	.42158	.05384	-.04775	.18015
.26	.34274	.06369	.02830	.10005
.28	.27205	.11840	-.08721	.02633
.30	.20978	.18720	-.14409	-.04322
.32	.15614	.14109	-.07551	-.10614
.34	.11161	.00491	-.05636	-.16067
.36	.07630	-.08531	.04745	-.21184
.38	.05070	-.02497	.06269	-.26065
.40	.03503	.10751	.14224	-.30169
.42	.02801	.14527	.16865	-.33213
.44	.02739	.06739	.19100	-.35190
.46	.02998	-.04262	.23165	-.36047
.48	.03383	-.09145	.08562	-.35900
.50	.03809	-.05195	-.12753	-.34615
.52	.04179	.01191	-.21215	-.32104
.54	.04293	.01527	-.19347	-.28205
.56	.03982	-.06811	-.20269	-.23011
.58	.03271	-.16191	-.17949	-.17263
.60	.02359	-.17695	-.05609	-.11461
.62	.01368	-.11689	-.04395	-.05861
.64	.00278	-.03754	-.02567	-.00656
.66	-.01102	-.00481	.07353	.04209
.68	-.02764	-.07829	.13091	.08568
.70	-.04620	-.14348	.09581	.12094
.72	-.05671	-.10550	.01598	.14963
.74	-.08480	-.04777	-.00009	.17384
.76	-.10327	-.04139	.03788	.19519
.78	-.12153	-.06884	.07954	.21491
.80	-.13900	-.11004	.06871	.23174
.82	-.15541	-.12412	.03423	.24424
.84	-.17133	-.09271	-.00820	.25160



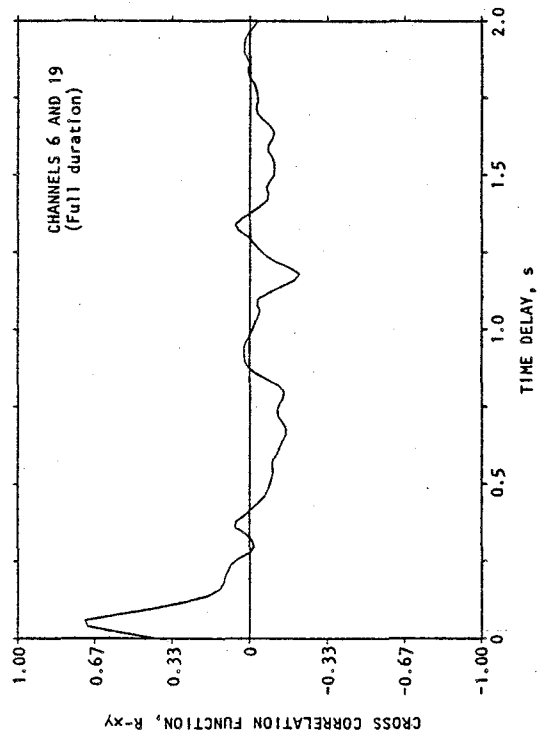
(a) Record Pair No. 1



(b) Record Pair No. 2

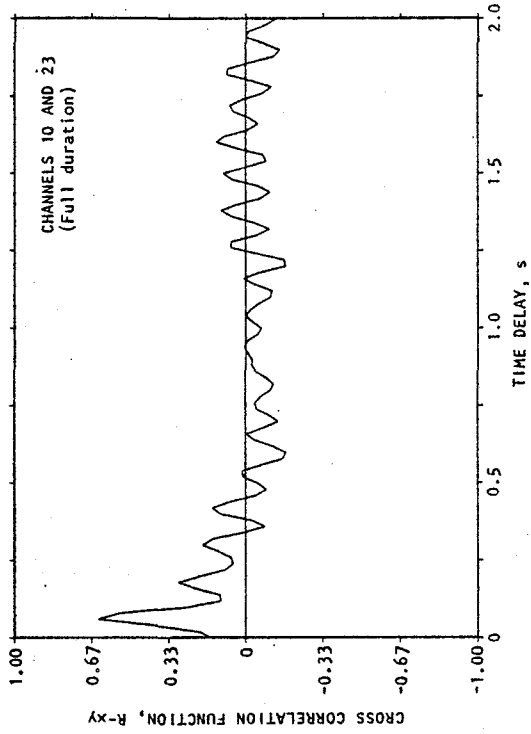


(c) Record Pair No. 3

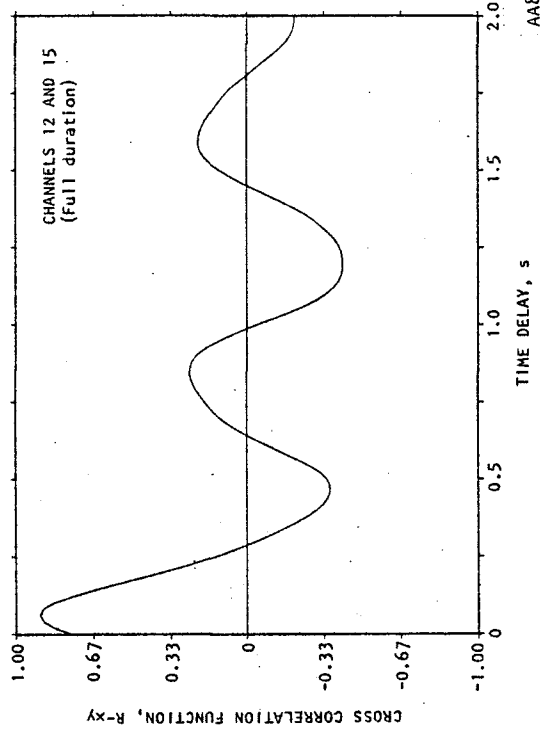


(d) Record Pair No. 4

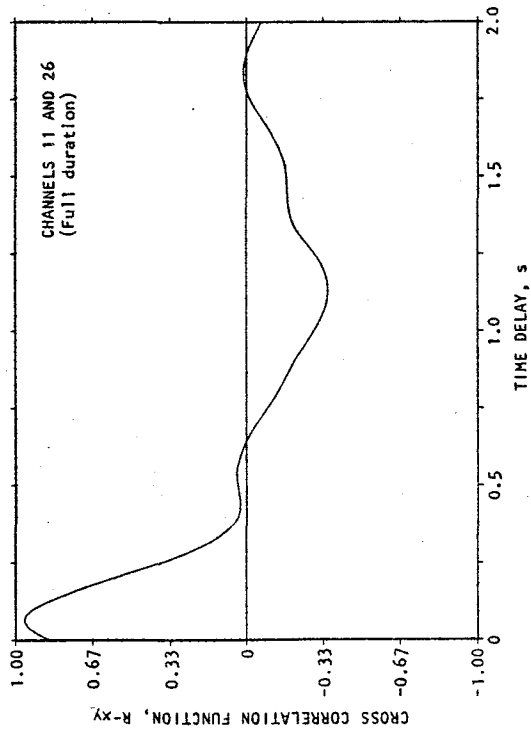
FIGURE 2-8. CROSS CORRELATION FUNCTIONS (BEFORE TIME SHIFT OF CHANNEL 1 TO 13 DATA)



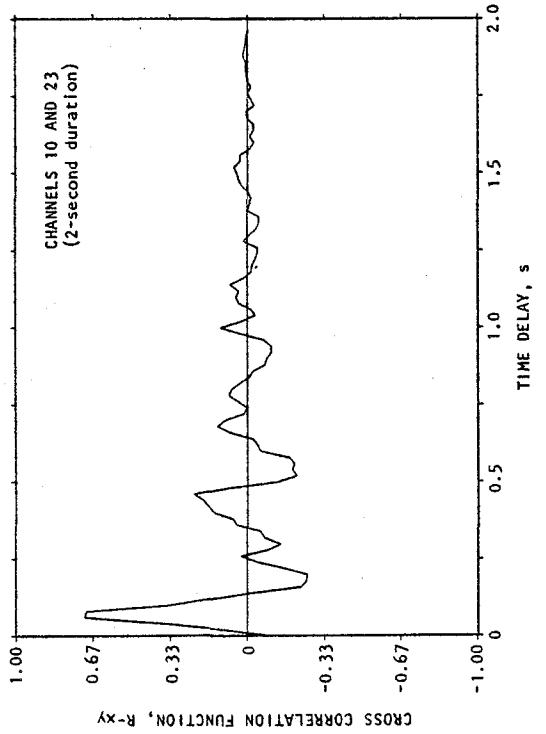
(f) Record Pair No. 6



(h) Record Pair No. 8



(e) Record Pair No. 5



(g) Record Pair No. 7

FIGURE 2-8. (CONCLUDED)



where ℓ is the distance between the instruments at the top and bottom of the central pier (~ 20 ft), $V_p (= \sqrt{E/\rho})$ is the P-wave propagation velocity, and E and ρ are the Young's modulus and mass density respectively of the reinforced concrete pier. Assuming a dynamic Young's modulus of about 4.5×10^6 psi and a weight density of 150 lb/ft^3 , $V_p = 11800$ fps and

$$t_s = \frac{17}{11800} = 0.0017 \text{ sec}$$

which is much smaller than the time lag of about 0.05 sec that results from the cross-correlation calculations. Therefore, traveling wave effects are seen to have an insignificant effect on this time lag, when compared to effects of recorder nonsynchronization.

2.3.3.2 Motions at Abutments and Embankments

The remaining record pairs shown in Table 2-2 correspond to motions measured at the abutments and embankments of the Meloland Road Overpass. Trends from these results are as follows:


- The accelerograms that comprise Record Pair No. 2 are both from Recorder A (for Channels 1 to 13), in which one accelerogram was measured at the north abutment and the other at the south abutment. Therefore, any phase time differences between these two accelerograms must be due to traveling wave effects and not to recorder nonsynchronization, since both accelerograms are from the same recorder. However, these accelerograms are seen to exhibit a vanishing phase time difference. This indicates that traveling wave effects are negligible for the Meloland Road Overpass; i.e., the apparent wavelengths of the predominant seismic waves that comprise the ground shaking at the Meloland Road Overpass (projected along the longitudinal axis of the bridge) are probably long when compared to the distances between the various abutment



and embankment accelerographs at this bridge structure.

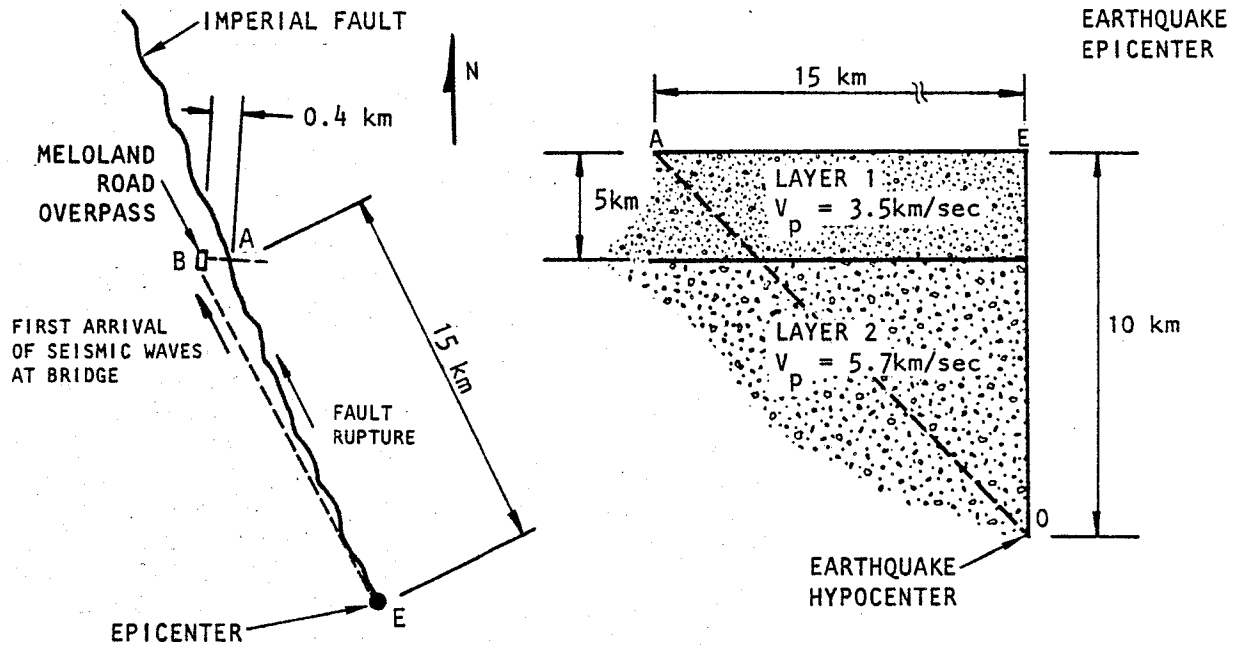
- Unlike Record Pair No. 2, Record Pairs 3 to 8 are each comprised of one accelerogram from Recorder A and the other from Recorder B. The instruments corresponding to these various record pairs are located on the abutments (for Record Pairs 3 and 4) and on the embankments (for Record Pairs 5 through 8), and these various comparisons involve both horizontal and vertical motions. If traveling wave effects were important at this bridge when compared to recorder nonsynchronization effects, certain systematic trends should appear in the comparisons of the phase time differences between (1) abutment motions vs. those of embankment motions; and (2) horizontal vs. vertical motions.* However, Table 2-1 shows that no such trends result from these cross-correlation calculations; i.e., for each of these record pairs, the phase time difference is about 0.060 sec.
- Comparison of cross-correlation results between Record Pairs 3 and 4 and between Record Pairs 6 and 7 are important for indicating whether the phase time differences were affected by any slight errors that may have occurred in the prior corrections for the periodic stalling of Recorder A (Sec. 2.2). As shown

*For example, if traveling wave effects were important, it should be expected that the phase time differences would be longer for the embankment motion correlations than for the correlations of abutment motions, since the propagation of waves between the embankment motion correlations involve somewhat longer propagation distances and slower wave propagation velocities. Also, it would appear that cross correlations of motions directed along the longitudinal axis of the bridge (for which P-waves should be most important) should yield smaller phase time differences than cross correlations of transverse or vertical motions (for which shear waves should play a greater role).



in Table 2-2, each of these sets of record pairs consider the same two accelerograms but with different durations; i.e., the full duration of motion is considered in Record Pairs 3 and 6 while, for Record Pairs 4 and 7, only the first 2 sec of shaking have been considered (which is before any recorder stalls took place). However, the phase time differences computed for each of these record pairs are nearly identical (about 0.060 sec) indicating that the recorder stall corrections had minor if any effects on these cross-correlation results.

- In Record Pairs 5 through 8, the instruments connected to Recorder A are on the *south* embankment, whereas those connected to Recorder B are located on the *north* embankment. This is in contrast to Record Pairs 3 and 4, in which the Recorder A instruments are located on the *north* abutment whereas those from Recorder B are on the *south* abutment. Despite this opposite orientation of the Recorder A and Recorder B instruments, the motions from Recorder A consistently lead those from Recorder B by about 0.060 sec. Although this further indicates that traveling wave effects are small when compared to recorder nonsynchronization effects, additional assessment of the effects of wave propagation on this trend is provided in Figure 2-9. In this, it might be expected from the Imperial Valley Earthquake's hypocentral location (southeast of the bridge) that the seismic waves propagating to the bridge from this hypocentral region should cause motions recorded on the south embankment and abutment to lead the motions recorded on the north embankment and abutment. However, as shown in Figure 2-9, the fault rupture propagates northward from the hypocenter to a location along the Imperial fault north of the



a) Plan View

b) Cross Section along Imperial Fault Plane

Definitions

- t_w = Minimum time for seismic P-waves to begin to arrive at bridge from the north (relative to time at which motion was first triggered at bridge)
- $t_{r,OA}$ = Time for fault rupture to propagate from hypocenter to point A (point along fault immediately east of bridge)
- t_{AB} = Time for seismic P-waves to propagate from point A to bridge
- t_{OB} = Time after initiation of fault rupture at which motion was first triggered at bridge (= time of first arrival of P-waves propagating from hypocenter)

Imperial Valley Earthquake data


- V_r = Fault rupture velocity = 2.0 - 2.5 km/sec
- OE = Hypocentral depth = 10 km (see above sketch)
- V_p = Average P-wave velocity of geologic layers (see above sketch)

Estimation of t_w (using fault geometry given in above sketches and average value of P-wave velocity, $V_{pa} = 5.0$ km/sec)

$$\begin{aligned}
 t_w &= t_{r,OA} + t_{AB} - t_{OB} \\
 &= \frac{OA}{V_r} + \frac{AB}{V_{pa}} - \frac{OB}{V_{pa}} \\
 &= \frac{18.0 \text{ km}}{2.5 \text{ km/sec}} + \frac{0.4 \text{ km}}{5.0 \text{ km/sec}} - \frac{18.0 \text{ km}}{5.0 \text{ km/sec}} = 3.7 \text{ sec}
 \end{aligned}$$

AA814

FIGURE 2-9. FIRST ARRIVAL TIME FOR SEISMIC WAVES PROPAGATING FROM NORTH OF THE MELOLAND ROAD OVERPASS (Based on data from Hartzell and Helmsberger, 1982)



bridge; therefore, it is conceivable the waves propagating southward to the bridge from this northerly ruptured fault segment might have contributed to the trends of Record Pairs 3 and 4, in which motions from the north abutment lead those from the south abutment. To assess this possibility, the simple wave propagation analysis provided in Figure 2-9 estimates the first arrival of waves propagating to the bridge from the east or north that could cause this trend. Results of this analysis show that the time of first arrival of such waves is well beyond the 2 sec duration of the motions considered in Record Pair 4, in which the Recorder A motions from the north abutment lead those from the south abutment by 0.060 sec. From this, it can be concluded that this time lead cannot be caused by wave propagation, and instead must be due to recorder nonsynchronization.

2.3.3.3 Corrections for Recorder Nonsynchronization

The results described in Sections 2.3.3.1 and 2.3.3.2 show that, for all of the cross correlations of pairs of records involving one accelerogram from Recorder A and one from Recorder B, the motions from Recorder A led those from Recorder B by about 0.060 sec. This consistent trend was shown to be independent of (1) the distance between the acceleration measurement locations; (2) whether the pairs of instruments were located on the soil embankments, the abutments, or the central pier of the bridge; (3) whether the measurements were for vertical, transverse, or longitudinal motion; (4) whether the instrument connected to Recorder A was located to the north or to the south of the instrument connected to Recorder B; or (5) whether only the first 2 sec of the records (before any stalls occurred in Recorder A) or the entire duration of the records was considered. Furthermore, cross correlations between



accelerograms that were both from the same recorder did not show any phase time shift; i.e., it was only when one accelerogram was from Recorder A and the other was from Recorder B that the above-indicated phase time shift of about 0.060 sec was obtained.

From all of this evidence, it is readily apparent that the above phase time shift is due primarily to recorder nonsynchronization, and the relative contributions to this time shift of traveling wave effects or any inaccuracies in the prior recorder stall corrections are small. Therefore, to correct the Meloland Road Overpass data for this nonsynchronization effect, the time coordinates of the accelerograms from Recorder A (i.e., for Channels 1 to 13) were retarded by 0.060 sec, with an appropriate number of zero acceleration ordinates inserted over the 0 to 0.060 sec time span for these accelerograms. Table 2-4 and Figure 2-10 provides cross-correlation results involving these time shifted records, showing that the prior recorder nonsynchronization effects have now been largely eliminated.

2.4 AVAILABILITY AND USE OF REPROCESSED DATA

To assist interested parties who may wish to use these reprocessed data, Appendix A provides plots of motion time histories, Fourier spectra, and response spectra for the reprocessed strong motion data from all 26 instruments at the Meloland Road Overpass. The appendix also describes how to directly obtain these data.



TABLE 2-4. PARTIAL TABULATION OF CROSS CORRELATION RESULTS
(AFTER TIME SHIFT OF CHANNEL 1 TO 13 DATA)

Time Lag, τ (sec)	Cross Correlation Function, R_{xy}			
	Record Pair No. 1 Channels 1 and CL1* Full Duration	Record Pair No. 2 Channels 3 and 13 Full Duration	Record Pair No. 3 Channels 6 and 19 Full Duration	Record Pair No. 4 Channels 6 and 19 2 sec Duration
0.	.88361	No time shift needed	.70810	.85523
.02	.58805		.56311	.56652
.04	.38061		.40920	.28328
.06	.32510		.27696	.04847
.08	.30570		.17760	-.09981
.10	.29182		.12766	-.14321
.12	.22376		.11099	-.14299
.14	.13365		.10558	-.18033
.16	.10999		.09169	-.30946
.18	.14945		.07973	-.31022
.20	.19125		.04742	-.22208
.22	.21902		-.00238	-.14040
.24	.23670		-.01993	-.06869
.26	.21763		-.01056	-.01813
.28	.16645		.02006	.05787
.30	.11486		.06152	.13794
.32	.07000		.05978	.21662
.34	.01623		.02299	.26356
.36	-.05541		-.00800	.22951
.38	-.12043		-.03701	.22577
.40	-.15001		-.06381	.12307
.42	-.15184		-.07839	-.06121
.44	-.16391		-.08840	-.19623
.46	-.18827		-.09577	-.28090
.48	-.19633		-.10258	-.27838
.50	-.18891		-.09746	-.23560
.52	-.19070		-.10187	-.17367
.54	-.20900		-.12126	-.10594
.56	-.20019		-.13204	-.07176
.58	-.18201		-.14317	.00082
.60	-.17983		-.15779	.07976
.62	-.17864		-.15936	.13913
.64	-.16601		-.14394	.12085
.66	-.13315		-.12518	.08667
.68	-.11172		-.12142	.07932
.70	-.11791		-.13071	.04397
.72	-.15744		-.14628	.07362
.74	-.20129		-.15017	.06268
.76	-.21561		-.12625	.01162
.78	-.20312		-.07694	-.04295
.80	-.16914		-.02453	-.12266
.82	-.13201		.00995	-.15880
.84	-.10394		.02264	-.15046

*Note: CL1 = Average vertical translation from channels 17 and 21

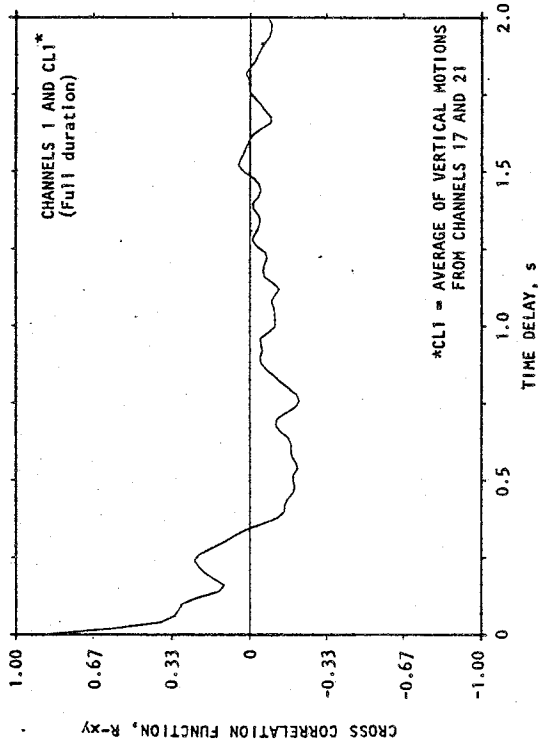


TABLE 2-4. (CONCLUDED)

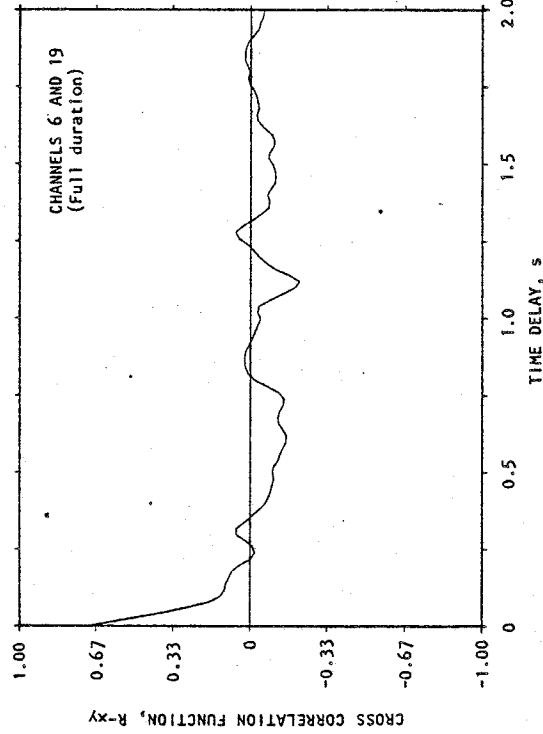
Time Lag, τ (sec)	Cross Correlation Function, R_{xy}			
	Record Pair No. 5 Channels 11 and 26 Full Duration	Record Pair No. 6 Channels 10 and 23 Full Duration	Record Pair No. 7 Channels 10 and 23 Full Duration	Record Pair No. 8 Channels 12 and 25 2 sec Duration
0.	.96219	.63985	.70363	.89490
.02	.95717	.54577	.69500	.88291
.04	.92683	.25007	.34126	.83763
.06	.87756	.10602	.18030	.76611
.08	.81646	.11011	-.00558	.67644
.10	.74725	.21947	-.23009	.57494
.12	.67103	.29301	-.25486	.46920
.14	.58936	.19788	-.25707	.36442
.16	.50456	.08780	-.16070	.26703
.18	.42046	.05370	-.04738	.17970
.20	.34183	.06352	.02853	.09801
.22	.27133	.11809	-.08683	.02627
.24	.20922	.18670	-.14299	-.04311
.26	.15572	.14071	-.07501	-.10587
.28	.11132	.00490	-.05670	-.16026
.30	.07619	-.08508	.04681	-.21130
.32	.05056	-.02490	.06232	-.25999
.34	.03494	.10723	.14215	-.30093
.36	.02794	.14488	.16812	-.33129
.38	.02732	.06721	.19062	-.35101
.40	.02990	-.04251	.23139	-.35957
.42	.03374	-.09121	.08575	-.35809
.44	.03798	-.05181	-.12759	-.34528
.46	.04168	.01188	-.21236	-.32022
.48	.04282	.01523	-.19310	-.28134
.50	.03971	-.06792	-.20064	-.22953
.52	.03262	-.16147	-.17628	-.17220
.54	.02352	-.17647	-.05314	-.11432
.56	.01365	-.11658	-.04244	-.05846
.58	.00277	-.03744	-.02502	-.00654
.60	-.01099	-.00479	.07437	.04198
.62	-.02757	-.07808	.13219	.08546
.64	-.04607	-.14309	.09738	.12064
.66	-.06531	-.10521	.01703	.14925
.68	-.08457	-.04764	.00114	.17340
.70	-.10299	-.04127	.03963	.19469
.72	-.12120	-.06865	.08086	.21437
.74	-.13863	-.10974	.06904	.23115
.76	-.15499	-.12378	.03324	.24362
.78	-.17086	-.09246	-.00872	.25096
.80	-.18580	-.04573	-.02417	.25076
.82	-.20028	-.02746	-.07448	.24153
.84	-.21569	-.02829	-.85186	.21974



NOTE:
NO RELATIVE TIME SHIFT WAS REQUIRED
FOR THE TWO ACCELOGRAMS IN RECORD
PAIR NO. 2, SINCE THEY WERE BOTH
OBTAINED FROM THE SAME RECORDER.
(See Fig. 2-8b)

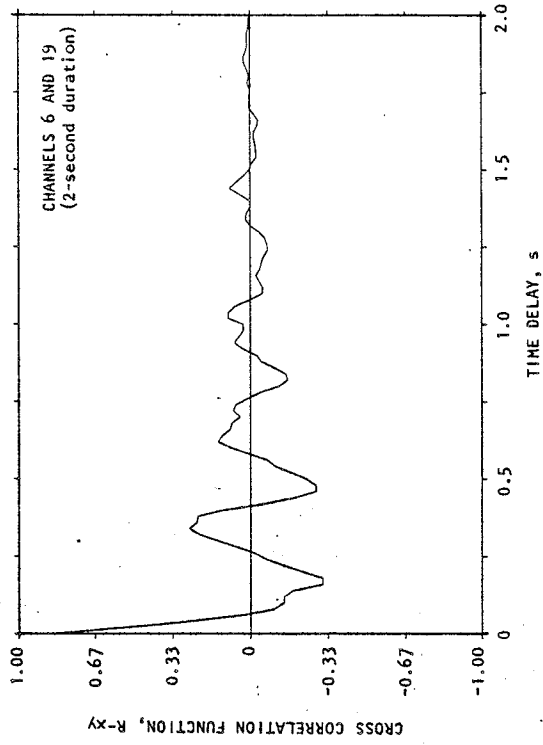


a) Record Pair No. 1



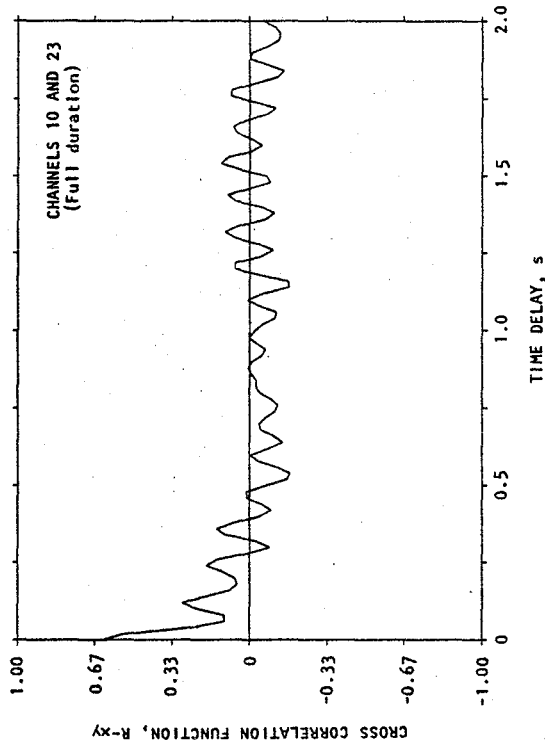
c) Record Pair No. 3

b) Record Pair No. 2

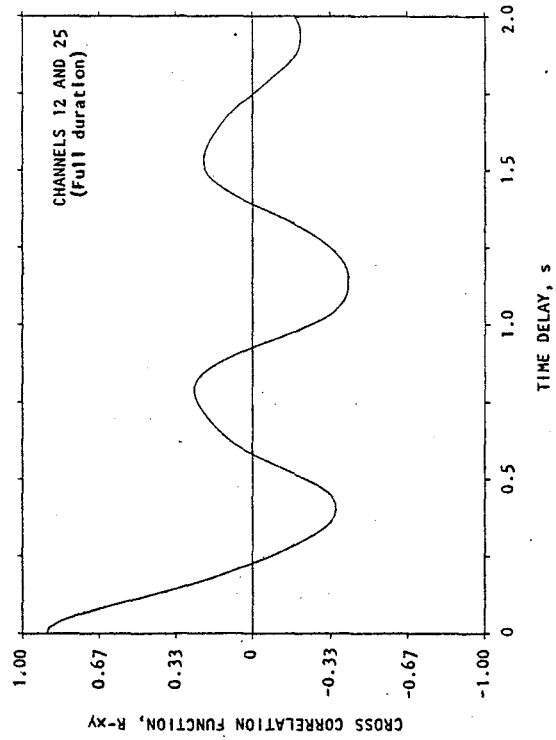


d) Record Pair No. 4

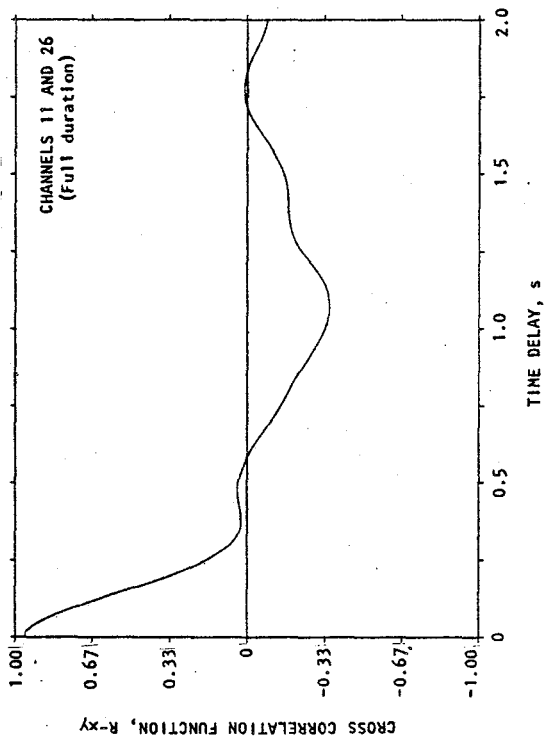
FIGURE 2-10. CROSS CORRELATION FUNCTIONS (AFTER TIME SHIFT OF CHANNEL 1 TO 13 DATA)



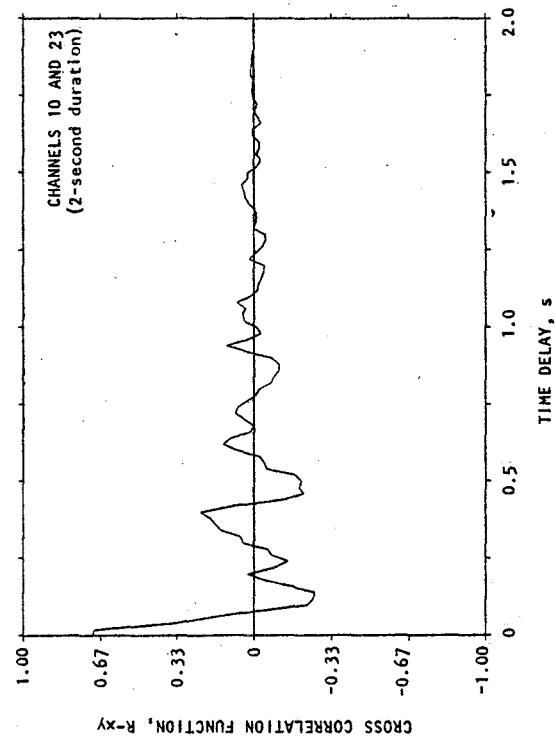
f) Record Pair No. 6



h) Record Pair No. 8



e) Record Pair No. 5



g) Record Pair No. 7

FIGURE 2-10. (CONCLUDED)



CHAPTER 3

MODAL IDENTIFICATION METHODOLOGY

An important objective of this project has involved the identification of pseudostatic and normal mode parameters of a linear model that characterizes the measured response of the Meloland Road Overpass during the 1979 Imperial Valley earthquake. To fulfill this objective, a new methodology has been derived and programmed under this study. This methodology, named MODE-ID, is applicable to any elastic structure with any arbitrary configuration, classical normal modes, any number of input and structural response measurements, and an initial at-rest position. It is an extension of a procedure originally developed by Beck (1978), for the case of a structure with a single base motion and response measurement.

The remainder of this chapter provides a comprehensive description of the MODE-ID methodology. It contains the formulation of the basic model treated by MODE-ID, a description of the numerical procedures used to implement MODE-ID, and an illustrative example in which MODE-ID is applied to a bridge-like structure.

3.1 FORMULATION OF THE MODEL

3.1.1 BASIC EQUATIONS OF MOTION

Consider an elastic structure/foundation system with classical normal modes that is initially at an at-rest position. Neglecting inertial coupling effects, the equations of motion for this system can be written in partitioned matrix form as follows

$$\begin{bmatrix} M_{11} & 0 \\ 0 & M_{22} \end{bmatrix} \begin{Bmatrix} \ddot{y} \\ \ddot{z} \end{Bmatrix} + \begin{bmatrix} C_{11} & C_{12} \\ C_{12}^T & C_{22} \end{bmatrix} \begin{Bmatrix} \dot{y} \\ \dot{z} \end{Bmatrix} + \begin{bmatrix} K_{11} & K_{12} \\ K_{12}^T & K_{22} \end{bmatrix} \begin{Bmatrix} y \\ z \end{Bmatrix} = \begin{Bmatrix} 0 \\ f \end{Bmatrix} \quad (3-1)$$



where the subscripts "1" and "2" denote the structure and foundation respectively, a dot denotes differentiation with respect to time, and

$[M], [C], [K]$ = Mass, damping, and stiffness matrices respectively

$\{f\}$ = Soil/foundation interaction force vector

$\{y\}, \{z\}$ = Structure and foundation response vectors respectively

It is noted from Equation 3-1 that the structure response is represented by the upper set of partitioned equations; therefore, in this formulation only this upper set requires consideration. These equations are

$$[M_{11}]\{\ddot{y}\} + [C_{11}]\{\dot{y}\} + [K_{11}]\{y\} = - [C_{12}]\{\dot{z}\} - [K_{12}]\{z\} \quad (3-2)$$

In Equation 3-2, $\{\ddot{y}\}$ can be expressed as

$$\{\ddot{y}\} = \{\ddot{s}\} + \{\ddot{x}\} \quad (3-3)$$

where, as described by Clough and Penzien (1975), $\{\ddot{s}\}$ is the "pseudostatic component" of the structure response (which represents the "static" effects of the multiple support movements on the response of the structure) and $\{\ddot{x}\}$ is the "dynamic component" (which represents the fixed base dynamic response of the structure, or the structure response relative to the zero-position of each support degree-of-freedom $\{z\}$). In this, it can be shown that

$$\{\ddot{s}\} = [R]\{\ddot{z}\} \quad (3-4)$$

where $[R]$, the pseudostatic influence matrix, is computed as

$$[R] = - [K_{11}]^{-1} [K_{12}] \quad (3-5)$$

Substituting Equations 3-3 and 3-4 into 3-2, the equations of motion take the form

$$\begin{aligned}
[M_{11}]\{\ddot{x}\} + [C_{11}]\{\dot{x}\} + [K_{11}]\{x\} = \\
- [M_{11}][R]\{\ddot{z}\} - ([C_{11}][R] + [C_{12}])\{\dot{z}\} \\
- ([K_{11}][R] + [K_{12}])\{z\}
\end{aligned} \tag{3-6}$$

Upon noting from Equation 3-5 that

$$[K_{11}][R] = - [K_{12}]$$

and neglecting the contributions of the damping terms to the effective earthquake forces (as suggested by Clough and Penzien, 1975), Equation 3-6 takes the form

$$[M_{11}]\{\ddot{x}\} + [C_{11}]\{\dot{x}\} + [K_{11}]\{x\} = - [M_{11}][R]\{\ddot{z}\} \tag{3-7}$$

3.1.2 MODAL EQUATIONS OF MOTION

It now remains to expand Equation 3-7 in terms of the fixed-base normal modes of the structure. To do this, we first express $\{x\}$ as

$$\{x\} = [\Phi]\{\eta\} \tag{3-8}$$

where $\{\eta\}$ is the vector of modal response amplitudes, and $[\Phi]$ is the modal matrix of the structure, normalized to satisfy the following orthogonality relationships

$$\begin{aligned}
[\Phi]^T [M_{11}] [\Phi] &= [I]_D \\
[\Phi]^T [C_{11}] [\Phi] &= [2\omega_r \zeta_r]_D \\
[\Phi]^T [K_{11}] [\Phi] &= [\omega_r^2]_D
\end{aligned} \tag{3-9}$$

In Equation 3-9, $[]_D$ depicts a diagonal matrix, $[I]_D$ is the unit diagonal matrix, and ζ_r and ω_r are the damping ratio and natural frequency respectively of the r th mode. The damping matrix is assumed to be diagonalized by the modal matrix so that classical normal modes exist.

The next step in the development of the modal equations of motion is to substitute Equation 3-8 into 3-7, and to premultiply the resulting set of matrix equations by $[\Phi]^T$. Then, after



satisfying the above modal orthogonality relationships (Eq. 3-9), the modal equations of motion become

$$[I]_D \{\ddot{\eta}\} + [2\omega_r \xi_r]_D \{\dot{\eta}\} + [\omega_r^2] \{\eta\} = - [\Gamma] \{\ddot{z}\} \quad (3-10)$$

where $[\Gamma]$ is the matrix of modal participation factors, defined as

$$[\Gamma] = [\phi]^T [M_{11}] [R] \quad (3-11)$$

3.1.3 IDENTIFIABLE MODEL

In order for a spatially discretized model of the form of Equation 3-1 to be realistic, a large number of degrees of freedom is required which typically exceeds the number of degrees of freedom at which the response of the structure is measured. For this reason, care must be taken to ensure that an identifiable model is used, that is, to ensure that the unknown parameters of the model can be determined uniquely from the response measured at a limited number of degrees of freedom (Beck, 1978). The approach used in this study is to identify certain modal parameters that fully describe the measured earthquake response. These identified parameters may then be used in a separate study of structural properties such as the effective moments of inertia of structural members or the fixity conditions at the structure/foundation interface.

An identifiable model based on the modal equations of motion is developed in this section. In this, we let

y_i ($i = 1, \dots, NR$) be the model displacement at each of the NR degrees of freedom at which the response is measured

z_j ($j = 1, \dots, NS$) be the displacement at each of the NS degrees of freedom at which the support motion is measured

s_i, x_i be the pseudostatic and dynamic components of the model displacement y_i

Suppose that NM modes contribute significantly to the response. Then from Equations 3-3, 3-4, and 3-8:

$$y_i(t) = s_i(t) + x_i(t) \quad (i = 1, \dots, NR) \quad (3-12)$$

where

$$s_i(t) = \sum_{j=1}^{NS} r_{ij} z_j(t) \quad (3-13)$$

$$x_i(t) = \sum_{r=1}^{NM} \phi_{ir} \eta_r(t)$$

and r_{ij} and ϕ_{ir} are the elements of the pseudostatic influence matrix $[R]$ and the modal matrix $[\Phi]$ respectively.

It is convenient to let x_{ir} ($= \phi_{ir}\eta_r$) denote the contribution of the r th mode to the dynamic component of the response at the i th degree of freedom. Then from the second of Equations 3-13:

$$x_i(t) = \sum_{r=1}^{NM} x_{ir}(t) \quad (3-14)$$

Equation 3-10 can be rewritten in terms of the x_{ir} as

$$\{\ddot{x}_{ir}\} + 2\zeta_r \omega_r \{\dot{x}_{ir}\} + \omega_r^2 \{x_{ir}\} = - [P^{(r)}] \{\ddot{z}\} \quad (3-15)$$

where $[P^{(r)}]$ is the effective participation factor matrix for the r th mode, defined as

$$[P^{(r)}] = \begin{bmatrix} \phi_{1r}^y r_1 & \phi_{1r}^y r_2 & \dots & \phi_{1r}^y r_{NS} \\ \phi_{2r}^y r_1 & \phi_{2r}^y r_2 & \dots & \phi_{2r}^y r_{NS} \\ \vdots & \vdots & & \vdots \\ \phi_{NR,r}^y r_1 & \phi_{NR,r}^y r_2 & \dots & \phi_{NR,r}^y r_{NS} \end{bmatrix} \quad (3-16)$$

In Equation 3-16, the element in the i th row and j th column of $[P^{(r)}]$, denoted as $p_{ij}^{(r)}$, is the effective participation factor at the i th response degree of freedom for the r th mode and the j th support degree of freedom; i.e.,



$$p_{ij}^{(r)} = \phi_{ir} \gamma_{rj} \quad (3-17)$$

where γ_{rj} is the conventional participation factor corresponding to the r th mode and the j th support degree of freedom (Eq. 3-11).

Equations 3-12 through 3-15 express the model used in the system identification. The parameters to be identified from the measured response and support motions are therefore the pseudo-static influence matrix:

$$\underline{\tilde{R}} = [R] = [r_{ij}] \quad (i = 1, \dots, NR; j = 1, \dots, NS) \quad (3-18)$$

and the modal parameters for each $r = 1, \dots, NM$:

$$\begin{aligned} \omega_r, & \text{ natural frequency} \\ \zeta_r, & \text{ damping ratio} \end{aligned} \quad (3-19)$$

$$\begin{aligned} \underline{\tilde{P}}^{(r)} &= [P^{(r)}] = [p_{ij}^{(r)}] \quad (i = 1, \dots, NR; j = 1, \dots, NS), \\ &= \text{matrix of effective participation factors} \end{aligned}$$

where to simplify the notation in Equations 3-18 and 3-19 and in the mathematical presentation in Section 3.2, the symbol \sim is adopted as an alternative representation of a matrix; e.g., $\underline{\tilde{R}} \equiv [R]$. Furthermore, it is assumed in this development that the initial conditions for the modal contributions calculated from Equation 3-15 correspond to the structure being initially at rest. If this were not the case, it would be necessary to identify additional parameters defining the nonzero initial conditions, along with the pseudostatic and modal response parameters indicated above.

The quantities $p_{ij}^{(r)}$ are treated as independent in this identification process. This is not strictly correct in general because, as shown in Equation 3-17, the $NR \times NS \times NM$ different $p_{ij}^{(r)}$ quantities can be derived from $(NR + NS) \times NM$ parameters γ_{rj} and ϕ_{ir} , which is a smaller number if $NR \geq 2$ and $NS \geq 2$. In addition, Equation 3-11 shows that each γ_{rj} in Equation 3-17 is

also dependent on the *complete* mode shape (that is, ϕ_{ir} for $i = 1, \dots, N$ where typically $N \gg NR$ for a realistic model), as well as the mass matrix (which could perhaps be estimated from structural plans) and the *complete* pseudostatic influence matrix. To further complicate matters, the complete mode shapes are subject to the nonlinear normalization constraint in the first of Equations 3-9.

Based on experience with the rigid-base case (Beck, 1978), it is not expected that the complete mode shape for any realistic model could be identified uniquely from the limited measurements usually available. Even if this were possible, the aforementioned nonlinear relationships involving the ϕ_{ir} and r_{ij} parameters would greatly complicate the parameter estimation process. Therefore, the approach taken in this study is to treat the $p_{ij}^{(r)}$ as independent and use their estimated values and Equation 3-17 to calculate the mode shape components at the degrees of freedom at which the response was measured.

In theory, by choosing any support degree of freedom j , the nonnormalized mode shape for mode r at the "measured" degree of freedom i is given directly by $p_{ij}^{(r)}$, since γ_{rj} in Equation 3-17 is a constant independent of i . However, under certain conditions, an ill-conditioning will occur which causes the estimates of each $p_{ij}^{(r)}$ to be unreliable but which does not affect the following sum to the same degree

$$\sum_{j=1}^{NS} p_{ij}^{(r)} = \phi_{ir} \sum_{j=1}^{NS} \gamma_{rj} \quad (3-20a)$$

This ill-conditioning arises when there is some degree of model error and/or noise in the data (as would occur in measured earthquake motions but not in motions computed from an analytical model), and when several of the support degrees of freedom have nearly identical motions. Equations 3-15 and 3-16 show that, if the support motions were actually identical (i.e., the "rigid base" situation), then the dynamic components of response



x_{ir} would be controlled by the above sum rather than by the individual values of $p_{ij}^{(r)}$. When the support motions are nearly but not exactly identical, and when we are dealing with measured (rather than analytical) data that contains some noise and/or model error, the sum should still be estimated reliably but the individual $p_{ij}^{(r)}$ will not; i.e., the individual $p_{ij}^{(r)}$ will be much more sensitive to model error or to noise in the data than will the sum. Therefore, under such conditions, the summed quantity $\sum_j p_{ij}^{(r)}$ should be used to obtain the mode shape for the r th mode ($r = 1, 2, \dots, NM$). This is carried out in MODE-ID by using the modal identification procedure (Sec. 3.2) to obtain $\sum_j p_{ij}^{(r)}$ at each structure response measurement location ($i = 1, 2, \dots, NR$). As shown in Chapter 4, this summation procedure produces reasonable mode shapes when applied to the actual earthquake records from the Meloland Road Overpass.

It is noted that the same ill-conditioning phenomenon is present in the estimation of the elements of the pseudostatic matrix from measured data that contains some degree of noise and/or model error. This ill-conditioning causes the individual elements of the pseudostatic matrix to be sensitive to model error or to noise in the data when the support motions are nearly but not exactly identical, but does not affect the following sum

$$\sum_{j=1}^{NS} r_{ij} = 1 \quad (i = 1, 2, \dots, NR) \quad (3-20b)$$

The above summation, which includes the elements of the i th row of the pseudostatic matrix, corresponds to the total displacement of the i th response degree of freedom due to simultaneously applying a unit static displacement to each support degree of freedom; i.e., this i th response component must attain a unit value. For nearly but not exactly identical support motions that contain some noise and/or model error, it is the above summation rather than the contributions of the individual elements that primarily governs the pseudostatic response.

As a final point, it is noted that the verification analysis described subsequently in Section 3.3, does not involve model error and was based on analytical (noise-free) response data rather than experimental data. This analysis is seen to produce excellent estimates of the individual effective participation factors and elements of the pseudostatic matrix, even though nearly identical support motions were applied to the bridge model considered in the analysis. Therefore, the necessity for considering the above sums of the effective participation factors and pseudostatic matrix elements when working with measured data arises from the combined effects of model error, data noise, and nearly identical support motions, rather than from nearly identical support motions alone.

3.2 IDENTIFICATION OF MODEL PARAMETERS

3.2.1 OVERVIEW

To identify the values of the modal and pseudostatic parameters described in the previous section, an optimization procedure is applied in MODE-ID to produce the "best" estimates from the measured seismic excitation and response. In this procedure, the following cost function, or measure of fit, is minimized with respect to the model parameters (denoted collectively by θ):

$$J(\theta) = \frac{1}{V} \sum_{i=1}^{NR} \sum_{n=0}^{NT} [a_i(n\Delta t) - \ddot{y}_i(n\Delta t; \theta)]^2 \quad (3-21)$$

where

a_i, \ddot{y}_i = Measured and model accelerations at degree of freedom i

$\theta = \{ \tilde{R}; \omega_r, \zeta_r, \underline{p}^{(r)}; r = 1, \dots, NM \}$

$\tilde{R} = [r_{ij}]$ ($i = 1, \dots, NR; j = 1, \dots, NS$), the pseudostatic response parameters



- ω_r = Natural frequency of mode r
 ζ_r = Damping ratio of mode r
 $\tilde{p}^{(r)}$ = $\left[p_{ij}^{(r)} \right]$ ($i = 1, \dots, NR; j = 1, \dots, NS$), the effective participation factor matrix of mode r
 Δt = Time step produced by the sample rate for the recorded seismic motions
 n = Time step number ranging from 0 to NT , corresponding to a time interval from 0 to $NT \times \Delta t$


and V is a normalizing constant chosen as:

$$V = \sum_{i=1}^{NR} \sum_{n=0}^{NT} a_i^2 (n\Delta t) \quad (3-22)$$

Therefore, J may be interpreted as the ratio of the mean-square error to the mean square of the measured response.

Any response quantity may be chosen in J . The acceleration is used in this study since it has the richest high frequency content and therefore allows more reliable estimation of the parameters of the high frequency modes.

By minimizing J , we are selecting those values of the model parameters that produce a least-squares match between the model and measured responses. This is different from ordinary least-squares schemes that identify the parameters by minimizing the sum of the squares of the residuals, which are the errors produced when the measured motions are substituted into the equations of motion. This latter scheme is sometimes called a least-squares equation-error approach to distinguish it from the technique used in this study, which may be referred to as a least-squares output-error approach. The advantage of using an output-error method is that it deals directly with the problem of major interest by showing how well the model can perform when the only freedom allowed is the variation of the values of the unknown parameters. In the least-squares equation-error approach, additional freedom is introduced by allowing the equations of motion to be satisfied in only an approximate sense. The penalty paid for the output-error formulation is that the



identification process becomes a nonlinear optimization problem even though the model equations are linear, since the model response is a nonlinear function of some of the parameters (the natural frequencies and damping ratios).

The minimization of J with respect to the model parameters may be implemented using any satisfactory optimization algorithm. The approach chosen here is an adaptation of the modal-sweep method developed by Beck (1978). This approach exploits the linearity of Equations 3-12 through 3-15 to obtain an iterative algorithm that is numerically efficient and has reliable convergence properties.

The modal-sweep algorithm is described in detail in the next section, but it is briefly summarized here. Basically, during each modal sweep, the estimates of the pseudostatic parameters are first updated by minimizing J with respect to these parameters only, and then the estimates of the parameters of each mode are successively updated by a series of single-mode minimizations of J . This minimization for each mode actually corresponds to least-squares matching of a modified measured response in which the contributions of the pseudostatic response and the other modes are subtracted out; these contributions are computed from the new parameter estimates for those modes already treated in the sweep, and from the prior parameter estimates for those modes not yet treated. A single sweep is completed when the pseudostatic response and all significant modes have been treated in this manner. Successive modal sweeps are performed until the fractional decrease in J is less than a prescribed amount, or until a prescribed maximum number of modal sweeps has been completed.

Usually only the first one or two of the strongest excited modes selected from the Fourier amplitude spectra of the records are initially included in the optimization process. Additional modes are then added, one at a time, by choosing appropriate initial estimates for the period and damping ratio. Successive



optimizations are performed until it is judged that all modes that significantly affect the response have been included. The modes are added successively in this manner so that it is easier to observe whether or not a mode has a significant effect on the match of the measured response.

3.2.2 MODAL SWEEP PROCEDURE

The modal sweep procedure is demonstrated by considering the case where the m th modal sweep has been completed, resulting in the parameter estimates $\{\theta\}_m = \{\underline{R}; \omega_r, \zeta_r, \underline{p}^{(r)}; r = 1, \dots, NM\}_m$. It is desired to proceed with the $(m + 1)$ th modal sweep which involves successive single-mode minimizations of J , first with respect to the pseudostatic parameters \underline{R} , and then with respect to the parameters for each mode, ω_r , ζ_r , and $\underline{p}^{(r)}$. In this process, the same approach is used for the estimation of the pseudostatic parameters as used for the effective participation factors of a mode. Indeed, the pseudostatic response can be visualized as a mode with a vanishing natural frequency, as can be seen by comparing the first of Equations 3-13 with Equation 3-15 for the case $\omega_r = 0$.

3.2.2.1 Pseudostatic Response Estimates

The first step in each modal sweep is to reestimate the pseudostatic response parameters.

Equations 3-12 through 3-16 show that the estimated acceleration at degree of freedom i after the m th modal sweep has been completed is:

$$\dot{y}_i(t; \{\theta\}_m) = \ddot{s}_i(t; \{\underline{R}\}_m) + \sum_{r=1}^{NM} \ddot{x}_{ir}(t; \{\omega_r, \zeta_r, \underline{p}^{(r)}\}_m) \quad (3-23)$$

The pseudostatic parameters \underline{R} are updated by minimizing:

$$J(\underline{R}) = \frac{1}{V} \sum_{i=1}^{NR} \sum_{n=0}^{NT} \left[a_i(n\Delta t) - \ddot{s}_i(n\Delta t; \underline{R}) - \sum_{r=1}^{NM} \ddot{x}_{ir}(n\Delta t; \{\omega_r, \zeta_r, \underline{p}^{(r)}\}_m) \right]^2 \quad (3-24)$$

In this equation, the quantity

$$a_i(n\Delta t) - \sum_{r=1}^{NM} \ddot{x}_{ir} \left(n\Delta t; \left\{ \omega_r, \zeta_r, \underline{P}^{(r)} \right\}_m \right)$$

to be matched by the pseudostatic response of the model represents a modified measured response in which the latest estimates of the modal contributions have been removed.

It is noted from the first of Equations 3-13 that the pseudostatic response \ddot{s}_i is a linear function of the elements of the matrix \underline{R} :

$$\ddot{s}_i(n\Delta t; \underline{R}) = \sum_{j=1}^{NS} r_{ij} \ddot{z}_j(n\Delta t) \quad (3-25)$$

For this reason, the condition for minimization of J ,

$$\frac{\partial J}{\partial r_{ij}} = 0, \quad (i = 1, \dots, NR; j = 1, \dots, NS) \quad (3-26)$$

leads to a linear system of equations for the estimates of the pseudostatic influence coefficients during the $(m + 1)$ th modal sweep:


$$\underline{E}^{(0)} \underline{P}^{(0)} = \underline{F}^{(0)} \quad (3-27)$$

where $\underline{P}^{(0)}$, $\underline{E}^{(0)}$, and $\underline{F}^{(0)}$ are $NS \times NR$, $NS \times NS$, and $NS \times NR$ matrices with elements:

$$P_{ki}^{(0)} = r_{ik} \quad (i = 1, \dots, NR; k = 1, \dots, NS) \quad (3-28)$$

$$E_{jk}^{(0)} = \sum_{n=0}^{NT} \ddot{z}_j(n\Delta t) \ddot{z}_k(n\Delta t), \quad (j, k = 1, \dots, NS) \quad (3-29)$$

$$F_{ji}^{(0)} = \sum_{n=0}^{NT} \ddot{z}_j(n\Delta t) \left[a_i(n\Delta t) - \sum_{r=1}^{NM} \ddot{x}_{ir} \left(n\Delta t; \left\{ \omega_r, \zeta_r, \underline{P}^{(r)} \right\}_m \right) \right] \quad (j = 1, \dots, NS; i = 1, \dots, NR) \quad (3-30)$$



so that $\underline{p}^{(0)}$ corresponds to the transpose of the pseudostatic influence matrix, \underline{R} . The square matrix $\underline{E}^{(0)}$ is symmetric, and it is also positive definite, and hence nonsingular, if the time histories of the support motions \ddot{z}_j , $j = 1, \dots, NS$, are linearly independent. The Gaussian elimination procedure is used to calculate the matrix $\underline{p}^{(0)}$ from Equation 3-27 to give the updated estimates for \underline{R} for the $(m + 1)$ th modal sweep.

3.2.2.2 Normal Mode Response Estimates

The next phase of the modal sweep process involves the reestimation of the normal mode parameters that together are used to compute the dynamic components of response at each response degree of freedom. This is carried out through a succession of single-mode minimizations of J , in which the parameters of the other modes and the pseudostatic response are held fixed at their latest estimates. The single-mode minimization of J to estimate the parameters of the r th mode is done by iterating with respect to ω_r and ζ_r only. For each iteration corresponding to an $\omega_r - \zeta_r$ pair, the effective participation factors $p_{ij}^{(r)}$, ($i = 1, \dots, NR$, $j = 1, \dots, NS$), which minimize J can be calculated explicitly by solving a linear system of equations; this is because the modal response is a linear function of these parameters. These "optimal" values of $p_{ij}^{(r)}$ are then used to compute the value of J corresponding to the given ω_r and ζ_r . By evaluating J in this manner, it can be minimized by performing a series of minimizations in one dimension in which J is repeatedly minimized with respect to ω_r with ζ_r held fixed, and then with respect to ζ_r with ω_r held fixed. Each one-dimensional minimization is achieved by finding the minimum of a parabola placed through three points enclosing the true minimum (Beck, 1978; Beck and Jennings, 1980). This technique for minimizing J with respect to ω_r and ζ_r turns out to be equivalent to the method of steepest descent but with the advantage that the gradient of J need not be computed.

The calculation of the "optimal" values of the effective participation factors for given values of ω_r and ζ_r during the

iterations in the (m+1)th modal sweep is based on the following theory. The first step is to express the "cost" function in the form:

$$J \left(\tilde{p}^{(r)} \right) = \frac{1}{V} \sum_{i=1}^{NR} \sum_{n=0}^{NT} \left[a_i^{(r)}(n\Delta t) - \ddot{x}_{ir}(n\Delta t; \omega_r, \zeta_r, \tilde{p}^{(r)}) \right]^2 \quad (3-31)$$

where the modified measured response

$$\begin{aligned} a_i^{(r)}(t) = & a_i(t) - \ddot{s}_i(t; \{R\}_{m+1}) \\ & - \sum_{s=1}^{r-1} \ddot{x}_{is}(t; \{\omega_s, \zeta_s, \tilde{p}^{(s)}\}_{m+1}) \\ & - \sum_{s=r+1}^{NM} \ddot{x}_{is}(t; \{\omega_s, \zeta_s, \tilde{p}^{(s)}\}_m) \end{aligned} \quad (3-32)$$

Thus, the latest estimates of the pseudostatic response and all modal contributions except that for mode r have been removed from the measured acceleration. In this way, $a_i^{(r)}$ is formed which, in turn, is to be matched by \ddot{x}_{ir} in a least-squares sense in order to estimate the elements of the matrix $\tilde{p}^{(r)} = [p_{ij}^{(r)}]$ corresponding to the given ω_r and ζ_r .

The next step is to notice that, from the linearity of Equation 3-15, \ddot{x}_{ir} can be expressed as a linear function of the $p_{ij}^{(r)}$:

$$\ddot{x}_{ir}(t) = \sum_{j=1}^{NS} p_{ij}^{(r)} \ddot{x}_j^{(r)}(t) \quad (3-33)$$

where each component $x_j^{(r)}$ satisfies the equation of motion:

$$\ddot{x}_j^{(r)} + 2\zeta_r \omega_r \dot{x}_j^{(r)} + \omega_r^2 x_j^{(r)} = -\ddot{z}_j(t) \quad (3-34)$$

Since each \ddot{z}_j is a measured support motion and ω_r and ζ_r have specified values at this stage of the iterative process, it follows that the $x_j^{(r)}$ may be calculated for each $j=1, \dots, NS$, independently of the $p_{ij}^{(r)}$. It can now be seen that the problem of minimizing J in Equation 3-31 with respect to the $p_{ij}^{(r)}$ can be



treated in the same way as the problem of minimizing J in Equation 3-24 with respect to the r_{ij} . Thus, setting

$$\frac{\partial J}{\partial p_{ij}^{(r)}} = 0, \quad (i = 1, \dots, NR; j = 1, \dots, NS) \quad (3-35)$$

leads to:

$$\underline{E}^{(r)} \left(\underline{p}^{(r)} \right)^T = \underline{F}^{(r)} \quad (3-36)$$

where $\left(\underline{p}^{(r)} \right)^T$ is the transpose of the effective participation factor matrix, and

$$E_{jk}^{(r)} = \sum_{n=0}^{NT} \ddot{x}_j^{(r)}(n\Delta t; \omega_r, \zeta_r) \ddot{x}_k^{(r)}(n\Delta t; \omega_r, \zeta_r) \quad (3-37)$$

(j, k = 1, \dots, NS)

$$F_{ji}^{(r)} = \sum_{n=0}^{NT} \ddot{x}_j^{(r)}(n\Delta t; \omega_r, \zeta_r) a_i^{(r)}(n\Delta t) \quad (3-38)$$


(j = 1, \dots, NS; i = 1, \dots, NR)

Equation 3-36 is solved for $\left(\underline{p}^{(r)} \right)^T$ using Gaussian elimination, and this result is substituted into Equation 3-31 to evaluate J for the given ω_r - ζ_r pair. This process allows J to be minimized with respect to all of the parameters of mode r during the $(m + 1)$ th modal sweep by iterating on only two parameters, ω_r and ζ_r .

3.2.2.3 Initialization of Modal Sweeps

The prior description of the modal sweep procedure has been applied to subsequent sweeps conducted after the procedure has first been initiated. However, it is necessary to apply a special procedure to the first modal sweep when starting this process, in order to avoid having to enter initial estimates for all the parameters of the model, many of which are difficult to estimate a priori. The procedure to be described here requires initial estimates for only the natural frequency and damping ratio for each mode which is to be included in the model.

The first modal sweep is initiated by estimating the pseudostatic response parameters through a least-squares matching of the measured response by the model pseudostatic response



alone. The procedure is similar to that described in Section 3.2.2.1 except that in Equations 3-24 and 3-30 there is no term involving modal contributions.

The first modal sweep is then continued by successively estimating the parameters of the modes which have been included initially in the model. Again, the procedure is similar to that described in Section 3.2.2.2 except that for mode r the modified measured response defined in Equation 3-32 does not contain the second sum involving the contributions of modes $r + 1$, $r + 2$, ..., NM .

The estimates of the parameters after the completion of the first modal sweep may not be particularly accurate, but since the process is iterative, they will be corrected in subsequent modal sweeps. The advantage of initializing the modal sweeps in this way is that the parameter estimation program is essentially self-starting. The only initial estimates which the user must provide are the natural frequencies and damping ratios of the modes to be included in the model, since these are needed to start the iterative process for these parameters. Only the frequencies need be chosen with care. The program will converge to the nearest local minimum of J for the given number of modes included. Thus, if initial frequencies were chosen without care, the program could converge to a set of modes which did not include an important mode of the structure. Plots of Fourier amplitude spectra and transfer functions between individual structural responses and support motions can provide important guidance in choosing initial frequencies. The initial damping ratios can usually be taken as say, 4%, since J is much less sensitive to these parameters than to the natural frequencies, so that initial large errors from the minimizing values have less effect.

The special procedure for the first modal sweep need not be selected in subsequent runs of MODE-ID when investigating the effects of introducing one additional mode at a time to the model. The initial estimates for all of the parameters except



those of the new mode can be input from an output file created by the previous run of the program. The user need only supply an initial frequency and damping ratio for the new mode. The first modal sweep then consists of only one single-mode minimization of J for the new mode and this follows the procedure described in Section 3.2.2.2.

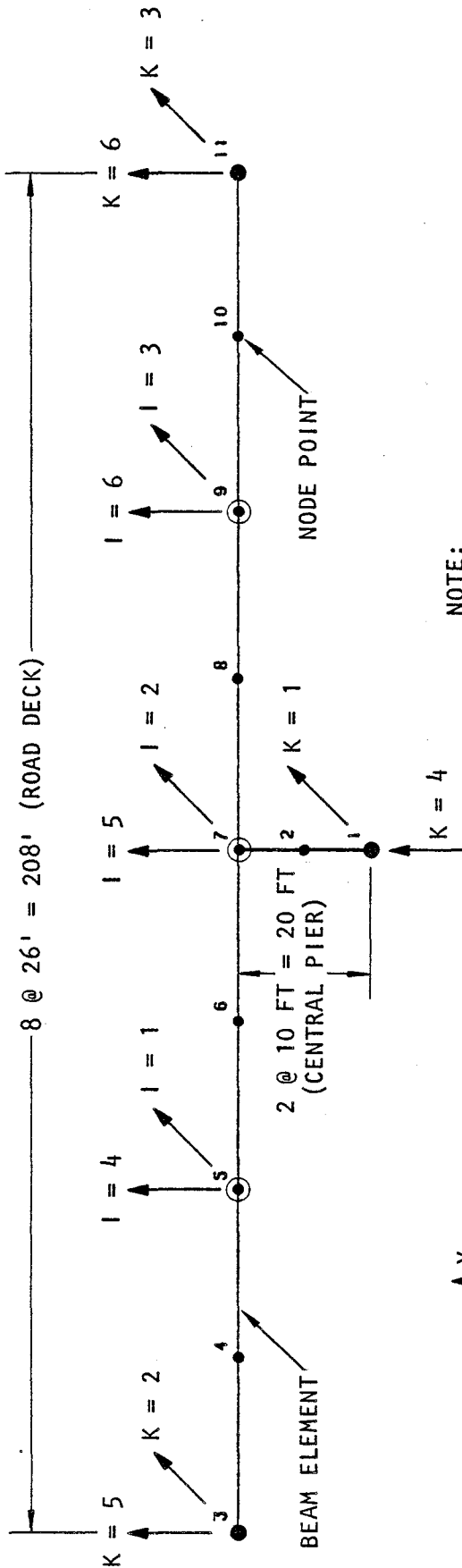
3.3 VERIFICATION ANALYSIS

3.3.1 OVERVIEW

To verify the accuracy of the foregoing methodology, MODE-ID is applied to a three-dimensional beam model of an idealized bridge structure with known pseudostatic and normal mode parameters. Input motions are applied at the multiple support points of this bridge model, and standard dynamic analysis procedures are used to compute the response at each of its degrees-of-freedom. These computed structure responses and the applied input motions are then treated as "measurements," and MODE-ID is applied to these measurements to estimate the pseudostatic and normal mode parameters of the bridge. Results of this application are seen to show excellent agreement with the original bridge parameters.

3.3.2 BRIDGE STRUCTURE

The structure considered in this verification analysis represents a hypothetical idealized bridge that is similar to the Meloland Road Overpass (see Fig. 3-1). The bridge is a two-span simply supported structure that is comprised of a road deck 208 ft long and a central pier 20 ft high. It is represented as a series of three-dimensional beam elements, and is excited by transverse and vertical input motions that are applied to the ends of the road deck and at the base of the central pier. Bridge responses monitored during the resulting dynamic analysis are the transverse and vertical motions at the center of each span and at the top of the central pier. Section



COMPUTER PRINTOUT LEGEND:

- K = SUPPORT DOF
- I = MONITORED RESPONSE DOF

NODE POINT LEGEND:

- SUPPORT MOTION NODE
- ⊙ MONITORED RESPONSE NODE
- ADDITIONAL RESPONSE NODE

BOUNDARY CONDITIONS AT SUPPORTS:

- DISPLACEMENTS — FIXED
- ROTATIONS — FREE

SECTION PROPERTIES AND MATERIAL PROPERTIES:

SEE TABLE 3-1.

FIGURE 3-1. VERIFICATION ANALYSIS: BRIDGE CONFIGURATION AND DEGREES-OF-FREEDOM



properties and material properties for the bridge are given in Table 3-1.

The pseudostatic influence matrix, R , for this bridge is assembled from a series of static analyses conducted using the SAP4 finite element program. In this, the j th column of R is obtained by applying a unit static displacement at the j th support degree-of-freedom (DOF) keeping all other support DOF fixed, and then computing the resulting displacement at each monitored response DOF (Fig. 3-2). The normal modes of the bridge that are included in this analysis are its fundamental transverse, antisymmetric vertical, and symmetric vertical modes. Mode shapes, natural frequencies, and effective modal participation factor matrices* for each of these modes were also computed from SAP4 and are shown in Figures 3-3 to 3-5, together with the damping ratios that were specified for each mode.

3.3.3 INPUT MOTIONS

The input motions applied at the various support degrees-of-freedom for this bridge are the transverse and vertical motions measured at the abutments and base of the central pier of the Meloland Road Overpass. The motions have been corrected for recorder stall and nonsynchronization effects as described in Chapter 2, and are shown in Figure 3-6.

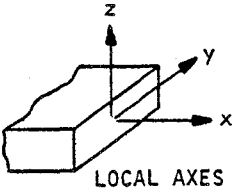
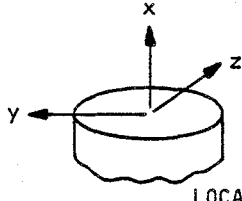
3.3.4 COMPUTATION OF SIMULATED MEASUREMENTS

As noted in Section 3.3.1, the computed dynamic response of the bridge subjected to the applied input motions serves as

* Figures 3-3 to 3-5 actually show the transpose of the effective participation factor matrices as expressed by Equation 3-16. As shown by this equation, the effective modal participation factors are computed as the product of the mode shape and the conventional modal participation factors (Eq. 3-11). It is noted that the conventional participation factors are dependent on how the mode shapes are normalized, whereas the effective participation factors are not.



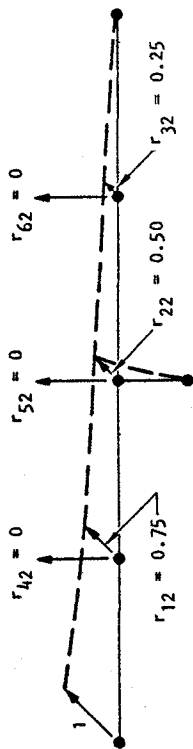
TABLE 3-1. BRIDGE PROPERTIES FOR VERIFICATION ANALYSIS

Property	Road Deck 	Central Pier 
Area (in. ²)	$A_x = 6782.4$	$A_x = 2822.4$
Bending Moments of Inertia (in. ⁴)	$I_y = 4.697 \times 10^6$ $I_z = 8.644 \times 10^7$	$I_y = 6.366 \times 10^5$ $I_z = 6.366 \times 10^5$
Torsional Moment of Inertia (in. ⁴)	$I_x = 1.265 \times 10^7$	$I_x = 12.732 \times 10^5$

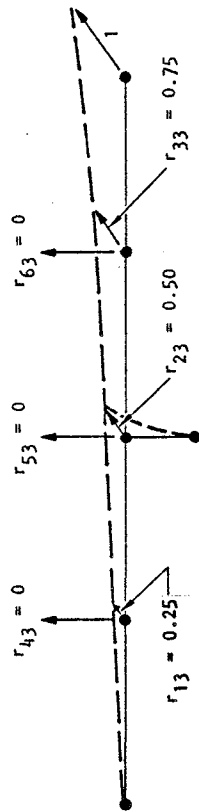
a) Section properties

Property	Value
Young's Modulus	$E = 3 \times 10^6 \text{ lb/in.}^2$
Poisson's Ratio	$\nu = 0.25$
Weight Density	$\gamma = 150 \text{ lb/ft}^3$

b) Material properties

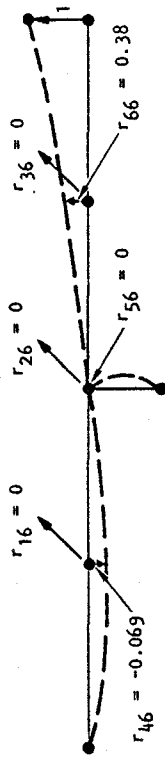


(a) Unit transverse displacement of base of central pier (K = 1).



(b) Unit transverse displacement of left abutment (K = 2)

(c) Unit transverse displacement of right abutment (K = 3)



(d) Unit vertical displacement of base of central pier (K = 4)

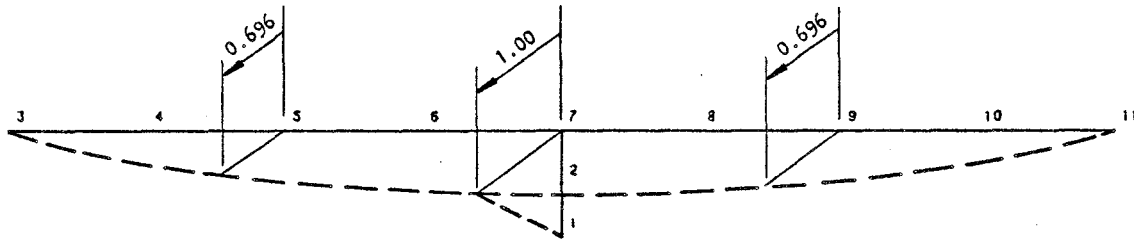
(e) Unit vertical displacement of left abutment (K = 5)

(f) Unit vertical displacement of right abutment (K = 6)

NOTE: STRUCTURE DISPLACEMENT VALUES SHOWN ROUNDED OFF TO TWO SIGNIFICANT FIGURES

AA801

FIGURE 3-2. CONSTRUCTION OF PSEUDOSTATIC INFLUENCE MATRIX FOR VERIFICATION ANALYSIS



MODE SHAPE

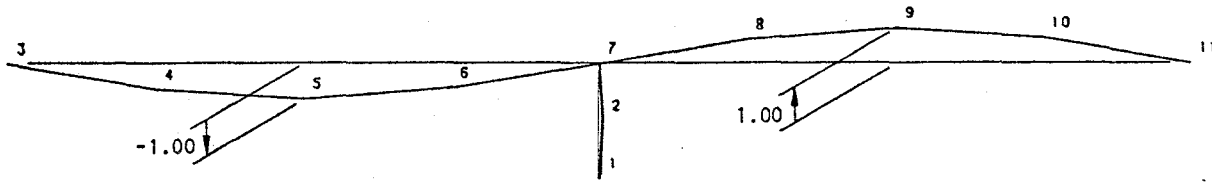
Natural frequency: $f_1 = 3.24$ Hz
 Damping ratio: $\zeta_1 = 0.0206$

Input		Response						Node Point (Input)
		Transverse			Vertical			
		I = 1	I = 2	I = 3	I = 4	I = 5	I = 6	
Transverse	K = 1	0	0	0	0	0	0	1
	K = 2	0.441	0.634	0.441	0	0	0	3
	K = 3	0.441	0.634	0.441	0	0	0	11
Vertical	K = 4	0	0	0	0	0	0	1
	K = 5	0	0	0	0	0	0	3
	K = 6	0	0	0	0	0	0	11
		5	7	9	5	7	9	
		Node Point (Response)						

Transpose of Effective Participation Factor Matrix (Eq. 3-16)

AA804

FIGURE 3-3. PROPERTIES OF FIRST TRANSVERSE MODE USED IN VERIFICATION ANALYSIS



MODE SHAPE

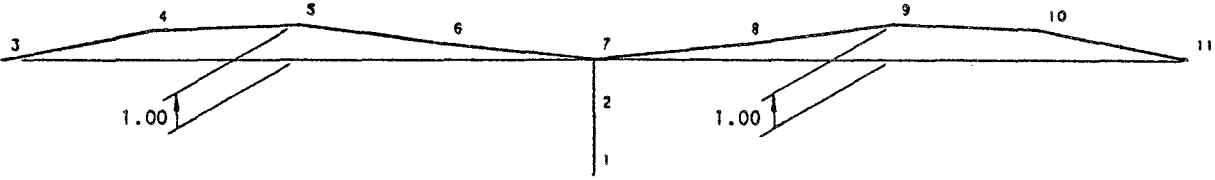
Natural frequency: $f_2 = 3.37$ Hz
 Damping ratio: $\zeta_2 = 0.0212$

Input		Response						Node Point (Input)
		Transverse			Vertical			
		I = 1	I = 2	I = 3	I = 4	I = 5	I = 6	
Transverse	K = 1	0	0	0	0	0	0	1
	K = 2	0	0	0	0	0	0	3
	K = 3	0	0	0	0	0	0	11
Vertical	K = 4	0	0	0	0.001	0	-0.001	1
	K = 5	0	0	0	0.288	0	-0.288	3
	K = 6	0	0	0	-0.289	0	0.289	11
		5	7	9	5	7	9	
Node Point (Response)								

Transpose of Effective Participation Factor Matrix (Eq. 3-16)

AA805

FIGURE 3-4. PROPERTIES OF FIRST ANTISYMMETRIC VERTICAL MODE USED IN VERIFICATION ANALYSIS



MODE SHAPE

Natural frequency: $f_3 = 4.721$ Hz

Damping ratio: $\zeta_3 = 0.030$

Input		Response						Node Point (Input)
		Transverse			Vertical			
		I = 1	I = 2	I = 3	I = 4	I = 5	I = 6	
Transverse	K = 1	0	0	0	0	0	0	1
	K = 2	0	0	0	0	0	0	3
	K = 3	0	0	0	0	0	0	11
Vertical	K = 4	0	0	0	0.736	0	0.736	1
	K = 5	0	0	0	0.231	0	0.231	3
	K = 6	0	0	0	0.233	0	0.233	11
		5	7	9	5	7	9	
Node Point (Response)								

Transpose of Effective Participation Factor Matrix (Eq. 3-16)

AA806

FIGURE 3-5. PROPERTIES OF FIRST SYMMETRIC VERTICAL MODE USED IN VERIFICATION ANALYSIS

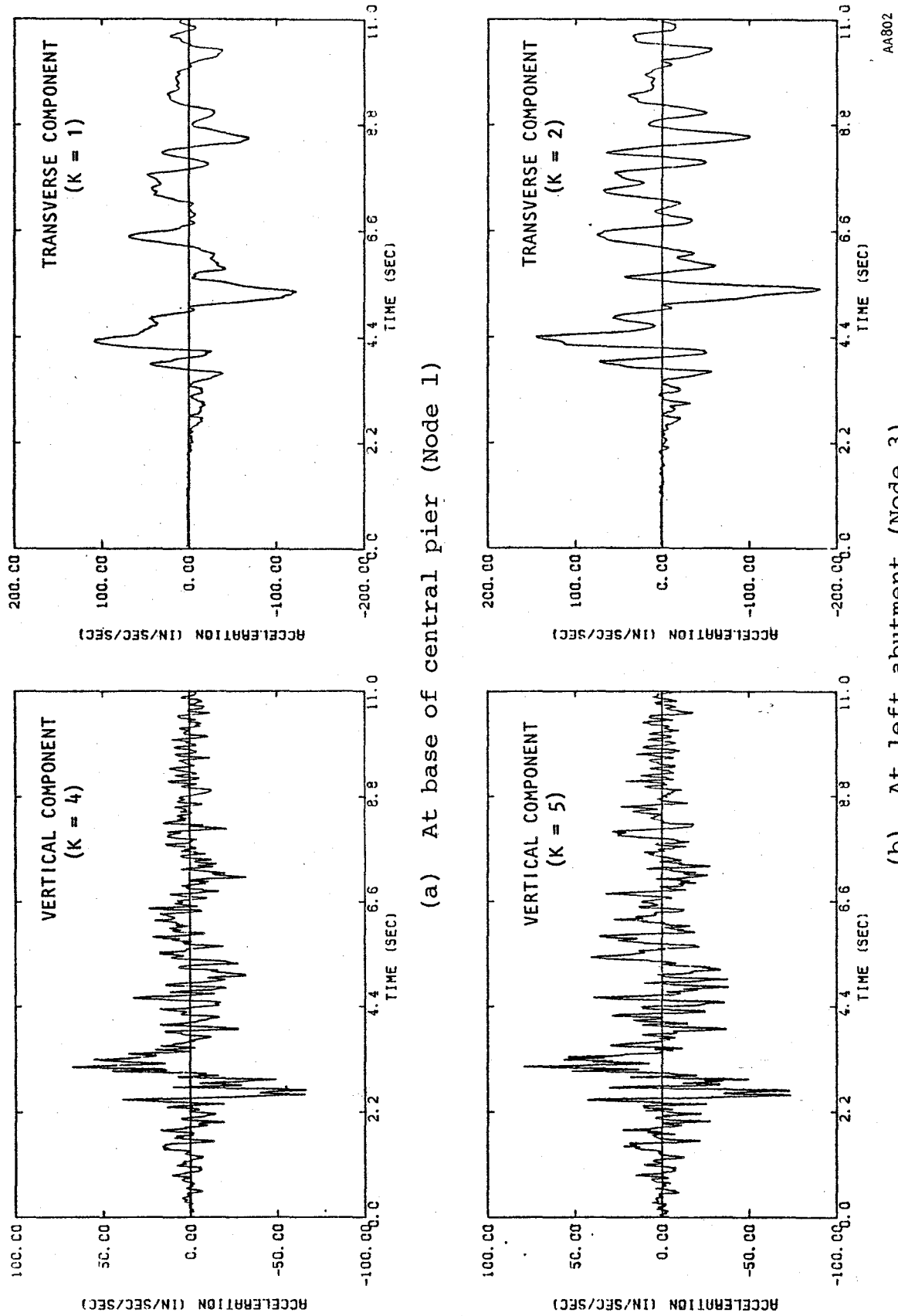
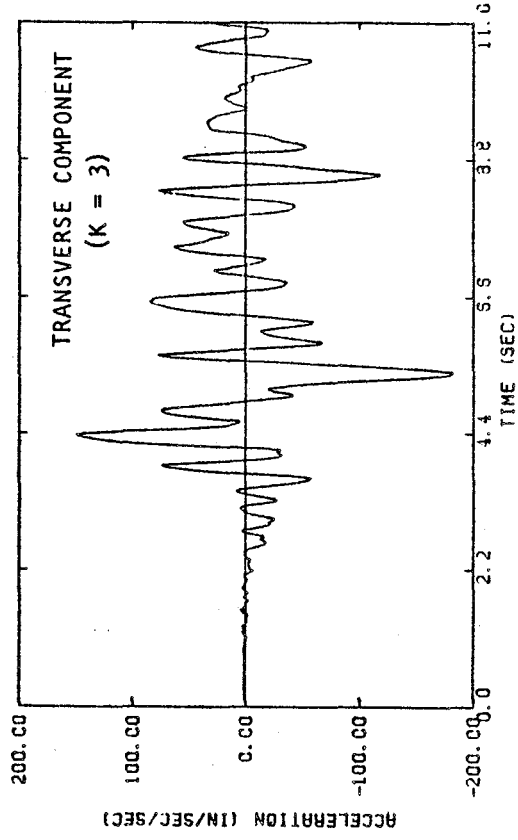
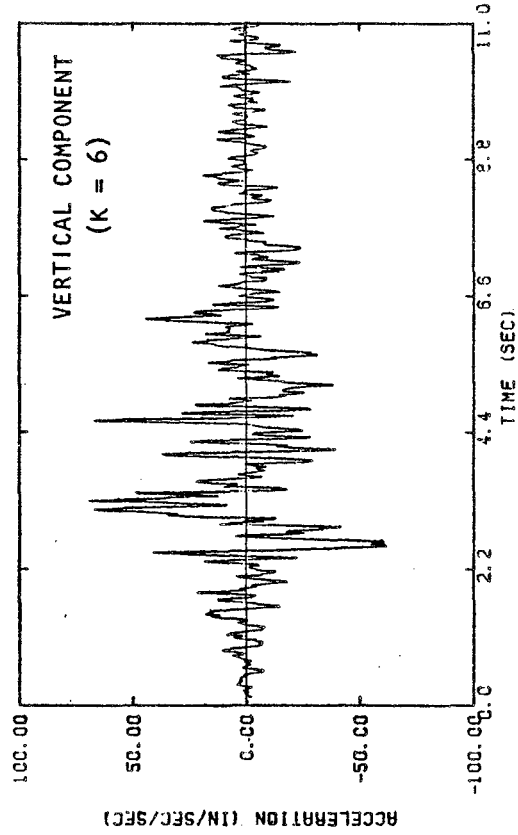


FIGURE 3-6. INPUT MOTIONS FOR VERIFICATION ANALYSIS



AA803



(c) At right abutment (Node 11)

FIGURE 3-6. (CONCLUDED)




simulated "response measurements" in these verification analyses. Model parameters are identified by applying MODE-ID to these "measurements," and are evaluated through comparison with the actual bridge parameters.

On this basis, two sets of dynamic response cases have been considered as part of this verification analysis. The first (Case 1) consists of computation of the bridge's pseudostatic response only, and subsequent application of MODE-ID to these computed responses to estimate the bridge's pseudostatic influence matrix \underline{R} . The second case (Case 2) involves computation of the total dynamic response of the bridge (pseudostatic and dynamic components), and use of MODE-ID with these total response results to estimate not only \underline{R} but the various normal mode parameters as well.

With this as background, the dynamic analysis of the bridge, which will provide the simulated "response measurements" for both the Case 1 and Case 2 applications, has been conducted in accordance with the following steps:

- Computation of the pseudostatic component of response at each structure degree-of-freedom using Equation 3-4. This step is all that is required to simulate the Case 1 "measurements," whereas the Case 2 simulation also requires the additional steps that follow.
- Computation of the modal response at each structure degree-of-freedom, by solving the equations of motion for each mode (see Eq. 3-15).
- Superposition of these modal responses to obtain the total dynamic component of response at each structure degree-of-freedom (see Eq. 3-14).
- Computation of the total response at each structure degree-of-freedom, by superposition of the pseudostatic and dynamic components (see Eq. 3-12).



3.3.5 CASE 1 RESULTS

The Case 1 estimates of the pseudostatic influence matrix, \underline{R} , as determined from the simulated "measurements" consisting of only the computed pseudostatic response of the bridge, are shown in Table 3-2. This table shows that the MODE-ID estimate of \underline{R} after only one modal sweep is nearly identical to the actual \underline{R} for the bridge, since there is no need to iterate in this case. In this as well as in all subsequent tables and figures, it is noted that I and K correspond to MODE-ID indices for response and support degrees of freedom respectively.

3.3.6 CASE 2 RESULTS

The Case 2 application of MODE-ID to the simulated total response "measurements" of the bridge response has produced estimates of \underline{R} and the normal mode parameters - i.e., all of the parameters that influence the total response. An unusually large number of modal sweeps (10 in all) was required for this application, because of the slow convergence of the vertical antisymmetric mode which was not strongly excited by the applied input motions. In fact, the natural period and damping ratio of the vertical symmetric mode and the transverse mode essentially reached their final values after about 5 modal sweeps; however the estimates of the corresponding parameters for the vertical antisymmetric mode were seen to be still changing noticeably even over the final modal sweeps.

Table 3-3 provides MODE-ID printout that compares the final estimates of \underline{R} and the normal mode parameters with the actual values of these quantities for the bridge. These comparisons show that MODE-ID has produced excellent estimates of \underline{R} and the normal mode parameters for the transverse and vertical symmetric modes - all of which were substantially excited by the applied input motions. However, the estimates for the vertical antisymmetric mode are poor, primarily because this mode was barely excited and is therefore not strongly represented in the



TABLE 3-2. CASE 1 RESULTS (Note legend in Fig. 3-1)

ABSOLUTE RESPONSE AT 6 DOF TO BE CALCULATED
FOR A MODE WITH 0 MODES.

CALCULATING PSEUDOSTATIC RESPONSE FROM FOLLOWING MATRIX:
(I IS OUTPUT DOF, K IS SUPPORT DOF)

	I=1	I=2	I=3	I=4	I=5	I=6
K=1	0.0000	0.0000	0.0000	0.0000	0.0000	0.0000
K=2	0.7500	0.5000	0.2484	0.0000	0.0000	0.0000
K=3	0.2500	0.5000	0.7516	0.0000	0.0000	0.0000
K=4	0.0000	0.0000	0.0000	0.6867	0.9988	0.6830
K=5	0.0000	0.0000	0.0000	0.3825	0.0000	-0.0690
K=6	0.0000	0.0000	0.0000	-0.0691	0.0000	0.3859

(a) Actual $[R]^T$ for bridge model

ACCELERATION MATCHING USED IN IDENTIFICATION

MINIMIZATION OF OUTPUT-ERROR MEASURE-OF-FIT J
TO ESTIMATE THE PSEUDOSTATIC INFLUENCE MATRIX AND
TO ESTIMATE THE MODAL PARAMETERS FOR 0 MODES.
CRITERION FOR CONVERGENCE WITHIN EACH MODE IS RELATIVE
CHANGE IN J LESS THAN 1.0E-04
THIS IS ALSO THE CRITERION FOR CONVERGENCE OF THE MODAL SWEEPS.
THE MAXIMUM NUMBER OF ITERATIONS WITHIN EACH MODE IS 10
AND THE MAXIMUM NUMBER OF MODAL SWEEPS ALLOWED IS 10

MODAL SWEEP NO 1

PSEUDOSTATIC INFLUENCE MATRIX
CALCULATED AS:

(I IS OUTPUT DOF, K IS SUPPORT DOF)

	I=1	I=2	I=3	I=4	I=5	I=6
K=1	-0.0000	-0.0000	-0.0000	-0.0000	-0.0000	-0.0000
K=2	0.7501	0.5001	0.2484	0.0000	0.0000	-0.0000
K=3	0.2499	0.4999	0.7516	-0.0000	0.0000	0.0000
K=4	0.0000	0.0000	-0.0000	0.6867	0.9988	0.6830
K=5	-0.0000	-0.0000	0.0000	0.3825	0.0000	-0.0690
K=6	-0.0000	-0.0000	0.0000	-0.0691	-0.0000	0.3859
SUM	1.0000	1.0000	1.0000	1.0001	0.9988	0.9999

(b) Estimated $[R]^T$ using MODE-ID



TABLE 3-3. CASE 2 RESULTS: MODE-ID PRINTOUT SHOWING ACTUAL AND ESTIMATED PARAMETERS
ABSOLUTE RESPONSE AT 6 DOF TO BE CALCULATED
FOR A MODE WITH 3 MODES.

MODAL SWEEP NOISE

PSEUDOSTATIC INFLUENCE MATRIX
CALCULATED AS:
(I IS OUTPUT DOF, K IS SUPPORT DOF)

	I=1	I=2	I=3	I=4	I=5	I=6
K=1	-0.0060	-0.0086	-0.0060	-0.0142	-0.0000	0.0152
K=2	0.7528	0.5039	0.2511	0.0366	0.0000	-0.0326
K=3	0.2526	0.5039	0.7543	-0.0251	0.0000	0.0206
K=4	0.0000	0.0000	0.0024	0.6271	0.9988	0.7415
K=5	-0.0015	-0.0022	-0.0015	0.4003	0.0000	-0.0780
K=6	0.0002	0.0005	0.0003	-0.0316	0.0000	0.3402
SUM	1.0006	1.0008	1.0006	0.9930	0.9988	1.0069

CALCULATING PSEUDOSTATIC RESPONSE FROM FOLLOWING MATRIX:
(I IS OUTPUT DOF, K IS SUPPORT DOF)

TRANSDUCER OF PSEUDOSTATIC INFLUENCE MATRIX

	I=1	I=2	I=3	I=4	I=5	I=6
K=1	0.0000	0.0000	0.0000	0.0000	0.0000	0.0000
K=2	0.7500	0.5000	0.2484	0.0000	0.0000	0.0000
K=3	0.2500	0.5000	0.7516	0.0000	0.0000	0.0000
K=4	0.0000	0.0000	0.6867	0.9988	0.6830	0.0000
K=5	0.0000	0.0000	0.3825	0.0000	-0.0490	0.0000
K=6	0.0000	0.0000	-0.0491	0.0000	0.3859	0.0000
SUM	1.0000	1.0000	1.0001	0.9988	0.9999	0.0000

MEASURE-OF-FIT= 1.230630E-04 ITERATIONS= 2
PERIOD= 0.308536 DAMPING= 2.0523(PERCENT)
PARTICIPATION FACTOR MATRIX:*

(I IS OUTPUT DOF, K IS SUPPORT DOF)

	I=1	I=2	I=3	I=4	I=5	I=6
K=1	0.0318	0.0460	0.0318	0.0028	-0.0000	-0.0281
K=2	0.4400	0.6326	0.4400	-0.0490	0.0000	0.0710
K=3	0.4486	0.6448	0.4486	0.0095	0.0000	-0.0031
K=4	0.0171	0.0252	0.0171	-0.0310	-0.0000	0.0003
K=5	-0.0015	-0.0022	-0.0015	0.1386	0.0000	-0.1236
K=6	-0.0089	-0.0134	-0.0089	0.1132	0.0000	0.1339
SUM	0.9271	1.3330	0.9271	-0.0463	0.0000	0.0504

CALCULATING MODE 1 RESPONSE USING FOLLOWING PARAMETERS:
PERIOD= 0.308600 DAMPING= 0.0206
PARTICIPATION FACTOR MATRIX:*

(I IS OUTPUT DOF, K IS SUPPORT DOF)

TRANSVERSE MODE

	I=1	I=2	I=3	I=4	I=5	I=6
K=1	0.0000	0.0000	0.0000	0.0000	0.0000	0.0000
K=2	0.4410	0.6340	0.4410	0.0000	0.0000	0.0000
K=3	0.4410	0.6340	0.4410	0.0000	0.0000	0.0000
K=4	0.0000	0.0000	0.0000	0.0000	0.0000	0.0000
K=5	0.0000	0.0000	0.0000	0.0000	0.0000	0.0000
K=6	0.0000	0.0000	0.0000	0.0000	0.0000	0.0000
SUM	0.8820	1.2680	0.8820	0.0000	0.0000	0.0000

MEASURE-OF-FIT= 1.149244E-04 ITERATIONS= 2
PERIOD= 0.298086 DAMPING= 1.6656(PERCENT)
PARTICIPATION FACTOR MATRIX:*

(I IS OUTPUT DOF, K IS SUPPORT DOF)

	I=1	I=2	I=3	I=4	I=5	I=6
K=1	-0.0327	-0.0474	-0.0327	-0.0186	0.0000	0.0429
K=2	0.0058	0.0084	0.0058	0.0645	-0.0000	-0.0790
K=3	0.0057	0.0080	0.0057	0.0105	-0.0000	-0.0179
K=4	-0.0242	-0.0354	-0.0242	-0.0083	0.0000	0.0359
K=5	0.0022	0.0031	0.0022	0.1656	-0.0000	-0.1711
K=6	0.0158	0.0233	0.0158	-0.1644	-0.0000	0.1369
SUM	-0.0504	-0.0728	-0.0504	0.0494	-0.0000	-0.0523

CALCULATING MODE 2 RESPONSE USING FOLLOWING PARAMETERS:
PERIOD= 0.299900 DAMPING= 0.0212
PARTICIPATION FACTOR MATRIX:*

(I IS OUTPUT DOF, K IS SUPPORT DOF)

ANTISYMMETRIC VERTICAL MODE

	I=1	I=2	I=3	I=4	I=5	I=6
K=1	0.0000	0.0000	0.0000	0.0000	0.0000	0.0000
K=2	0.0000	0.0000	0.0000	0.0000	0.0000	0.0000
K=3	0.0000	0.0000	0.0000	0.0000	0.0000	0.0000
K=4	0.0000	0.0000	0.0000	0.0010	0.0000	-0.0010
K=5	0.0000	0.0000	0.0000	0.2880	0.0000	-0.2880
K=6	0.0000	0.0000	0.0000	-0.2870	0.0000	0.2870
SUM	0.0000	0.0000	0.0000	0.0000	0.0000	0.0000

MEASURE-OF-FIT= 1.148756E-04 ITERATIONS= 2
PERIOD= 0.212000 DAMPING= 2.9992(PERCENT)
PARTICIPATION FACTOR MATRIX:*

(I IS OUTPUT DOF, K IS SUPPORT DOF)

	I=1	I=2	I=3	I=4	I=5	I=6
K=1	-0.0022	-0.0032	-0.0022	0.0022	-0.0000	-0.0025
K=2	0.0011	0.0015	0.0011	-0.0006	-0.0000	0.0006
K=3	0.0003	0.0004	0.0002	-0.0018	0.0000	0.0008
K=4	0.0020	0.0028	0.0020	0.7330	-0.0000	0.7385
K=5	0.0005	0.0008	0.0005	0.2305	0.0000	0.2315
K=6	-0.0013	-0.0018	-0.0013	0.2352	0.0000	0.2304
SUM	0.0004	0.0005	0.0003	1.1985	-0.0000	1.1993

CALCULATING MODE 3 RESPONSE USING FOLLOWING PARAMETERS:
PERIOD= 0.212000 DAMPING= 0.0300
PARTICIPATION FACTOR MATRIX:*

(I IS OUTPUT DOF, K IS SUPPORT DOF)

SYMMETRIC VERTICAL MODE

	I=1	I=2	I=3	I=4	I=5	I=6
K=1	0.0000	0.0000	0.0000	0.0000	0.0000	0.0000
K=2	0.0000	0.0000	0.0000	0.0000	0.0000	0.0000
K=3	0.0000	0.0000	0.0000	0.0000	0.0000	0.0000
K=4	0.0000	0.0000	0.0000	0.7360	0.0000	0.7360
K=5	0.0000	0.0000	0.0000	0.2310	0.0000	0.2310
K=6	0.0000	0.0000	0.0000	0.2330	0.0000	0.2330
SUM	0.0000	0.0000	0.0000	1.2000	0.0000	1.2000

MAXIMUM NO. OF MODAL SWEEPS REACHED SO ITERATIONS STOPPED
THE RELATIVE CHANGE IN J OVER THE LAST MODAL SWEEP WAS 1.37E-01

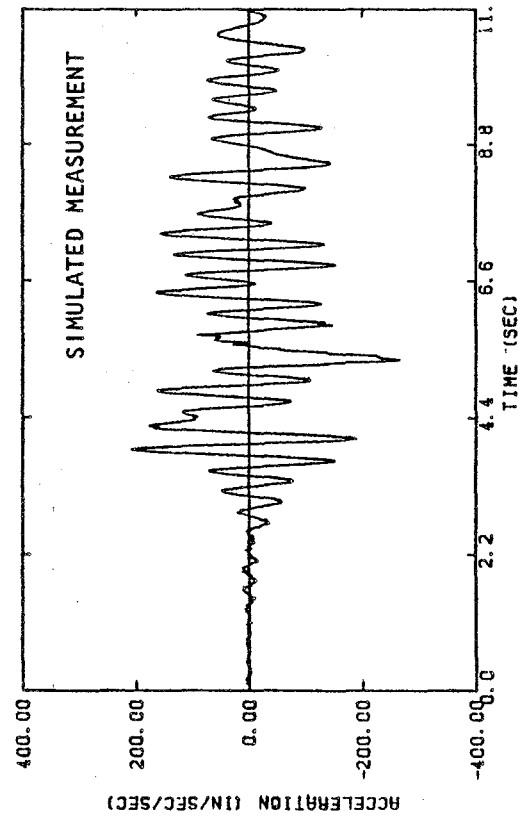
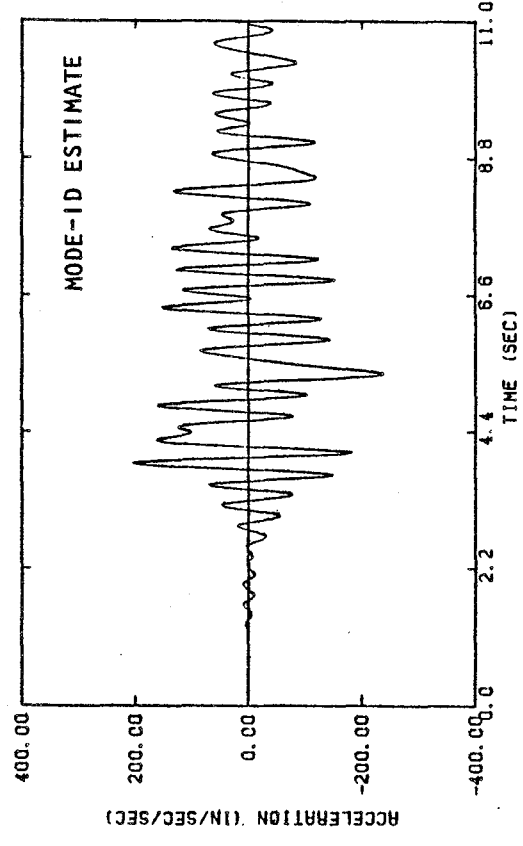
* NOTE: THIS CORRESPONDS TO TRANSPOSE OF EFFECTIVE PARTICIPATION FACTOR MATRIX GIVEN BY EQ. 3-16

(a) Actual Parameters (b) Estimated Parameters

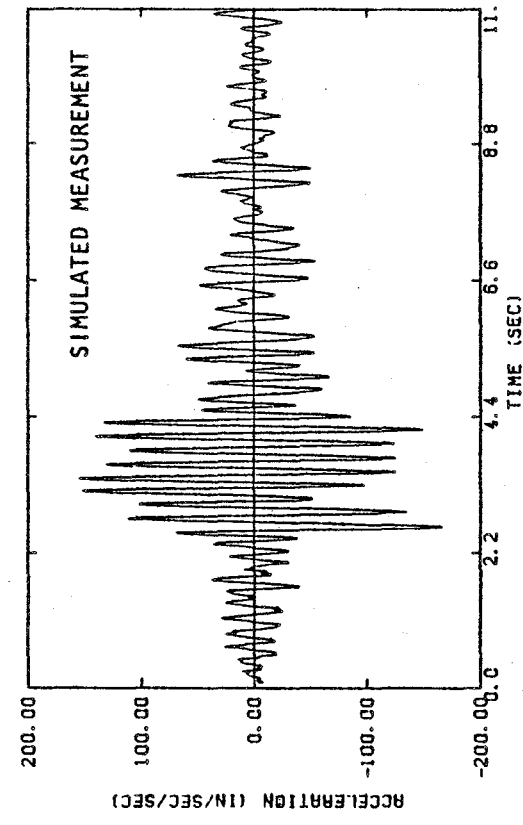
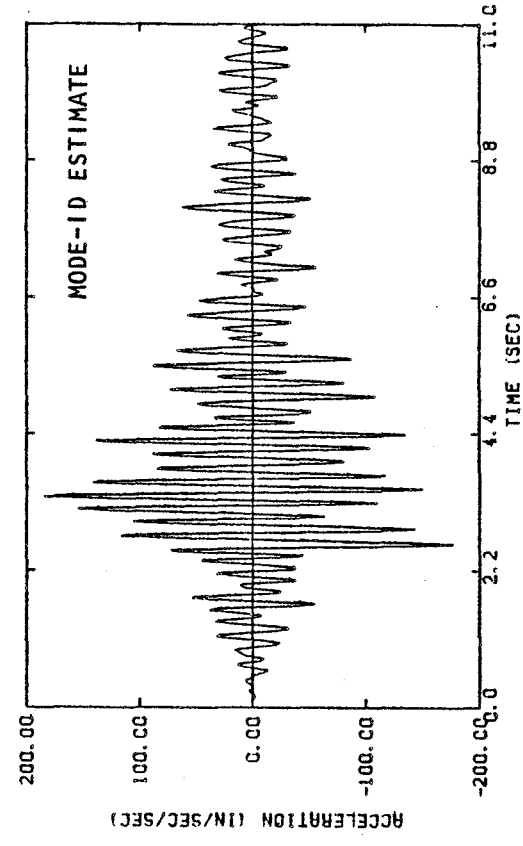


simulated "measurements" (i.e., in the computed bridge response). Also, because this mode and the transverse mode have almost the same natural frequency, their effective participation factors show a tendency for the two modes to trade off. To illustrate, it is seen that if corresponding columns of the transpose of the identified effective participation factor matrix for these two modes are summed and compared to the same sum for the actual matrices, the agreement is excellent. Therefore for such closely spaced modes in which one mode is weakly excited, it is the sums of the two sets of effective participation factor matrices that are most reliably identified by MODE-ID.

Further results along these lines are provided as comparisons between the simulated "measurements" at each node point and the estimated bridge motions computed using the parameters identified by MODE-ID (Figs. 3-7 to 3-9). These comparisons show that the agreement is so close that the "measured" and estimated motions are virtually indistinguishable. Such excellent comparisons are a further indication of (1) the lack of sensitivity of the bridge response to the vertical antisymmetric mode, whose estimate using MODE-ID was poor; and (2) the ability of MODE-ID to provide excellent estimates of those pseudostatic and normal mode parameters whose effect on the bridge response is more substantial. Of course, the comparison between the "measured" and estimated motions is better than would be expected if the measurements from an actual bridge were used, since then the model used in the system identification would not be as exact as it is for the idealized hypothetical bridge considered in this test case. Nevertheless, as shown subsequently in Chapter 4, the ability of MODE-ID to identify a model that closely matches the measured seismic response of the Meloland Road Overpass is remarkably good.



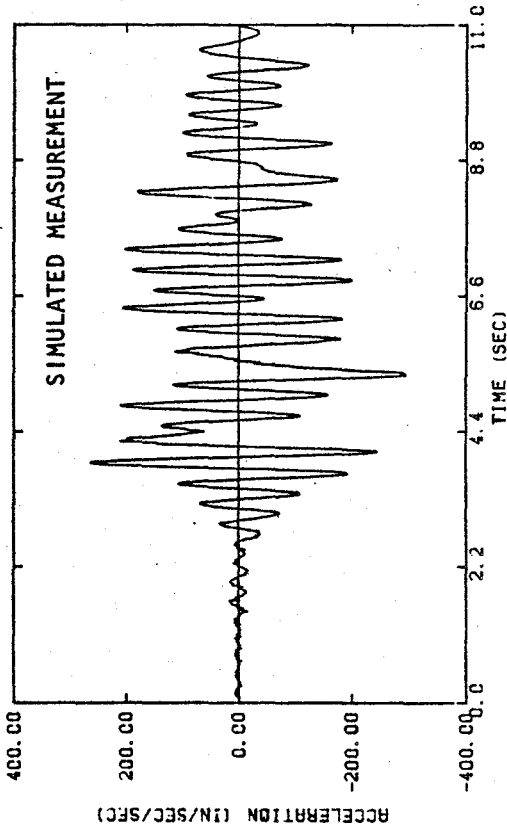
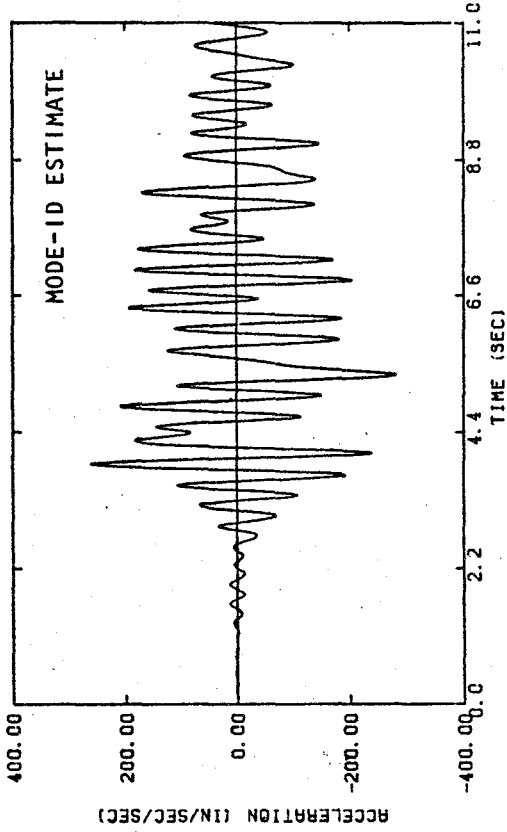
(a) Transverse motion (I = 1)



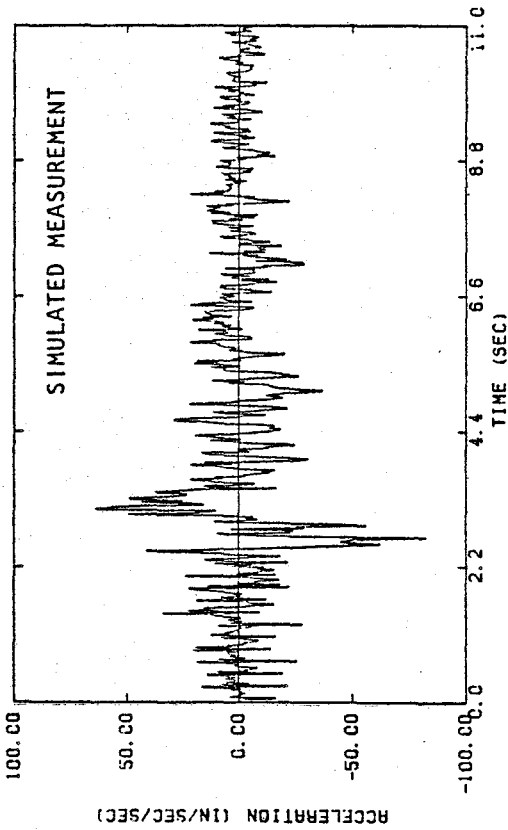
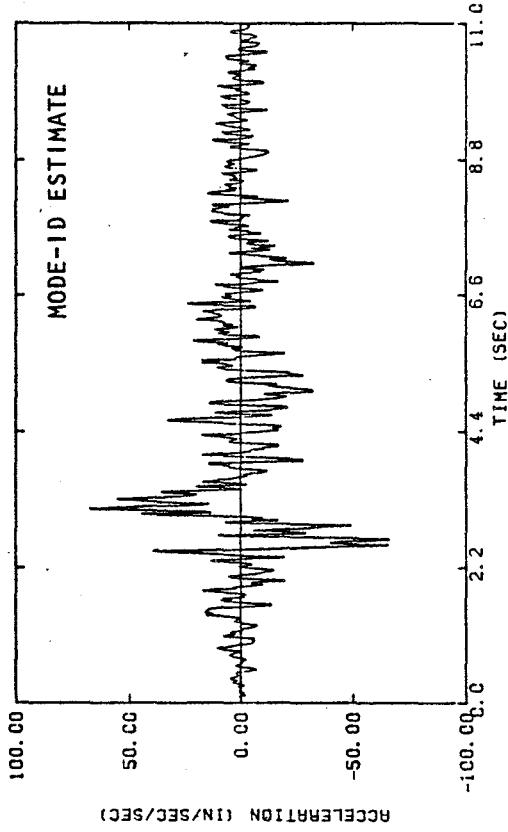
(b) Vertical motion (I = 4)

AA807

FIGURE 3-7. COMPARISON OF SIMULATED MEASUREMENTS AND ESTIMATED MOTIONS: NODE 5



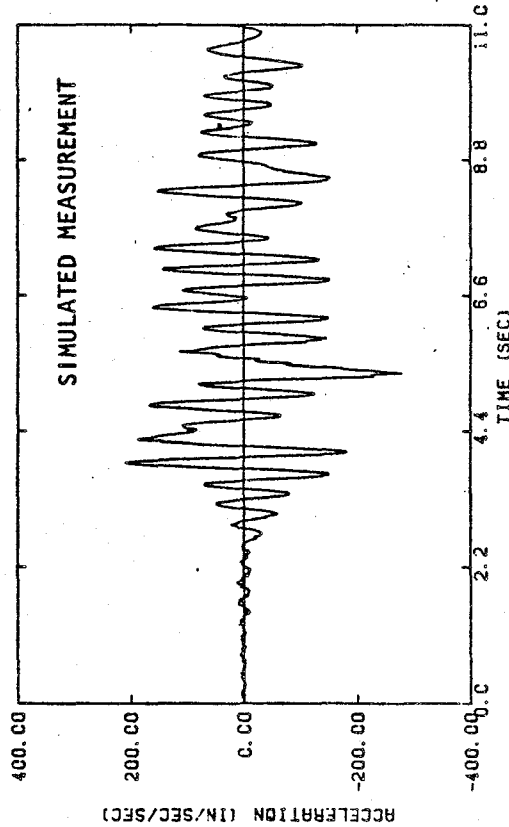
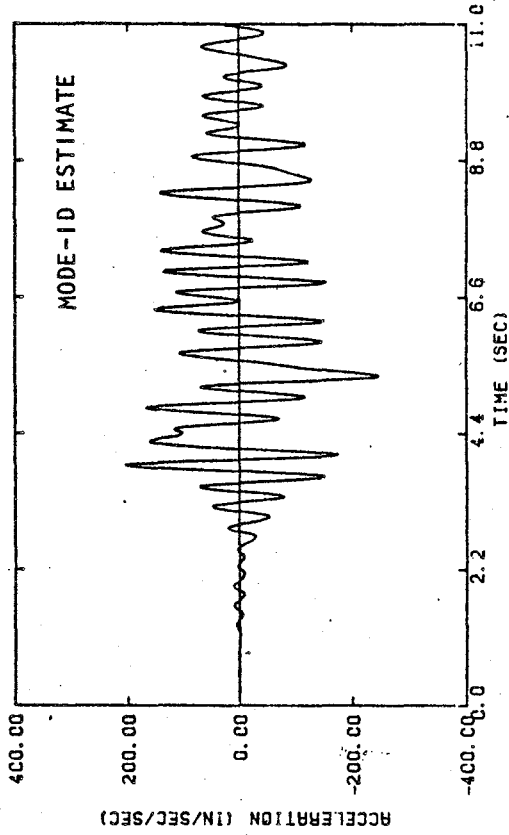
(a) Transverse motion (I = 2)



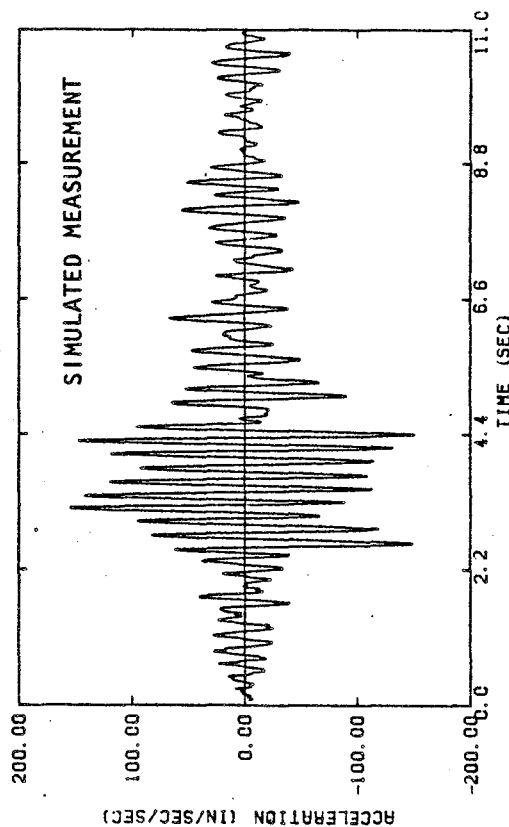
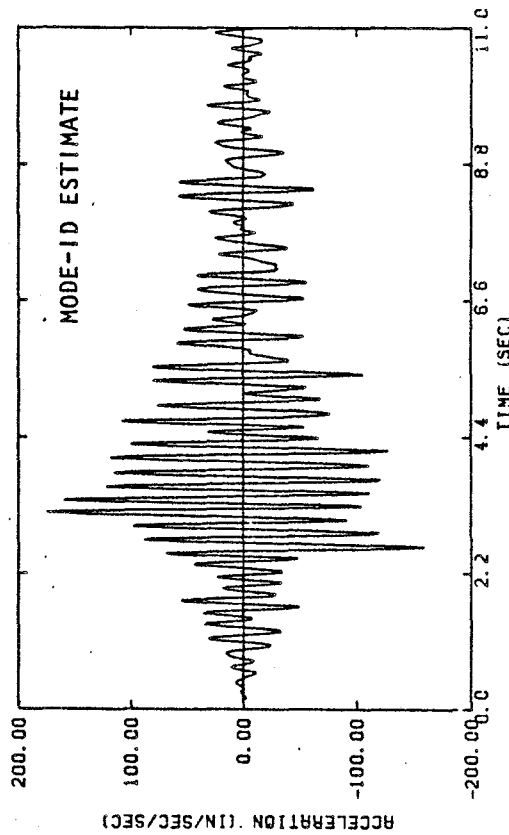
(b) Vertical motion (I = 5)

AA808

FIGURE 3-8. COMPARISON OF SIMULATED MEASUREMENTS AND ESTIMATED MOTIONS: NODE 7



(a) Transverse motion (I = 3)



(b) Vertical motion (I = 6)

AA809

FIGURE 3-9. COMPARISON OF SIMULATED MEASUREMENTS AND ESTIMATED MOTIONS: NODE 9

11
12
13
14
15
16
17
18
19
20
21
22
23
24
25
26
27
28
29
30
31
32
33
34
35
36
37
38
39
40
41
42
43
44
45
46
47
48
49
50
51
52
53
54
55
56
57
58
59
60
61
62
63
64
65
66
67
68
69
70
71
72
73
74
75
76
77
78
79
80
81
82
83
84
85
86
87
88
89
90
91
92
93
94
95
96
97
98
99
100
101
102
103
104
105
106
107
108
109
110
111
112
113
114
115
116
117
118
119
120
121
122
123
124
125
126
127
128
129
130
131
132
133
134
135
136
137
138
139
140
141
142
143
144
145
146
147
148
149
150
151
152
153
154
155
156
157
158
159
160
161
162
163
164
165
166
167
168
169
170
171
172
173
174
175
176
177
178
179
180
181
182
183
184
185
186
187
188
189
190
191
192
193
194
195
196
197
198
199
200
201
202
203
204
205
206
207
208
209
210
211
212
213
214
215
216
217
218
219
220
221
222
223
224
225
226
227
228
229
230
231
232
233
234
235
236
237
238
239
240
241
242
243
244
245
246
247
248
249
250
251
252
253
254
255
256
257
258
259
260
261
262
263
264
265
266
267
268
269
270
271
272
273
274
275
276
277
278
279
280
281
282
283
284
285
286
287
288
289
290
291
292
293
294
295
296
297
298
299
300
301
302
303
304
305
306
307
308
309
310
311
312
313
314
315
316
317
318
319
320
321
322
323
324
325
326
327
328
329
330
331
332
333
334
335
336
337
338
339
340
341
342
343
344
345
346
347
348
349
350
351
352
353
354
355
356
357
358
359
360
361
362
363
364
365
366
367
368
369
370
371
372
373
374
375
376
377
378
379
380
381
382
383
384
385
386
387
388
389
390
391
392
393
394
395
396
397
398
399
400
401
402
403
404
405
406
407
408
409
410
411
412
413
414
415
416
417
418
419
420
421
422
423
424
425
426
427
428
429
430
431
432
433
434
435
436
437
438
439
440
441
442
443
444
445
446
447
448
449
450
451
452
453
454
455
456
457
458
459
460
461
462
463
464
465
466
467
468
469
470
471
472
473
474
475
476
477
478
479
480
481
482
483
484
485
486
487
488
489
490
491
492
493
494
495
496
497
498
499
500
501
502
503
504
505
506
507
508
509
510
511
512
513
514
515
516
517
518
519
520
521
522
523
524
525
526
527
528
529
530
531
532
533
534
535
536
537
538
539
540
541
542
543
544
545
546
547
548
549
550
551
552
553
554
555
556
557
558
559
560
561
562
563
564
565
566
567
568
569
570
571
572
573
574
575
576
577
578
579
580
581
582
583
584
585
586
587
588
589
590
591
592
593
594
595
596
597
598
599
600
601
602
603
604
605
606
607
608
609
610
611
612
613
614
615
616
617
618
619
620
621
622
623
624
625
626
627
628
629
630
631
632
633
634
635
636
637
638
639
640
641
642
643
644
645
646
647
648
649
650
651
652
653
654
655
656
657
658
659
660
661
662
663
664
665
666
667
668
669
670
671
672
673
674
675
676
677
678
679
680
681
682
683
684
685
686
687
688
689
690
691
692
693
694
695
696
697
698
699
700
701
702
703
704
705
706
707
708
709
710
711
712
713
714
715
716
717
718
719
720
721
722
723
724
725
726
727
728
729
730
731
732
733
734
735
736
737
738
739
740
741
742
743
744
745
746
747
748
749
750
751
752
753
754
755
756
757
758
759
760
761
762
763
764
765
766
767
768
769
770
771
772
773
774
775
776
777
778
779
780
781
782
783
784
785
786
787
788
789
790
791
792
793
794
795
796
797
798
799
800
801
802
803
804
805
806
807
808
809
810
811
812
813
814
815
816
817
818
819
820
821
822
823
824
825
826
827
828
829
830
831
832
833
834
835
836
837
838
839
840
841
842
843
844
845
846
847
848
849
850
851
852
853
854
855
856
857
858
859
860
861
862
863
864
865
866
867
868
869
870
871
872
873
874
875
876
877
878
879
880
881
882
883
884
885
886
887
888
889
890
891
892
893
894
895
896
897
898
899
900
901
902
903
904
905
906
907
908
909
910
911
912
913
914
915
916
917
918
919
920
921
922
923
924
925
926
927
928
929
930
931
932
933
934
935
936
937
938
939
940
941
942
943
944
945
946
947
948
949
950
951
952
953
954
955
956
957
958
959
960
961
962
963
964
965
966
967
968
969
970
971
972
973
974
975
976
977
978
979
980
981
982
983
984
985
986
987
988
989
990
991
992
993
994
995
996
997
998
999
1000



CHAPTER 4

SEISMIC RESPONSE CHARACTERISTICS OF
MELOLAND ROAD OVERPASS

This chapter describes our investigation of the strong motion records measured at the Meloland Road Overpass (MRO) during the main shock of the 1979 Imperial Valley earthquake, and our resulting evaluation of the bridge's seismic response characteristics. The chapter is divided into four main sections. The first of these sections (Sec. 4.1) describes trends observed from direct examination of the basic time histories and Fourier amplitude spectra of the recorded motions at the MRO. The second section (Sec. 4.2) addresses the use of MODE-ID for identification of normal modes and pseudostatic response characteristics, including an overview of the basic modal identification procedures and a description of the combinations of input and response channels that were considered. Detailed descriptions and interpretations of the results of these various applications are provided in the remaining sections of this chapter (Secs. 4.3 and 4.4).

4.1 EXAMINATION OF RECORDED MOTIONS

Although the major emphasis of this evaluation of dynamic response characteristics of the MRO is the identification of pseudostatic and normal mode parameters, there is much that can first be learned from a direct examination of the time histories and Fourier amplitude spectra of the recorded motions at the MRO. Such an examination has been undertaken to indicate basic response characteristics of the bridge, and also to provide information for planning the subsequent modal identification calculations and for interpreting their results.

The remainder of this section is divided into three parts that address the bridge's transverse response characteristics (Sec. 4.1.1), vertical response characteristics (Sec. 4.1.2),



and longitudinal response characteristics (Sec. 4.1.3). The locations of the various acceleration response channels that are referred to in these discussions are shown in Figure 4-1.

4.1.1 TRANSVERSE RESPONSE CHARACTERISTICS

The transverse response characteristics of the MRO are indicated by acceleration, velocity, and displacement histories of the transverse motions measured on or near the bridge, Fourier amplitude spectra of these motions, and tabulations of peak response. Trends from examination of these data are described in the paragraphs that follow for the embankments and free field (Sec. 4.1.1.1), for the bridge abutments and the base of its central pier (Sec. 4.1.1.2), and for the bridge deck (Sec. 4.1.1.3).

4.1.1.1 Free-Field and Embankment Response

The time variation of the transverse motions measured at the two embankments are seen from Figure 4-2 to be generally similar to each other and to the free field. However, the amplitudes of the embankment motions are somewhat greater than those of the free field, particularly for accelerations (Table 4-1), and the embankment motion time histories exhibit a greater high frequency content. The strongest segment of these motions occurs over the time interval extending from about 2.5 sec to 10 sec after the start of the shaking.

The frequency content of the transverse motions measured at the free field and in the embankments is represented by the Fourier amplitude spectra provided in Figure 4-3. These spectra show that both the free-field and embankment motions have a predominant frequency of about 0.5 Hz (period = 2.0 sec). In addition, the embankment motions are seen to be amplified relative to the free field in the 1-to-2 Hz range (period range of 0.5 sec to 1.0 sec). At higher frequencies, neither the embankments nor the free-field exhibit a significant response.

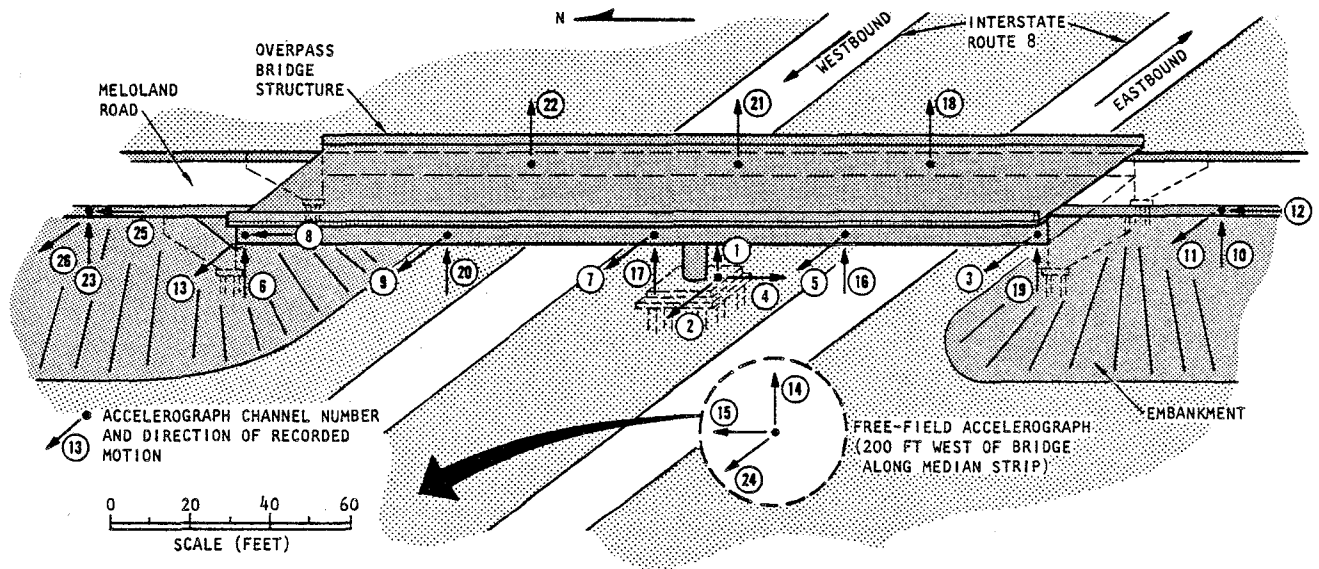
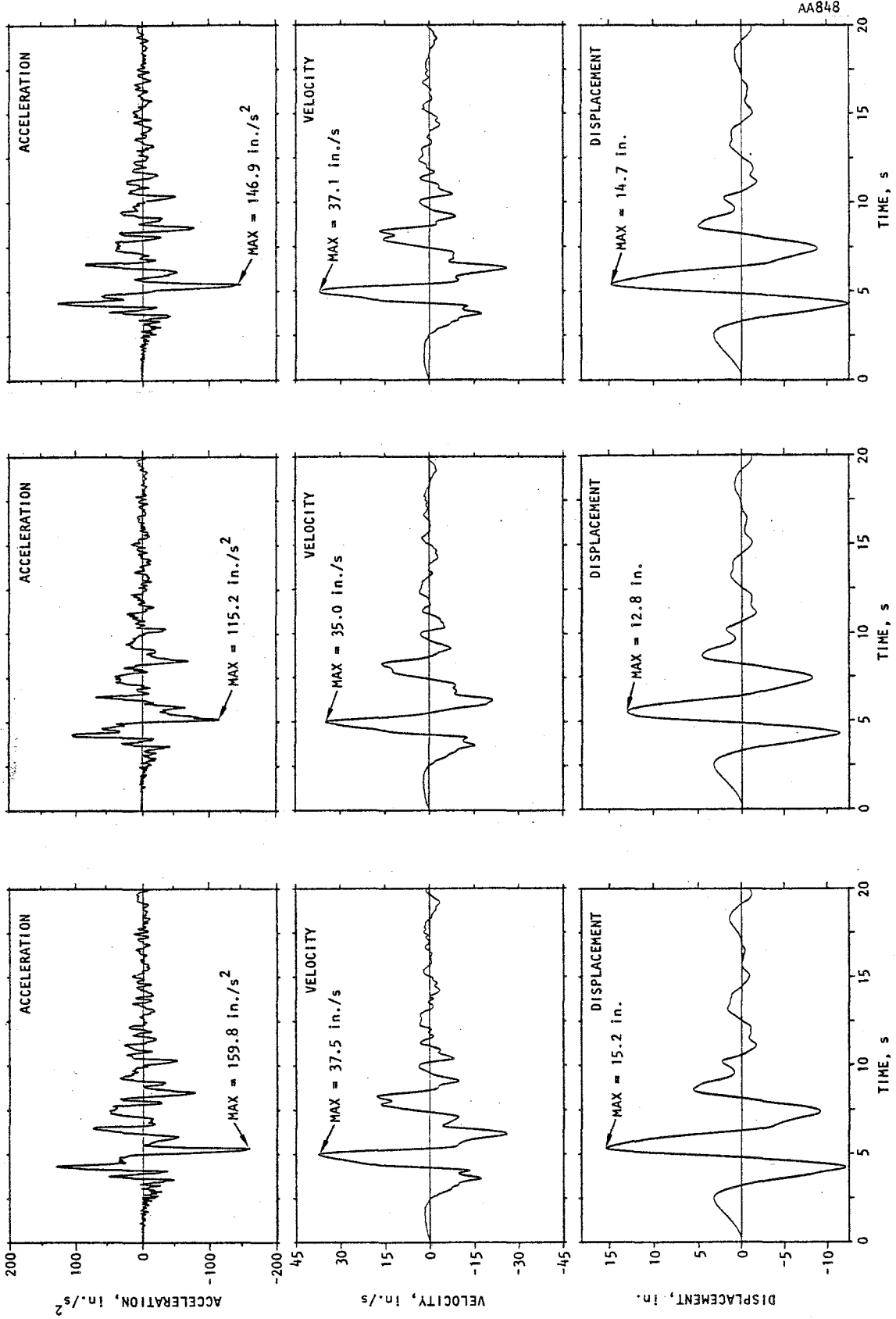


FIGURE 4-1. MELOLAND ROAD OVERPASS CHANNEL LOCATIONS



(a) South embankment
(Channel 11)

(b) Free field
(Channel 24)

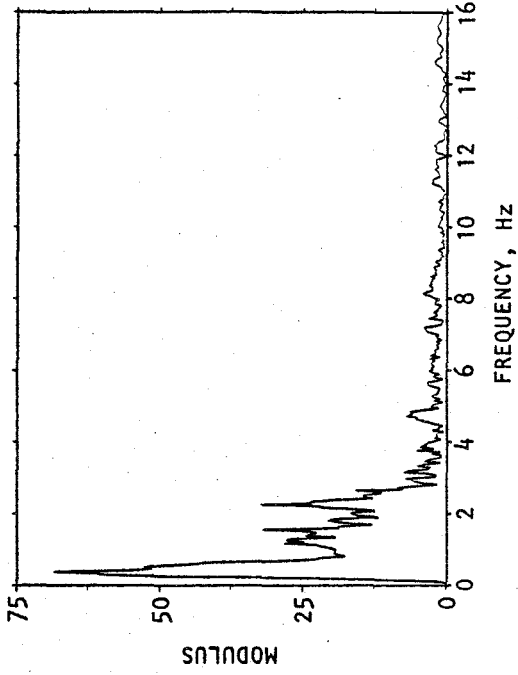
(c) North embankment
(Channel 26)

FIGURE 4-2. TRANSVERSE RESPONSE AT EMBANKMENTS AND FREE FIELD: TIME HISTORIES

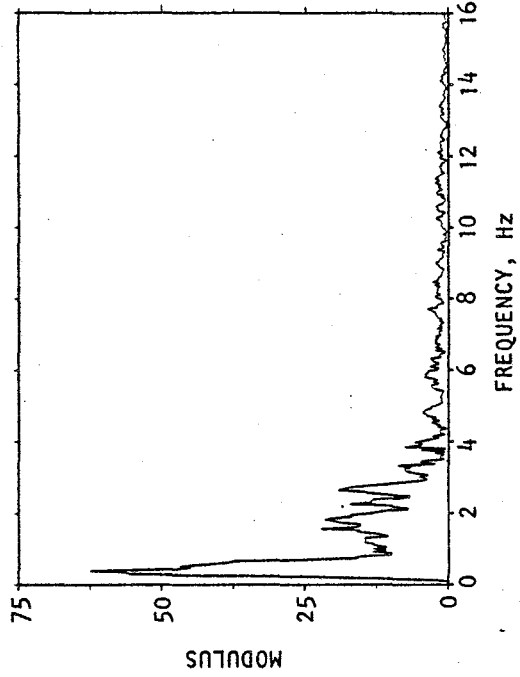


TABLE 4-1. PEAK MOTIONS RECORDED AT MRO

Direction	Channel		Peak Response		
	Location	Number	Acceleration IPS ²	Velocity IPS	Displacement in.
Transverse	Free Field	24	115.2	35.0	12.8
	South Embankment	11	159.8	37.5	15.2
	North Embankment	26	146.9	37.1	14.7
	South Abutment	3	181.1	34.3	14.7
	North Abutment	13	181.9	36.8	14.9
	Base of Central Pier	2	122.6	32.7	13.4
	Deck: Midlength of South Span	5	192.4	36.9	15.4
	Deck: Over Central Pier	7	190.4	36.7	15.2
	Deck: Midlength of North Span	9	187.6	37.0	15.1
Vertical	Free Field	14	75.1	10.5	2.7
	South Embankment	10	94.7	11.5	3.0
	North Embankment	23	85.0	10.9	3.0
	South Abutment	19	79.1	11.1	3.0
	North Abutment	6	69.4	11.0	3.1
	Base of Central Pier	1	67.6	11.2	2.9
	Deck: West Face				
	Midlength of South Span	16	188.3	16.0	3.6
	Over Central Pier	17	87.8	12.0	3.1
	Midlength of North Span	20	166.5	15.8	3.6
	Deck: East Face				
	Midlength of South Span	18	170.8	15.0	3.4
Over Central Pier	21	87.0	11.1	3.1	
Midlength of North Span	22	153.5	12.9	3.2	
Longitudinal	Free Field	15	116.7	28.1	6.5
	South Embankment	12	107.4	31.2	7.2
	North Embankment	25	126.7	31.0	6.8
	North Abutment	8	152.0	32.6	7.1
	Base of Central Pier	4	110.7	31.5	7.6

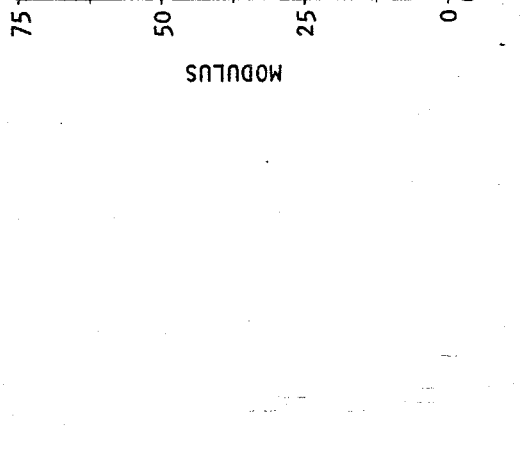


(a) South embankment (Channel 11)



AA849

(b) North embankment (Channel 26)



(c) Free field (Channel 24)

FIGURE 4-3. TRANSVERSE RESPONSE AT EMBANKMENTS AND FREE FIELD: FOURIER AMPLITUDE SPECTRA



4.1.1.2 Bridge Support Response

The basic characteristics of the measured transverse response of the bridge abutments and central-pier base can be evaluated through assessment of the time histories of the measured motions (Fig. 4-4), their corresponding Fourier amplitude spectra (Fig. 4-5), and tabulations of peak motions (Table 4-1). Comparisons of these bridge support motions with those previously described for the free field and embankments were also useful in this evaluation process.

The time history and peak motion data indicated above show that the transverse motions at the two abutments are generally similar to each other. They are stronger than the motions of the central-pier base, and exhibit larger accelerations and comparable velocities and displacements to those in the embankments. The transverse motion at the central-pier base is similar in amplitude and frequency content to that of the free field (Figs. 4-2b, 4-3c), indicating that soil/structure interaction does not have a strong effect on these particular motions. The strong shaking segment of the transverse motions at each of the bridge supports extends from about 2.5 sec to about 10 sec after the start of the shaking, and is comparable in duration to that previously observed for the embankments and free field.

Examination of the Fourier amplitude spectra from Figures 4-3 and 4-5 shows that the transverse response of the abutments at low frequencies (less than about 2 Hz) is generally comparable to that of the embankments. However, at a frequency of about 2.5 Hz (period of about 0.4 sec), the transverse motions of the abutments are substantially amplified relative to those of the embankments, the central-pier base, and the free field. This amplified abutment response is an important transverse response characteristic of the bridge and, in fact, is shown from the modal identification results presented later in this chapter to correspond to a significant transverse response mode of the MRO (Sec. 4.4).

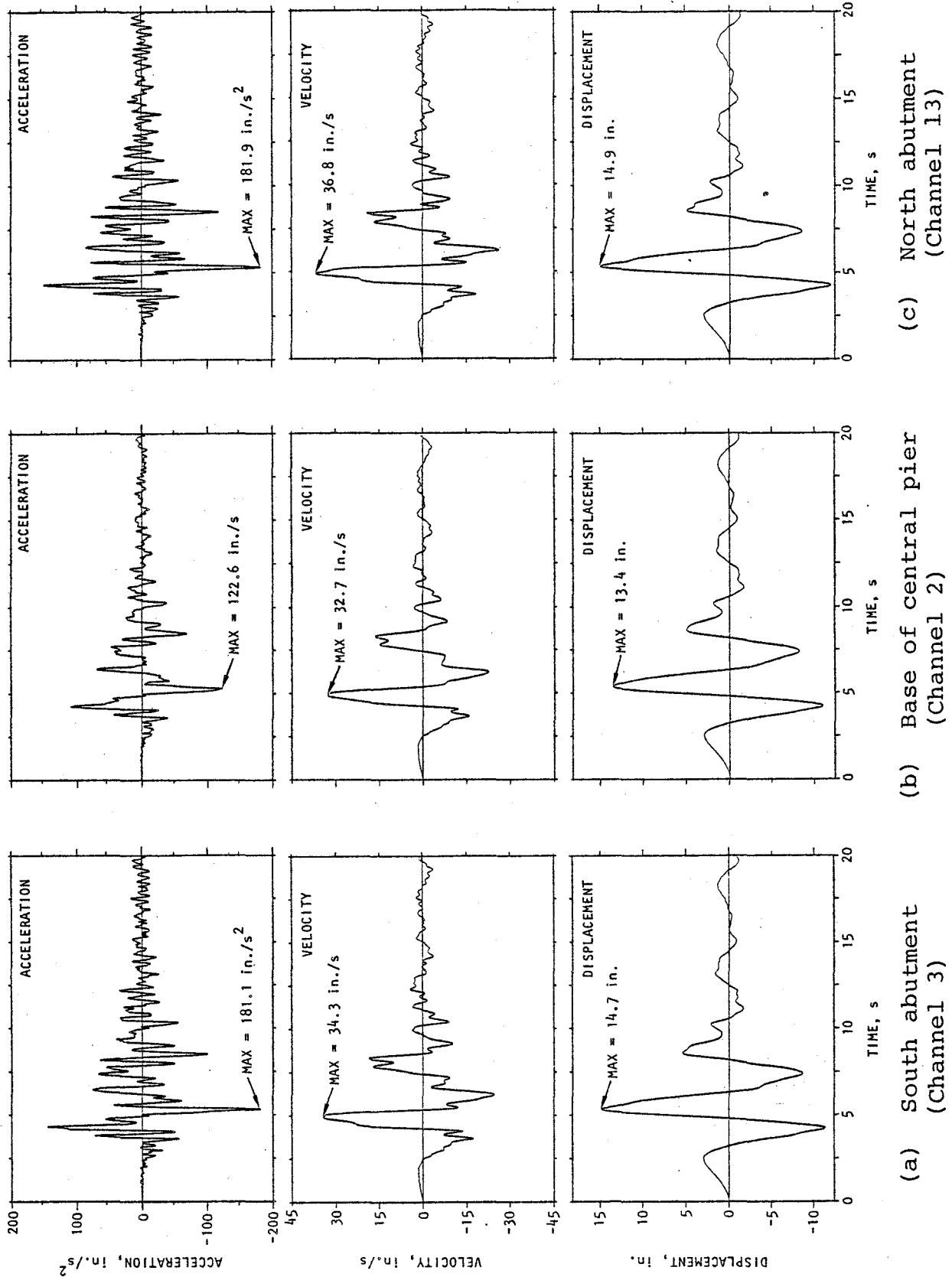
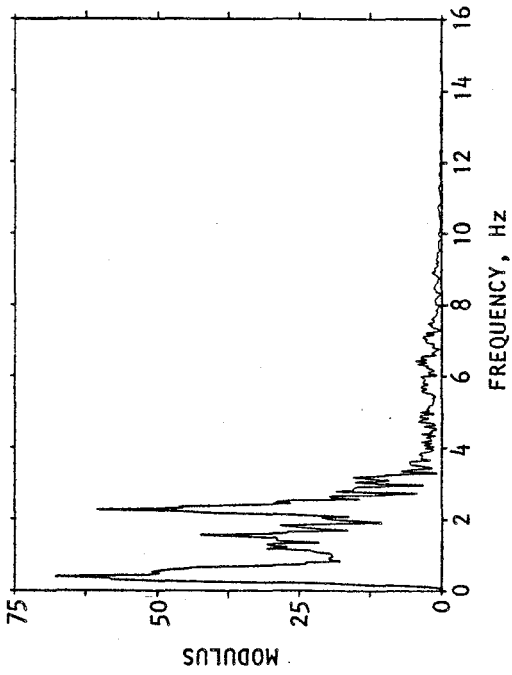
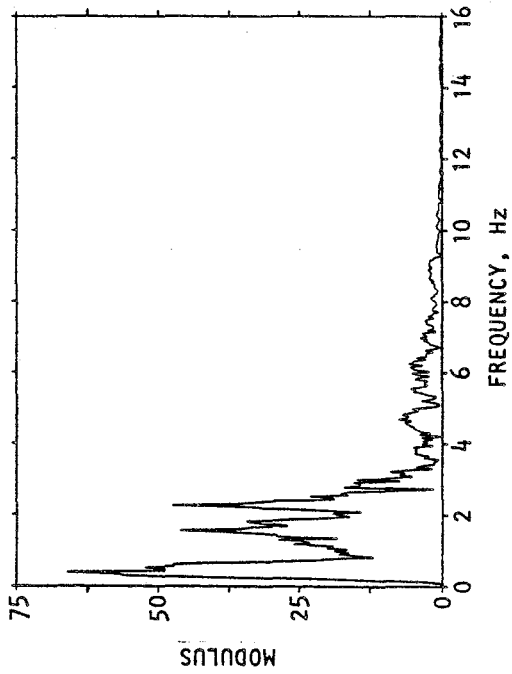


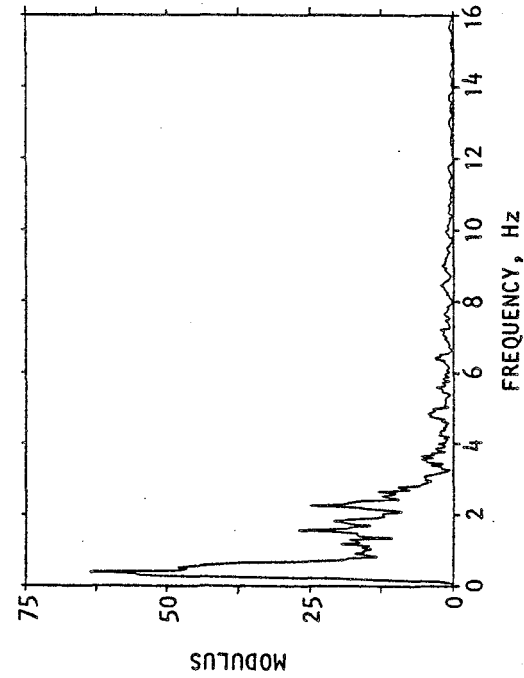
FIGURE 4-4. TRANSVERSE RESPONSE AT BRIDGE SUPPORTS: TIME HISTORIES



(b) North abutment (Channel 13)



(a) South abutment (Channel 3)



(c) Base of central pier (Channel 2)

AA851

FIGURE 4-5. TRANSVERSE RESPONSE AT BRIDGE SUPPORTS: FOURIER AMPLITUDE SPECTRA



4.1.1.3 Bridge Deck Response

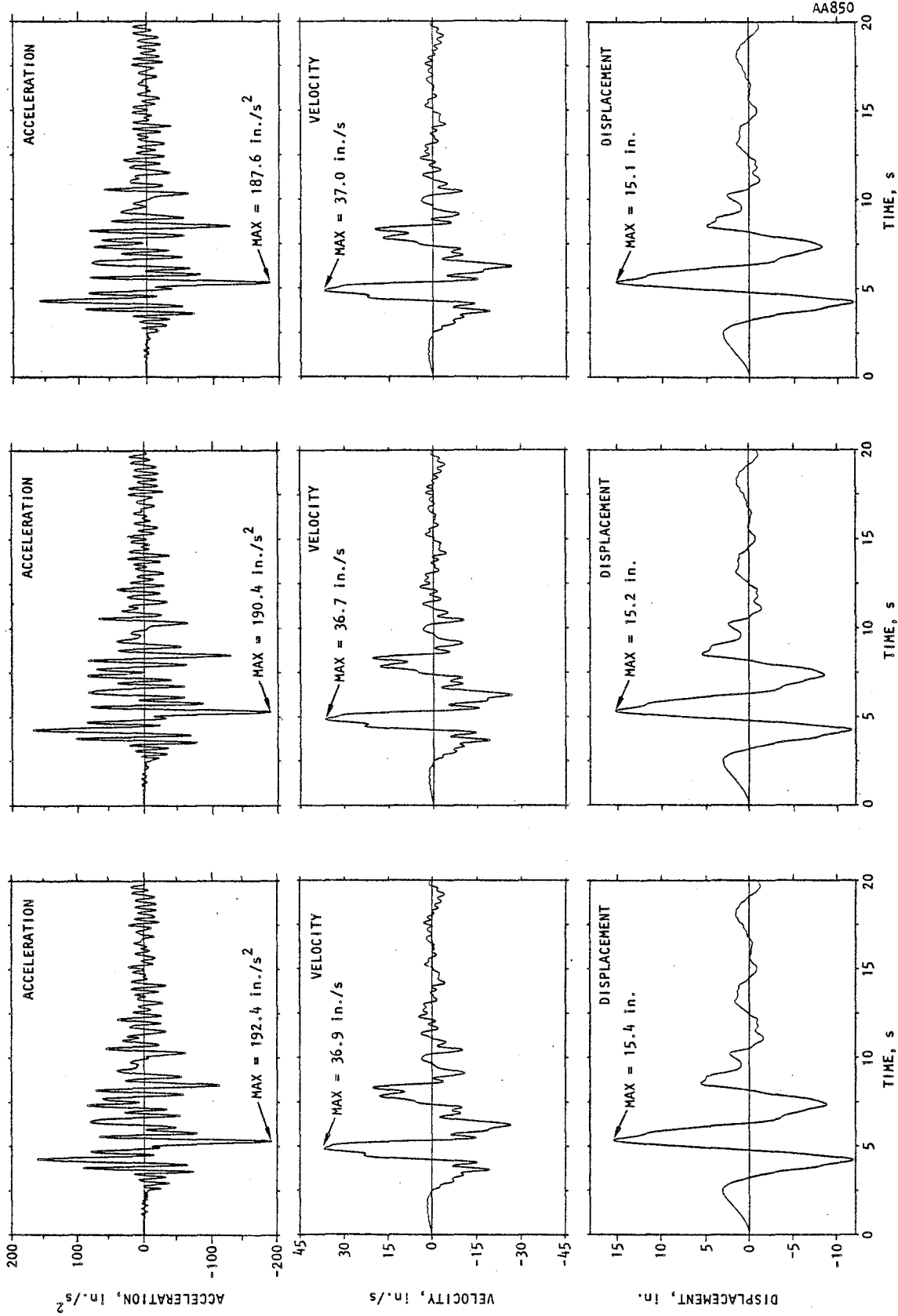
The transverse response of the bridge deck itself is indicated by plots of motion time histories along the length of the deck (Fig. 4-6), corresponding Fourier amplitude spectra (Fig. 4-7), and tabulations of peak motions (Table 4-1). These results show that the transverse motions measured at each deck response channel are quite comparable. Also, the time variation, frequency content, and peak values of the deck's transverse motions are very similar to those of the abutments, with only a slight further dynamic amplification. This shows that the deck's transverse response is essentially following the motions of the abutments - a trend that is further demonstrated by the modal identification results presented later in this chapter.

4.1.2 VERTICAL RESPONSE CHARACTERISTICS

The vertical response characteristics of the MRO are presented in a similar manner as for the transverse response. In this, motion time histories, Fourier amplitude spectra, and tabulations of peak response at the various vertical motion channels are examined to identify trends for the vertical response of the embankments and free field (Sec. 4.1.2.1), the bridge abutments and central pier base (Sec. 4.1.2.2), and the bridge deck (Sec. 4.1.2.3).

4.1.2.1 Free-Field and Embankment Response

The time variation of the vertical motions at the embankments and the free field is shown in Figure 4-8. This figure indicates that the vertical motion at these locations has considerably more high frequency content than does the transverse motion, although the duration of strong shaking is comparable. Also, the acceleration and velocity histories at the two embankments, while reasonably similar, exhibit more noticeable differences than do the corresponding transverse motions. The overall character of the time variation of the

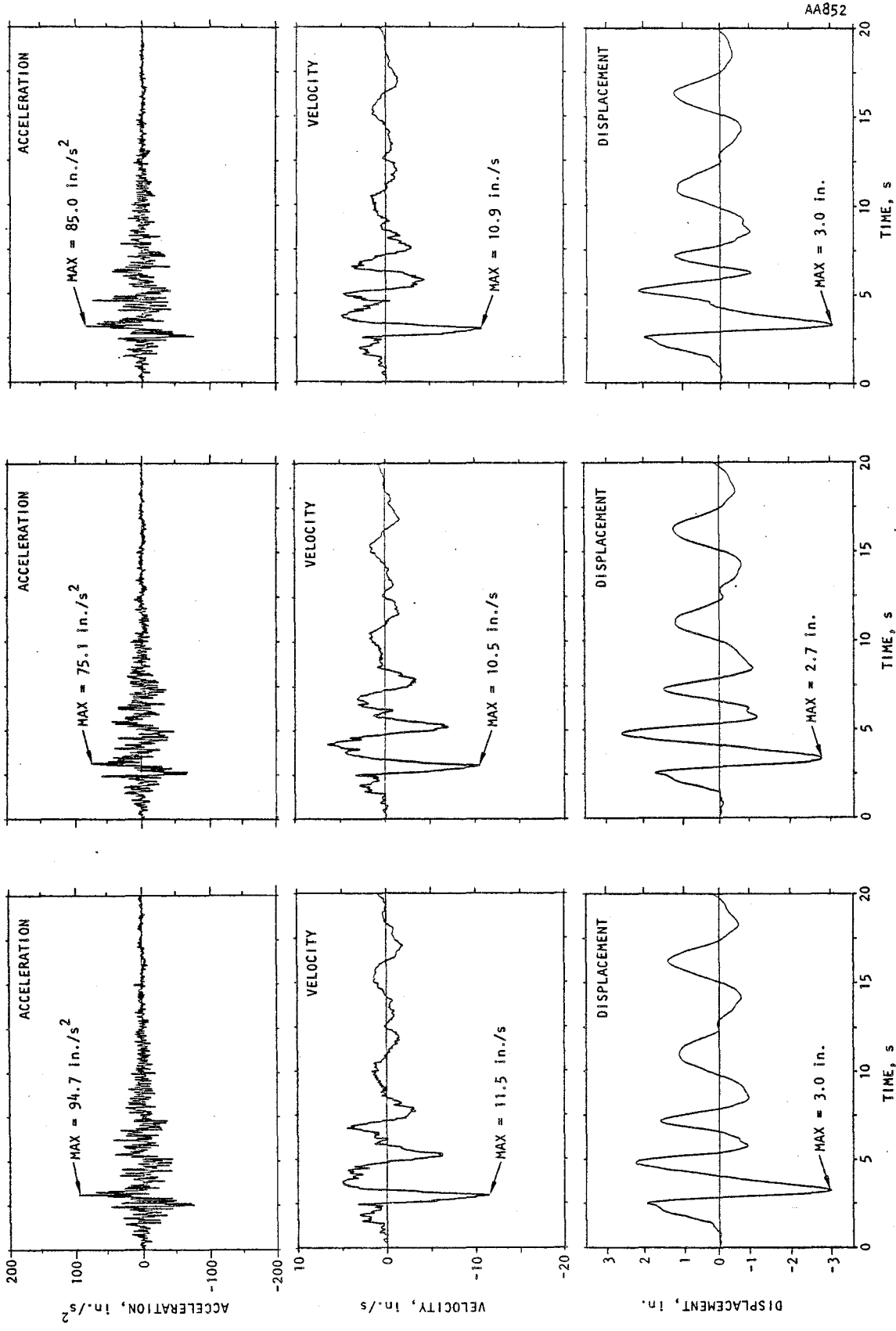


(a) Midlength of south span (Channel 5)

(b) Over central pier (Channel 7)

(c) Midlength of north span (Channel 9)

FIGURE 4-6. TRANSVERSE RESPONSE ALONG BRIDGE DECK: TIME HISTORIES



(a) South embankment
(Channel 10)

(b) Free field
(Channel 14)

(c) North embankment
(Channel 23)

FIGURE 4-8. VERTICAL RESPONSE AT EMBANKMENTS AND FREE FIELD: TIME HISTORIES



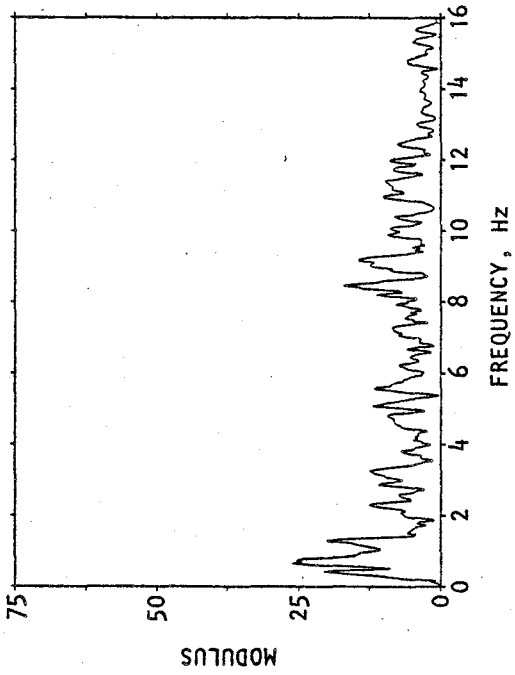
embankment motions is similar to that of the free field. The peak velocities and displacements at the embankments and the free field are nearly identical, and the peak accelerations at the embankments are amplified somewhat relative to those of the free field (see also Table 4-1).

The frequency content of these motions is indicated by the Fourier amplitude spectra provided in Figure 4-9. These spectra exhibit moderate peaks in both the free-field and embankment motions over the frequency range of about 0.5 to 1.5 Hz (period range of about 0.67 sec to 2.0 sec). Beyond that range, the embankment and free-field spectra are generally similar and of uniform overall intensity, although the embankment spectra exhibit some amplification relative to the free field in the 4.0 to 5.0 Hz range (period range of about 0.2 sec to 0.25 sec) and in the 8.5 to 9.5 Hz range (i.e., at periods around 0.11 sec).

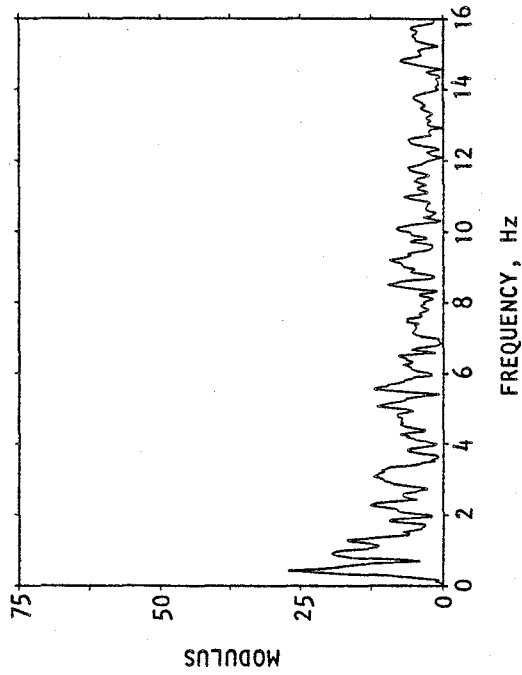
4.1.2.2 Bridge Support Response

The time histories of the vertical motions at the MRO abutments and central-pier base are provided in Figure 4-10. They show that the vertical motions at these locations are generally quite similar. The strong shaking segment of the vertical motion at the abutments and central-pier base is seen to be comparable to that observed for the embankments and free field, as is the general character of the time variation, the duration of strong shaking, and the peak values of these motions (also see Table 4-1).

The Fourier amplitude spectra for these bridge support motions are given in Figure 4-11. They exhibit the same moderate peaks in the 0.5 Hz to 1.5 Hz frequency range as was observed in the spectra for the embankment and free-field vertical motions. Otherwise, the spectra are generally uniform over a frequency range extending through about 10 Hz, with some minor peaks observed over the 2 to 4 Hz frequency range (0.25 sec to 0.5 sec period range).



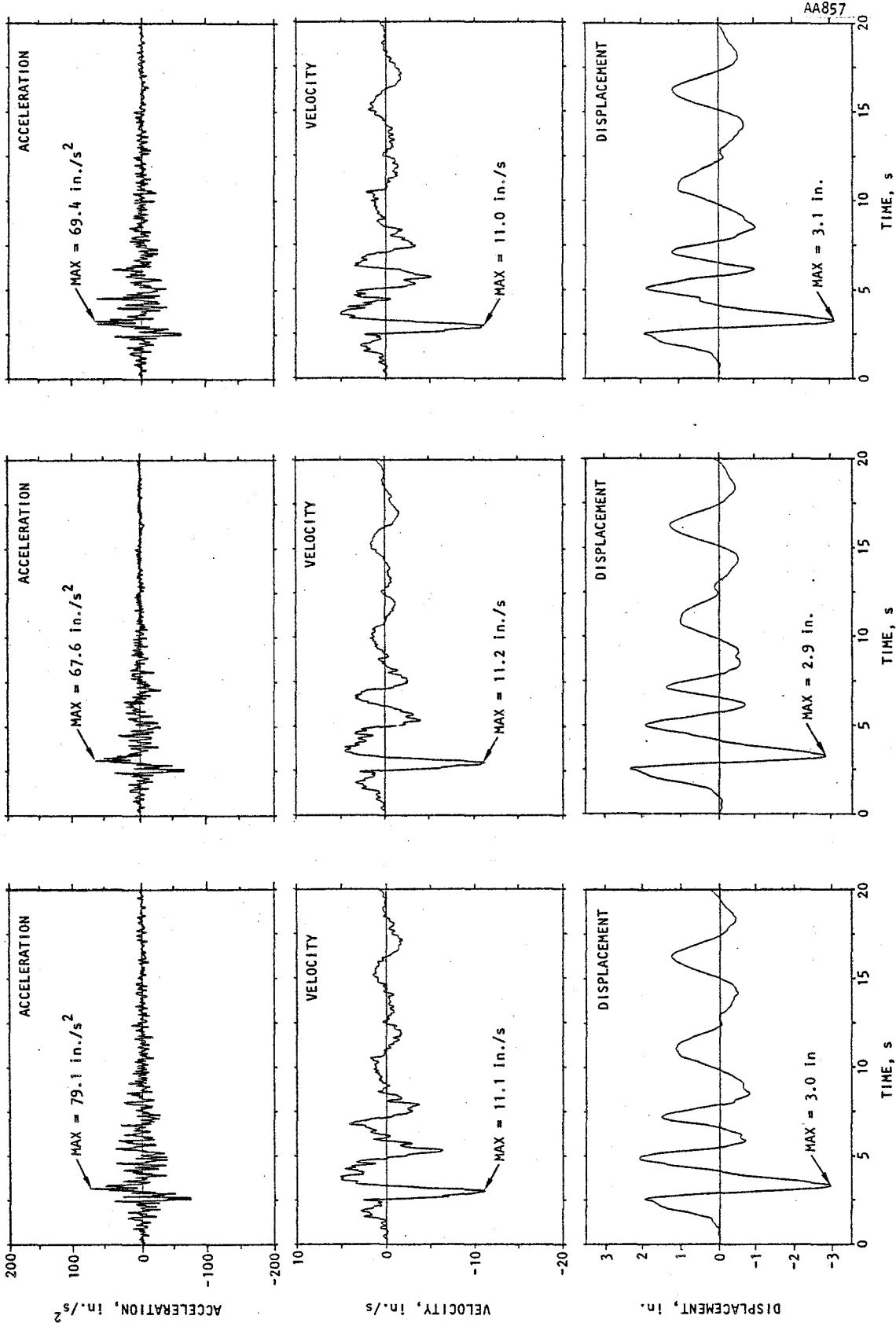
(a) South embankment (Channel 10)



(b) North embankment (Channel 23)

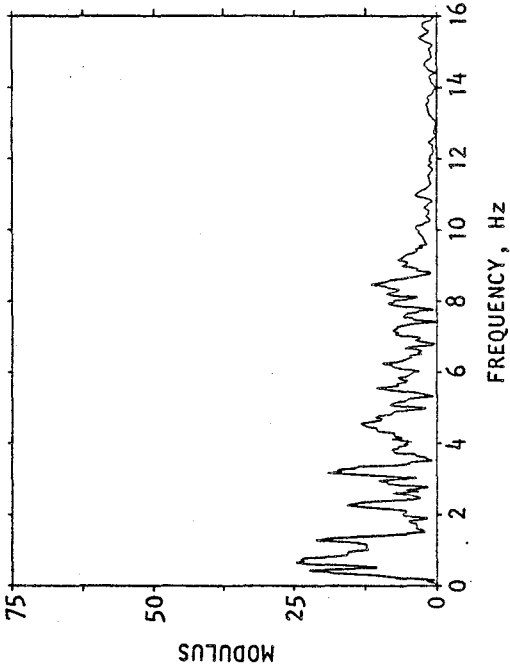
AA856

FIGURE 4-9. VERTICAL RESPONSE AT EMBANKMENTS AND FREE FIELD: FOURIER AMPLITUDE SPECTRA

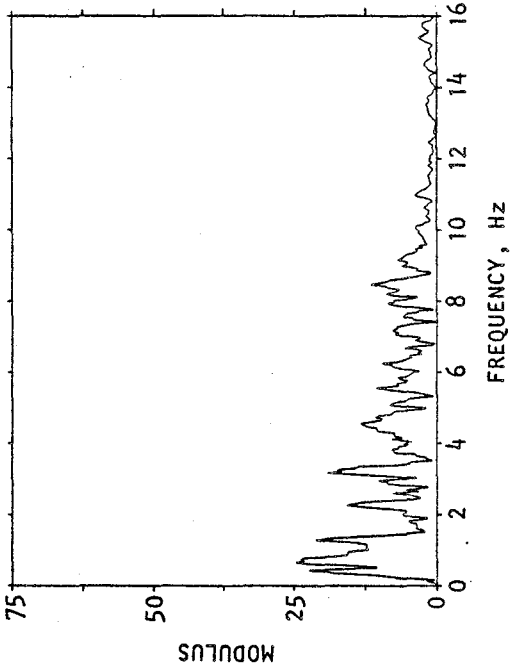


(a) South abutment (Channel 19) (b) Base of central pier (Channel 1) (c) North abutment (Channel 6)

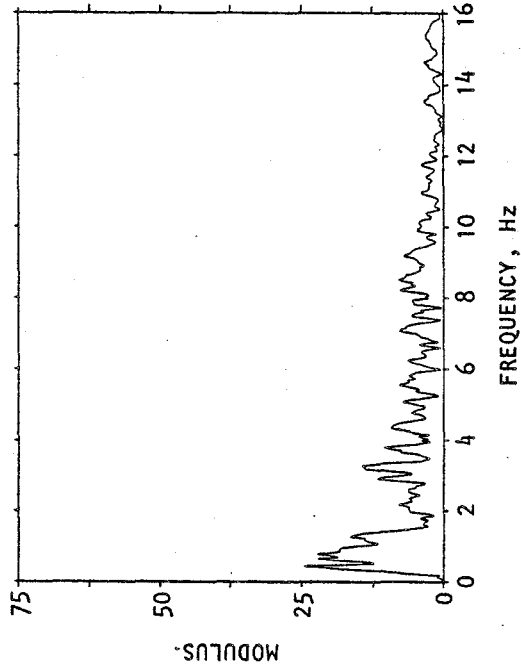
FIGURE 4-10. VERTICAL RESPONSE AT BRIDGE SUPPORTS: TIME HISTORIES



(a) South abutment (Channel 19)



(b) North abutment (Channel 6)



(c) Base of central pier (Channel 1)

AA858

FIGURE 4-11. VERTICAL RESPONSE AT BRIDGE SUPPORTS: FOURIER AMPLITUDE SPECTRA

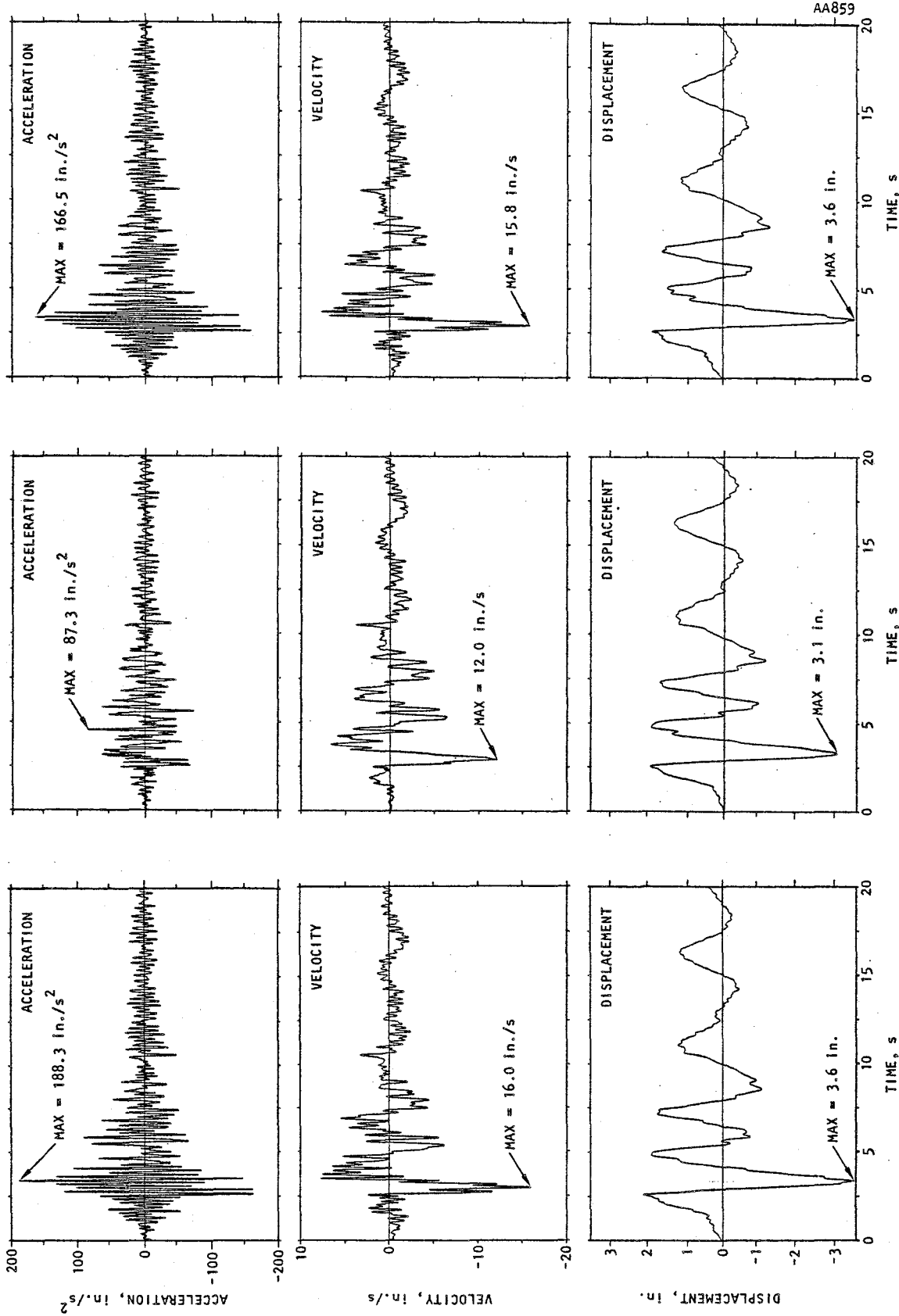


4.1.2.3 Bridge Deck Response

The time histories of vertical response along the west face and east face of the MRO bridge deck are provided in Figures 4-12 and 4-13, respectively. These time histories, together with the tabulations of peak motions provided in Table 4-1, indicate significant vertical response at the midlength of each span of the deck. These deck midspan motions are substantially greater than are the vertical motions measured at the central pier, abutments, embankments, and free field; in fact, they represent the dominant feature of the MRO's vertical seismic response. The deck's overall duration of vertical strong motion is generally comparable to that described earlier, although the particularly strong shaking at the midlength of each deck span occurs over a somewhat shorter time segment that extends from about 2.5 sec to about 5.0 sec after the start of the shaking.

The corresponding Fourier amplitude spectra of the vertical motions along the west face and east face of the bridge deck are shown in Figure 4-14. They indicate a very prominent peak in the spectral amplitudes of the motions measured at the midlength of each span, over a frequency range centered at about 4.5 Hz (i.e., over a period range centered at about 0.22 sec). This prominent frequency of response that occurs at these deck midspan locations is not exhibited by the vertical motions measured elsewhere at the bridge or within the free field, and is therefore a major vertical response characteristic of the deck spans themselves. It is noted that the modal identification results presented subsequently in this chapter show that this frequency corresponds to the dominant vertical response mode of the MRO (Secs. 4.3 and 4.4).

To further assess the nature of the bridge's vertical response, the vertical motions measured at each face of the bridge deck are expressed as the superposition of two components: (1) a vertical translation along the centerline of the deck's cross section; and (2) a rotation that represents the

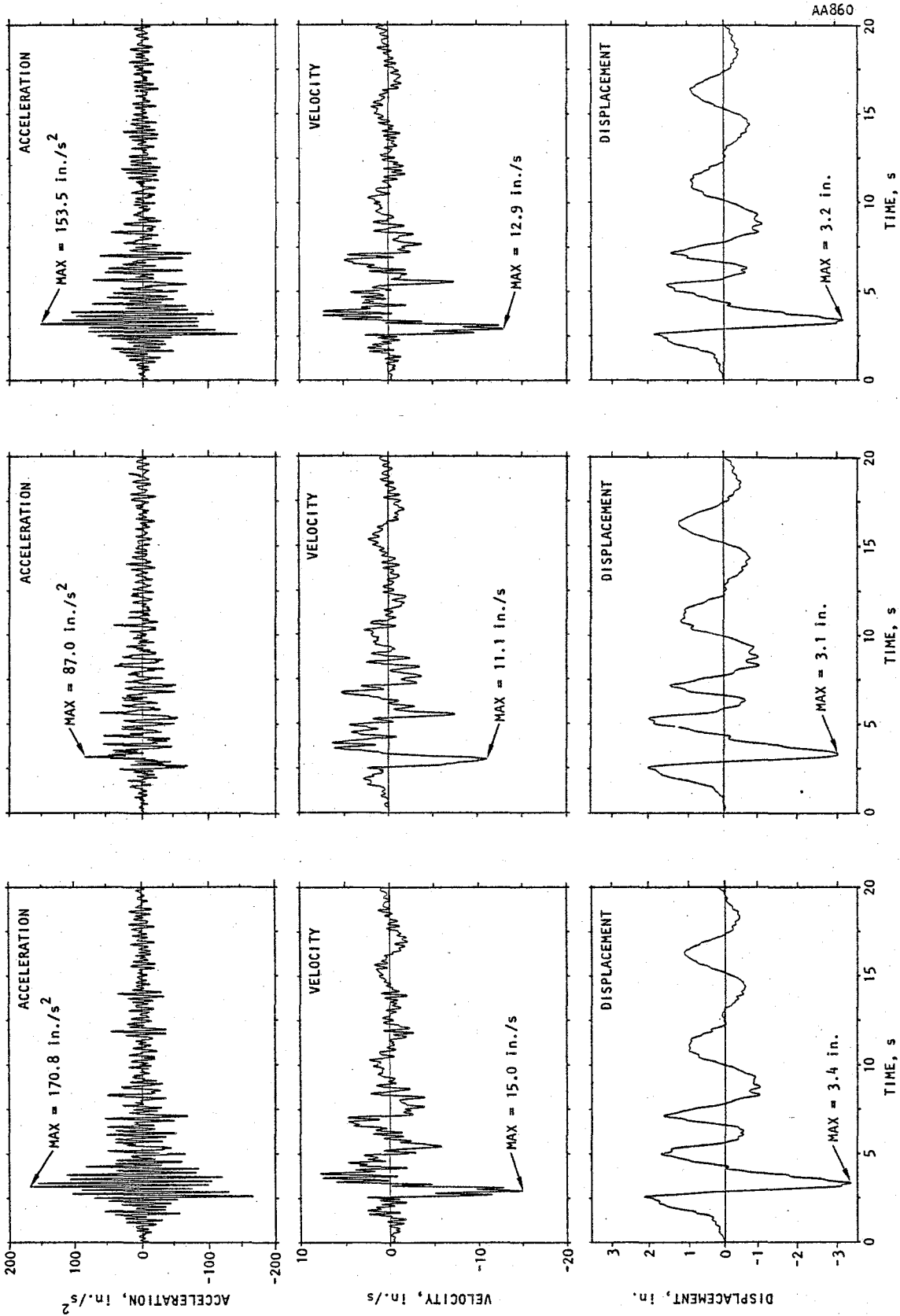


(a) Midlength of south span (Channel 16)

(b) Over central pier (Channel 17)

(c) Midlength of north span (Channel 20)

FIGURE 4-12. VERTICAL RESPONSE ALONG WEST FACE OF BRIDGE DECK: TIME HISTORIES

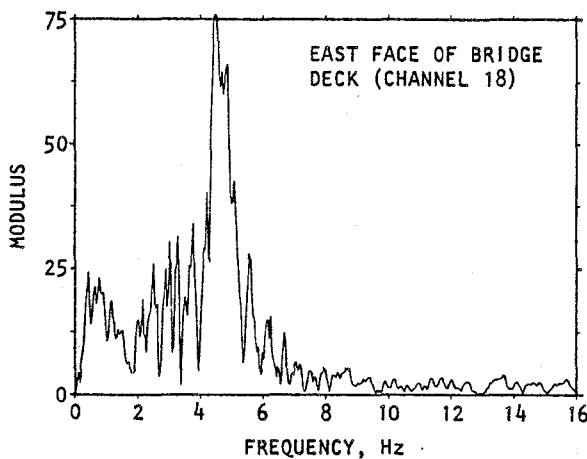
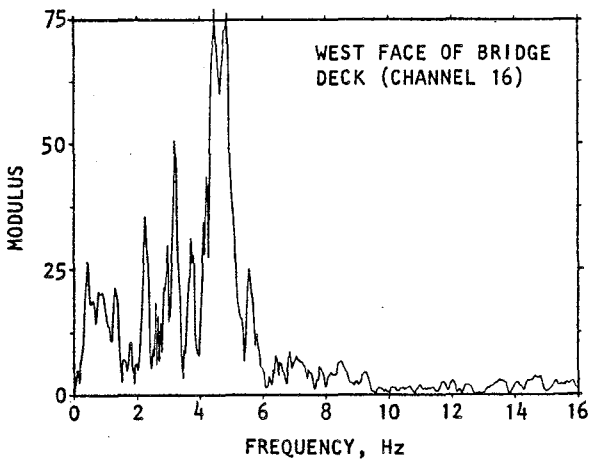


(a) Midlength of south span (Channel 18)

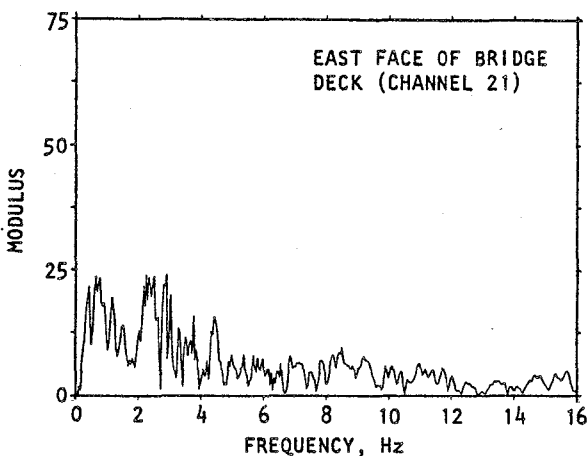
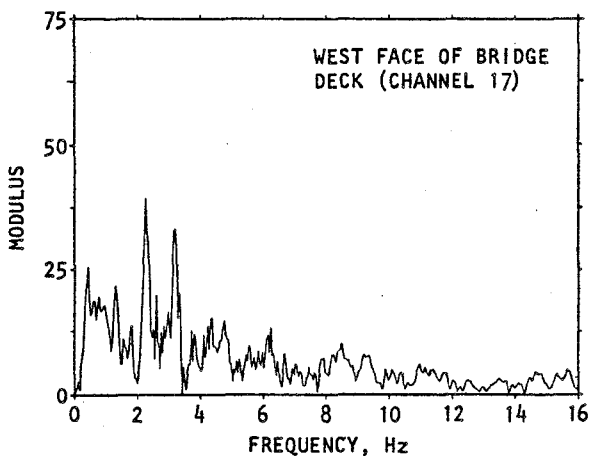
(b) Over central pier (Channel 21)

(c) Midlength of north span (Channel 22)

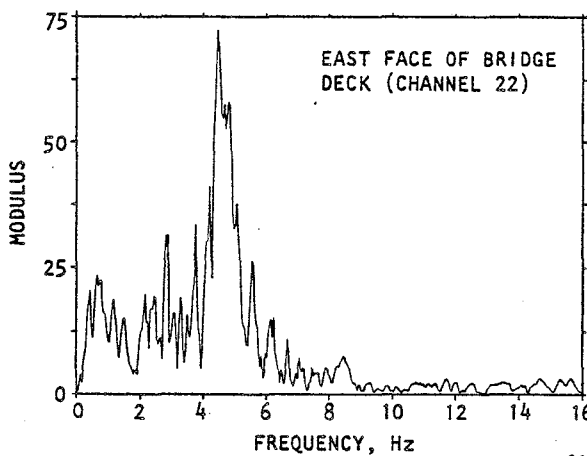
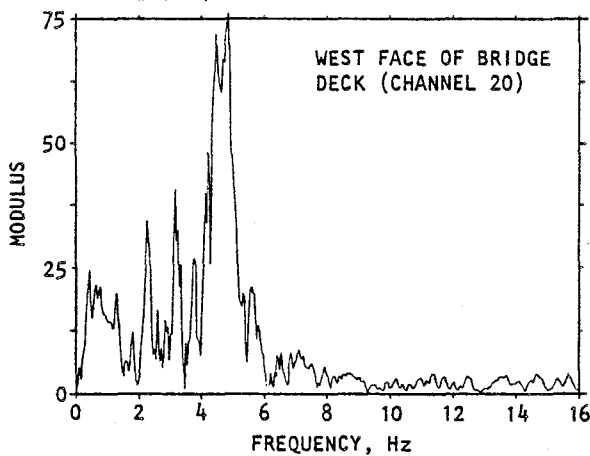
FIGURE 4-13. VERTICAL RESPONSE ALONG EAST FACE OF BRIDGE DECK: TIME HISTORIES



(a) Midlength of south span



(b) Over central pier



(c) Midlength of north span

AA861

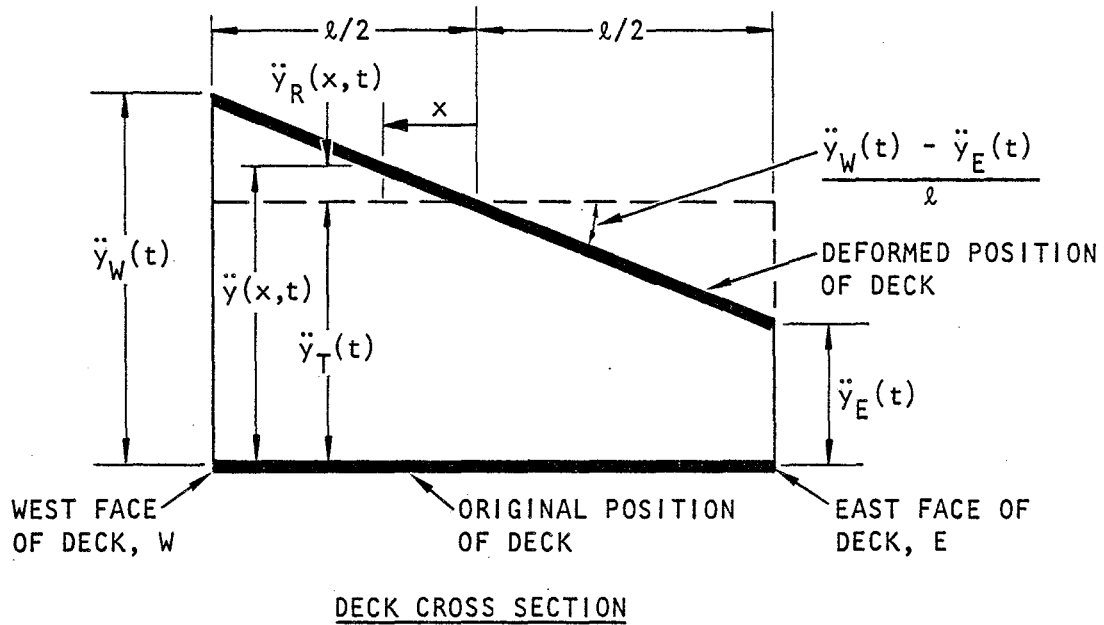
FIGURE 4-14. VERTICAL RESPONSE OF BRIDGE DECK: FOURIER AMPLITUDE SPECTRA



contribution of the deck's torsional response to the total vertical motion measured at each face of the deck (Fig. 4-15). Fourier amplitude spectra of these translational and rotational components are provided in Figure 4-16. They show that the primary contributor to the significant 4.5 Hz vertical response at the midlength of each deck span is the translational component; i.e., rotational (torsion) contributions to the deck's vertical motion at these locations and predominant frequency are small. However, this trend does not hold for the vertical motions measured at those deck channels located above the central pier, where the amplitudes of motion are much smaller and the above-indicated 4.5 Hz predominant frequency does not appear. At such locations, the relative contribution of the rotational component of the deck's vertical response is now relatively more important, although it is still smaller than the translational component. As expected, the Fourier amplitude spectrum of the deck translational component of vertical motion above the central pier closely follows that of the vertical motions measured at the base of the central pier (see Figs. 4-11c and 4-16b). Also, the small peak apparent at about 2.5 Hz in the deck's spectra for its rotational component of vertical motion will be shown later in this chapter to represent torsional motion inherent in the bridge's significant transverse response mode at this frequency (see Sec. 4.1.1.2).

4.1.3 LONGITUDINAL RESPONSE CHARACTERISTICS

The principal longitudinal response characteristics at the MRO can be defined from its measured response at the free-field, embankments, and bridge support locations; i.e., an array of longitudinal response accelerometers along the bridge deck is not necessary because of the deck's large stiffness in its longitudinal (axial) direction. For this reason, only a limited number of longitudinal response accelerometers have been deployed at the MRO. These instruments are located at the free field (Channel 15), the base of the central pier (Channel 4),



Total vertical acceleration of deck at location x and time t:

$$\ddot{y}(x,t) = \ddot{y}_T(t) + \ddot{y}_R(x,t)$$

where

$$\begin{aligned} \ddot{y}_T(t) &= \text{Translational component} = 0.5 [\ddot{y}_W(t) + \ddot{y}_E(t)] \\ \ddot{y}_R(x,t) &= \text{Rotational (torsion) component} = [\ddot{y}_W(t) - \ddot{y}_E(t)] \frac{x}{l} \end{aligned}$$

$$\left. \begin{array}{l} \ddot{y}_W(t) \\ \ddot{y}_E(t) \\ x \\ l \end{array} \right\} = \text{As defined in above sketch}$$

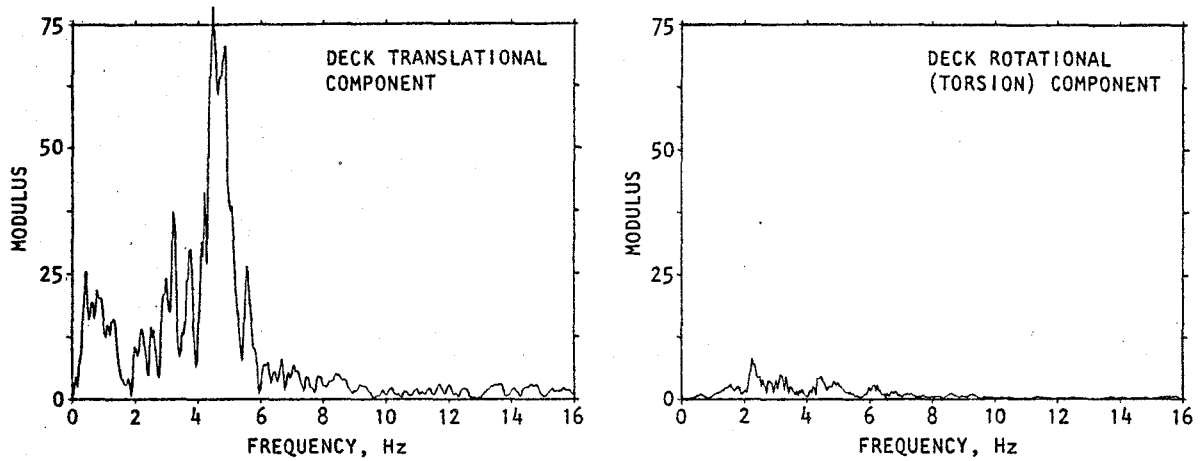
at $x = \frac{l}{2}$:

$$\ddot{y}(x,t) = \ddot{y}_W(t)$$

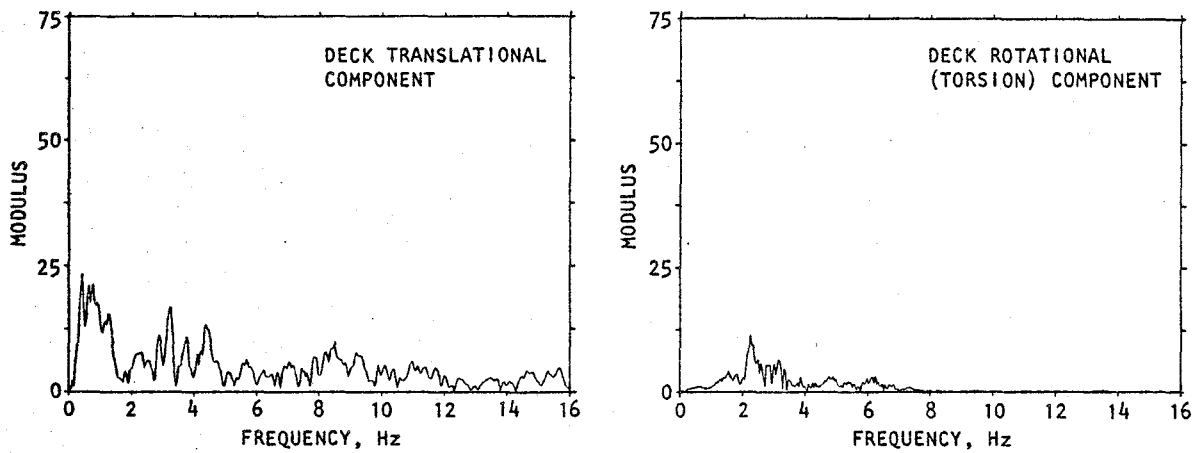
and

$$\left. \begin{array}{l} \ddot{y}_T = 0.5 [\ddot{y}_W(t) + \ddot{y}_E(t)] \\ \ddot{y}_R = 0.5 [\ddot{y}_W(t) - \ddot{y}_E(t)] \end{array} \right\} \begin{array}{l} \text{Translational and rotational} \\ \text{components depicted in} \\ \text{Figure 4-16} \end{array}$$

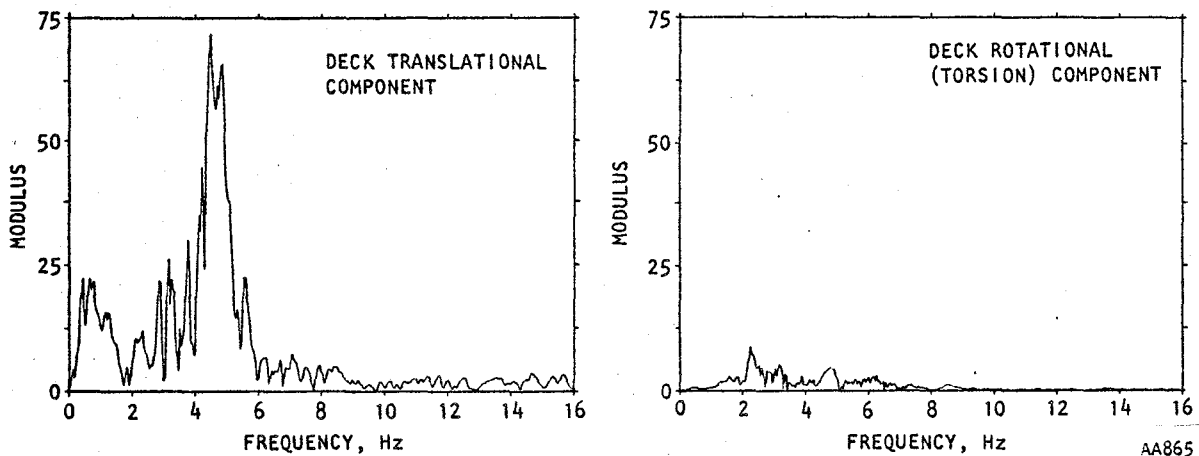
FIGURE 4-15. TRANSLATIONAL AND ROTATIONAL COMPONENTS OF VERTICAL RESPONSE OF BRIDGE DECK



(a) Midlength of south span



(b) Over central pier



(c) Midlength of north span

FIGURE 4-16. VERTICAL RESPONSE OF BRIDGE DECK: FOURIER AMPLITUDE SPECTRA OF DECK TRANSLATIONAL AND ROTATIONAL COMPONENTS



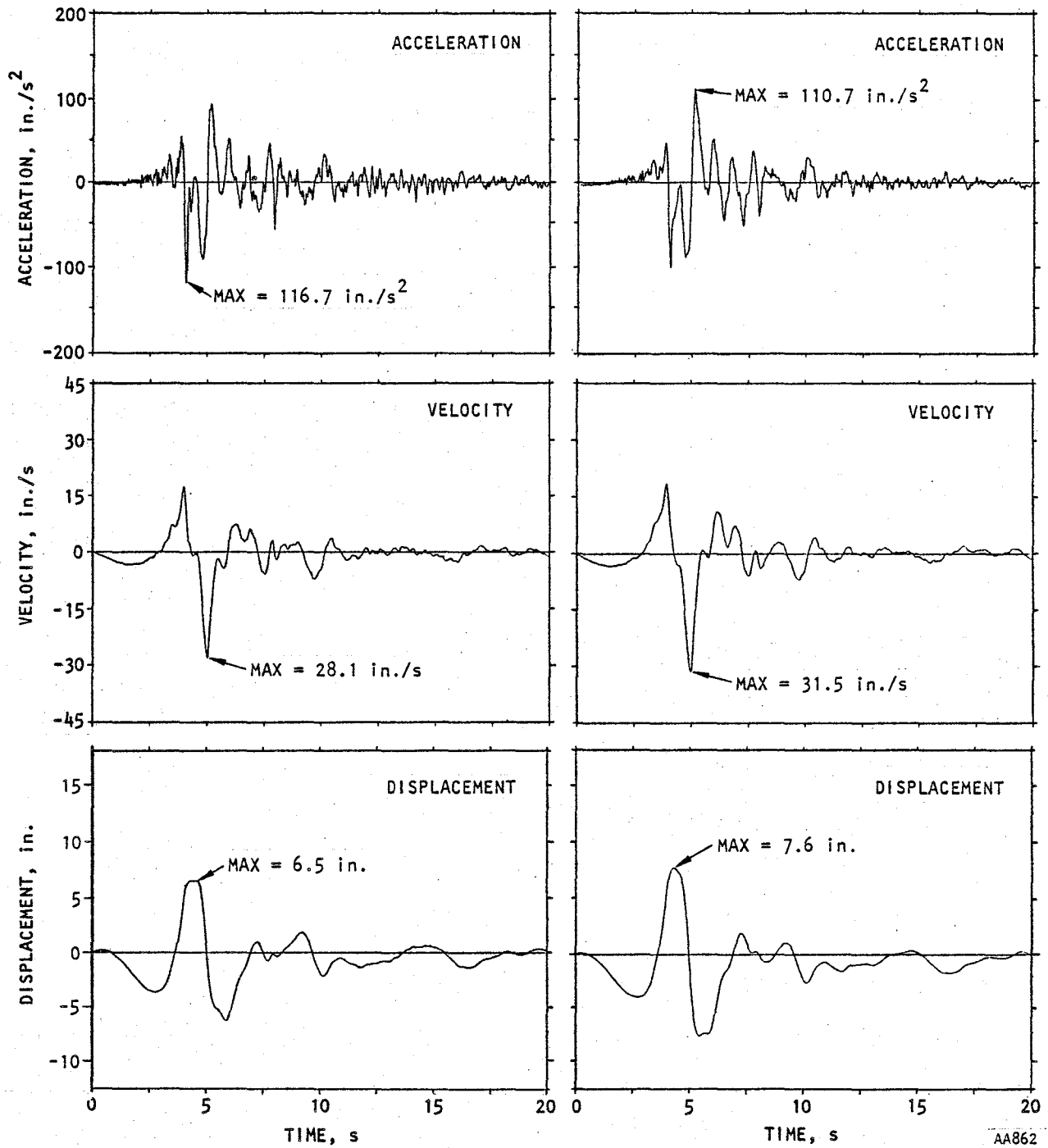
the south and north embankments (Channels 12 and 25), and the north abutment (Channel 8).

Motion time histories from these various channels are provided in Figures 4-17 and 4-18. They show that the time variations of the longitudinal motions at the embankments, central pier base, and north abutment are all generally comparable to each other and to the free field. These figures, together with Table 4-1, also show that the peak longitudinal displacements and velocities at the embankments and bridge supports are slightly amplified relative to those of the free field. The peak accelerations at the south embankment and central pier base locations are comparable to those of the free field whereas, at the north embankment and abutment, the peak accelerations are somewhat larger. In general, this array of longitudinal motions exhibits less intense shaking than the transverse motions at corresponding locations, and more intense shaking than the vertical motions.

Fourier amplitude spectra of these longitudinal motions are provided in Figure 4-19. They show that the principal longitudinal response at the bridge embankments, central pier base, and north abutment occurs at frequencies of less than 2.0 Hz (i.e., at periods longer than 0.5 sec), where the motions closely follow those of the free field. At higher frequencies, the longitudinal bridge response at the central pier base and south embankment is also comparable to that of the free field whereas, at the north embankment and abutment, moderate spectral amplifications relative to the free field are observed at frequencies of about 2.5 Hz and 3.3 Hz (i.e., at periods of about 0.4 sec and 0.3 sec).

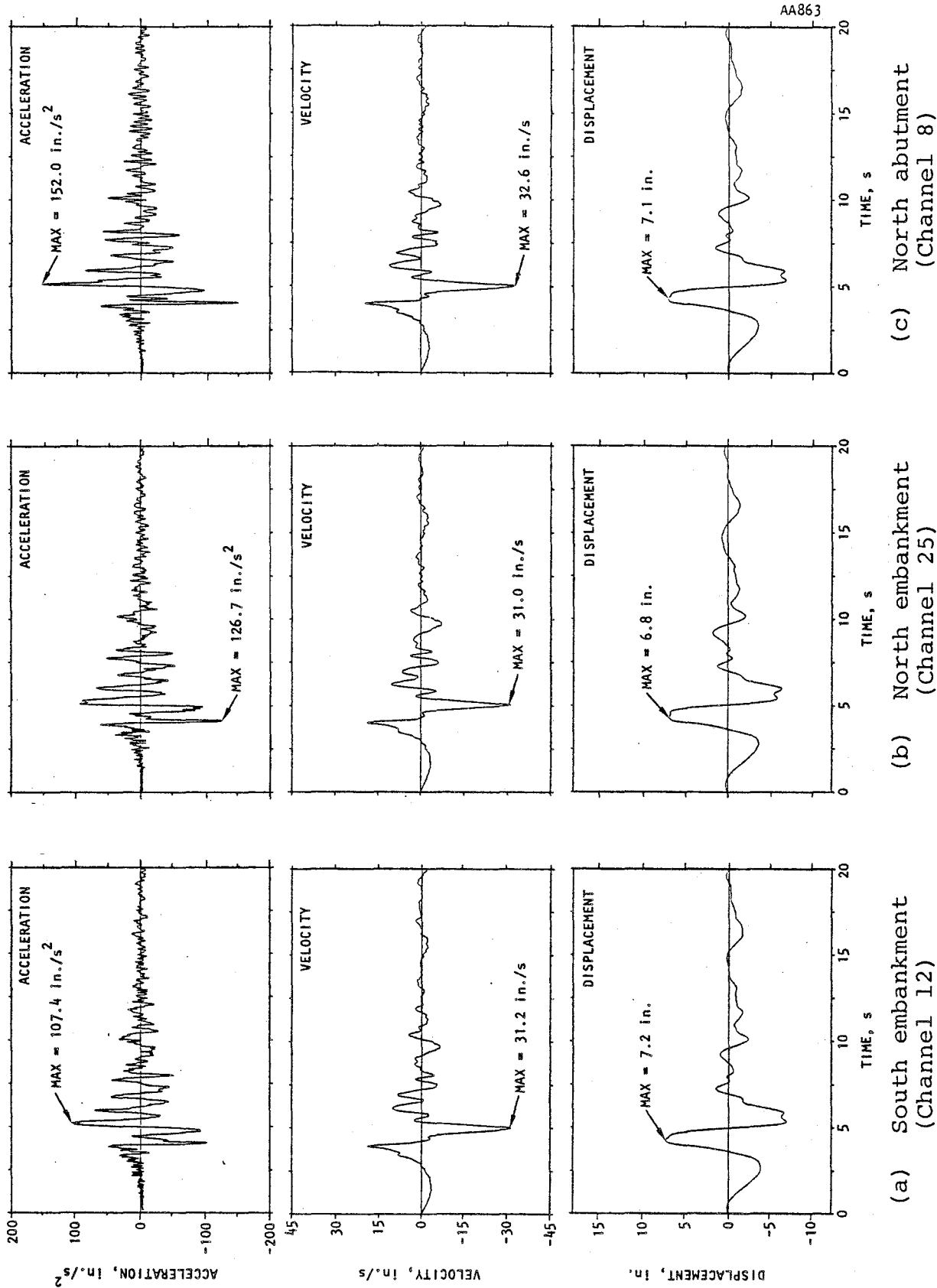
4.2 OVERVIEW OF MODAL IDENTIFICATION PROCESS

The above trends from our evaluation of the MRO's response time histories and Fourier amplitude spectra not only provide important insights into basic response characteristics of the MRO, but also serve as important background for a main emphasis



(a) Free field (Channel 15)

(b) Base of central pier
(Channel 4)FIGURE 4-17. LONGITUDINAL RESPONSE AT FREE FIELD AND
BASE OF CENTRAL PIER: TIME HISTORIES

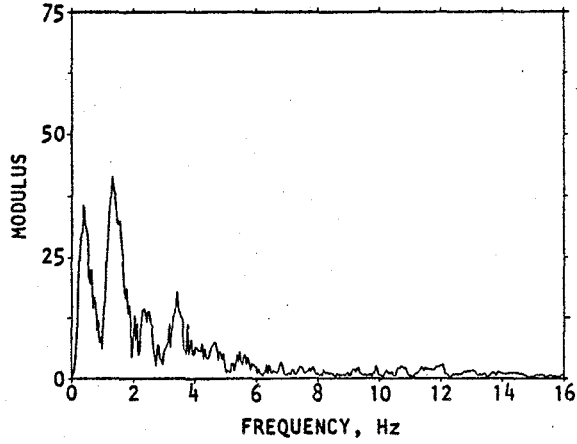


(a) South embankment (Channel 12)

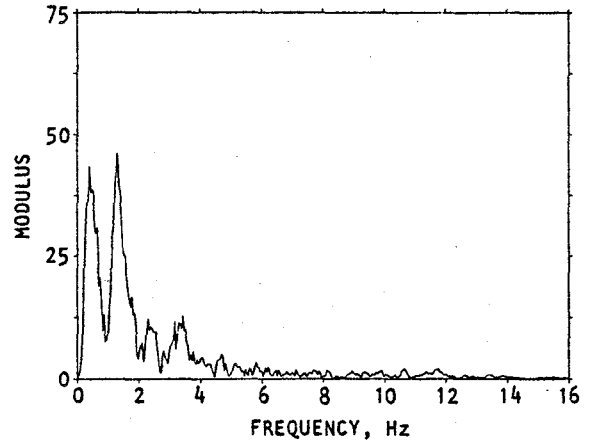
(b) North embankment (Channel 25)

(c) North abutment (Channel 8)

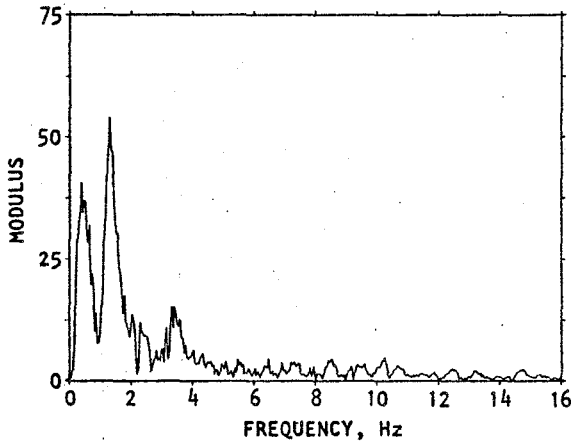
FIGURE 4-18. LONGITUDINAL RESPONSE AT EMBANKMENTS AND NORTH ABUTMENT: TIME HISTORIES



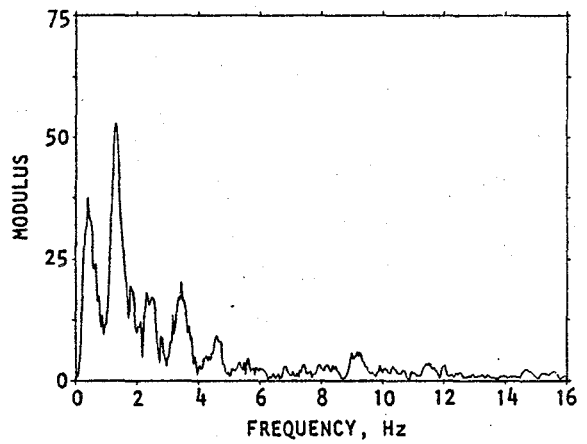
(a) Free field
(Channel 15)



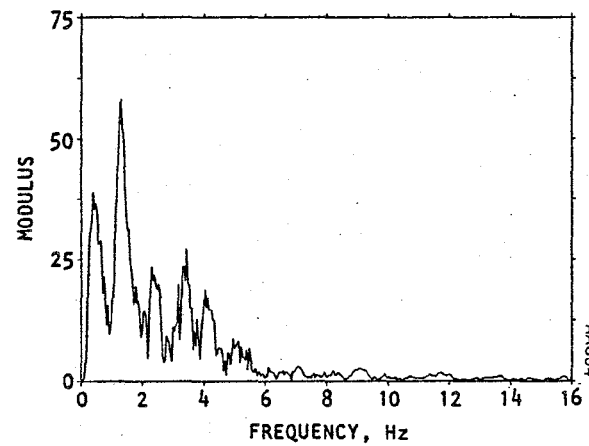
(b) Base of central pier
(Channel 4)



(c) South embankment
(Channel 12)




(d) North embankment
(Channel 25)



(e) North abutment (Channel 8)

FIGURE 4-19. LONGITUDINAL RESPONSE OF BRIDGE: FOURIER AMPLITUDE SPECTRA



of this research project: the identification of normal modes of response of the MRO. This modal identification process involves the application of the MODE-ID methodology developed under this project (Chapter 3) to the MRO's strong motion records as specially processed during the project (Chapter 2).

This section provides a general overview and background for this modal identification application. It describes the various combinations of MRO input and response channels that have been considered (Sec. 4.2.1), the initialization of the modal identification process (Sec. 4.2.2), and the general MODE-ID application procedure (Sec. 4.2.3). Following this, the results of the MODE-ID applications to the MRO data are provided in Sections 4.3 and 4.4. It is noted here that the modes identified for the MRO only incorporate the bridge's transverse and vertical response; i.e., the bridge's longitudinal response is not included in this modal identification application.

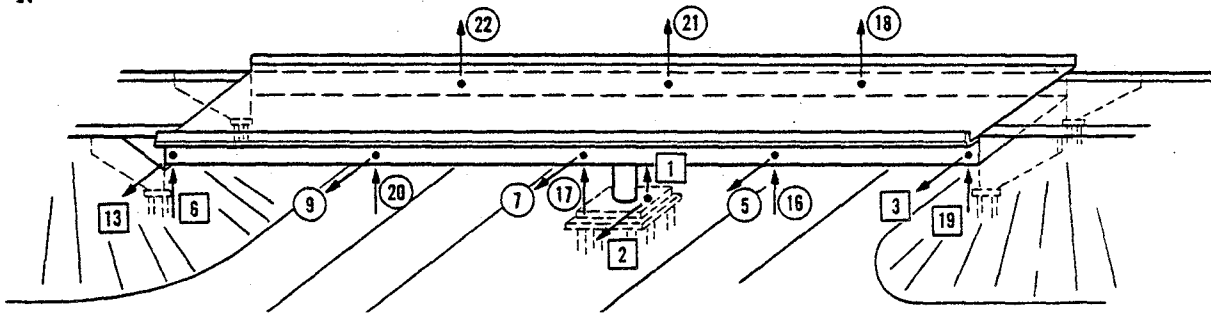
4.2.1 INPUT AND RESPONSE CHANNEL COMBINATIONS

The pseudostatic response and normal modes identified by MODE-ID are obviously dependent on the combination of input and response channels that is considered. As discussed in Chapter 3, the identified normal modes represent the fixed-base modal characteristics of the portion of the structure represented by the response channels, whereas the "static" contributions of the input (support) motions to the bridge response are represented through the pseudostatic influence matrix. In this project, two different combinations of input and response channels have been considered, in order to investigate dynamic characteristics of two alternative subsystems of the bridge.

The first combination, denoted as Case 1, considers the response channels to be from those instruments located along the road deck, and the input channels to be from the instruments at the abutments and central-pier base (Fig. 4-20a). This combination emphasizes the dynamic characteristics of a subsystem



N ←

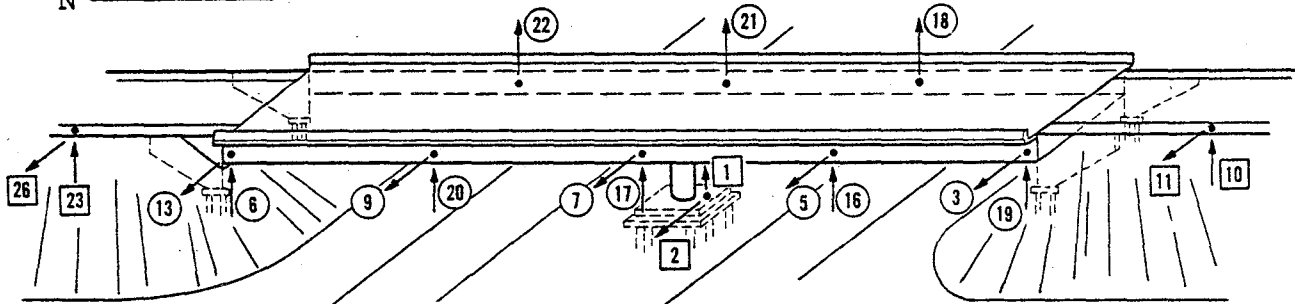


(a) Case 1

LEGEND:

- = INPUT CHANNELS
- = RESPONSE CHANNELS

N ←



(b) Case 2

LEGEND:

- = INPUT CHANNELS
- = RESPONSE CHANNELS

FIGURE 4-20. COMBINATION OF DESIGNATED INPUT AND RESPONSE CHANNELS CONSIDERED IN MRO MODAL IDENTIFICATIONS



consisting of the road deck and central pier, whose contributions to the overall bridge response are represented through the fixed-base normal modes that are identified. The pseudostatic influence matrix that is also identified from this Case 1 combination of channels represents the additional "static" effects of the abutments, embankments, central-pier foundation, and underlying soil medium on the overall bridge response.

In the second combination of input and response channels, denoted as Case 2, the response channels are from those instruments located along the road deck and at the abutments, and the input channels are from the instruments located on the embankments and at the base of the central pier (Fig. 4-20b). This combination of channels differs from that of Case 1 in that it emphasizes the dynamic characteristics of a subsystem that now includes the abutments and part of the embankments, as well as the road deck and the central pier; these dynamic characteristics are represented through the fixed-base normal modes identified from this Case 2 subset of measured motions. The identified pseudostatic influence matrix, on the other hand, now represents the "static" contributions of the portion of the embankments that extend beyond the embankment instruments, the foundation/soil system beneath the central-pier base, and the soil medium that underlies the embankments and the MRO.

4.2.2 INITIALIZATION PROCESS

Necessary input to the application of MODE-ID to the measured earthquake motions at the MRO consists of initial estimates of the MRO's significant modes of vibration. The direct interpretation of the MRO's measured motion time histories and corresponding Fourier amplitude spectra, as described in Section 4.1, represents a key set of results for this purpose. In addition, because of the importance of this step, several other initialization procedures have been applied under this project. These include the use of (1) transfer functions developed from the Fourier spectra of the measured



records; (2) sensitivity studies using simple analytical models of the bridge; and (3) application of a simplified single-input/single-output version of MODE-ID. These initialization procedures are described in the paragraphs that follow.

4.2.2.1 Transfer Functions from Fourier Spectra

One initialization approach used in this MRO application has involved "transfer functions" derived from Fourier spectra of a single input channel, $X(\omega)$, and response channel, $Y(\omega)$. Such "transfer functions," designated here as $H(\omega)$, have been developed for each of several input-channel/response-channel combinations according to the following expression*

$$H(\omega) = \frac{Y(\omega)}{X(\omega)} = H_r + iH_i \quad (4-1)$$

If we express $Y(\omega)$ and $X(\omega)$ in terms of their real and imaginary components, i.e.,

$$Y(\omega) = Y_r + iY_i \quad (4-2)$$

$$X(\omega) = X_r + iX_i$$

then it can be shown that

$$H_r = \frac{Y_r X_r + Y_i X_i}{X_r^2 + X_i^2} \quad (4-3)$$

$$H_i = \frac{Y_i X_r - X_i Y_r}{X_r^2 + X_i^2}$$

* This is not the actual transfer function between a single set of input and response channels, because the measured bridge response at any given channel is excited simultaneously by all of the input motions. Determination of the actual transfer function between any input and response channel would require suppression of all of the input motions except the designated one. However, the "transfer function" given by Equation 4-1 should still show pronounced peaks at the natural frequencies of lightly damped modes that are strongly excited by the earthquake.



Under this "transfer function" approach, initial estimates of the bridge modes are provided by identifying those frequencies where, for several different combinations of input and response channels, the amplitude of $H(\omega)$, denoted as

$$|H(\omega)| = \sqrt{H_r^2 + H_i^2} \quad (4-4)$$

consistently exhibits a predominant peak, and the phase angle of $H(\omega)$, denoted as

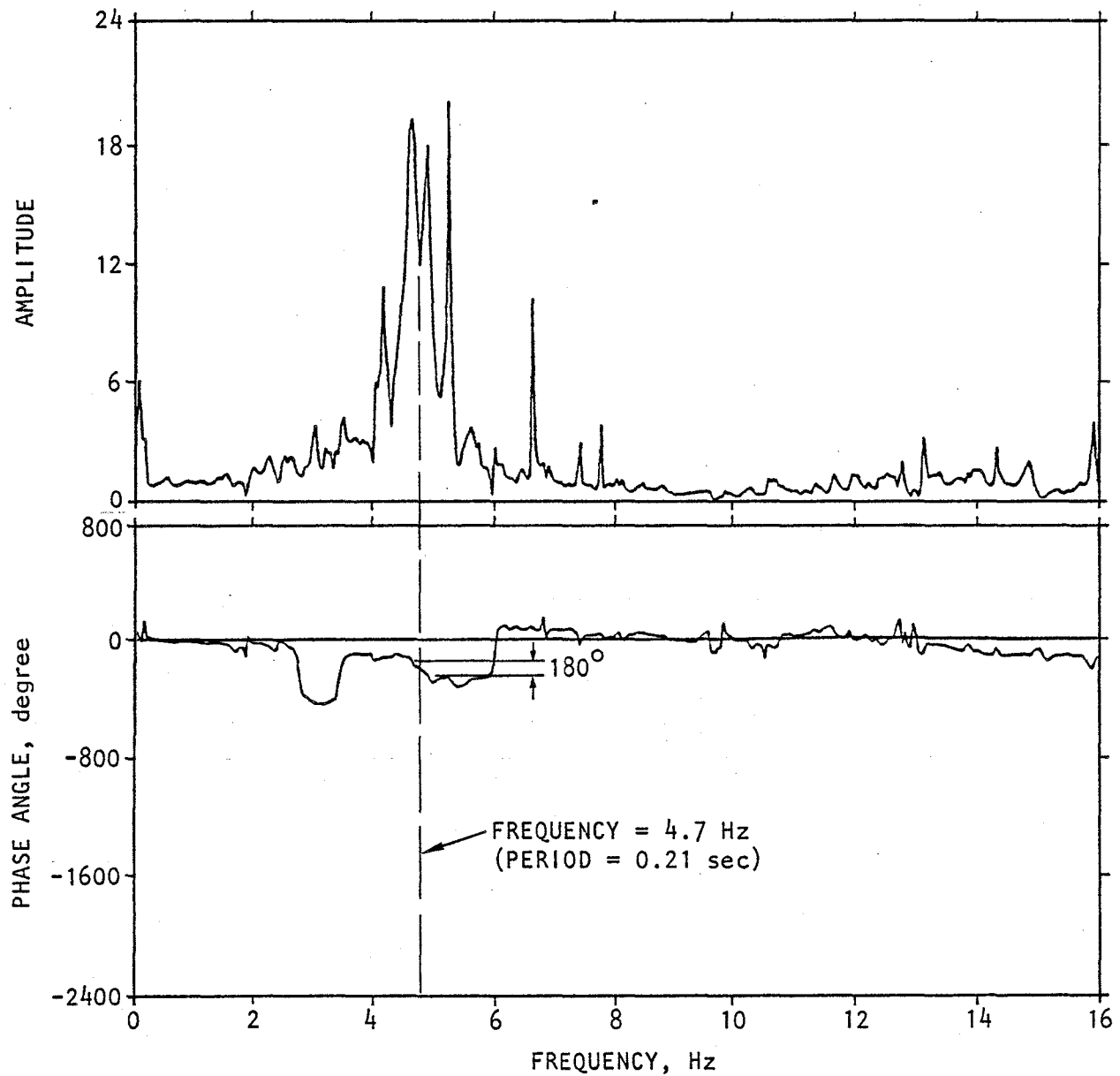
$$\phi(\omega) = \tan^{-1} \frac{H_i}{H_r} \quad (4-5)$$

consistently exhibits a 180-deg phase shift (Fig. 4-21). An estimate of the corresponding mode shape can be developed from plots of $|H(\omega)|$ for the various input-channel/response-channel combinations, taking account of whether the motions at the various locations are in phase or 180-deg out of phase. However, because of the approximations involved with this method and the complications caused by inherent noise in the strong motion data, such estimates should be interpreted as providing only qualitative representations of the actual mode shape. More reliable estimates of the mode shapes, and also the modal damping ratios, are obtained from the subsequent application of MODE-ID to the MRO's strong motion records (Secs. 4.3 and 4.4).

4.2.2.2 Sensitivity Studies Using Simple Analytical Models

Another initialization approach that has been used has involved simple analytical models of the bridge to compute mode shapes and frequencies. These computations have been carried out as sensitivity studies in which reasonable variations of the model stiffness and mass parameters have been considered, and mode shapes and frequencies have been computed for each set of parameters. From this, bounds on the modal characteristics of the actual structure have been estimated.


Under this project, the analytical model of the bridge used in the sensitivity studies has been comprised of beam elements,



NOTE:

INPUT CHANNEL — VERTICAL RESPONSE AT CENTRAL PIER BASE (CHANNEL 1)
RESPONSE CHANNEL — TRANSLATIONAL COMPONENT OF VERTICAL RESPONSE AT
MIDLENGTH OF SOUTH SPAN $\left(\frac{\text{CHANNEL 16} + \text{CHANNEL 18}}{2}\right)$

FIGURE 4-21. TRANSFER FUNCTION APPROACH FOR INITIAL ESTIMATE OF NORMAL MODES



while simple spring elements have been used to represent the constraint of the foundations at the two abutments and at the base of the central pier. A matrix of parametric analysis cases was then defined, in which variations in each of the resulting structure/foundation model parameters were considered. The greatest variations that were considered were in the foundation spring constants, in which baseline values estimated according to procedures suggested by Scott (1983) were varied up to the limiting conditions of fixed and pinned boundary conditions.

For each combination of parameters considered in the matrix of cases, mode shapes and frequencies of the model's normal modes have been computed using the SAP7 computer program. Sample results from these analyses are shown in Table 4-2.

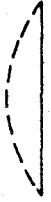



4.2.2.3 Single-Input/Single-Output Modal Identification

The last initialization procedure used under this project has employed a single-input/single-output version of MODE-ID, named IDSISO. Since only a single input motion is used, IDSISO is strictly applicable only if all support motions are identical (i.e., if "rigid base" conditions apply). Nevertheless, IDSISO represents a numerically efficient means of obtaining approximate estimates of the natural frequencies of the various normal modes of the MRO.

When initially searching for the whereabouts of the various modes in the frequency domain, a useful first step involves application of a program called PROFIL. In this program, a measure-of-fit parameter, J , (analogous to that described in Chapt. 3) is computed as a function of natural period, using motions from any designated input and response channel and a fixed damping ratio. This process involves an optimization of the modal participation factor so as to minimize J for each specified period. It can be carried out for any assumed number of modes, and results in a plot of J vs. natural period in which a pronounced local minimum in J corresponds to the natural period of a mode of vibration. These plots therefore provide a



TABLE 4-2. SAMPLE RESULTS OF SENSITIVITY STUDIES: VARIATIONS OF FOUNDATION ROTATIONAL SPRING CONSTANTS

Predominant Direction of Response	Mode	Mode Shape	Natural Period (sec) for Various Values of Foundation Rotational Spring Constants				
			Pinned	Fixed	Baseline	0.1 x Baseline	0.5 x Baseline
Transverse	First Symmetric		0.309	0.120	0.300	0.309	0.308
	First Antisymmetric		0.076	0.049	0.076	-	0.076
Vertical	First Antisymmetric		0.300	0.194	0.268	0.298	0.282
	First Symmetric		0.212	0.147	0.195	0.212	0.203

AA921

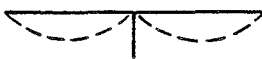




visual indication of the various periods at which normal modes occur. For example, Figure 4-22 shows the minima in J that are produced by two transverse modes of response of the MRO.

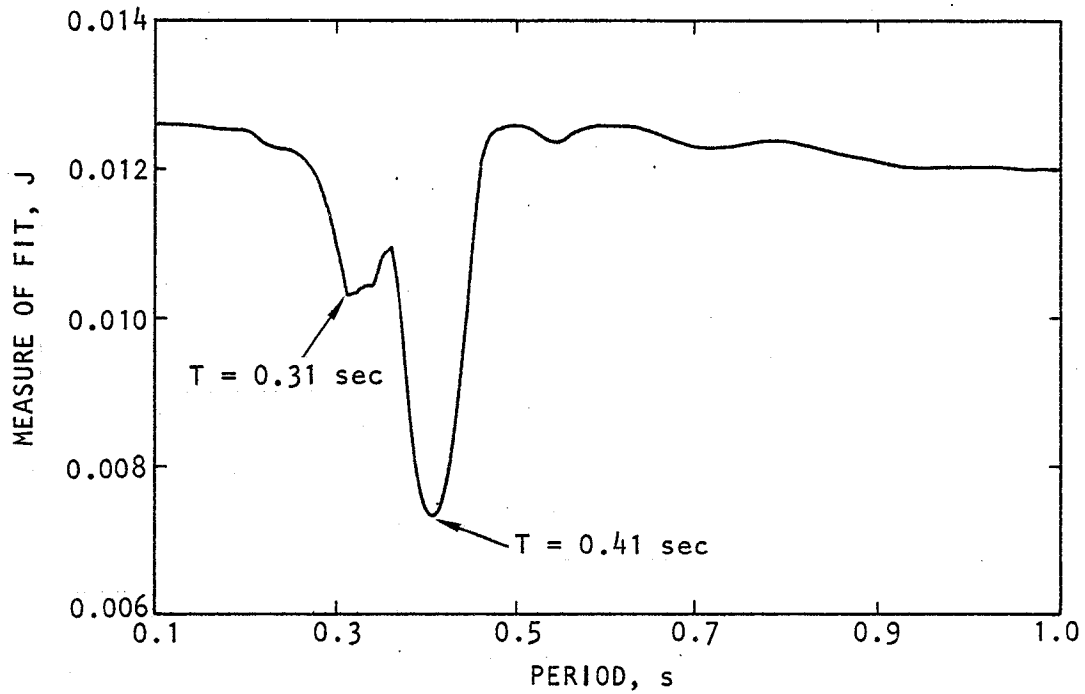
4.2.2.4 Summary of Initialization Results

Results of the normal mode estimates from each of the initialization procedures described above is provided in Table 4-3. This table indicates three significant modes of response of the MRO, which correspond to (1) a symmetric vertical response mode of the deck, with a natural period (T) of about 0.21 sec; (2) a fundamental symmetric transverse response mode (termed the system transverse mode) which features transverse response of the deck/abutment system and has a natural period of about 0.4 sec; and (3) a second symmetric transverse response mode (termed the deck transverse mode) which features prominent deck response amplitudes and smaller abutment response amplitudes, and has a natural period of about 0.31 sec. It is shown in the subsequent modal identification results that orthogonality between the two transverse modes is satisfied through embankment mode shape amplitudes (not shown in Table 4-3) that are apparently 180 deg out-of-phase between the

TABLE 4-3. SUMMARY OF INITIAL ESTIMATES OF BRIDGE MODES

Mode	Approximate Mode Shape	Natural Period (Sec)	Damping Ratio
Deck Vertical		0.21	0.03
Deck Transverse		0.31	0.01
Deck/Abutment System Transverse		0.40	0.10

AA920




NOTE:

DIRECTION OF MOTION: TRANSVERSE

INPUT CHANNEL NUMBER: 1 (BASE OF CENTRAL PIER)

RESPONSE CHANNEL NUMBER: 7 (MIDSPAN OF DECK)

FIGURE 4-22. SINGLE MODE PROFIL PLOT



two modes (see Sec. 4.4). Also, it is noted that the initial estimates of the modal damping ratios shown in Table 4-3 have been obtained from the IDSISO calculations. However, such damping ratio estimates are not necessarily reliable because they are based on a simplified model in which only one input motion and one response motion is treated at a time.

A breakdown of the natural period estimates for the various modes, according to each of the various initialization procedures, is provided in Table 4-4. This table indicates that very similar estimates of the natural period of the deck vertical response mode were developed from each of the four initialization procedures. The two transverse response modes were each estimated from three of the four procedures and, for these modes, each of the natural period estimates are also quite close. This suggests that a reasonable degree of confidence can be attached to the initial natural period estimates for the vertical mode and for both of the transverse modes.

It is important to note here that the initial period estimates developed according to each of the above initialization procedures represent only one set of parameters that characterize the overall response of the MRO. Additional parameters needed to fully represent the bridge response are its mode shapes, modal damping ratios, modal participation factor matrices, and pseudostatic influence matrices (see Chapt. 3). However, reliable estimates of all of these parameters cannot be readily obtained using the above simplified initialization procedures. Also, because of the simplifications and approximations involved, these procedures may suggest the presence of "modes" which are not real. For these reasons, the more extensive procedures that comprise MODE-ID have been applied, in which all input and response channels are considered simultaneously and in a mathematically rigorous manner, so as to provide a more complete basis for identifying the full set of modal parameters needed to characterize the response of the MRO.



TABLE 4-4. ESTIMATION OF MODAL NATURAL PERIODS BY VARIOUS ESTIMATION PROCEDURES

Mode	Examination of Motion Time Histories and Fourier Amplitude Spectra (Sec. 4.1)		Transfer Functions From Fourier Spectra (Sec. 4.2.2.1)		Sensitivity Studies Using Analytical Model (Sec. 4.2.2.2)*		IDSISO Modal Identification (Sec. 4.2.2.3)	
	Frequency (Hz)	Period (Sec)	Frequency (Hz)	Period (Sec)	Frequency (Hz)	Period (Sec)	Frequency (Hz)	Period (Sec)
Deck Vertical	4.5	0.22	4.9	0.21	5.0	0.20	4.9	0.21
Deck Transverse	-	-	3.5	0.29	3.3	0.30	3.2	0.31
Deck/Abutment System Transverse	2.5	0.40	2.2	0.45	-	-	2.5	0.40

*Natural frequencies and periods shown from sensitivity study results correspond to baseline foundation spring parameters estimated from procedure suggested by Scott (1983), and to best a priori estimates of other parameters.



4.2.3 MODE-ID APPLICATION PROCEDURE

Following development of initial estimates of the periods of the MRO's significant modes as described above, MODE-ID is applied to the Case 1 and Case 2 subsets of strong motion data according to the following procedure:

1. Confirmation of Modes. Further assessment of possible bridge modes is carried out by applying MODE-ID in two separate and relatively simple calculations that consider (1) all vertical response and input channels only; and (2) all transverse response and input channels only. These calculations neglect the presence of any coupled vertical and transverse components in the MRO's modes of response; however they provide a relatively efficient method of confirming or rejecting the presence of "modes" determined by the preliminary and more approximate procedures described in Section 4.2.2. Also, they are valuable for obtaining improved estimates of the natural periods of the significant modes of the MRO, that will be used as input to the subsequent superrun calculations.
2. Superrun Calculation. The next step in the MODE-ID implementation consists of a "superrun" calculation that simultaneously includes all of the MRO's coupled transverse and vertical response and support motion measurements for Case 1 and Case 2. Because of this, the superrun calculation will provide more reliable estimates of the pseudostatic parameters and modal parameters (particularly the mode shapes, participation factors, and damping ratios) than will the prior MODE-ID calculations carried out under Step 1 above. In the superruns, MODE-ID is implemented on a step-by-step basis, by adding one mode at a time and evaluating each mode's significance by assessing its



relative influence on the measure-of-fit, J (Eq. 3-21). When the identification process is completed, overlaid plots of measured vs. model motions at each channel location are also obtained to provide a visual indication of how well the identified model represents the measured bridge response.

3. Interpretation of Identified Response Characteristics.

Following the superrun, MODE-ID is used again to further interpret the modes identified under the superrun calculations. This involves additional computation of the measure-of-fit, J , and additional plotting of overlaid model vs. measured response time histories so as to (1) isolate the relative contributions of the pseudostatic component and each of the various normal modes to the total response of the MRO; and (2) assess the significance of any particular unusual features of the modes identified during the MODE-ID superrun.

In all of the above MODE-ID applications, the mode shape components for each mode are determined by (1) summing the elements of each row of the effective participation factor (EPF) matrix separately over the vertical-input and transverse-input degrees of freedom, (in which each row corresponds to a response degree of freedom); and (2) obtaining the mode shape as the ratio of each of these summations (which hereafter are termed "partial row-sums"). These summations are necessitated by the ill-conditioning phenomena described in Section 3.1.3, and also by certain simplifications in the MODE-ID identification process so as to avoid the various nonlinear constraints between the parameters of a classical-mode model (also described in Section 3.1.3). Because of the same ill-conditioning phenomena, the results of the pseudostatic influence matrix identification are examined through use of the same partial row-sums which, for pseudostatic response, should approach unity. It is noted that it is these partial row-sums of the elements of the EPF and pseudostatic matrices, rather than the individual elements of



these matrices, that primarily control the spatial variation of the MRO's modal and pseudostatic response.* These partial row-sums can be reliably estimated by application of MODE-ID to the MRO's array of strong motion measurements, while estimates of the individual elements of these matrices are not as reliable.

4.3 CASE 1 RESULTS

This section describes results from the application of MODE-ID to the identification of MRO pseudostatic and modal response parameters for the bridge deck and central pier, using the Case 1 set of input and response channels (see Fig. 4-23). The section is divided into four main subsections that address each step in the application procedure that was described in Section 4.2.3. These correspond to the confirmation of modes (Sec. 4.3.1), the superrun calculations (Sec. 4.3.2), and detailed interpretations of the identified response characteristics (Secs. 4.3.3 and 4.3.4).

4.3.1 CONFIRMATION OF MODES

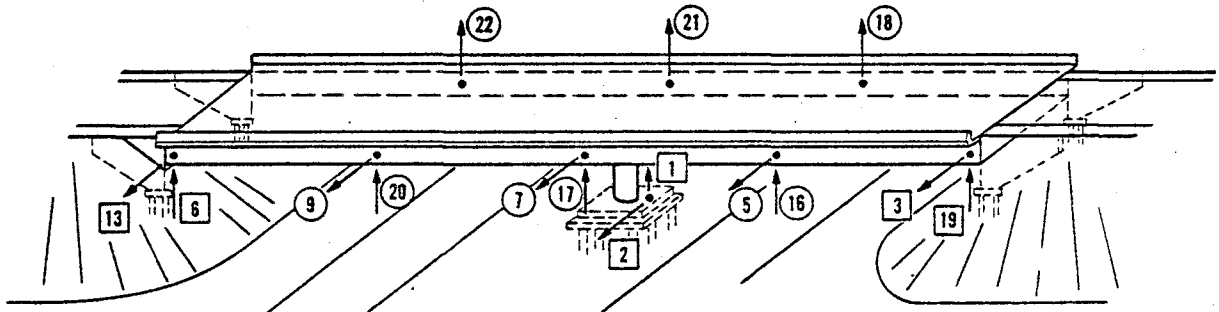
Before implementing the final modal identification in the MODE-ID superrun, a confirmation of the suspected modes of the bridge is first obtained by applying MODE-ID to data from two subsets of the Case 1 channels. These subsets correspond to the transverse input and transverse response channels, and to the vertical input and vertical response channels. The deck's transverse and vertical mode natural periods, as estimated from the prior initialization procedures (Sec. 4.2.2 and Table 4-3) are used as input to these initial MODE-ID calculations.

*This is because the partial row-sums are the controlling parameters when all input motions are identical. For the MRO, these input motions are nearly identical when separated into vertical motion and transverse motion groups.



LEGEND:

- = INPUT CHANNELS
- = RESPONSE CHANNELS




(a) Channel locations

Channel Type	Location	Number	Direction
Input Channels	Base of Central Pier	1	Vertical
		2	Transverse
	South Abutment	19	Vertical
		3	Transverse
	North Abutment	6	Vertical
		13	Transverse
Response Channels	Along Road Deck	16, 17, 18 20, 21, 22	Vertical
		5, 7, 9	Transverse

(b) Channel tabulations

FIGURE 4-23. CASE 1 SUBSET OF INPUT AND RESPONSE CHANNELS



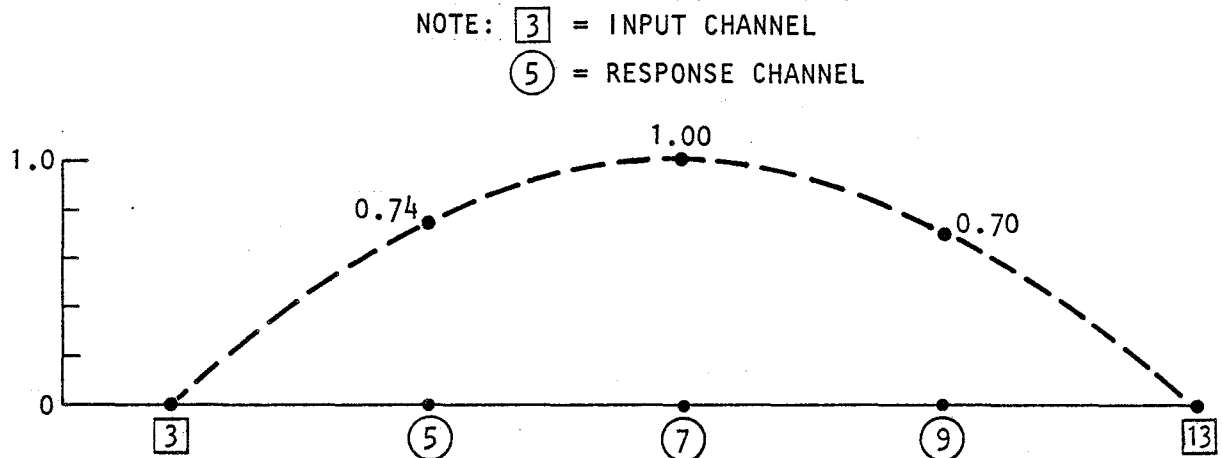
Results of these applications confirmed the presence of two significant modes, which are shown in Figures 4-24 and 4-25. These results show that the natural periods of the transverse and vertical deck modes have changed only slightly relative to the prior estimates shown in Table 4-3, whereas the damping ratios have changed markedly. Of particular interest in these results is the measure-of-fit, J . For the transverse input and response channels, J is quite small ($J = 0.020$) indicating that the pseudostatic matrix and normal modes identified for this subset of channels produces a total transverse response that compares closely with the measured transverse motions of the MRO bridge deck. However, when MODE-ID is applied to the vertical input and response channels, the resulting value of J is much larger ($J = 0.26$), indicating a less satisfactory fit with the measured vertical motions. This trend occurs because (1) this initial estimate of the bridge modes neglects the possible presence of any coupled vertical and transverse components in the various mode shapes; and (2) the fit between the model and measured vertical motions is more sensitive to these neglected coupling effects than is the fit between the model and measured transverse motions. The subsequent superrun results (Sec. 4.3.2) show that, when these coupling effects are included in the modal identification process, the fit between the model and measured vertical response improves markedly.

It is also observed from Figure 4-25 that partial row-sums of the the pseudostatic influence matrix for the vertical-input/vertical-response model often deviate considerably from the theoretically correct value of 1.0. This suggests that MODE-ID may have attempted to compensate for the above-mentioned missing coupling effects by adjusting the pseudostatic influence matrix. In contrast to this, the partial row-sums of the pseudostatic influence matrix for the transverse-input/transverse-response model attain values quite close to 1.0 (Fig. 4-24). These results, together with the above-indicated low value of J , show

Natural Period: $T = 0.280$ secDamping Ratio: $\zeta = 0.051$ Measure-of-Fit: $J = 0.020$
(Eq. 3-21)

Item	Channel Number		
	5	7	9
Sum of elements in rows of pseudostatic influence matrix	1.10	1.04	1.02
Sum of elements of rows in effective participation factor matrix	0.46	0.62	0.44
Normalized mode shape	0.74	1.00	0.71

(a) Tabulation of results



(b) Plot of normalized mode shape

FIGURE 4-24. CASE 1: APPLICATION OF MODE-ID TO TRANSVERSE INPUT AND RESPONSE CHANNELS



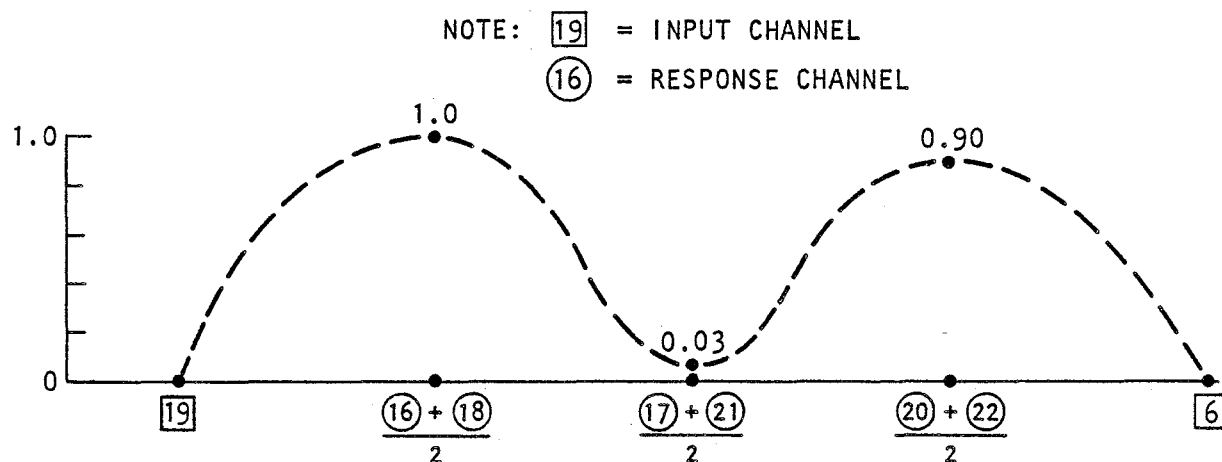
Natural Period: $T = 0.210$ sec

Damping Ratio: $\zeta = 0.056$

Measure-of-fit: $J = 0.26$
(Eq. 3-21)

Item	Channel Along West Face of MRO			Channel Along East Face of MRO		
	16	17	20	18	21	22
Sum of elements in rows of pseudostatic influence matrix	1.22	1.10	1.19	1.07	0.82	0.78
Sum of elements in rows of effective participation factor matrix	1.22	~0	1.09	1.23	0.08	1.10
Normalized mode shape	0.99	0	0.89	1.0	0.07	0.90

(a) Tabulation of results



(b) Plot of normalized mode shape (translational component)

FIGURE 4-25. CASE 1: APPLICATION OF MODE-ID TO VERTICAL INPUT AND RESPONSE CHANNELS



that the total transverse response of the MRO deck is well represented by the pseudostatic and modal parameters identified from the transverse-input/transverse-response model.

4.3.2 SUPERRUN RESULTS

Now that the significant deck modes of the MRO's seismic response have been confirmed, the next step in the MODE-ID application is to consider the Case 1 transverse and vertical response measurements simultaneously in a superrun that provides the final identification of the Case 1 pseudostatic influence matrix and normal mode parameters. Results of this application are provided in the paragraphs that follow.

4.3.2.1 Adequacy of Identified Model

The overall results of this superrun calculation are presented in two forms. First, the parameters of the identified model and its measure-of-fit with the measured MRO response are provided in tabulated form (Table 4-5). Second, for selected MRO response channels, superrun results are provided as overlaid plots of motion time histories from the MRO measurements vs. those from computations using MODE-ID model (Figs. 4-26 to 4-28).

The identified Case 1 superrun model is comprised of a pseudostatic influence matrix, a deck vertical response mode, and a deck transverse response mode. This model provides an excellent representation of the MRO's measured seismic response, as demonstrated by the low value of J in Table 4-5 ($J = 0.056$), and by the close comparisons between the overlaid motion time history plots from the measurements and the model. The Case 1 model is discussed further in the paragraphs that follow.

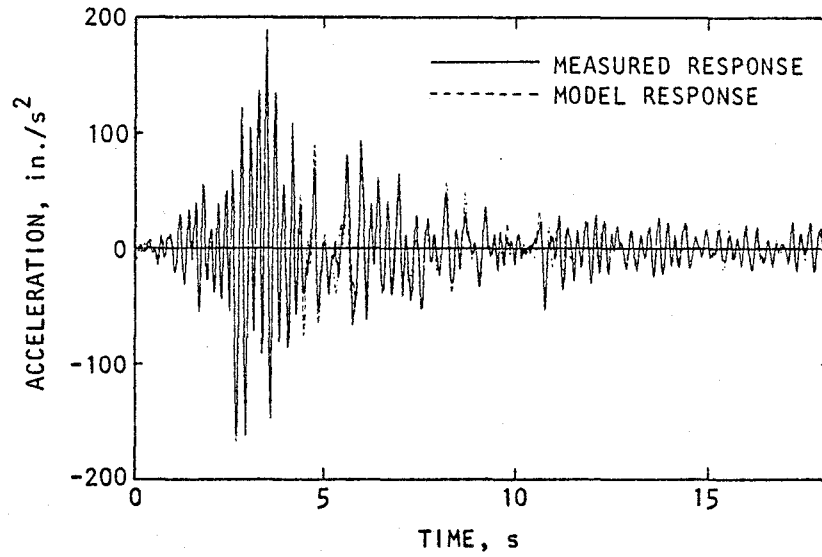
4.3.2.2 Pseudostatic Influence Matrix

Table 4-5 provides the identified pseudostatic influence matrix in terms of the partial row-sums of the matrix. These

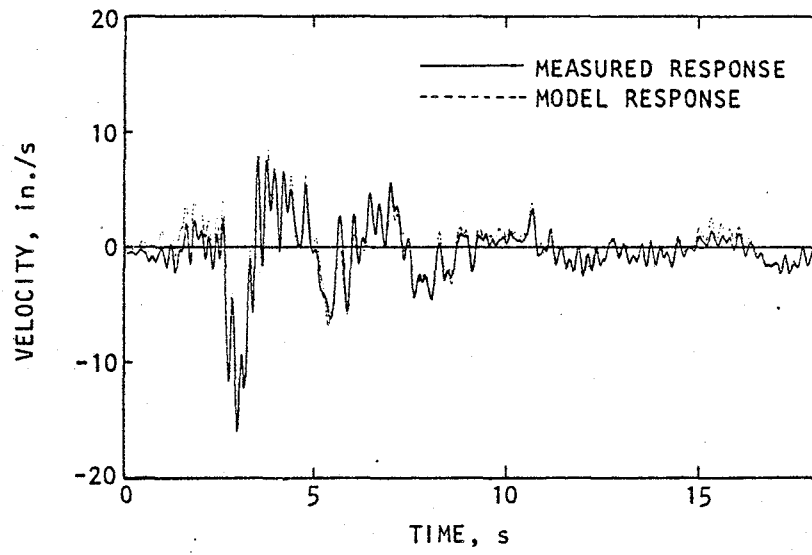


TABLE 4-5. CASE 1 SUPERRUN RESULTS: TABULATION AND SUMMARY

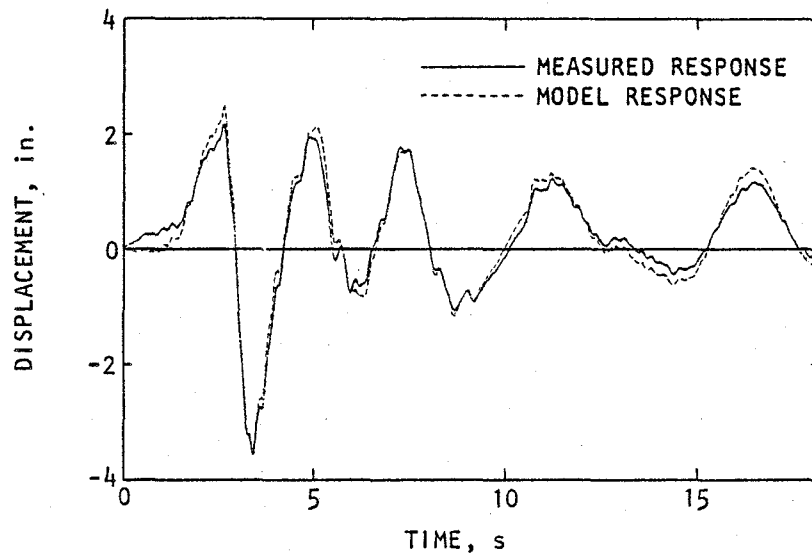
Mode	Natural Period (Sec)	Damping Ratio	Summation of Elements in Each Row of Pseudostatic Influence Matrix or Effective Participation Factor Matrix														Measure of Fit, J (Eq. 3-21)
			Input Channels	Transverse						Vertical							
				5	7	9	16	17	20	18	21	22					
Pseudostatic	-	-	Transverse (2, 3, 13)	1.10	1.04	1.02	-0.01	-0.03	0.0	0.01	0.01	0.01	0.01	0.01	0.01	0.056	
			Vertical (1, 19, 6)	0.0	0.01	-0.01	1.11	0.98	1.05	1.10	0.93	0.84					
Deck Transverse	0.269	0.066	Transverse (2, 3, 13)	0.47	0.59	0.43	0.09	-0.42	0.14	0.86	0.46	0.76	0.056				
			Vertical (1, 19, 6)	-0.01	-0.05	-0.03	0.08	-0.04	-0.14	-0.11	-0.03	-0.04					
Deck Vertical	0.211	0.066	Transverse (2, 3, 13)	0.11	0.13	0.10	-1.17	-0.29	-1.34	-1.15	0.07	-0.88	0.056				
			Vertical (1, 19, 6)	-0.01	0.03	0.02	1.19	0.02	1.11	1.25	0.08	1.10					



(a) Acceleration



(b) Velocity



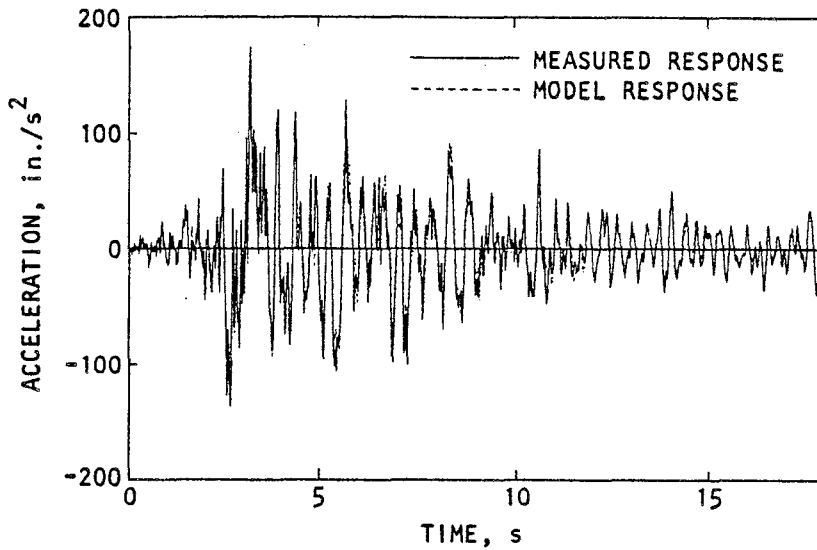
AA866

(c) Displacement

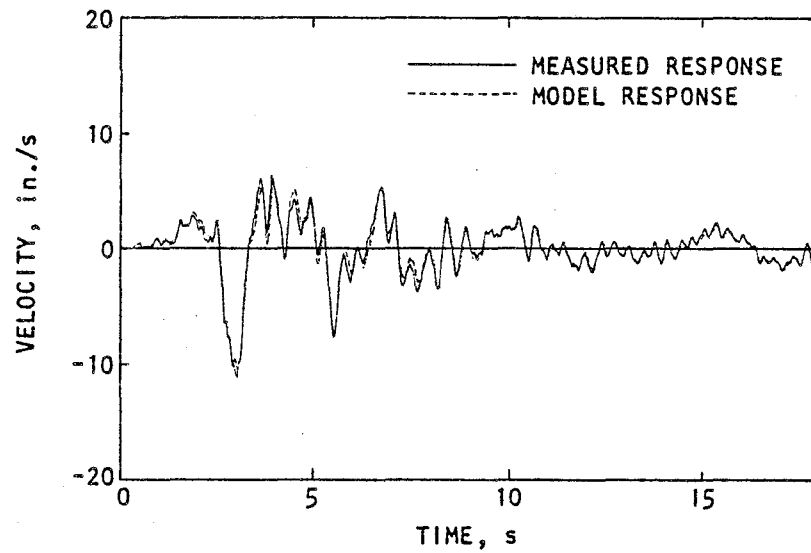
FIGURE 4-26. CASE 1 SUPERRUN RESULTS: COMPARISON OF MEASURED AND MODEL VERTICAL RESPONSE AT CHANNEL 16 (MIDLENGTH OF SOUTH SPAN ALONG WEST FACE OF BRIDGE DECK)



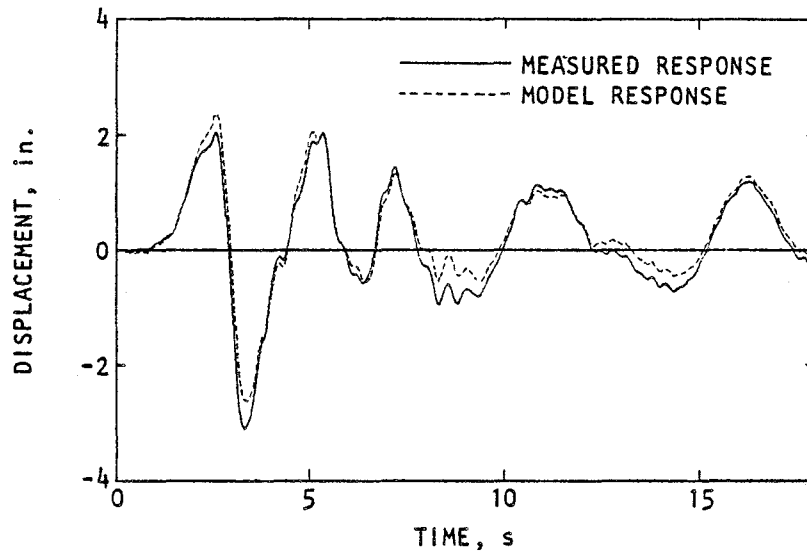
R-8222-5603



(a) Acceleration



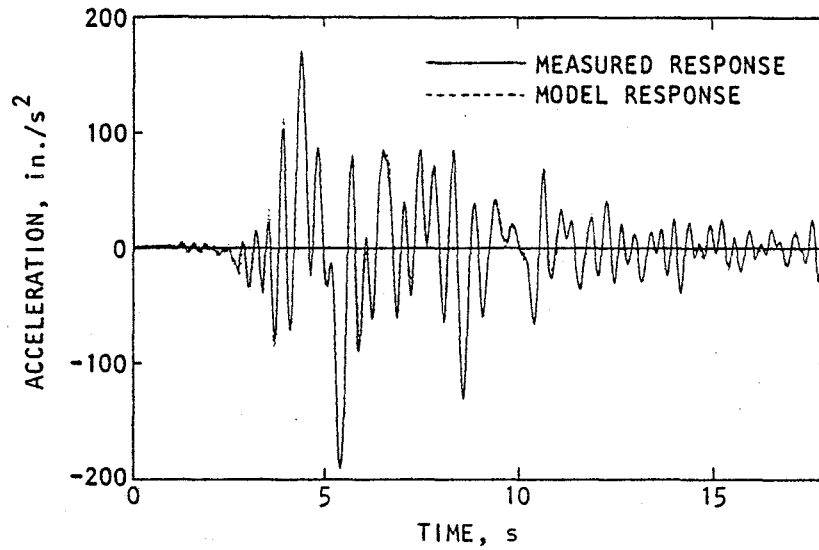
(b) Velocity



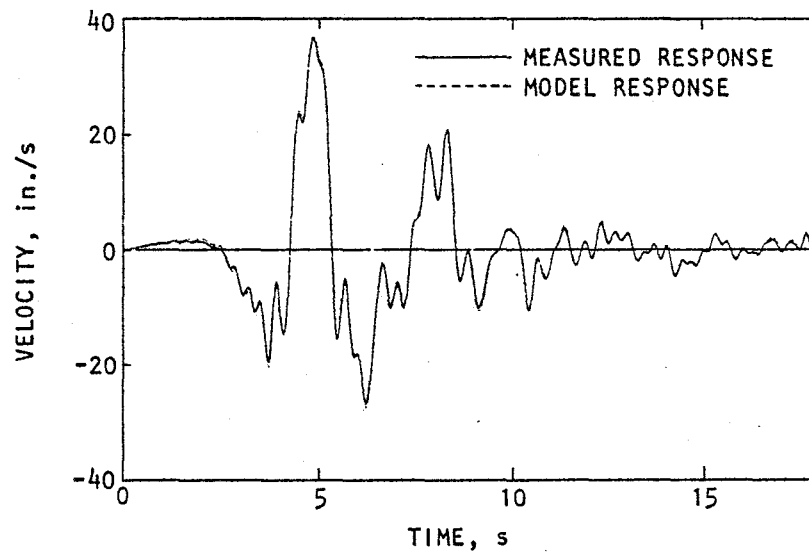
(c) Displacement

AA868

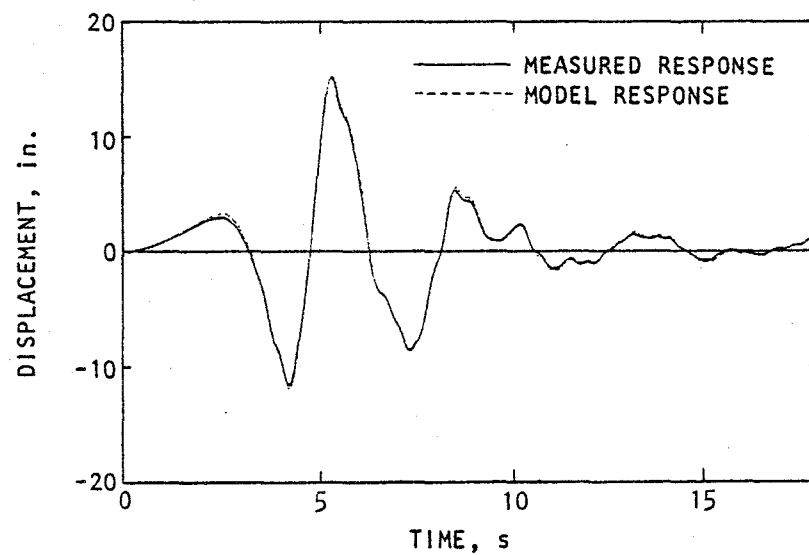
FIGURE 4-27. CASE 1 SUPERRUN RESULTS: COMPARISON OF MEASURED AND MODEL VERTICAL RESPONSE AT CHANNEL 21 (OVER CENTRAL PIER ALONG EAST FACE OF BRIDGE DECK)



(a) Acceleration



(b) Velocity



(c) Displacement

AA867

FIGURE 4-28. CASE 1 SUPERRUN RESULTS: COMPARISON OF MEASURED AND MODEL TRANSVERSE RESPONSE AT CHANNEL 7 (OVER CENTRAL PIER)



summations show that, as expected, the transverse input motions are the primary contributors to the pseudostatic response at the various transverse response channel locations, and the vertical input motions are the main contributors to the pseudostatic response at the vertical response channels. The sums corresponding to each response channel are all reasonably close to the theoretically correct values of either zero or unity.

4.3.2.3 Deck Vertical Response Mode

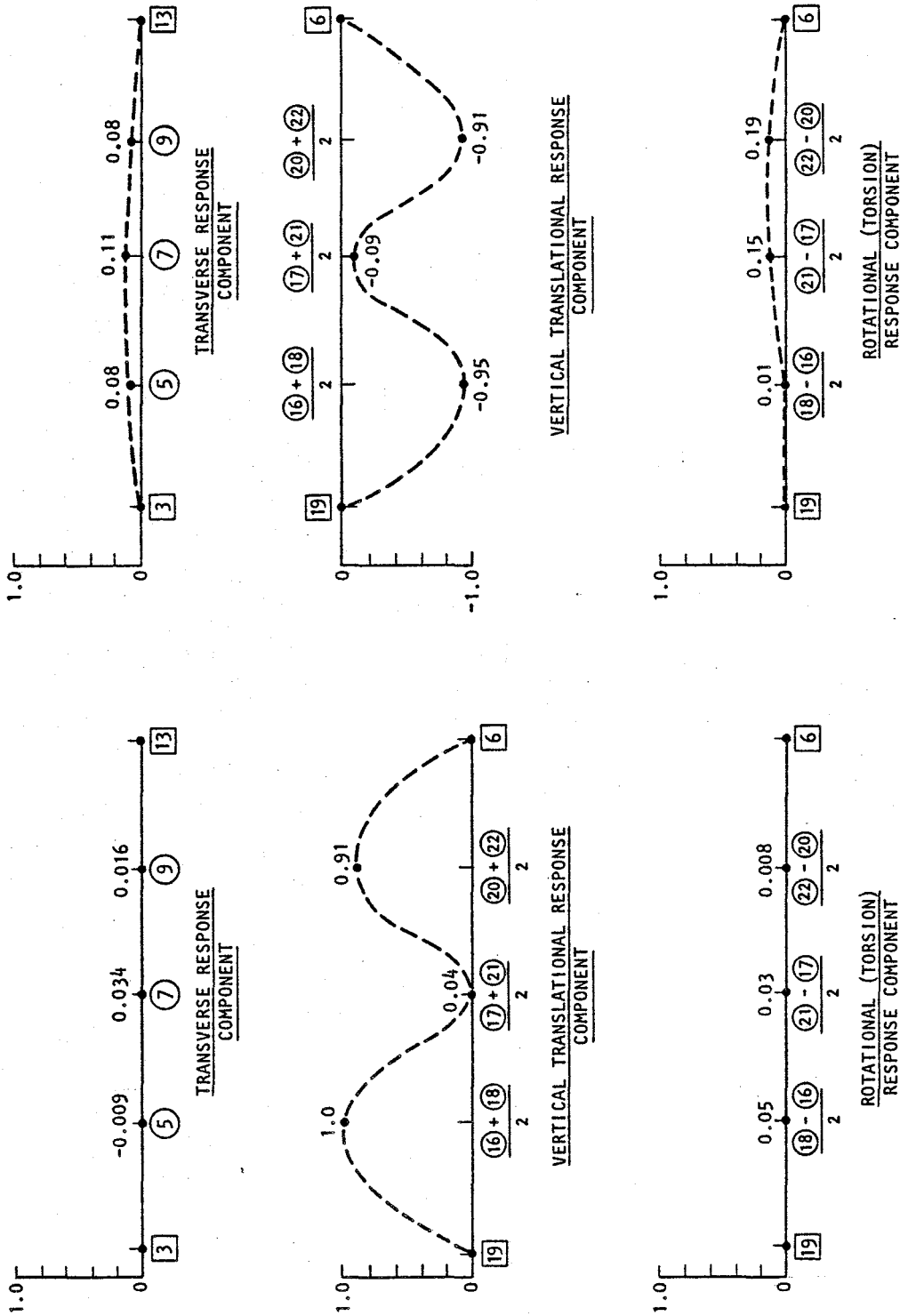
The vertical response mode of the MRO bridge deck has been identified in this superrun as having a natural period ($T = 0.211$ sec) that is nearly the same as that identified for the prior vertical-input/vertical-response model, and a damping ratio ($\xi = 0.066$) that is somewhat higher. However, the partial row-sums of the superrun's effective participation factor (EPF) matrix have certain features not present in the vertical-input/vertical-response model, and are discussed below.

Two sets of partial row-sums of the EPF matrix are given in Table 4-5 for this mode (and for the deck transverse response mode as well). One set represents a row-sum over the columns of the matrix that correspond to the transverse input motions (Channels 2, 3, and 13), and the other set represents a row-sum over those columns that correspond to the vertical input motions (Channels 1, 19, and 6). These are used to develop two corresponding sets of mode shape plots that have all been normalized to a common scale (Fig. 4-29). These plots provide a means for assessing whether the mode shapes established from the partial row-sums for transverse input and for vertical input are consistent, which they should be according to Equation 3-16. Also, the use of a common scale factor in developing the plots provides a graphic means for examining the relative values of the EPFs due to transverse input and to vertical input, in order to see if they are physically reasonable.



AA844

NOTE: **3** = INPUT CHANNEL
5 = RESPONSE CHANNEL



(a) Due to vertical input motions (Channels 1, 19, 6) (b) Due to transverse input motions (Channels 2, 3, 13)

FIGURE 4-29. CASE 1 SUPERRUN RESULTS: NORMALIZED MODE SHAPES FOR DECK VERTICAL RESPONSE MODE.



With this as background, Table 4-5 and Figure 4-29 show that both sets of EPF partial row-sums lead to mode shape components with the following physically plausible trends: (1) the transverse and rotational (torsion) components are small when compared to the vertical translational components; and (2) the vertical translational components have large amplitudes at the midlength of each deck span, and are reasonably symmetric about the midspan of the bridge. However, the set of EPF partial row-sums that corresponds to summations over the transverse input degrees of freedom gives values for the vertical translational response that are negative and much too large (Fig. 4-29b). In evaluating this anomaly, it should be noted that

- Even though the EPFs for vertical translations due to transverse input are large, the resulting vertical response need not be, since this also depends on the transverse excitation of the bridge supports at the vertical mode frequency. In fact, Figure 4-5 shows that this excitation is indeed very low.
- The implausibility of these large EPFs is apparent in view of the near symmetry of the MRO configuration and its measured response and input motions (Sec. 4.1). This near-symmetry strongly suggests that the vertical translational components corresponding to vertical input motions should dominate the MRO's response in its vertical mode.
- Although the EPFs for vertical translational response due to transverse input motions are overly large, they produce a mode shape that is very similar to that for vertical translational response due to vertical input



motions.* This is consistent with theory (e.g., Eq. 3-16) which indicates that the partial row-sums should produce the same mode shape regardless of whether the summation is over the transverse input terms of the EPF matrix or the vertical input terms.

Causes for the large vertical response EPFs due to transverse input may be related to (1) the limited array of support motion measurements obtained at the MRO, which does not fully define the excitation of the bridge deck and pier; and (2) limitations in the applicability of a linear elastic and classical mode model to represent a real structure. This is discussed further in Section 4.3.4.

4.3.2.4 Deck Transverse Response Mode

The transverse response mode of the MRO bridge deck has been identified in this superrun as having a natural period ($T = 0.269$ sec) that is somewhat reduced relative to that identified for the prior transverse-input/transverse-response models, and a damping ratio ($\xi = 0.066$) that is somewhat greater. However, the partial row-sums of the EPF matrix for this transverse response mode contain certain features not present in the transverse-input/transverse-response model. These features are discussed below.

Two sets of partial row-sums of the EPF matrix are given in Table 4-5 for this deck transverse response mode. The first set, which corresponds to a sum over the transverse input degrees of freedom, leads to a reasonably symmetric distribution of the transverse response components of the mode shape that is

* The fact that the normalized mode shape for vertical translations has a different sign in Figure 4-29b as compared to Figure 4-29a is because of (1) the choice of normalization; and (2) the fact that the conventional participation factors for transverse input motions are opposite in sign to those for vertical input motions.



similar to that identified previously for the transverse-input/transverse-response model (Fig. 4-30a). It also leads to physically plausible rotational (torsion) components of the mode shape that, as expected, are reasonably symmetric about the midlength of the MRO and are largest at that location. However, the vertical translational response components that result from this set of partial row-sums are unreasonably large relative to the transverse response components. This same physical anomaly was previously noted for the deck vertical response mode except that (1) the vertical translational response components due to transverse input were negative instead of positive; and (2) the mode shapes for vertical response due to transverse input motions and due to vertical input motions were comparable whereas, for the deck transverse mode they are not* (Figs. 4-30a, b). Such results are discussed further in Section 4.3.4.

The second set of partial row-sums of the EPF matrix that are shown in Table 4-5 for this mode correspond to a summation over the vertical input degrees of freedom. This table and Figure 4-30b both show that, as expected, the EPFs corresponding to the vertical input degrees of freedom are small when compared to the EPFs corresponding to the transverse input degrees of freedom.

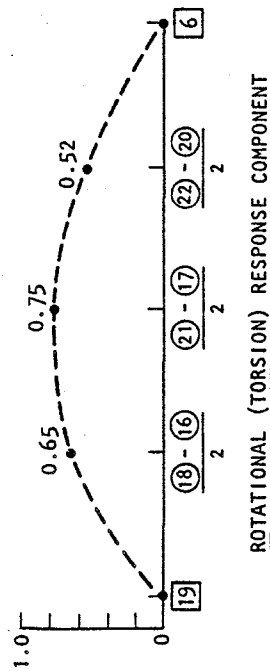
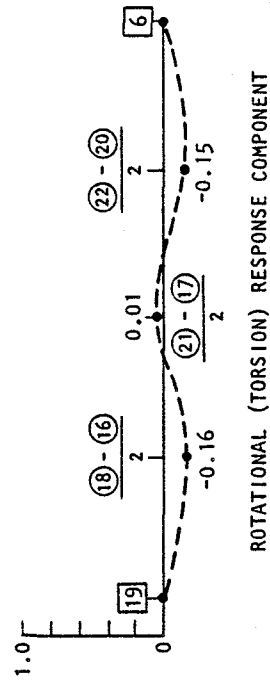
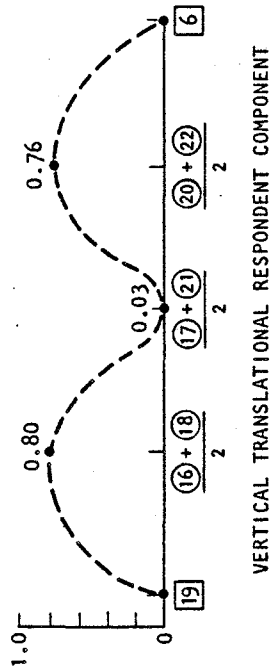
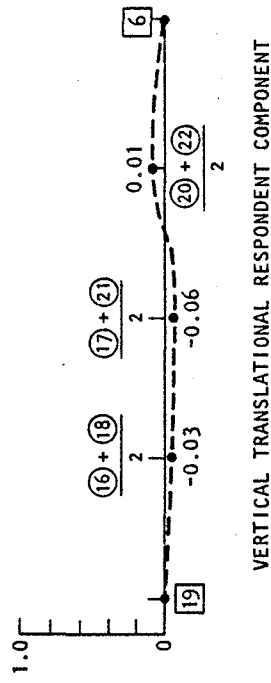
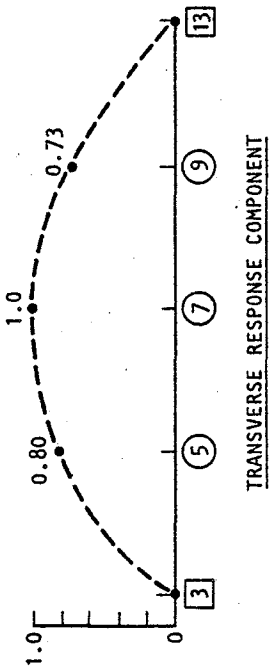
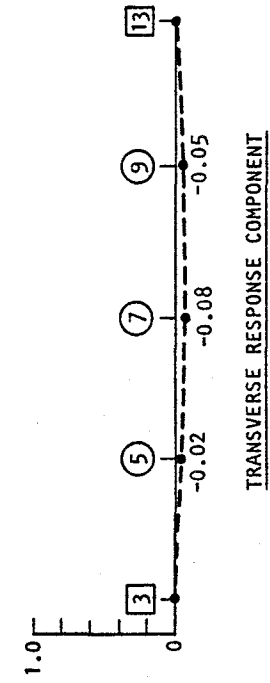
4.3.3 RELATIVE IMPORTANCE OF INDIVIDUAL MODES

This section provides results of an assessment of the relative importance of each mode of the Case 1 model (including pseudostatic) through comparison of their individual contributions to the total fit with the measured MRO response. These results are provided (1) as tabulations of the effect of each

*As previously noted in Section 4.3.2.3, Equation 3-16 indicates that all partial row-sums should produce the same mode shape regardless of whether the summation is over the transverse input terms of the EPF matrix or the vertical input terms.



NOTE: 3 = INPUT CHANNEL
5 = RESPONSE CHANNEL



AA845

(a) Due to transverse input motions (Channels 2, 3, 13)

(b) Due to vertical input motions (Channels 1, 19, 6)

FIGURE 4-30. CASE 1 SUPERRUN RESULTS: NORMALIZED MODE SHAPES FOR DECK TRANSVERSE RESPONSE MODE

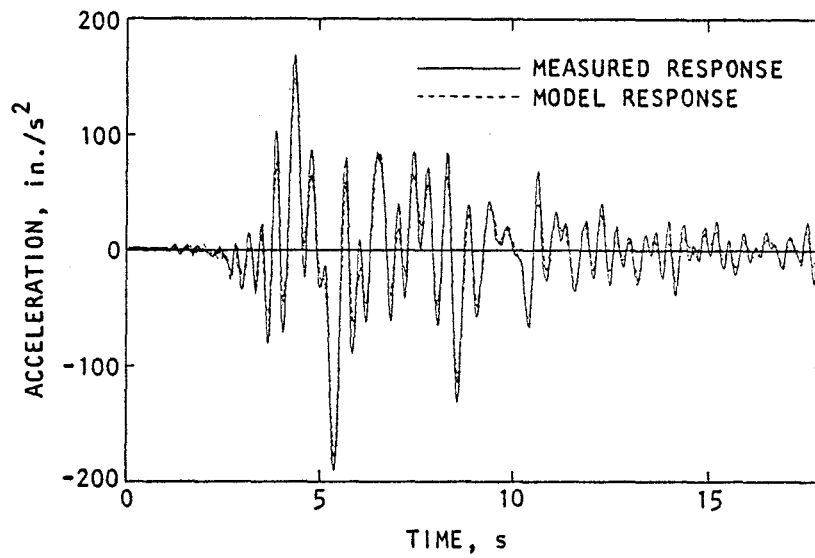


mode on the measure-of-fit, J , (Table 4-6); and (2) as visual comparisons of these effects through overlaid plots of measured vs. model acceleration histories at selected channels, as the contribution of each mode is added to the model response (Figs. 4-31 to 4-33). Trends from these results are as follows:

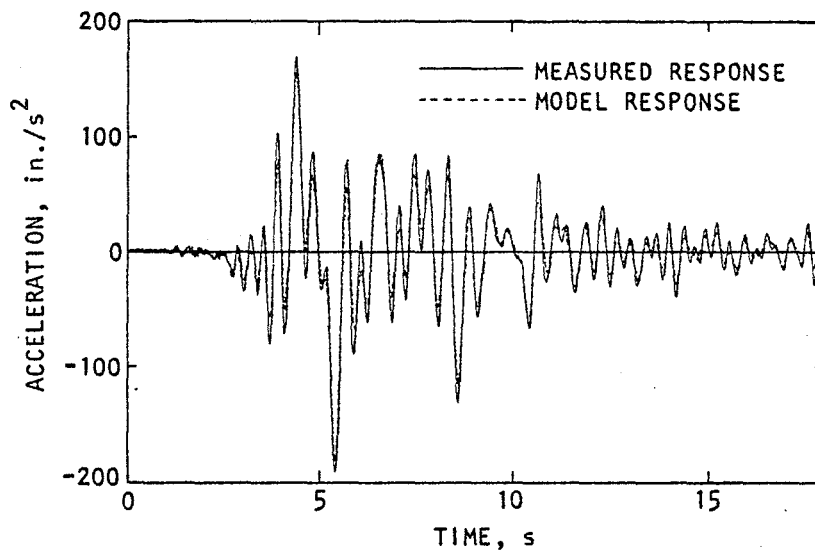
TABLE 4-6. CASE 1 RESULTS: RELATIVE CONTRIBUTIONS OF INDIVIDUAL MODES TO MEASURE OF FIT WITH MEASURED BRIDGE RESPONSE

Model Response	Measure of Fit, J (Eq. 3-21)	Percent Reduction in J
Pseudostatic Only	0.351	-
Pseudostatic Plus Deck Vertical Response Mode	0.109	68.9
Pseudostatic Plus Deck Vertical Response Mode and Deck Transverse Response Mode (Superrun)	0.056	48.7

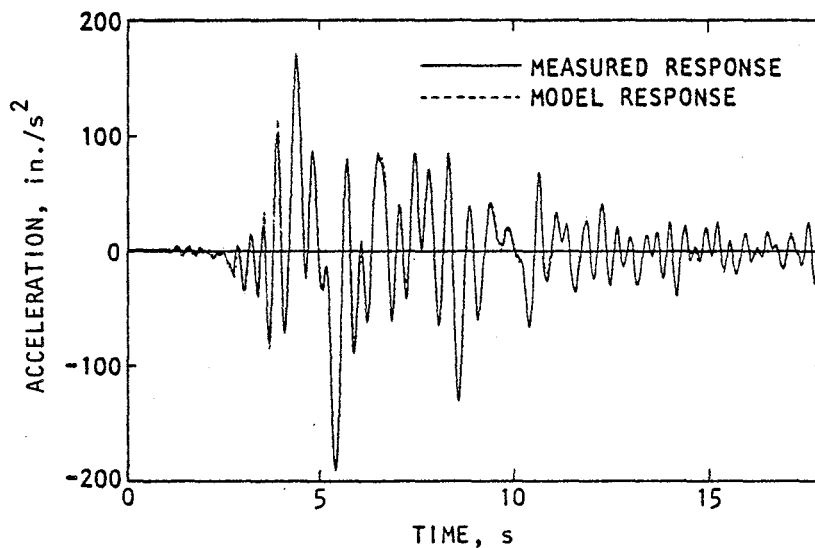
- The deck vertical response mode is seen to lead to a larger reduction in J than does the deck transverse response mode, and therefore has a greater effect on the fit between the model response and the measured response (Table 4-6).
- Visual comparison of the contributions of each mode to the fit with the deck's measured transverse acceleration histories shows that the deck's transverse response is dominated by the pseudostatic component (Fig. 4-31a). This demonstrates that the transverse response of the MRO is most directly affected by those elements of the bridge whose contributions are represented as pseudostatic response; in Case 1, these are the bridge abutment and foundation supports, including



(a) Model response = pseudostatic only



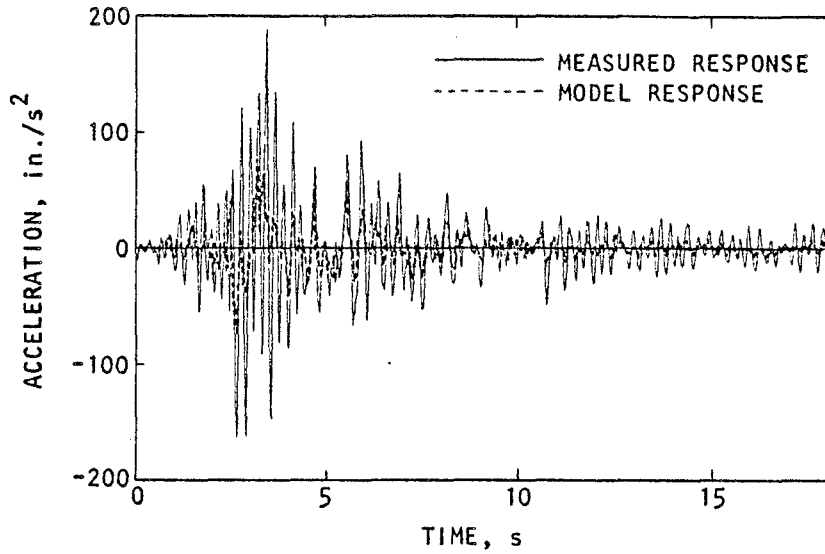
(b) Model response = pseudostatic and vertical mode



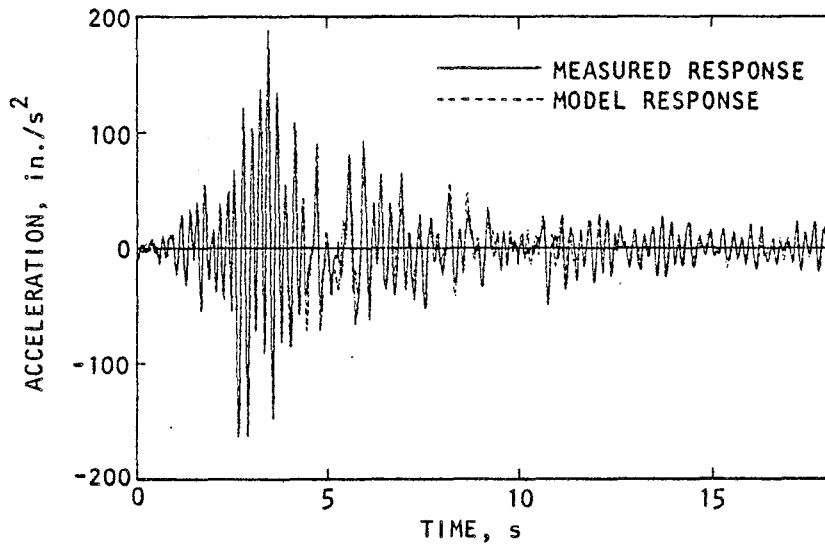
AA875

(c) Model response = pseudostatic and all modes (Superrun)

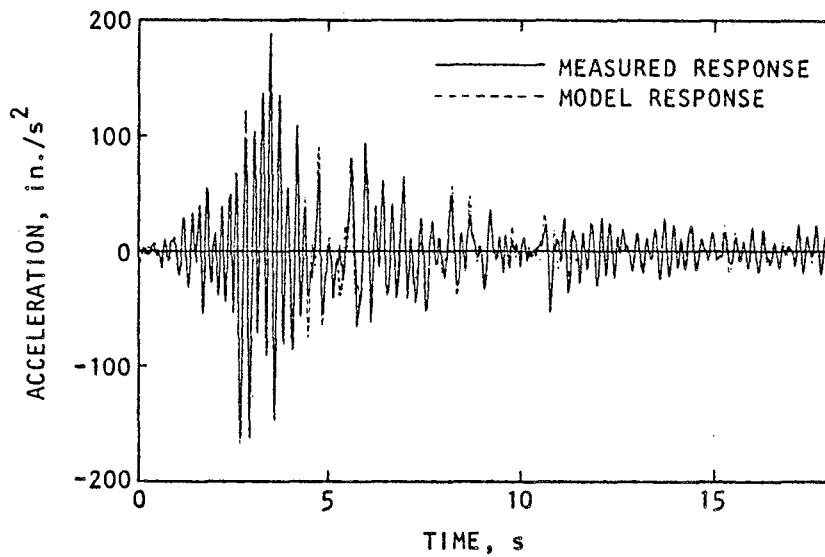
FIGURE 4-31. CASE 1 RESULTS: RELATIVE CONTRIBUTIONS OF INDIVIDUAL MODES TO FIT OF TRANSVERSE ACCELERATION HISTORY AT CHANNEL 7 (OVER CENTRAL PIER)



(a) Model response = pseudostatic only



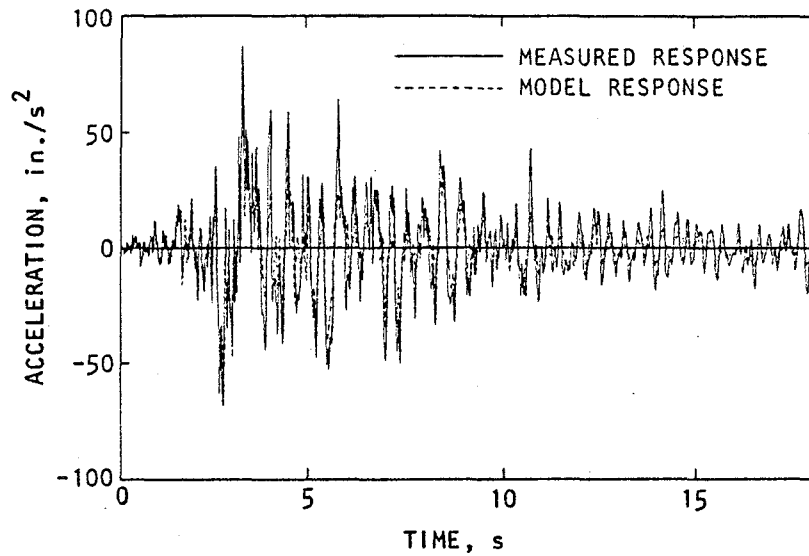
(b) Model response = pseudostatic and vertical mode



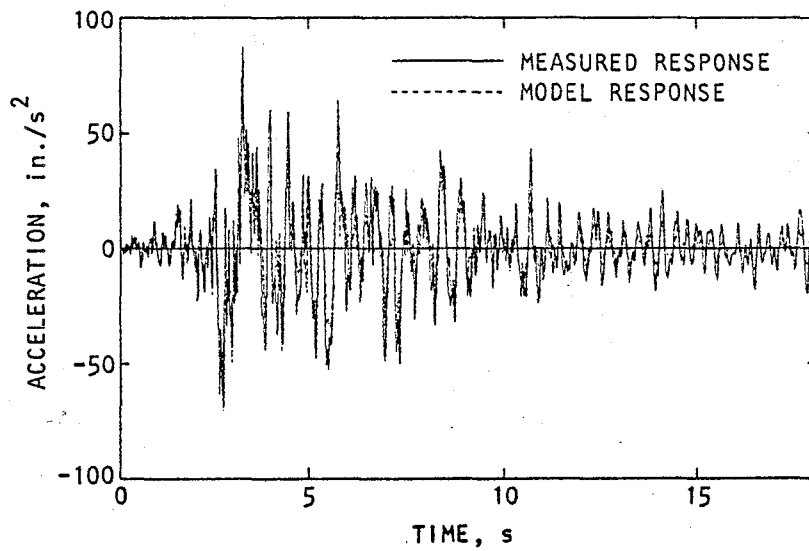
AA876

(c) Model response = pseudostatic and all modes (Superrun)

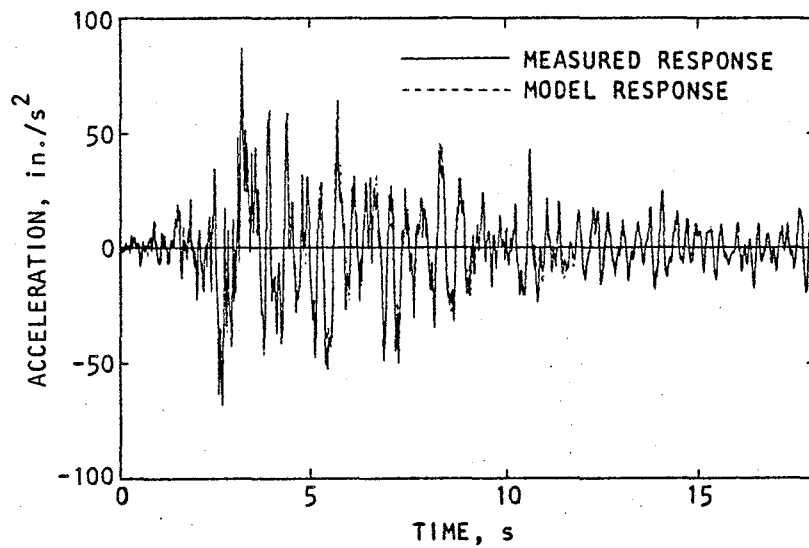
FIGURE 4-32. CASE 1 RESULTS: RELATIVE CONTRIBUTIONS OF INDIVIDUAL MODES TO FIT OF VERTICAL ACCELERATION HISTORY AT CHANNEL 16 (MIDLENGTH OF SOUTH SPAN, ALONG WEST FACE)



(a) Model response = pseudostatic only




(b) Model response = pseudostatic and vertical mode



AA885

(c) Model response = pseudostatic and all modes (Superrun)

FIGURE 4-33. CASE 1 RESULTS: RELATIVE CONTRIBUTIONS OF INDIVIDUAL MODES TO FIT OF VERTICAL ACCELERATION HISTORY AT CHANNEL 21 (OVER CENTRAL PIER, ALONG EAST FACE)



the surrounding soil medium.* The vertical mode has virtually no effect on the fit of the model vs. measured transverse response, and the deck transverse mode has only a minor additional contribution to this fit (Figs. 4-31b, 4-31c).

- Visual comparison of the contributions of each mode to the fit with the deck's measured vertical acceleration histories at the midlength of each span shows that the vertical response at these locations is dominated by the deck's vertical response mode (Fig. 4-32b). The pseudostatic response, by itself, provides a rather poor fit with these measured vertical motions (Fig. 4-32a); this indicates that the bridge support motions do not strongly affect these deck motions, which are instead most directly influenced by the dynamic response characteristics of the deck itself. The deck transverse response mode (which incorporates vertical motions of the deck due to torsion) has only a minor further contribution to the fit between the measured vs. model vertical response at the midlength of each deck span (Fig. 4-32c).
- Visual comparison of the contributions of each mode to the fit with the deck's measured vertical acceleration histories over the central pier shows that the vertical response mode now has a much smaller effect (Fig. 4-33b). This is because the deck's mode shape for this mode has very small amplitudes at this central pier location. Therefore, the primary contributors to the deck's vertical response over the central pier are the pseudostatic effects from the

* This trend is consistent with observations from our prior direct examination of the MRO's transverse motion measurements (Sec. 4.1.1) which showed that the deck's transverse response closely follows that of the abutments.



support motions at the base of the central pier (Fig. 4-33a) and the torsional motions from the deck's transverse response mode (Fig. 4-33c).


4.3.4 DISCUSSION OF APPARENT ANOMALIES IN SUPERRUN RESULTS

4.3.4.1 Possible Causes

The Case 1 superrun calculations described in Section 4.3.2 have resulted in a model that fits quite closely with the response measured at the various accelerometers along the MRO bridge deck. However, in both the transverse and vertical modes that were identified, the EPFs corresponding to vertical response due to transverse input motions are overly large and are therefore judged to be physically anomalous.* The ensuing paragraphs discuss possible causes of these anomalies, followed by a series of calculations that demonstrate the influence of each anomaly on the fit of the model response to the measured MRO motions.

One possible contributor to the above anomalies could be the basic MODE-ID methodology. The extent of such contributions can be assessed in the context of the results of the MODE-ID verification analysis described in Section 3.3 of Chapter 3. This analysis was based on an idealized bridge structure that had classical normal modes and a configuration, section properties, and material properties that were similar (except for the assumed modal damping ratios) to those of the MRO. The structure had pinned boundary conditions at the abutment and

* As noted in Section 4.3.2, the anomalies in the vertical and transverse modes are of opposite sign. This suggests some possible canceling of the total model response produced by the two anomalies.



central-pier-base supports, and transverse and vertical input motions were applied at these support locations that were identical to those measured at the MRO. The dynamic transverse and vertical motion time histories were then computed at each structure degree-of-freedom; these computed motions were, in turn, treated as simulated "measurements" to which MODE-ID was applied in order to identify the modes of the structure. It is noted that no longitudinal motions were incorporated in these computations.


The pseudostatic and normal mode response parameters identified by MODE-ID from the above simulated "measurements" were seen to be nearly identical to the given values of the idealized structure* and were generally similar to those identified for the MRO from the Case 1 superrun (Table 3-4). Also, the EPF matrix identified for the transverse and vertical modes of the idealized structure did not exhibit any of the anomalies that appeared in the EPF matrix identified for the MRO.

The above discussion demonstrates that the anomalies in the EPFs identified for the MRO are caused by differences between the conditions represented by the real earthquake motions vs. the simulated "measurements" computed under the verification analysis. One such difference is the presence of measurement noise in the real motions, which is absent in the simulated "measurements." However, the major difference between the two situations is that the MODE-ID model used in the system identification of the MRO is only an approximation to the real structure whereas, in the verification analysis, it is capable of exactly representing the idealized structure. The reasons for the model being only an approximation for the MRO include:

* Only for the vertical antisymmetric mode, which was not strongly excited by the applied input motions, did the MODE-ID results differ to any notable degree from those of the original idealized bridge structure in the verification analysis.



- Nonlinear Bridge Response. There are several possible sources of nonlinear behavior of bridge structures, which include the inelastic stress/strain characteristics of the soil and the reinforced concrete materials, separation of the pile and pile caps, frictional characteristics along the pile/soil interfaces, etc. At the MRO, there was no significant earthquake-induced damage (e.g., structural cracking, residual tilting or displacement offsets, soil/structure separation at the abutments), or changes over time in frequencies exhibited by the response time history plots. Nevertheless, in view of the large relative vertical displacements along the deck and the major contributions of the foundation/soil system to the bridge's transverse response, it is likely that the MRO experienced at least some degree of nonlinear behavior.
- Use of Classical Uncoupled Normal Mode Model. The modeling of real structures in terms of classical uncoupled normal modes has been widely used in dynamic analysis applications. However, such models have certain limitations when used to represent the measured response of such structures, even at lower excitation levels where nonlinear phenomena may not be significant. For example, it is known that the response of linear soil/structure systems does not exhibit uncoupled normal modes, and the various elements of the structure may not vibrate exactly in phase in a given mode.
- Incomplete Specification of Support Motions. In the MODE-ID verification analysis presented in Chapter 3, the input motions were considered to be pure transverse and vertical translations applied at pinned



support points; i.e., in that analysis, the constraints and degrees of freedom of the supports were fully defined. However, this is not the situation for the Case 1 system of input channels at the MRO (Fig. 4-23), which is insufficient to (a) distinguish between translational and rotational motions at each structure support; and (b) define the amplitude and relative phasing of the longitudinal motions at the two abutments, which could conceivably affect the vertical response of the bridge deck.* Therefore, MODE-ID could possibly be compensating for the missing pseudostatic effects due to this incomplete set of input motion measurements, through artificial adjustment of the identified EPF matrices.

Now let us consider how MODE-ID might compensate for the above differences between the assumed model and the actual bridge. To do this, it is first appropriate to note that MODE-ID separately identifies each element of the EPF matrix for a mode. This is because there are complicated nonlinear constraints among the various matrix elements in the assumed linear

* Figure 4-19 shows that the longitudinal motions at the north abutment exhibit a prominent peak at about 4 Hz that is not found in the longitudinal motions at the north embankment. No longitudinal motions were measured at the south abutment; however if its longitudinal motions were out-of-phase with those at the north abutment, additional near-symmetric vertical motions of the deck would be induced that are analogous to a P- Δ effect and are not now represented, either through the MRO's pseudostatic influence matrix or through its vertical or transverse mode of vibration. Furthermore, the fact that this 4 Hz frequency of amplified longitudinal motion is near the natural frequency of both the deck vertical and transverse response modes suggests that neglecting the longitudinal abutment motions could influence the vertical components of the MRO response in both of these modes.




model. Because these relationships are difficult to treat computationally, they have not been incorporated in MODE-ID (Sec. 3.1.3, Chapt. 3).

Since MODE-ID can separately identify each element in the EPF matrix, it will determine each of these elements so as to optimize the fit between the computed model response and the actual measured response of the MRO, ignoring the above-indicated constraints between the elements that are inherent in the model. If the true structural system is accurately described by the model and its input motions, the MODE-ID results will provide a close representation of the actual structure behavior, as was demonstrated by the verification analysis in Chapter 3. However, the fact that the model will not exactly describe reality and that all components of input motions are not specified could lead to identification of certain terms in the EPF matrix that, while optimizing the fit between measurements and model responses, are not physically plausible. This may account for the unusual features of the MRO response characteristics identified from the Case 1 superrun.

4.3.4.2 Effect of Anomalies on Fit of Model and Measured Response

With the above discussion as background, the effects of the various modal anomalies on the fit between the measured response and the Case 1 model response are now evaluated. This evaluation is implemented by defining four modified Case 1 models (denoted as Models A through D) whose EPF matrices are changed relative to those of the original Case 1 superrun model, so as to isolate the effects of each anomaly. Then, for each modified model, the measure-of-fit, J , is recomputed and compared to that from the original Case 1 superrun model. In addition, acceleration time histories at selected channel locations are recomputed using each modified model, and plots of these time histories are



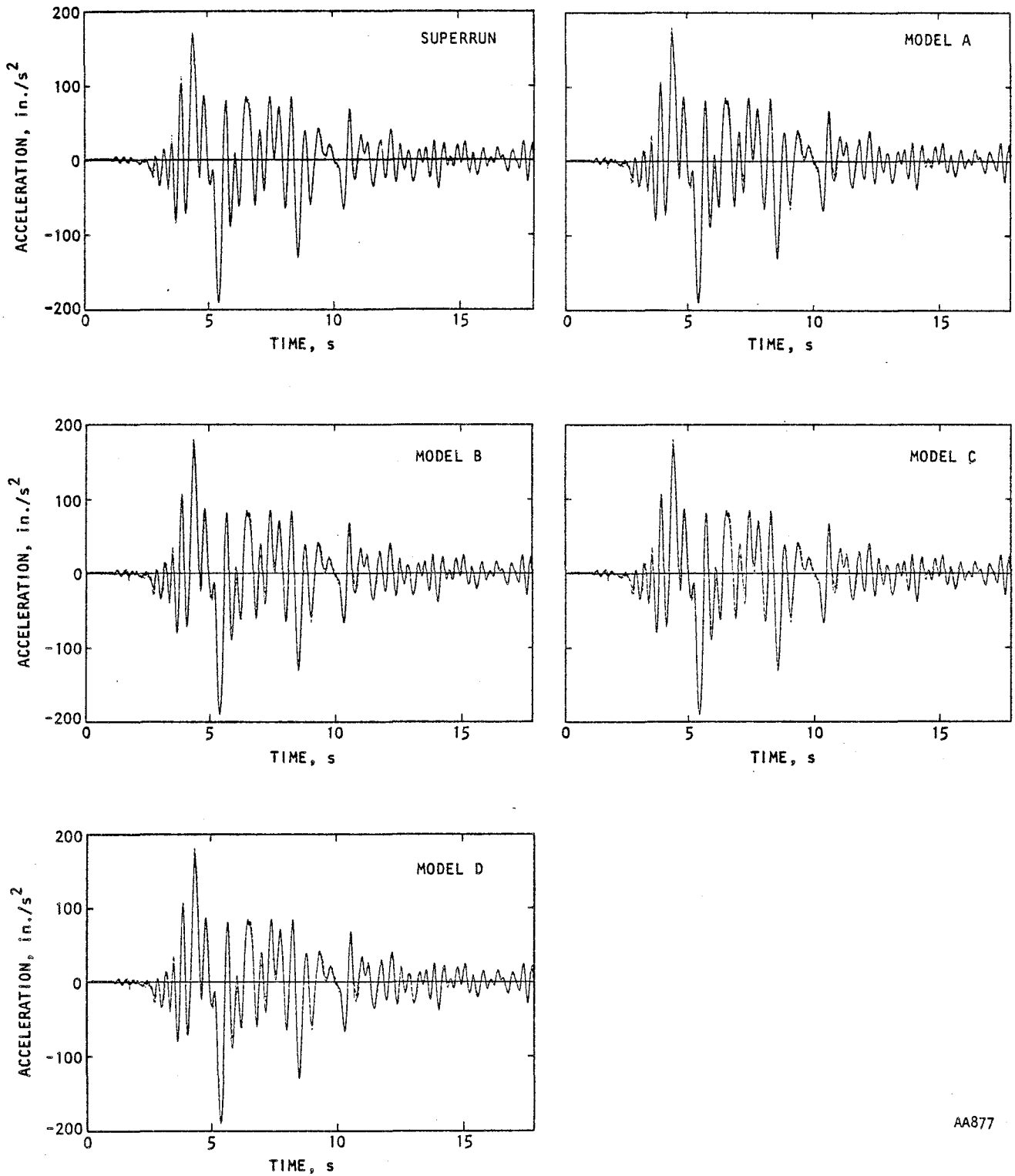
overlaid onto time-history plots from the actual MRO acceleration measurements. These overlaid plots provide a visual indication of how the individual anomalies, as represented through the modified models, affect the fit with the measured bridge motions.

Models A through D and the various modifications of the EPF matrix that they entail are defined in Table 4-7. The new values of J that were computed using each model are also given in this table, and overlaid plots of the measured vs. computed acceleration histories for selected channels are provided in Figures 4-34 through 4-36. These results show the following trends:

- Models A through D give almost the same fit to the measured transverse accelerations as the superrun, and these are excellent (Fig. 4-34). This shows that the EPFs that represent transverse response due to vertical input motions (in both the transverse and vertical modes), have only a very small effect on the fit to the measured transverse motions.
- Comparison of results from the superrun with those from Model A indicates that, when the EPFs that represent vertical translational response due to transverse input motions are deleted from the EPF matrix of both the vertical and transverse mode, the resulting fit with the measured vertical response is worsened substantially over the 4-to-5 sec time segment, and is not markedly affected elsewhere. This does, however, essentially double the value of J .
- Comparison of results from Models A and B show that when the EPFs that represent vertical translational response due to transverse input motions are deleted from the EPF matrix for the vertical mode only (i.e., is included only in the EPF matrix for the transverse mode), the fit between the model vs. measured vertical



————— MEASURED RESPONSE
- - - - - MODEL RESPONSE



AA877

FIGURE 4-34. CASE 1 RESULTS: EFFECT OF MODAL ANOMALIES ON FIT OF MODEL AND MEASURED TRANSVERSE ACCELERATION HISTORIES AT CHANNEL 7

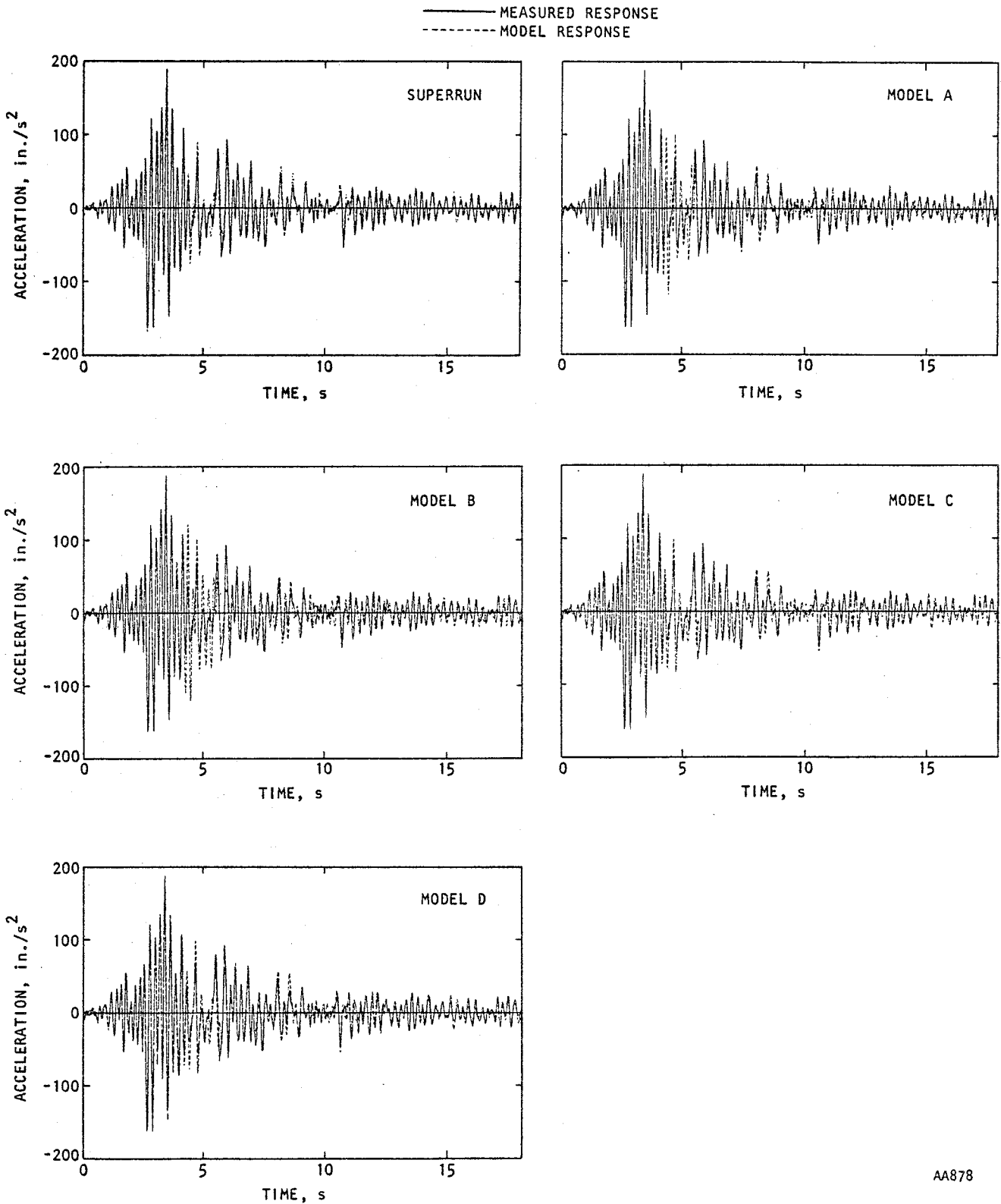
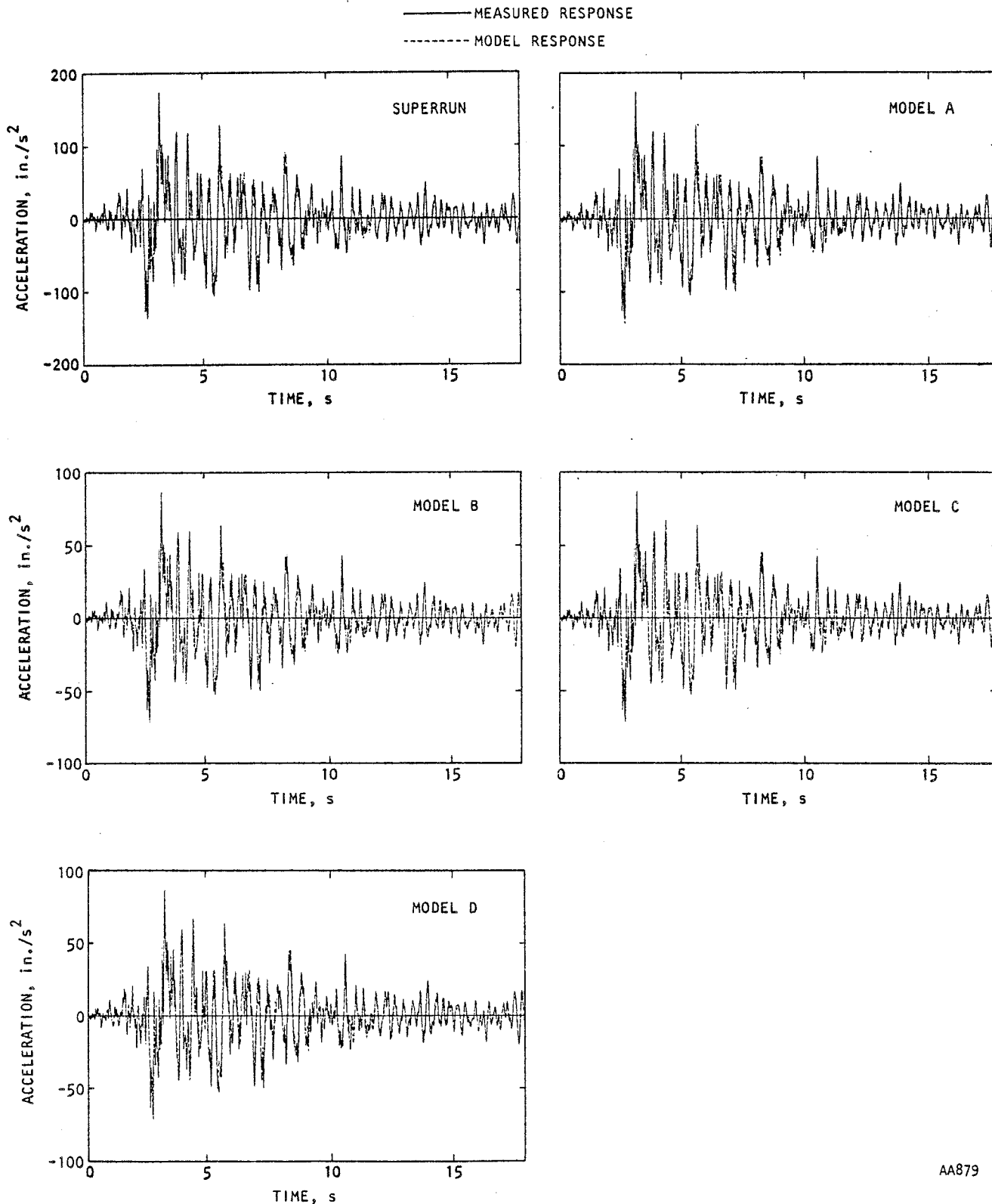


FIGURE 4-35. CASE 1 RESULTS: EFFECT OF MODAL ANOMALIES ON FIT OF MODEL AND MEASURED VERTICAL ACCELERATION HISTORIES AT CHANNEL 16



AA879

FIGURE 4-36. CASE 1 RESULTS: EFFECT OF MODAL ANOMALIES ON FIT OF MODEL AND MEASURED VERTICAL ACCELERATION HISTORIES AT CHANNEL 21




response actually worsens. Only when these EPFs are included in the EPF matrices for both the transverse and vertical modes (Model C) does the fit with the measured vertical response dramatically improve, primarily in the 4-to-5 sec time range.

- Comparison of results from Models C and D indicates that, when the EPFs that represent vertical translational response due to transverse input motions are included in the EPF matrix for the vertical mode, the deletion of these EPFs from the EPF matrix for the transverse mode causes only a very slight worsening of the fit between the model vs. measured vertical response.

The above trends indicate two interesting elements of the various anomalies in the Case 1 superrun results. First, they show that a classical mode model estimated by removing the anomalies from the MODE-ID results (Model A) provides a good overall fit with the measured response of the MRO, except over a short time segment (extending from about 4 sec to about 5 sec after triggering of the instruments). Also, they show that the anomaly in the EPFs for the vertical mode is much more important to the fit with the measured MRO response than is the anomaly in the EPFs for the transverse mode. In fact, since the transverse mode's anomaly actually worsens the fit when considered without the vertical mode's anomaly, it may represent an attempt by MODE-ID to compensate for an overcorrection to the fit by the vertical mode's anomaly alone. This contention is supported by the fact that these anomalies produce vertical motion of opposite sign (Figs. 4-29b, 4-30a).

4.4 CASE 2 RESULTS

The second of the MODE-ID applications to the MRO seismic response measurements considers the input motions to be those motions measured at the embankments and at the central-pier base, and the response motions to be those motions measured at



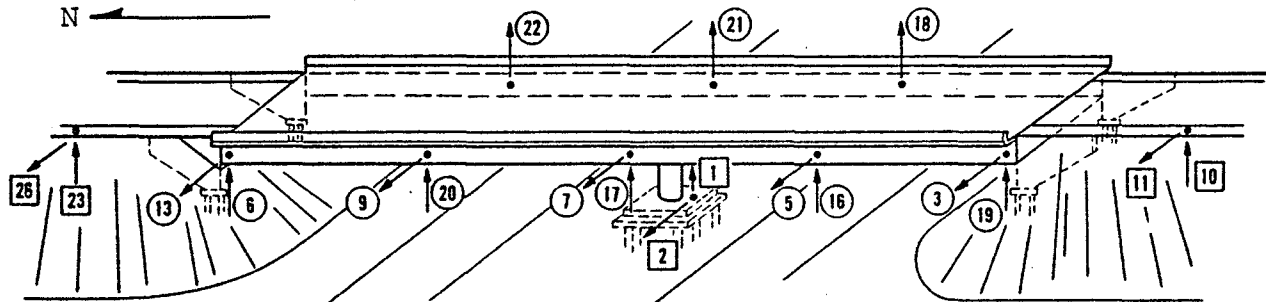
the abutments and along the road deck (Fig. 4-37). Therefore, this Case 2 application differs from that of Case 1 in that (1) the response of the abutments and part of the embankments is now incorporated in the normal modes of vibration; and (2) the pseudostatic response now represents the "static" contributions of the portion of the embankments that extend beyond the locations of the embankment instruments, the foundation/soil system at the central-pier base, and the soil medium that underlies the MRO.

The Case 2 results are presented in accordance with the same general sequence as followed for Case 1. This presentation covers the confirmation of suspected modes for the Case 2 model (Sec. 4.4.1), the Case 2 superrun results (Sec. 4.4.2), and detailed interpretations of these results (Secs. 4.4.3 to 4.4.5).

4.4.1 CONFIRMATION OF MODES

The first step in the identification of the Case 2 model involves use of MODE-ID to confirm the significant modes and to obtain improved estimates of their natural periods that will be used as input to the subsequent superrun calculations. As in Case 1, this entails application of MODE-ID to two subsets of the Case 2 channels - one corresponding to the transverse input and response channels only, and the other corresponding to the vertical input and response channels only.

Results from the application of MODE-ID to the Case 2 transverse input and response channels are summarized in Figure 4-38. These results show that two symmetric modes of vibration and a pseudostatic influence matrix are identified, and these produce an excellent fit to the measured Case 2 transverse response (as indicated by the low value of J shown in Figure 4-38). The fundamental symmetric mode, termed the system transverse response mode, did not appear in the prior Case 1 calculations because it primarily involves significant abutment motions that were represented in Case 1 through the pseudostatic



LEGEND:

- = INPUT CHANNELS
- = RESPONSE CHANNELS

(a) Channel locations

Channel Type	Location	Number	Direction
Input Channels	Base of Central Pier	1	Vertical
		2	Transverse
	South Embankment	10	Vertical
		11	Transverse
	North Embankment	23	Vertical
		26	Transverse
Response Channels	South Abutment	19	Vertical
		3	Transverse
	Along Road Deck	16,17,18 20,21,22	Vertical
		5,7,9	Transverse
	North Abutment	6	Vertical
		13	Transverse

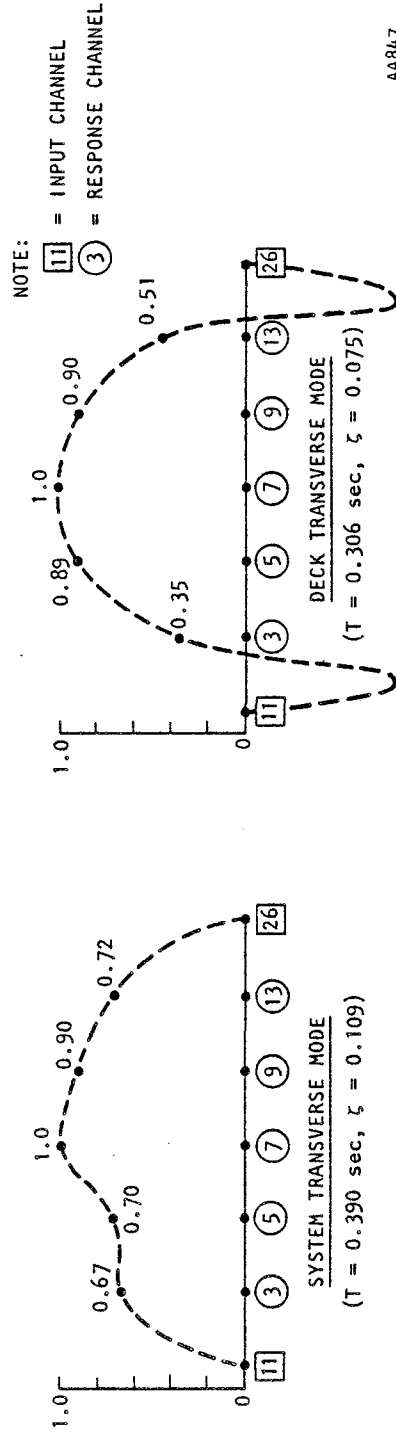
(b) Channel tabulations

FIGURE 4-37. CASE 2 SUBSET OF INPUT AND RESPONSE CHANNELS



Mode	Natural Period, Sec	Damping Ratio	Pseudostatic and Modal Response Characteristics	Channel Numbers					Measure of Fit, J (Eq. 3-21)
				3	5	7	9	13	
Pseudostatic Response	-	-	Sum of elements in rows of pseudostatic influence matrix	0.95	1.07	1.04	1.01	0.98	0.048
Deck/Abutment System Mode	0.390	0.109	Sum of elements in rows of effective participation factor matrix	0.27	0.28	0.40	0.36	0.29	
			Normalized mode shape	0.67	0.70	1.0	0.90	0.72	
Deck Transverse Mode	0.306	0.075	Sum of elements in rows of effective participation factor matrix	0.23	0.58	0.65	0.59	0.33	
			Normalized mode shape	0.35	0.89	1.00	0.91	0.51	

(a) Tabulation of results



AA847

(b) Plots of mode shapes

FIGURE 4-38. CASE 2: APPLICATION OF MODE-ID TO TRANSVERSE INPUT AND RESPONSE CHANNELS FOR 2-MODE MODEL



influence matrix. It has a natural period of 0.390 sec, and was shown from our earlier assessment of the measured MRO motions to represent a significant contributor to the overall transverse response of the MRO (see Sec. 4.1). The second symmetric mode identified from this transverse-input/transverse-response application is similar to the deck transverse response mode that was identified under Case 1. It has a natural period ($T = 0.306$ sec) and a damping ratio ($\xi = 0.075$) that are somewhat greater than those shown by the Case 1 results. Reasons for this trend, as well as for the large negative mode shape amplitudes shown along the embankments (Fig. 4-38b), are discussed in Section 4.4.2.4.*

The application of MODE-ID to the Case 2 subset of vertical input and response channels is summarized in Figure 4-39. The only significant mode identified from this application is a deck vertical response mode that was also identified in Case 1. Its natural period ($T = 0.216$ sec) is nearly identical to that identified under Case 1 and its damping ratio ($\xi = 0.056$) is somewhat lower. The large value of J shown in Figure 4-39 indicates that these identified pseudostatic and modal parameters provide a rather poor fit to the vertical motions that were measured at the MRO. As in Case 1, this is because these initial modal estimates neglect the presence of any coupled transverse and vertical components in the mode shapes for the various modes - an assumption that particularly affects the fit between the model vs. measured vertical motions. The subsequent Case 2 superrun, which includes these coupling effects, identifies a model whose computed vertical motions compare much more favorably with those measured at the MRO.

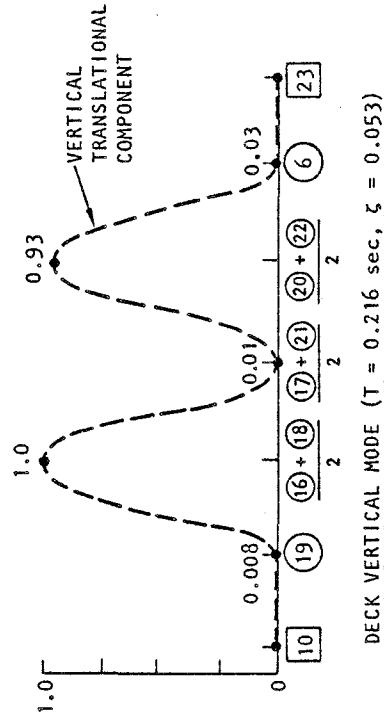
* It is noted here that all mode shapes are identified only at the discrete locations of the strong motion instruments. The dashed curves shown in the mode shape plots represent the expected variation between these instrument locations.



Mode	Natural Period, Sec	Damping Ratio	Pseudostatic and Modal Response Characteristics	Channel Numbers				Measure of Fit, J (Eq. 3-21)	
				19	16 18	17 21	20 22		6
Pseudostatic Response	-	-	Sum of elements in rows of pseudostatic influence matrix	0.95	1.17 1.11	1.01 0.88	1.22 0.94	1.01	0.307
Deck Vertical Mode	0.216	0.053	Sum of elements in rows of effective participation factor matrix	0.02	1.25 1.12	0.01 0.03	1.11 1.09	0.08	0.307
			Normalized mode shape	0.016	1.0 0.90	0.008 0.020	0.89 0.87	0.06	

(a) Tabulation of results

NOTE:
10 = INPUT CHANNEL
19 = RESPONSE CHANNEL



AA846

(b) Plot of mode shape

FIGURE 4-39. CASE 2: APPLICATION OF MODE-ID TO VERTICAL INPUT AND RESPONSE CHANNELS



4.4.2 SUPERRUN RESULTS

With the significant modes now established, MODE-ID is next applied in a superrun that considers all Case 2 transverse and vertical input and response channels simultaneously, so as to identify final values of the Case 2 model parameters. The paragraphs that follow discuss the overall adequacy of the identified superrun model and the characteristics of its pseudostatic influence matrix and normal modes.

4.4.2.1 Adequacy of Identified Model

The overall results of this superrun calculation are presented in tabulated form (Table 4-8), and in plotted form as overlaid plots of motion time histories from MRO measurements and from computations using the identified MODE-ID model (Figs. 4-40 to 4-44). Table 4-8 shows that the identified Case 2 superrun model is comprised of a pseudostatic influence matrix, a deck vertical response mode, and two symmetric transverse response modes. In the remainder of this chapter, the two transverse modes are named the system transverse response mode and the deck transverse response mode (this latter name was chosen to be consistent with the terminology used for a similar mode identified in Case 1). It should be noted, however, that these two modes are actually the bridge's fundamental symmetric transverse mode and second symmetric transverse mode respectively, and the mode shapes for both modes include translations of the abutments as well as the road deck.

The low value of J indicated by the tabulated results ($J = 0.093$) and the close comparisons between the overlaid motion time history plots both show that the identified Case 2 model closely represents the MRO's measured seismic response. However, this value of J is now slightly higher than that from the Case 1 results (which was $J = 0.056$), indicating that Case 2 model does not fit the measured response quite as well as does the Case 1 model. Examination of the overlaid motion time history plots from the two cases shows that this difference in

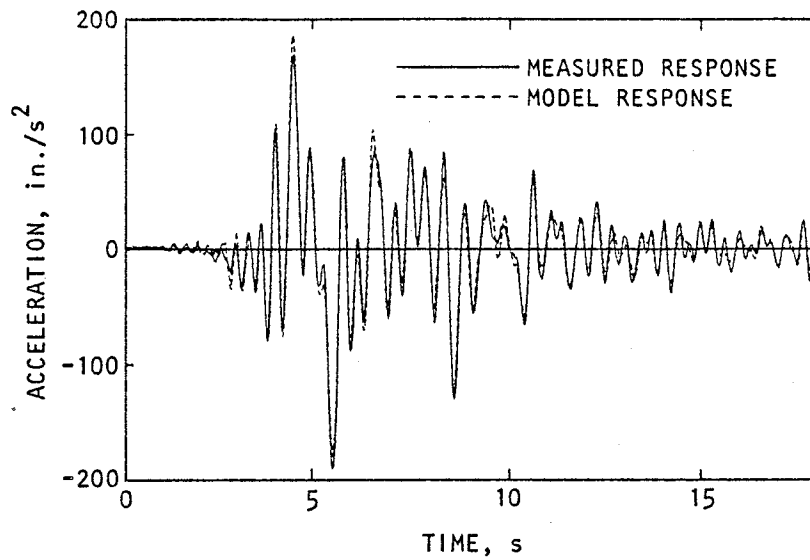


TABLE 4-8. CASE 2 SUPERRUN RESULTS: TABULATION AND SUMMARY

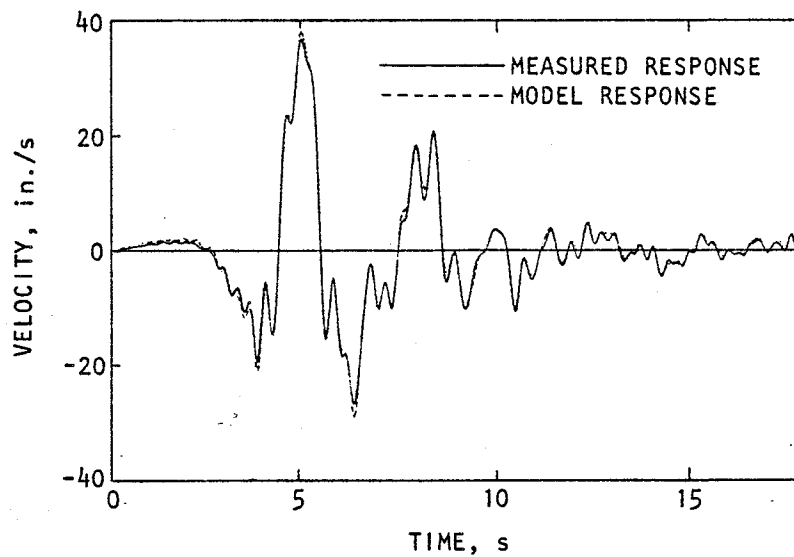
Mode	Natural Period (Sec)	Damping Ratio	Summation of Rows of Pseudostatic Influence Matrix or Effective Participation Factor Matrix																		Measure of Fit, J (Eq. 3-21)
			Input Channels						Response Channels												
			Transverse						Vertical												
			3	5	7	9	13	19	16	17	20	18	21	22	6						
Pseudostatic	-	-	Transverse (2, 11, 26)	0.96	1.04	1.02	0.98	0.95	0.0	-0.05	-0.02	-0.05	0.02	0.0	-0.03	0.0					
			Vertical (1, 10, 23)	-0.01	0.0	-0.01	-0.01	0.01	0.98	1.10	0.94	1.10	1.06	0.92	0.94	0.99					
System Transverse	0.390	0.103	Transverse (2, 11, 26)	0.18	0.10	0.24	0.23	0.20	-0.10	-0.04	-0.12	0.14	0.05	0.03	0.01						
			Vertical (1, 10, 23)	-0.04	-0.05	-0.09	-0.10	-0.06	0.08	-0.17	0.03	-0.20	-0.29	-0.07	-0.17	0.02					
Deck Transverse	0.309	0.073	Transverse (2, 11, 26)	0.30	0.62	0.70	0.64	0.39	-0.06	-0.40	-0.55	0.44	0.49	0.39	-0.15						
			Vertical (1, 10, 23)	-0.02	0.04	0.03	0.03	0.04	-0.05	-0.10	-0.10	-0.20	-0.11	0.0	-0.69	0.0					
Deck Vertical	0.219	0.056	Transverse (2, 11, 26)	0.10	0.05	0.02	0.08	0.13	-0.10	-0.42	-0.15	-0.69	0.01	-0.49	-0.03						
			Vertical (1, 10, 23)	0.03	-0.02	0.0	0.02	0.04	0.03	1.30	0.0	1.20	1.24	0.07	1.21	0.06					



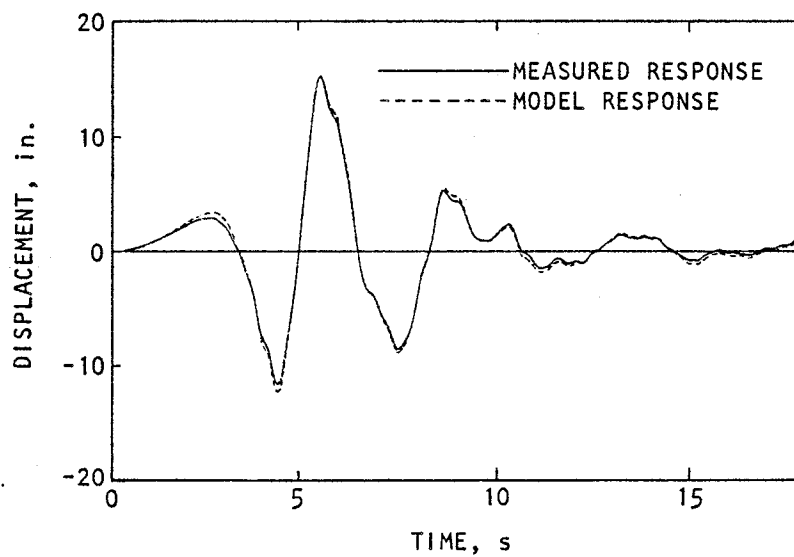
R-8222-5603



(a) Acceleration



(b) Velocity



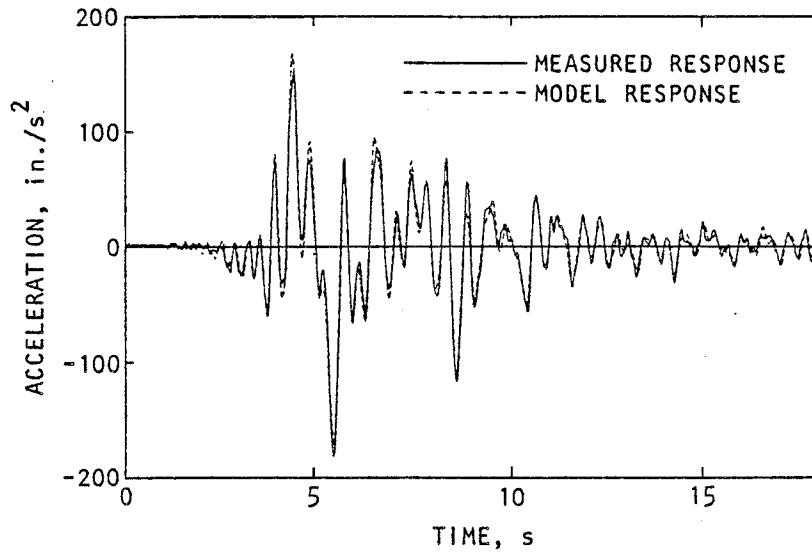
(c) Displacement

AA880

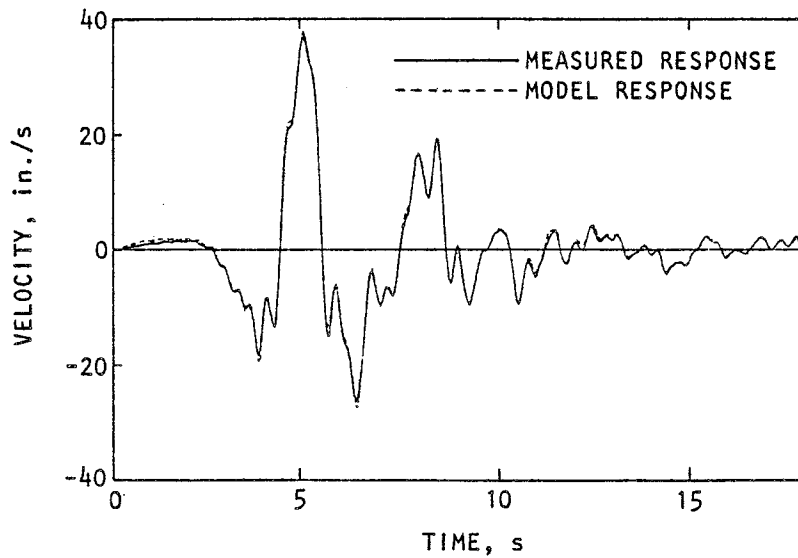
FIGURE 4-40. CASE 2 SUPERRUN RESULTS: COMPARISON OF MEASURED AND MODEL TRANSVERSE RESPONSE AT CHANNEL 7 (OVER CENTRAL PIER)



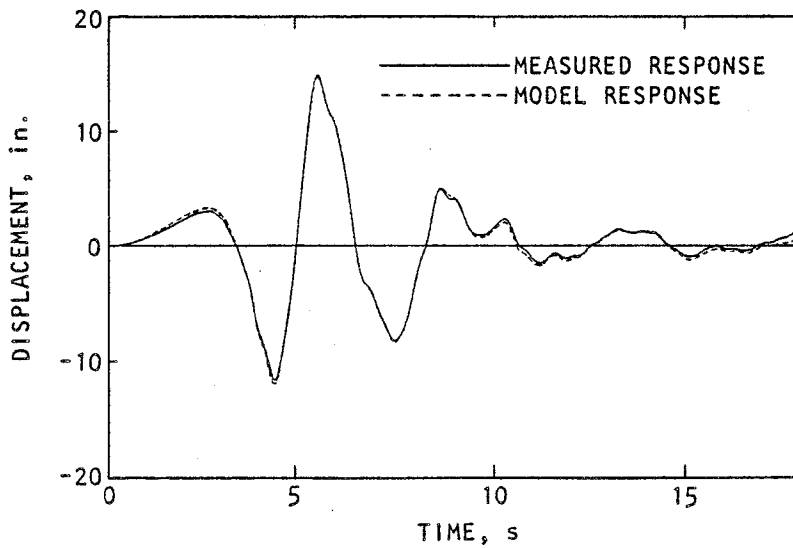
R-8222-5603



(a) Acceleration



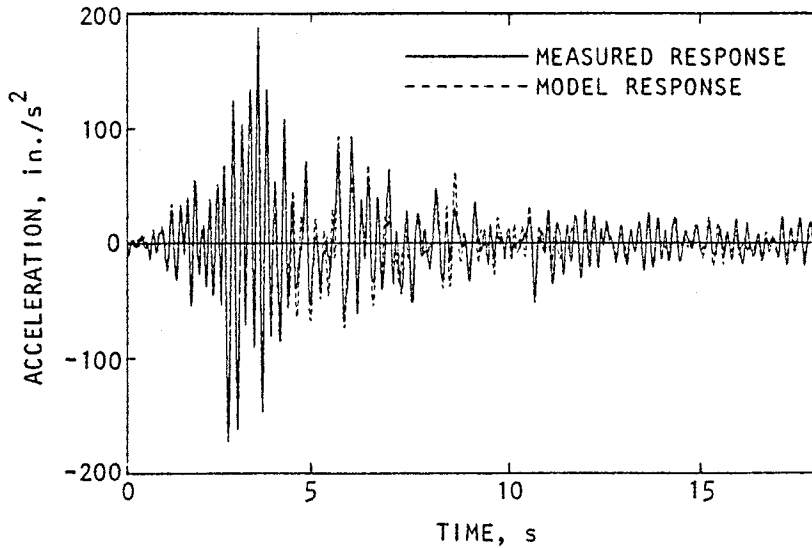
(b) Velocity



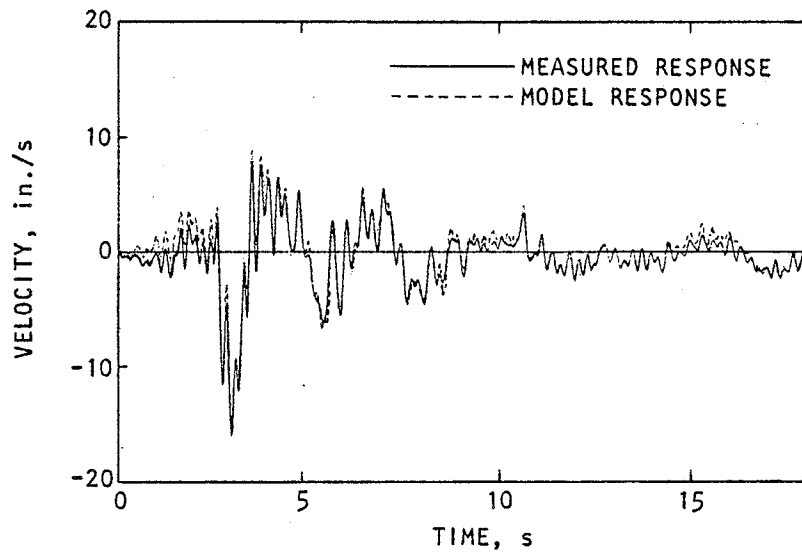
(c) Displacement

AA881

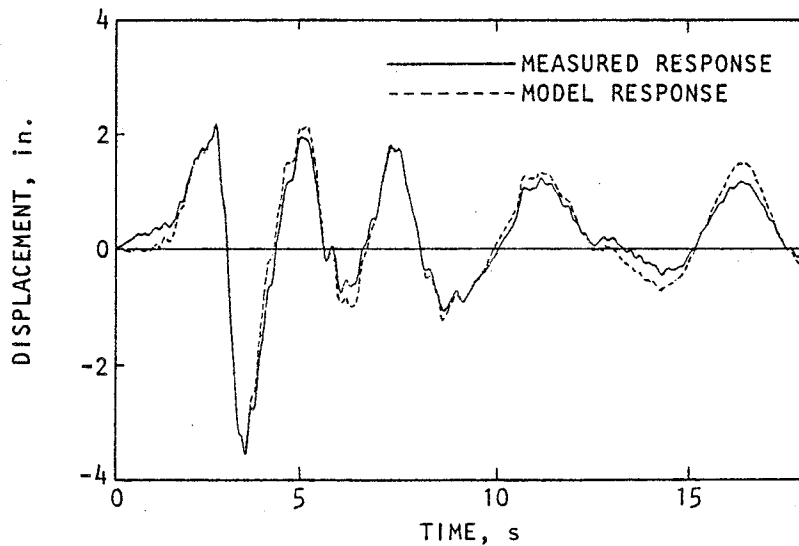
FIGURE 4-41. CASE 2 SUPERRUN RESULTS: COMPARISON OF MEASURED AND MODEL TRANSVERSE RESPONSE AT CHANNEL 13 (WEST FACE OF NORTH ABUTMENT)



(a) Acceleration



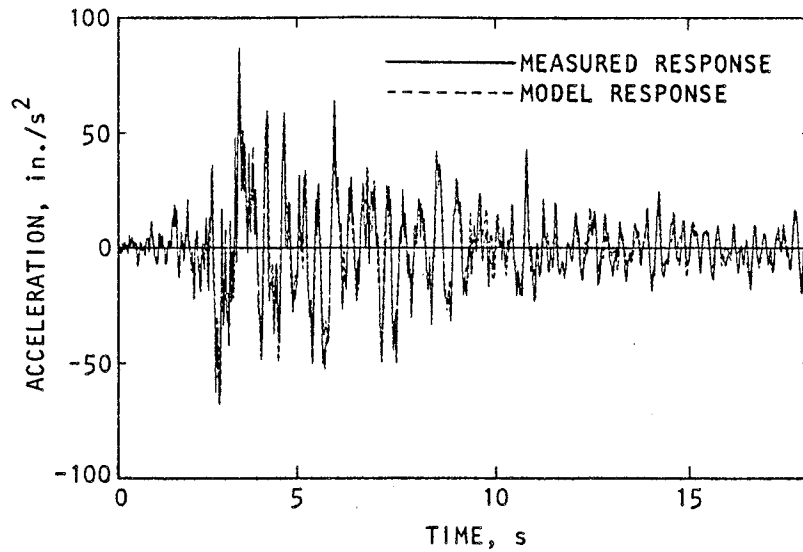
(b) Velocity



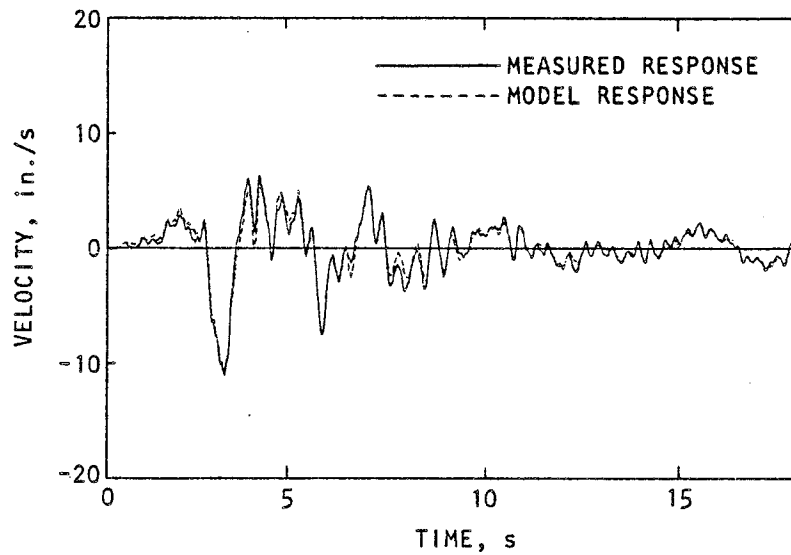
(c) Displacement

AA882

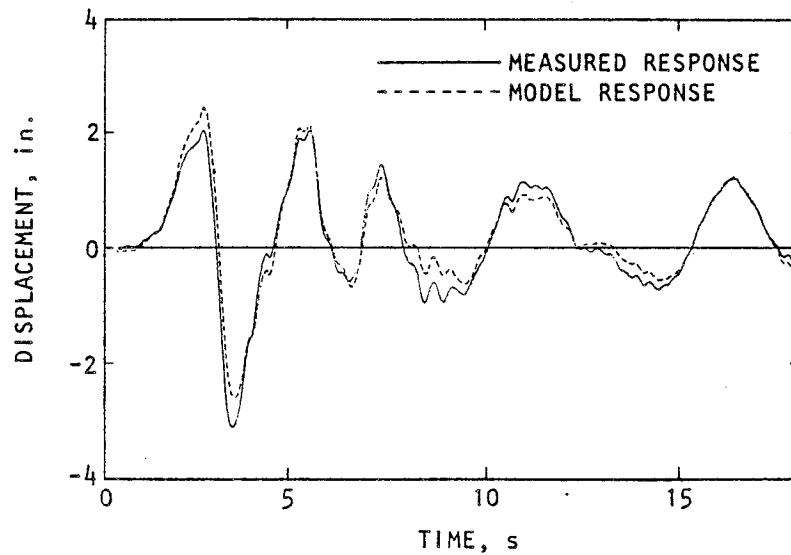
FIGURE 4-42. CASE 2 SUPERRUN RESULTS: COMPARISON OF MEASURED VS. MODEL VERTICAL RESPONSE AT CHANNEL 16 (MIDLENGTH OF SOUTH SPAN, ALONG WEST FACE OF BRIDGE DECK)



(a) Acceleration



(b) Velocity



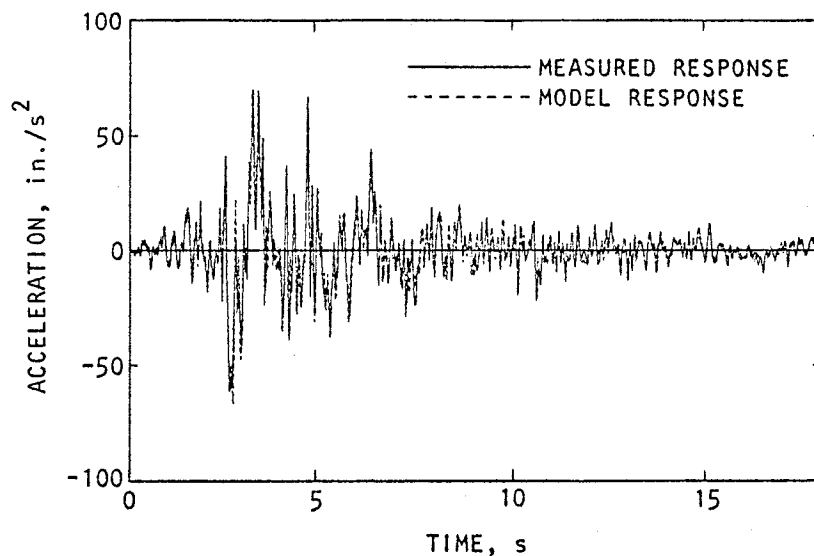
(c) Displacement

AA883

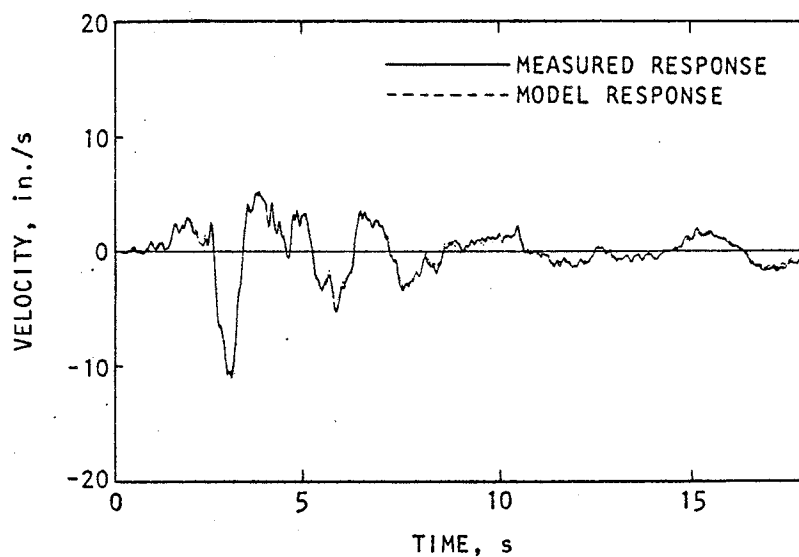
FIGURE 4-43. CASE 2 SUPERRUN RESULTS: COMPARISON OF MEASURED VS. MODEL VERTICAL RESPONSE AT CHANNEL 21 (OVER CENTRAL PIER, ALONG EAST FACE OF BRIDGE DECK)



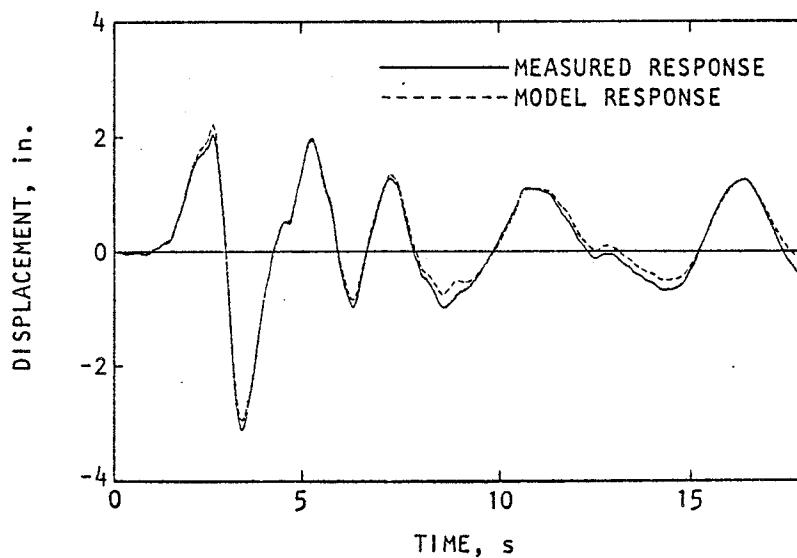
R-8222-5603



(a) Acceleration



(b) Velocity



(c) Displacement

FIGURE 4-44. CASE 2 SUPERRUN RESULTS: COMPARISON OF MEASURED VS. MODEL VERTICAL RESPONSE AT CHANNEL 6 (WEST FACE OF NORTH ABUTMENT)

AA884



fit is primarily in the vertical motions; i.e., the Case 1 model provides a somewhat closer fit to the measured vertical motions than does the Case 2 model. Both models, however, provide an excellent overall fit to the measured transverse motions of the MRO. These results will be interpreted and discussed further in Sections 4.4.3 to 4.4.5.

4.4.2.2 Pseudostatic Influence Matrix

The partial row-sums provided in Table 4-8 for the pseudostatic influence matrix show that, as in Case 1, the transverse input motions are the primary contributors to the pseudostatic response at the various transverse response channel locations, and the vertical input motions are the main contributors to the pseudostatic response at the vertical response channels. Furthermore, as before, the partial row-sums corresponding to each response channel are all reasonably close to the theoretically correct values of zero or unity.

4.4.2.3 System Transverse Response Mode

The system transverse response mode of the MRO abutment/superstructure system is identified in this Case 2 superrun as having a natural period ($T = 0.392$ sec) and a damping ratio ($\xi = 0.103$) that are nearly identical to those identified from the transverse-input/transverse-response calculation. The mode shape for this mode features significant transverse response components at the abutments, and is an important contributor to the overall transverse response of the MRO. As previously noted, it is the fundamental symmetric mode of transverse vibration of the bridge.

The partial row-sums of the EPF matrix that correspond to transverse input motions and to vertical input motions are tabulated in Table 4-8, and the corresponding normalized mode

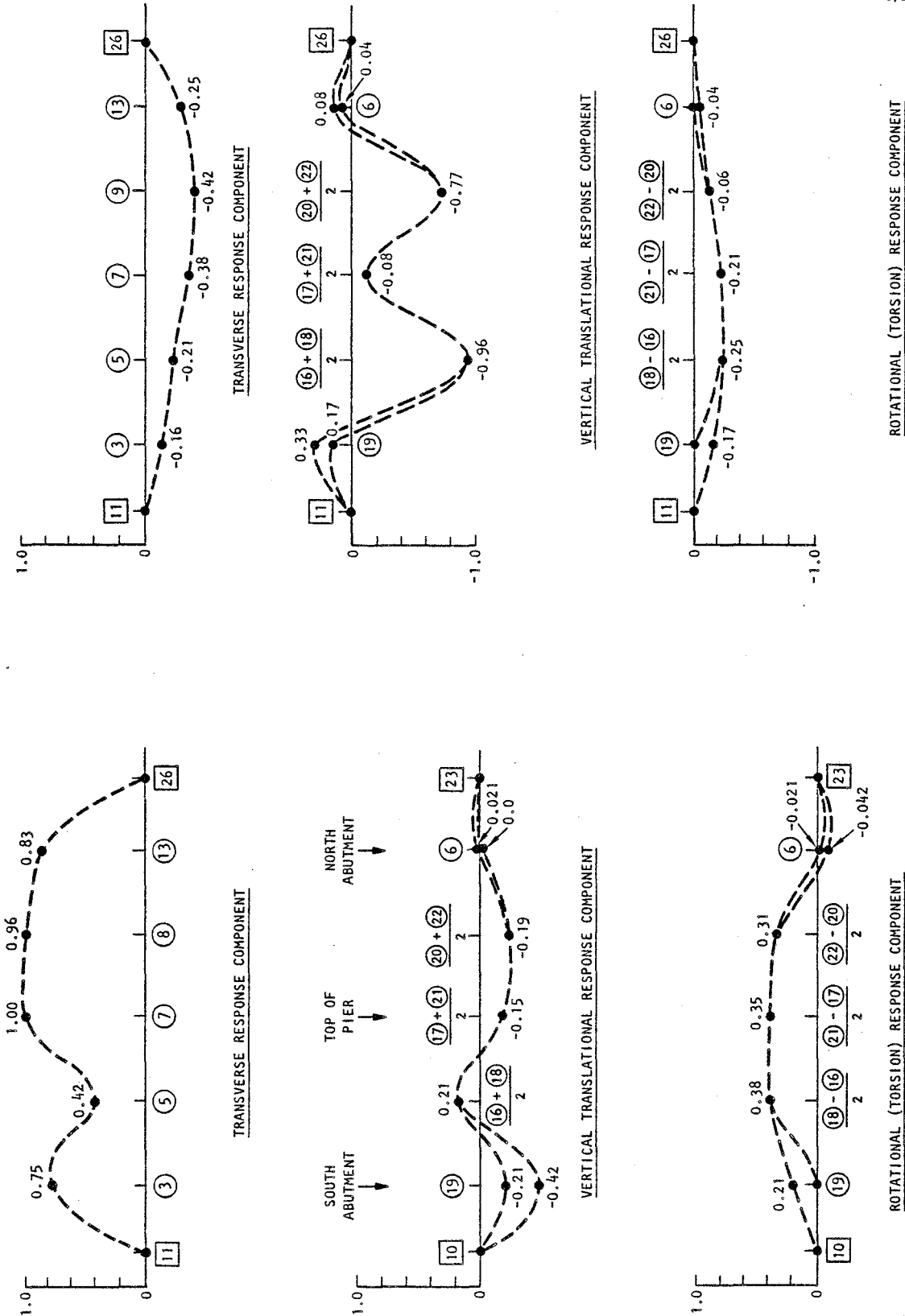


shapes are plotted in Figure 4-45.* The features of these partial row-sums and corresponding mode shapes are as follows:

- The transverse response component due to transverse input motions is reasonably symmetric about the mid-span of the MRO, except for a pronounced kink in the mode shape amplitude at the midlength of the south span (Channel 5). Possible causes of this kink are discussed in Section 4.4.4.
- The rotational (torsion) response component due to transverse input motions is reasonably uniform along the length of the deck. In the vicinity of the abutments, the amplitude of this rotational component decreases markedly, probably because of the significant torsional stiffness of the abutments and their underlying pile supports.
- Figure 4-45 also shows noticeable vertical translational response components due to transverse input motions, and prominent transverse, vertical, and torsional response components due to vertical input motions. These appear to be physical anomalies of the type discussed under Case 1, and are interpreted in Section 4.4.5.

It is noted that the single vertical response measurement at each abutment is insufficient to separate the relative contributions of the translational and rotational (torsion) components to the total vertical response at the abutments. For this reason, the mode shape amplitudes that correspond to these two components are shown in Figure 4-45 to have two bounding values at the abutments. The first bound assumes that the abutment's geometry and distribution of pile supports leads to a


*For reasons previously discussed under Case 1 (Sec. 4.3.2.3), these mode shape plots for both the transverse and vertical input motions, are normalized to a common scale factor. The same is true of mode shape plots shown subsequently for the other modes identified under Case 2.



(a) Due to transverse input motions (Channels 2, 11, 26)

(b) Due to vertical input motions (Channels 1, 10, 23)

FIGURE 4-45. CASE 2 SUPERRUN RESULTS: NORMALIZED MODE SHAPE FOR SYSTEM TRANSVERSE RESPONSE MODE ($T = 0.392$ sec, $\zeta = 0.113$)

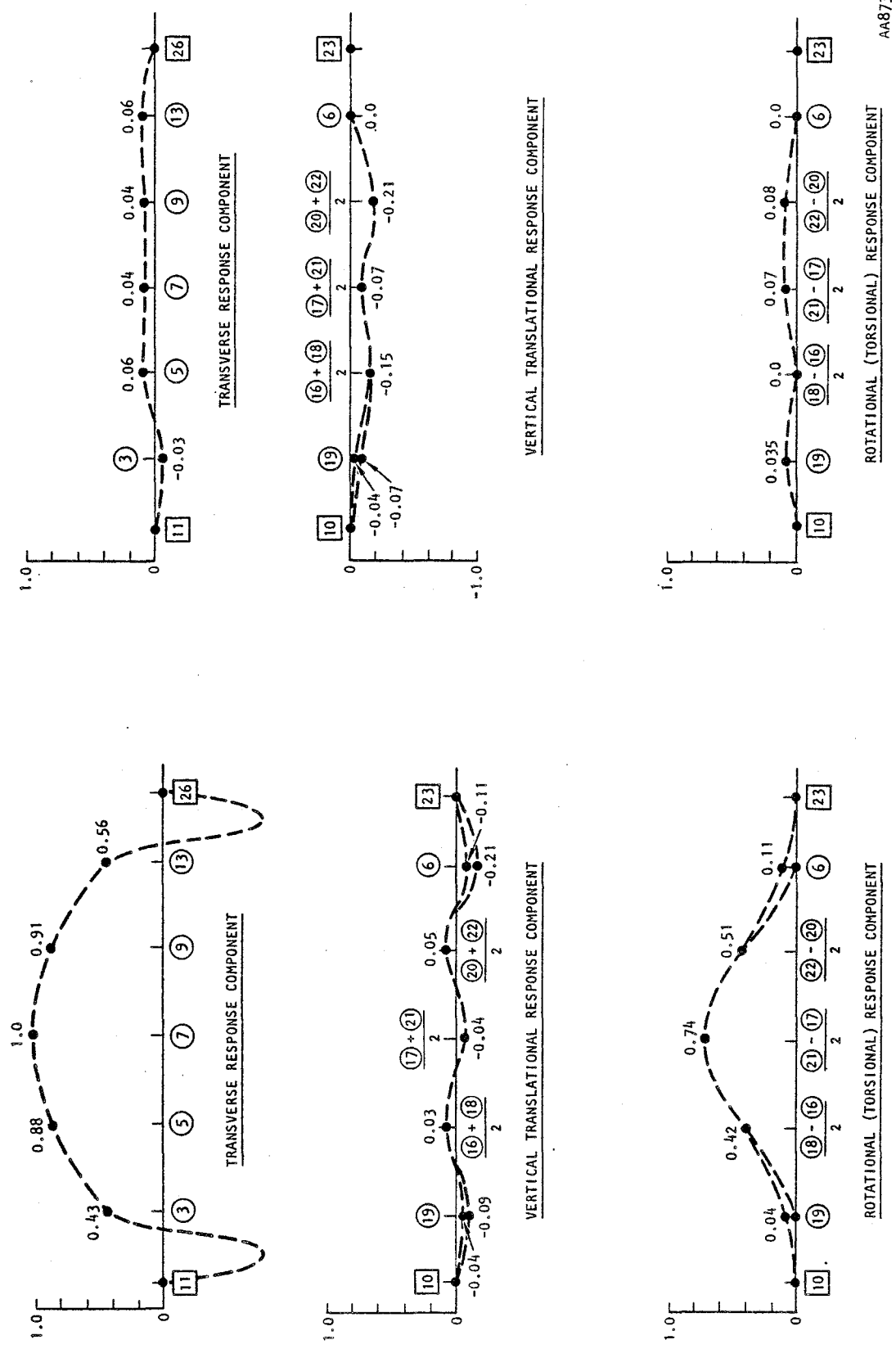


large torsional stiffness that prevents any torsional rotation from occurring at the abutments; i.e., all of the motion at the single vertical accelerometer at each abutment is assumed to arise from vertical translations only. The second bound assumes that the abutments undergo finite vertical translations and torsional rotations that contribute equally to the motion measured at each abutment's single vertical accelerometer. These same two bounds will also be shown in the plots of mode shapes from the remaining superrun results presented in this section.

4.4.2.4 Deck Transverse Response Mode

The second transverse response mode identified for this Case 2 model has a mode shape with near-symmetric transverse translations and torsional rotations of the deck, and with transverse translations of the abutment as well (Fig. 4-46). This mode, which corresponds to a similar mode from Case 1, has a natural period ($T = 0.306$ sec) and a damping ratio ($\xi = 0.078$) that are both larger than those of the Case 1 model. This is because of the previously noted differences in how the Case 1 and Case 2 models incorporate the measured transverse motions of the two abutments, which are strongly affected by the soils in the adjacent embankments and in the underlying geologic media. Because of these differences, the Case 2 model incorporates abutment/soil system response characteristics through its normal modes of vibration whereas, in Case 1, these characteristics were incorporated through the pseudostatic influence matrix. In view of this, together with the particularly strong influence of the abutment response on the MRO's transverse response (Sec. 4.1) and the inherently low stiffness and high damping of the adjacent soils, it follows that the natural period and damping ratio of transverse response mode should be greater in Case 2 than in Case 1.

Another interesting comparison between the Case 1 and Case 2 results for this mode involves the relative values of the



(a) Due to transverse input motions (Channels 2, 11, 26)


(b) Due to vertical input motions (Channels 1, 10, 23)

FIGURE 4-46. CASE 2 SUPERRUN RESULTS: NORMALIZED MODE SHAPE FOR DECK TRANSVERSE RESPONSE MODE ($T = 0.306$ sec, $\zeta = 0.079$)



various partial row-sums of the EPF matrix. Figure 4-46 shows that the Case 2 set of input and response measurements result in partial row-sums that lead to a physically plausible set of mode shape components whose amplitudes are significant only for the transverse translational and torsional components due to transverse input; i.e., all other mode shape components shown in Figure 4-46 are small. In contrast to this, the partial row-sums for the similar mode in Case 1 showed a significant vertical translational component due to transverse input (Fig. 4-30a). This component from Case 1 was judged to be physically implausible, and the corresponding elements of the EPF matrix for that mode were shown in Section 4.3.3 to have an insignificant effect on the fit of the model motions to the measured motions. The rationale for ignoring this component in the Case 1 results is further strengthened by the results from Case 2, which shows that this questionable component disappears almost entirely when a different set of input and response channels is considered. This is further discussed in Section 4.4.5.

The transverse-input/transverse-response component of the mode shape for this deck transverse mode also warrants discussion. Figures 4-45 and 4-46 show that this mode shape component exhibits embankment translations that are 180 deg out of phase with the deck translations for this mode. These out-of-phase embankment translations were not actually computed by MODE-ID, because of the limited strong motion instrumentation within the embankments. Rather, in view of this limited instrumentation, they were inserted as an assumed vehicle for maintaining orthogonality between the deck and system transverse response modes. This assumption was supported by approximate orthogonality calculations that accounted for the large mass of the embankment soil medium. These calculations showed that for reasonable assumptions regarding possible locations of nodes (i.e., zero points) in the region of the mode shape along the embankments, only small-to-moderate values of the out-of-phase embankment translations are required to satisfy orthogonality

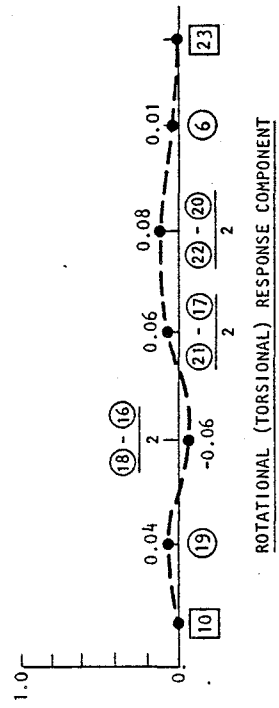
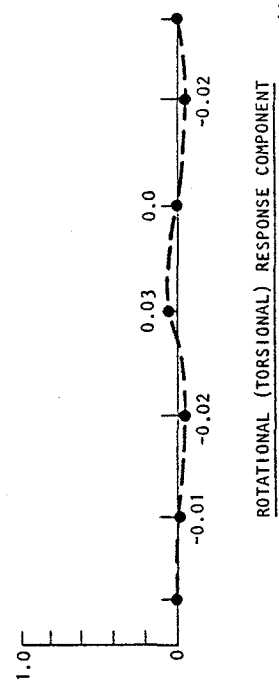
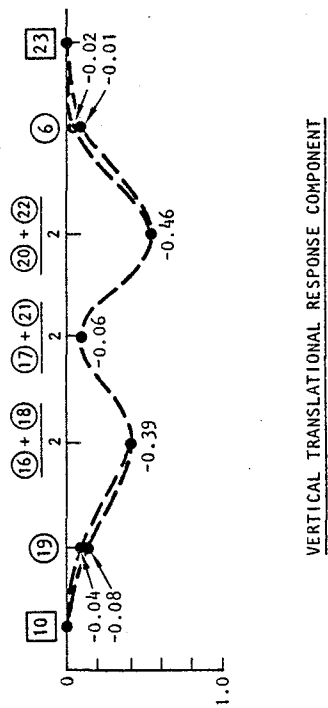
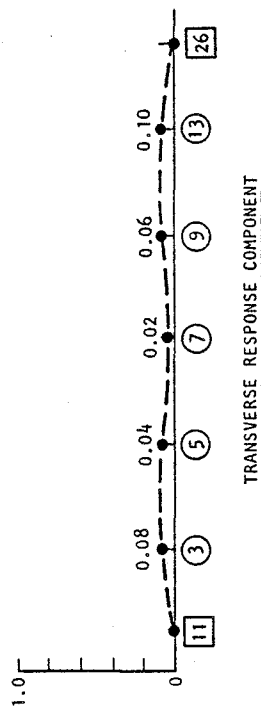
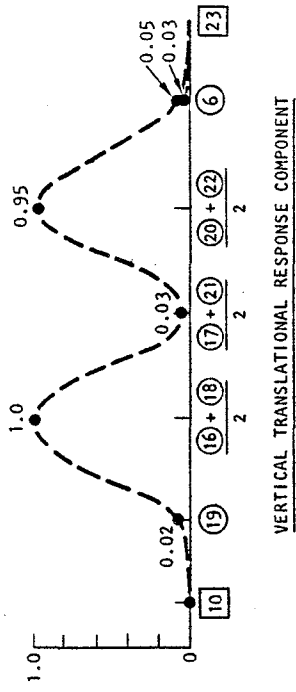
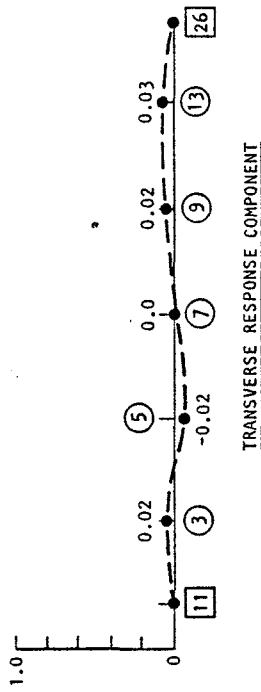


between the two transverse modes. Of course, the calculations are based on the locations of the embankment instruments being points of fixity in the mode shape, because these locations are input points in the Case 2 applications. This would not necessarily be the case if sufficient instrumentation existed within the embankments to permit a more complete assessment of their contributions to the MRO's transverse response characteristics. Nevertheless, even if the point of fixity changes, the assumed existence of out-of-phase embankment translations in the deck transverse mode remains as a physically plausible basis for maintaining the required modal orthogonality relationships.

4.4.2.5 Deck Vertical Response Mode

A deck vertical response mode has been identified from the Case 2 superrun that was also identified in Case 1. Its natural period ($T = 0.219$ sec) is only slightly greater than that for Case 1, and its damping ratio ($\xi = 0.058$) is slightly reduced. This reduction in damping ratio, although slight, occurs despite the fact that the Case 2 normal modes include effects of the abutments and a portion of the embankment soil medium, whereas the Case 1 modes do not. These abutment/soil effects would tend to increase the modal damping ratio if their contributions to the modal response characteristics were significant. However, this is not the case for the deck vertical response mode, which is instead dominated by the dynamic response characteristics of the deck itself.* In fact, the contributions of the abutment/soil effects in this mode are probably sufficiently small so as to be overshadowed by the uncertainties and numerical difficulties inherent in the estimation of damping ratios. This, in

*The predominant effects of the deck properties on this vertical response mode have been established from our prior assessment of the MRO's strong motion data (Sec. 4.1). This hypothesis is further supported by the Case 2 EPFs established for this mode (Fig. 4-47) which show that, in the vertical response component due to vertical input, the abutment EPFs are small when compared to those of the road deck.




AA874

(b) Due to vertical input motions (Channels 1, 10, 23)

(a) Due to transverse input motions (Channels 2, 11, 26)

FIGURE 4-47. CASE 2 SUPERRUN: NORMALIZED MODEL SHAPE FOR DECK VERTICAL RESPONSE MODE ($T = 0.219$ sec, $\zeta = 0.058$)



turn, would account for the slight reduction in the damping ratio identified for this mode in Case 2 relative to Case 1.

The various partial row-sums of the EPF matrix for this mode are shown as normalized mode shapes in Figure 4-47. This figure shows that the partial row-sums that corresponds to vertical translations induced by vertical input are dominant; in addition, the resulting mode shape is quite similar to that from Case 1 (Fig. 4-29). However, there is an interesting and important difference between the Case 1 and Case 2 results for this mode - namely in the partial row-sum of the EPF matrix that represents the vertical translational response component due to transverse input motions. In Case 1, this response component had unrealistically large EPF amplitudes, whose numerical values were similar to those of the vertical translational component due to vertical input. This result, although physically implausible, had an important effect on the fit between the measured motions and the Case 1 model motions (Sec. 4.4). The Case 2 EPFs differ from those of Case 1 in that the EPFs that represent the vertical translational response component due to transverse input now have amplitudes that are less than half the amplitudes of the corresponding component due to vertical input (Fig. 4-47). The significant reduction in the amplitude of these EPFs that results when a different set of input and response channels is used under Case 2, strengthens the prior assessment that they are indeed physically implausible. Further discussion of this anomaly is provided in Section 4.4.5.

4.4.3 RELATIVE IMPORTANCE OF INDIVIDUAL MODES

This section provides results of an assessment of the relative importance of each mode of the Case 2 model (including pseudostatic). This assessment follows the same procedure as previously described for Case 1 (Sec. 4.3.3). It involves comparison of the contribution of each individual mode to the total fit with the measured MRO response through (1) tabulations

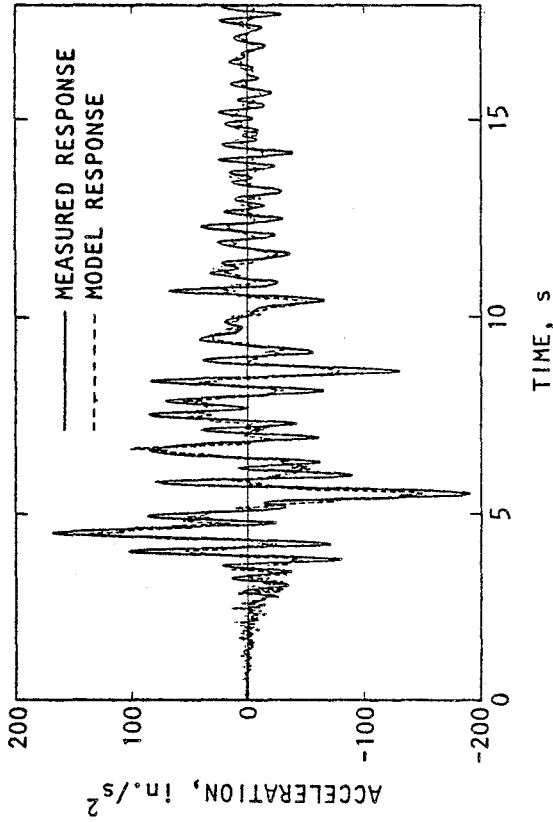


of the effect of each mode on the measure of fit, J (Table 4-9); and (2) visual comparisons of these effects through overlaid plots of measured vs. model acceleration histories at selected channels as the contribution of each mode is added to the model response (Figs. 4-48 to 4-52). Trends from these results are as follows:

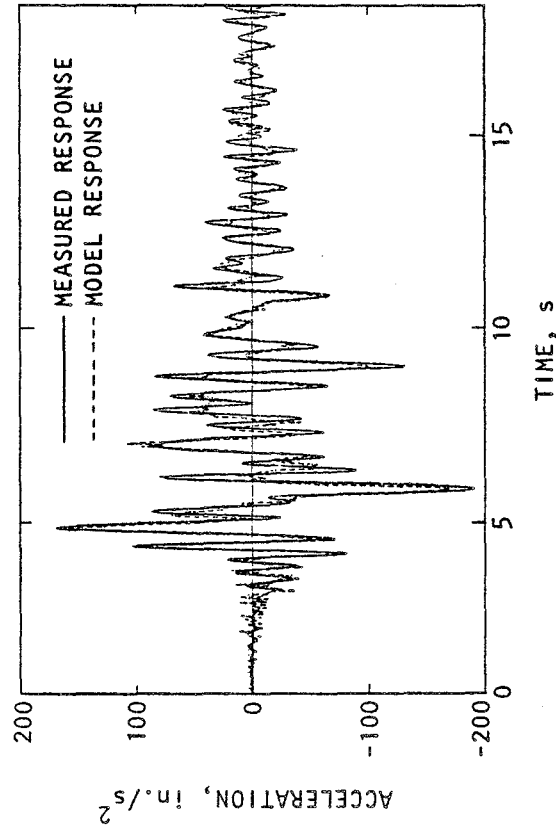
- The system transverse response mode and the deck vertical response mode lead to much larger reductions in J than does the deck transverse response mode (Table 4-9). This trend is consistent with our prior assessment of the MRO strong motion records (Sec. 4.1), which illustrated the importance of the system transverse and deck vertical response modes.

TABLE 4-9. CASE 2 RESULTS: RELATIVE CONTRIBUTIONS OF INDIVIDUAL MODES TO MEASURE OF FIT WITH MEASURED BRIDGE RESPONSE

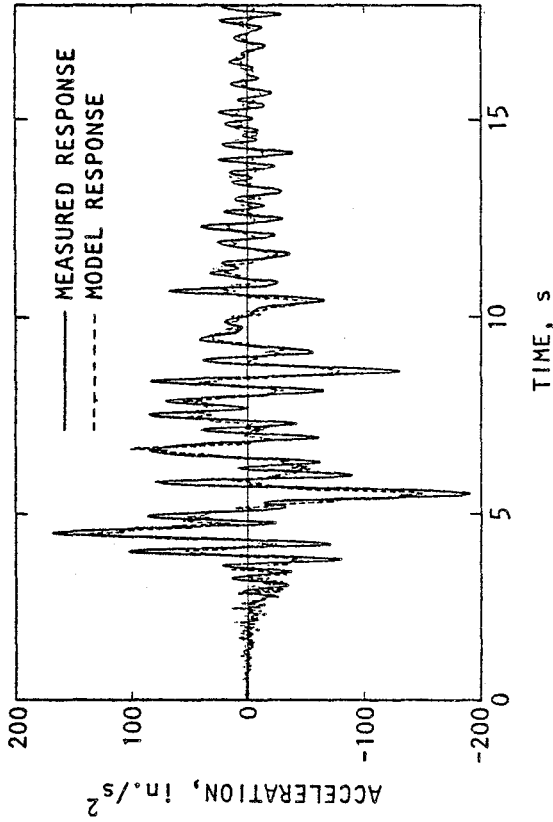
Model Response	Measure of Fit, J (Eq. 3-21)	Percent Reduction in J
Pseudostatic Only	0.499	-
Pseudostatic Plus Deck Vertical Response Mode	0.275	44.9
Pseudostatic Plus Deck Vertical Response and Transverse Response Modes	0.209	24.0
Pseudostatic Plus Deck Vertical Response Mode, Deck Transverse Response Mode, and System Transverse Response Mode (Superrun)	0.093	55.5



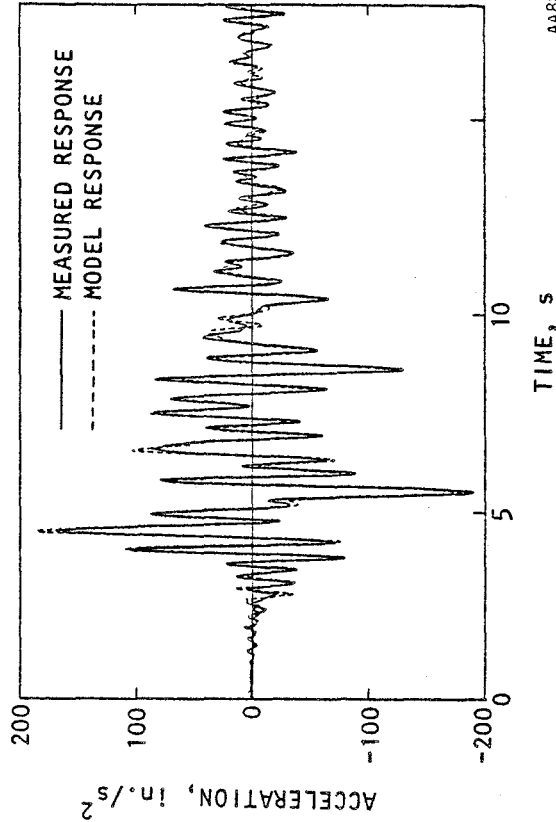
(a) Model response = pseudostatic only



(b) Model response = pseudostatic, deck vertical mode, and deck transverse mode



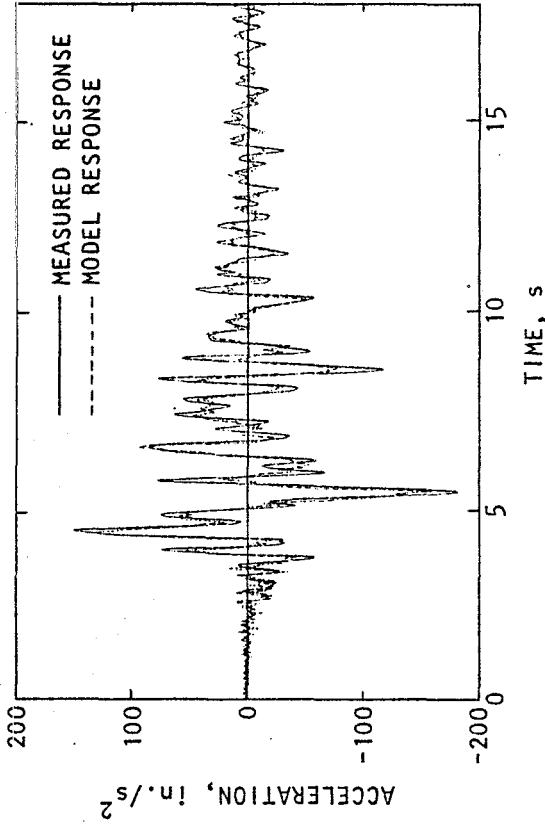
(c) Model response = pseudostatic and deck vertical mode



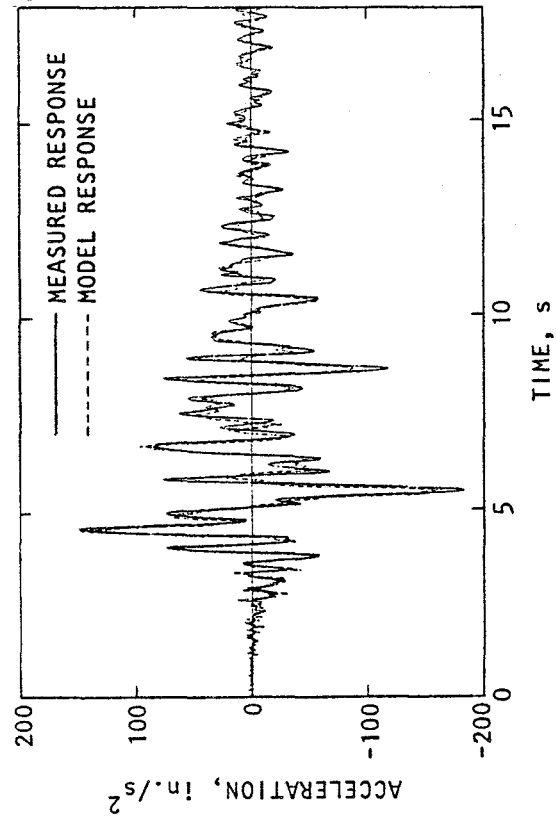
(d) Model response = pseudostatic and all modes (Superrun)

AA886

FIGURE 4-48. CASE 2 RESULTS: RELATIVE CONTRIBUTIONS OF INDIVIDUAL MODES TO FIT OF TRANSVERSE ACCELERATION HISTORY AT CHANNEL 7 (OVER CENTRAL PIER)

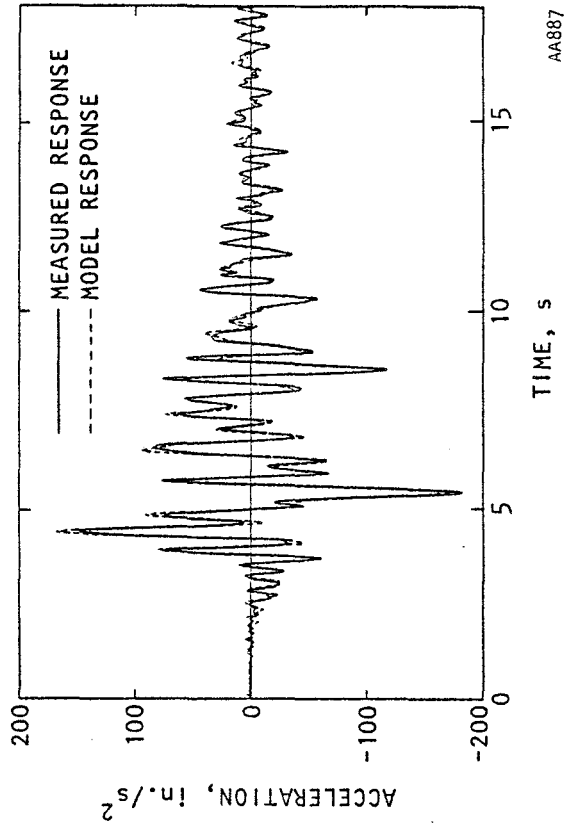


(a) Model response = pseudostatic only



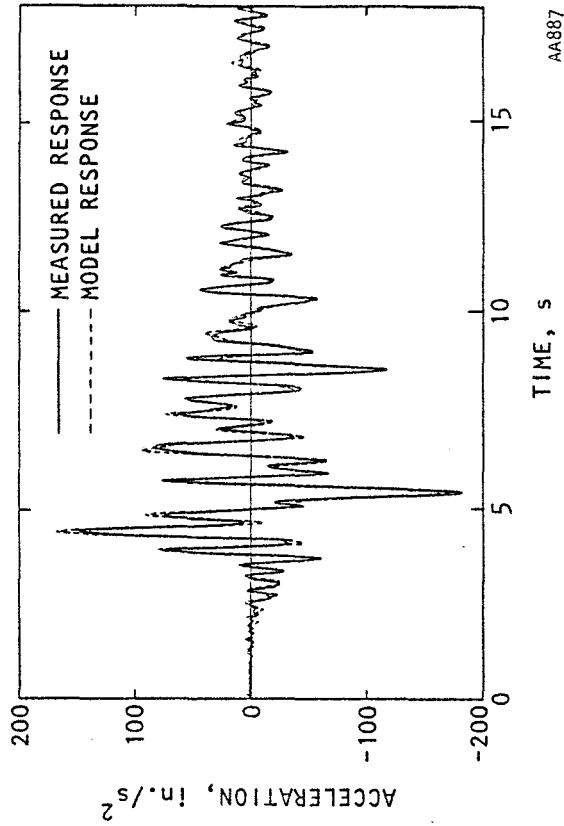
(b) Model response = pseudostatic and deck vertical mode

4-98



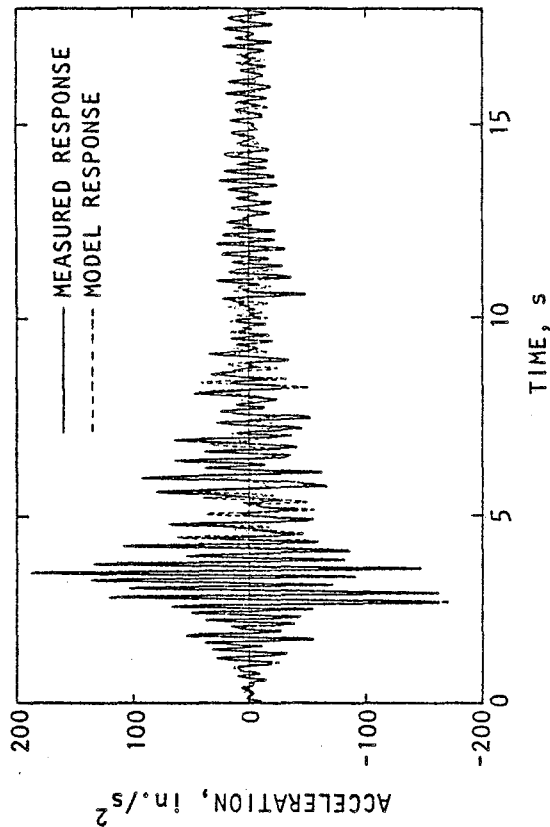
(c) Model response = pseudostatic, deck vertical mode, and deck transverse mode

AA887

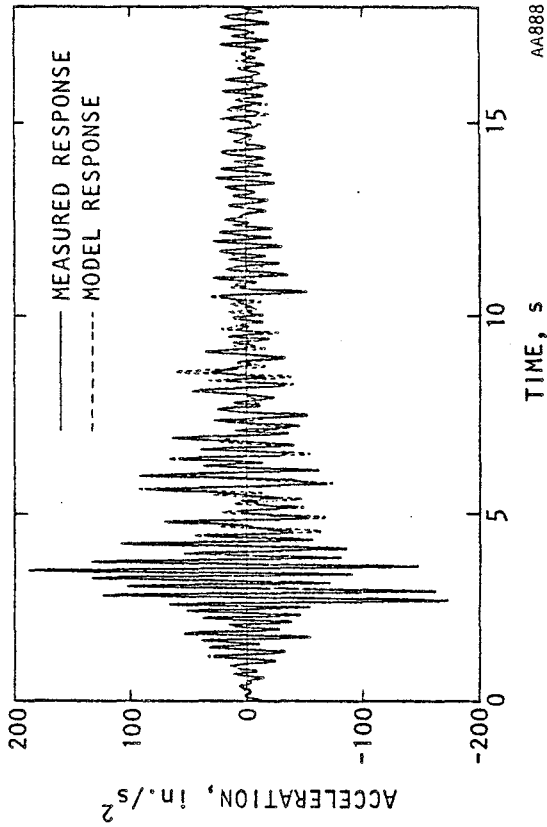


(d) Model response = pseudostatic and all modes (Superrun)

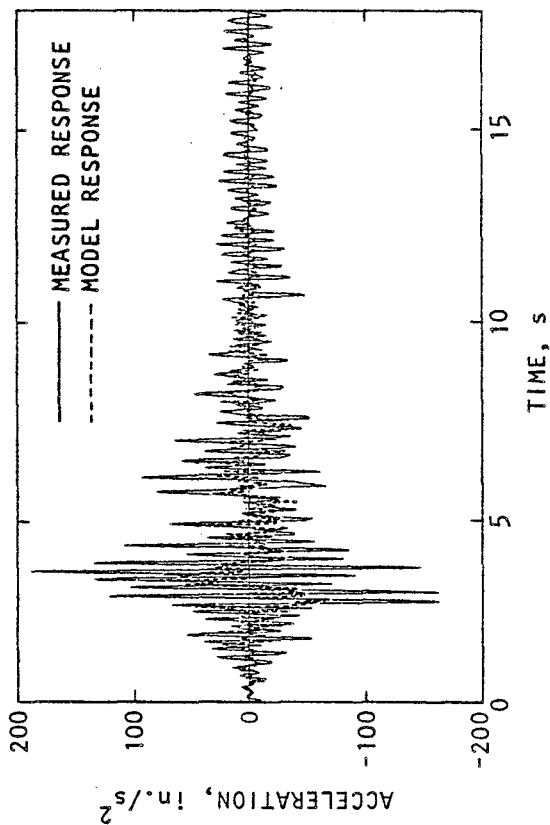
FIGURE 4-49. CASE 2 RESULTS: RELATIVE CONTRIBUTIONS OF INDIVIDUAL MODES TO FIT OF TRANSVERSE ACCELERATION HISTORY AT CHANNEL 13 (WEST FACE OF NORTH ABUTMENT)



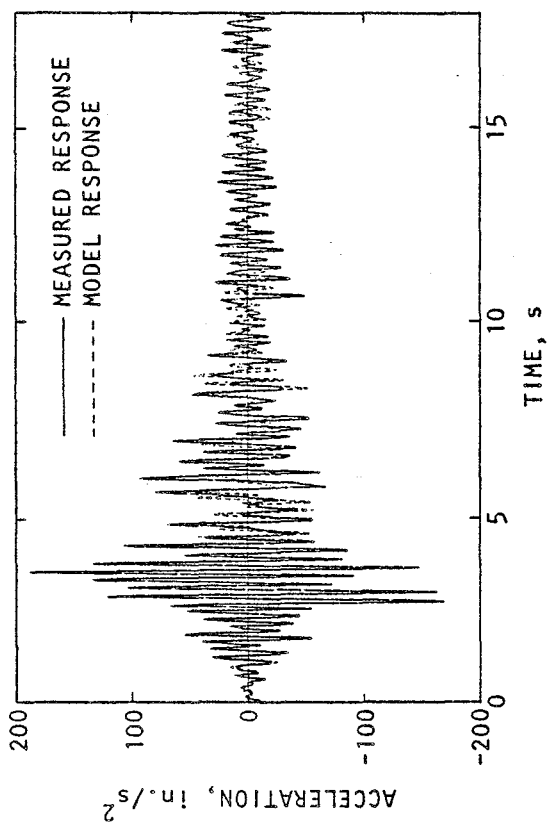
(a) Model response = pseudostatic only



(b) Model response = pseudostatic and deck vertical mode



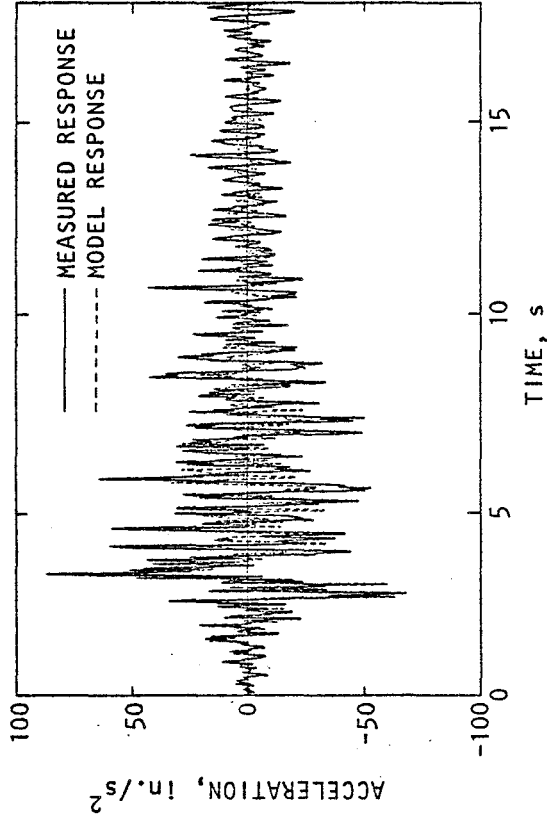
(c) Model response = pseudostatic, deck vertical mode, and deck transverse mode



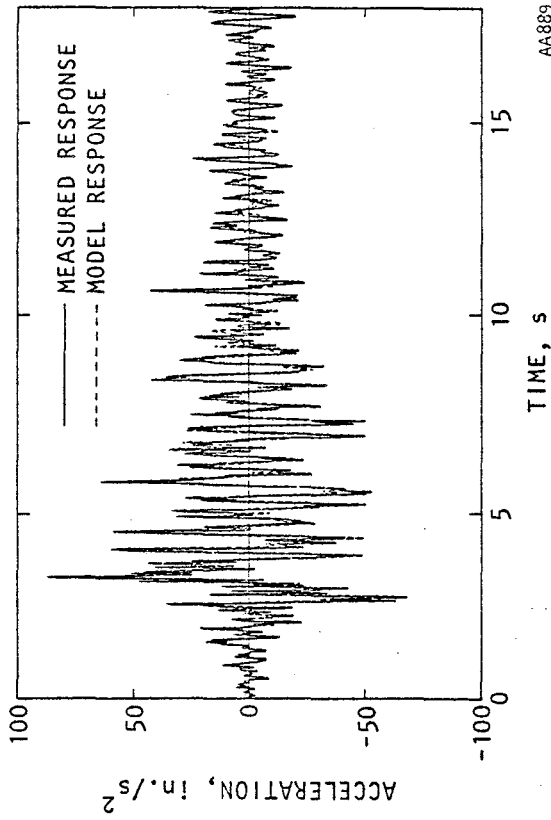
(d) Model response = pseudostatic and all modes (Superrun)

AA888

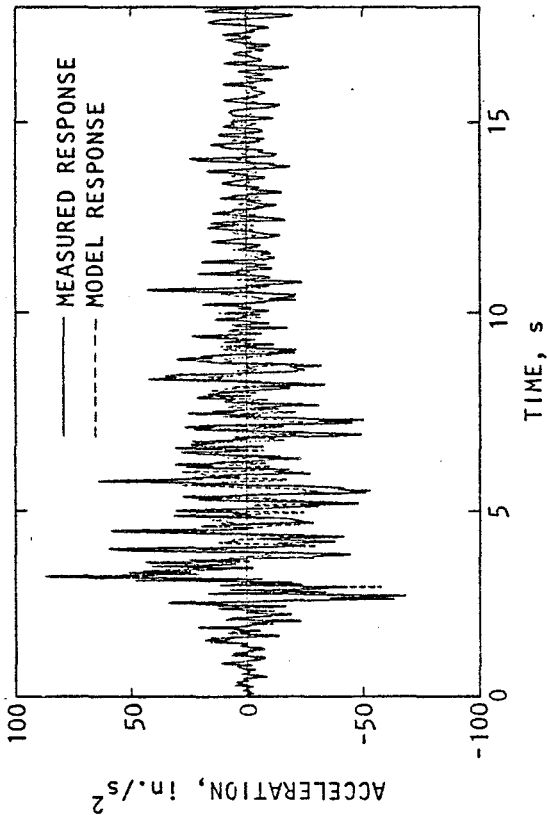
FIGURE 4-50. CASE 2 RESULTS: RELATIVE CONTRIBUTIONS OF INDIVIDUAL MODES TO FIT OF VERTICAL ACCELERATION HISTORY AT CHANNEL 16 (MIDLENGTH OF SOUTH SPAN, ALONG WEST FACE)



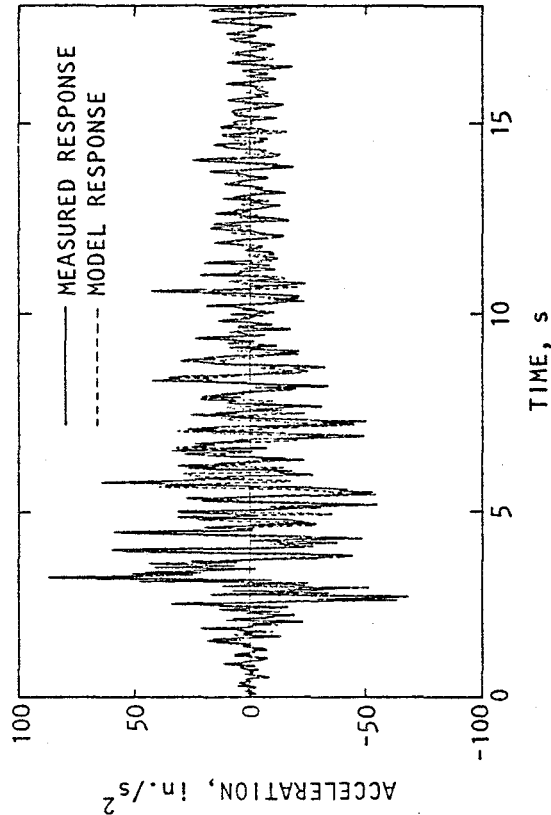
(a) Model response = pseudostatic only



(b) Model response = pseudostatic and deck vertical mode



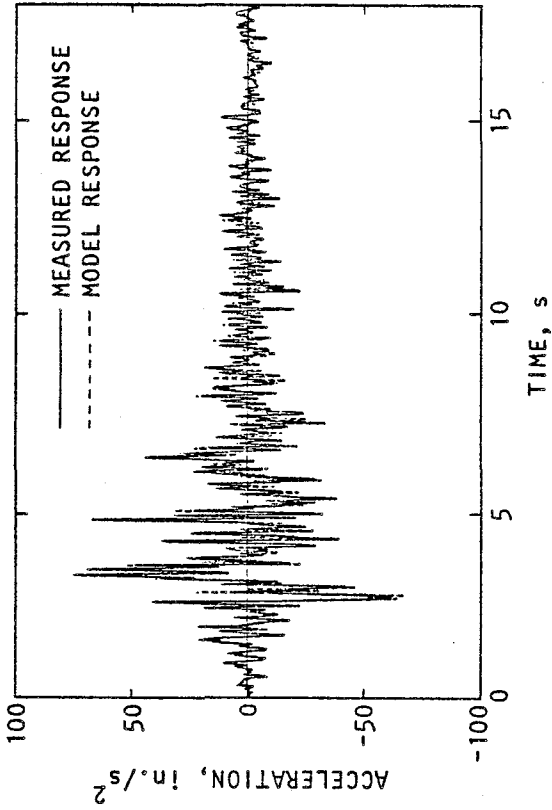
(c) Model response = pseudostatic, deck vertical mode, and deck transverse mode



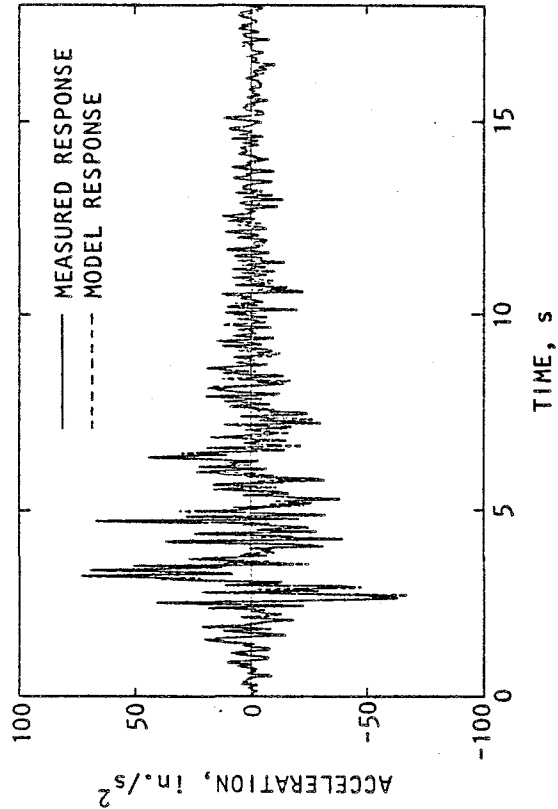
(d) Model response = pseudostatic and all modes (Superrun)

AA889

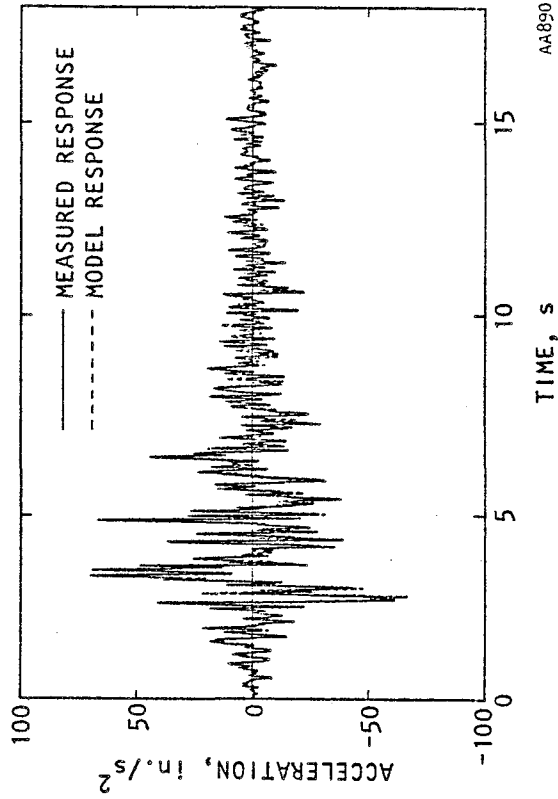
FIGURE 4-51. CASE 2 RESULTS: RELATIVE CONTRIBUTIONS OF INDIVIDUAL MODES TO FIT OF VERTICAL ACCELERATION HISTORY AT CHANNEL 21 (OVER CENTRAL PIER, ALONG EAST FACE)



(a) Model response = pseudostatic only



(b) Model response = pseudostatic and deck vertical mode



(c) Model response = pseudostatic and all modes (Superrun)

AA890

(d) Model response = pseudostatic, deck vertical mode, and deck transverse mode

FIGURE 4-52. CASE 2 RESULTS: RELATIVE CONTRIBUTIONS OF INDIVIDUAL MODES TO FIT OF VERTICAL ACCELERATION HISTORY AT CHANNEL 6 (WEST FACE OF NORTH ABUTMENT)

- Visual comparison of the contributions of each mode to the fit with the bridge's measured transverse acceleration histories along its deck (Channel 7) and at its north abutment (Channel 13) shows that the pseudostatic response by itself provides a fit to the measured transverse response that is good, but not quite as close as for Case 1 (Figs. 4-48a, 4-49a, and 4-31a). This is because the pseudostatic response for Case 2 now no longer includes the significant transverse response contributions of the abutments, which are instead incorporated in the normal modes of vibration.
- The additional contributions of the deck vertical response mode and the deck transverse response mode to the fit with the measured transverse response at the above locations are small when compared to the contributions of the pseudostatic response (Figs. 4-48b, 4-48c, 4-49b, and 4-49c). However, when the contributions of the system transverse response mode are added, a more prominent further improvement in this fit is noted (Figs. 4-48d and 4-49d).
- Visual comparison of the contributions of each mode to the fit with the deck's measured vertical acceleration history at the midlength of each span shows that, as in Case 1, the vertical response at these locations is dominated by the deck's vertical response mode (Fig. 4-50b). The pseudostatic response, by itself, provides a poor fit to these measured vertical motions (Fig. 4-50a), and only a slight further improvement to this fit takes place when the torsional response contributions of the two transverse response modes are included (Figs. 4-50c and 4-50d).
- Visual comparison of the contributions of each mode to the fit with the deck's measured vertical acceleration



histories above the central pier and at the abutments shows that the deck's vertical response mode now has a much smaller effect (Fig. 4-51 and 4-52). This is because the translational components of the deck's vertical response mode are small at these deck support locations. Therefore, the principal contributors to the vertical response at the deck supports are the pseudostatic effects of the support motions themselves, and the torsional components of the MRO's two transverse response modes.

4.4.4 INTERPRETATION OF MODE SHAPE KINK FROM SYSTEM TRANSVERSE RESPONSE MODE RESULTS

The Case 2 superrun results described in Section 4.4.2.3 indicate that the system transverse response mode exhibits a noticeable kink in its mode shape amplitude at the midlength of the south span. In view of the important effects of this mode on the overall system transverse response characteristics, it is appropriate to identify possible causes of this unusual and prominent feature. Sensitivity study calculations using SAP7 and further transverse-input/transverse-output modal identification using MODE-ID are employed for this purpose.

4.4.4.1 SAP7 Calculations

The first step in the interpretation of this mode shape kink involves a special series of simple sensitivity studies using the SAP7 finite element program. This entails computation of normal modes of the MRO, based on nominal properties of the bridge superstructure and a spring/effective-mass representation of the contributions of the foundation/soil system to these modes. The objective of these calculations is to see if the computed mode shapes provide possible clues regarding the occurrence of the mode shape kink for the system transverse response mode.

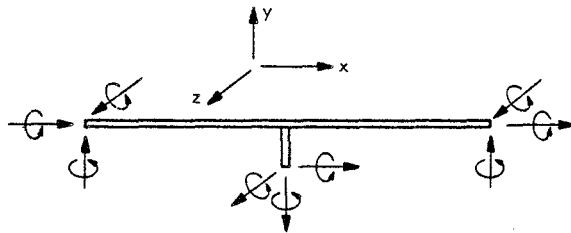


Sample results from this sensitivity study are provided in Tables 4-10a and 4-10b. Table 4-10a shows that a system transverse response mode is computed using SAP7 as having a symmetric mode shape, without the kink exhibited by the Case 2 superrun results. However, this symmetric mode is accompanied by an antisymmetric mode with a nearly identical natural period. Table 4-10b shows that, for nominal properties of the foundation/soil springs, the natural periods of these modes are strongly dependent on the effective mass of the foundation/soil system. In fact, it is seen that when the effective mass attains a value of about 1.27×10^5 lb-sec²/ft, the natural periods of these symmetric and antisymmetric modes are virtually identical and have values ($T = 0.40$ sec) very close to that identified for the system transverse response mode identified during the Case 2 superrun ($T = 0.392$ sec).

The above results indicate a possible cause for the mode shape kink observed from the Case 2 superrun results for the system transverse response mode. It is conceivable that this mode, which should have an essentially symmetric mode shape, could be accompanied by a closely spaced antisymmetric mode. Furthermore, it is possible that this antisymmetric mode would not be readily apparent because (1) it is not strongly excited by the nearly symmetric excitations applied to the MRO during the earthquake; and (2) its natural period is very close to that of the symmetric mode, which is much more prominent because of the nearly symmetric input excitations. Therefore, the modal identification process carried out in MODE-ID might represent these closely spaced strong symmetric and weak antisymmetric modes as a single equivalent mode, whose characteristics are representative of the combined characteristics of the two closely spaced modes. Furthermore, the mode shape of this equivalent mode could be essentially symmetric, except for a kink that results from adding the effects of the weak antisymmetric mode. Finally, it is noted that the damping ratio of the equivalent mode would be higher than that of either of the two



TABLE 4-10. CASE 2 RESULTS: MODES IDENTIFIED FROM SPECIAL SAP7 SENSITIVITY STUDIES



Note: k_x, k_y, k_z = Springs that provide restraint at bridge model supports against translation in x, y, and z directions respectively (lb/ft)

k_{rx}, k_{ry}, k_{rz} = Springs that provide restraint at bridge model supports against rotations about x, y, and z axes respectively (lb-ft/rad)

m, m_r = Effective mass at bridge supports corresponding to translations (lb-sec²/ft) and rotations (lb-ft-sec²/ft) respectively

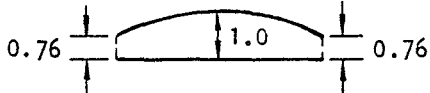
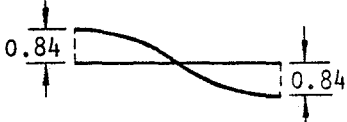
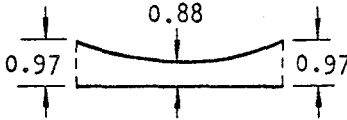
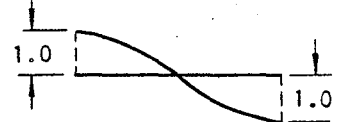
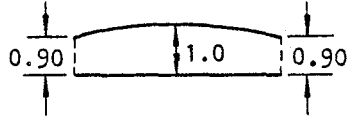
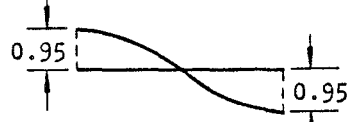
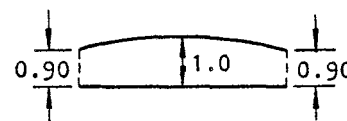
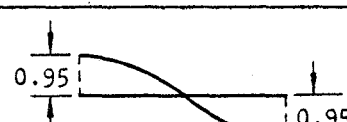
Case Number	Abutments	Column	Mode No.	Period, (Sec)	Mode Shape
SPEST	$k_x = 72.5 \cdot 10^6$ $k_y = 24 \cdot 10^8$ $k_z = 33.6 \cdot 10^6$ $k_{rx} = 10^8$ $k_{ry} = 2.2 \cdot 10^8$ $k_{rz} = 17 \cdot 10^8$ $m = 1,000,000$ $m_r = 4,000$	$k_x = k_z = \text{fixed}$ $k_y = \text{fixed}$ $k_{rx} = 2.5 \cdot 10^8$ $k_{ry} = 420 \cdot 10^8$ $k_{rz} = 2.5 \cdot 10^8$ $m = 8,300$ $m_r = 4,000$	1	0.363	(TRANSVERSE)
			2	0.351	(TRANSVERSE)
			3	0.297	(VERTICAL)
			4	0.227	(TRANSVERSE)
			5	0.212	(VERTICAL)
			6	0.080	(VERTICAL)
			7	0.073	(TRANSVERSE)
			8	0.069	(VERTICAL)

AA911

(a) Sample results of sensitivity studies




TABLE 4-10. (CONCLUDED)

Effective Mass (Translational) at Abutments, $\frac{\text{lb}/\text{sec}^2}{\text{ft}}$ *	Mode	Natural Period, Sec.	Mode Shape
100,000	Symmetric	0.363	
	Antisymmetric	0.350	
200,000	Symmetric	0.489	
	Antisymmetric	0.488	
125,000	Symmetric	0.397	
	Antisymmetric	0.390	
127,000	Symmetric	0.400	
	Antisymmetric	0.400	

AA907

*Note: Foundation spring constants correspond to values given in Table 4-10a

(b) Influence of effective translational mass at abutments of system transverse response modes

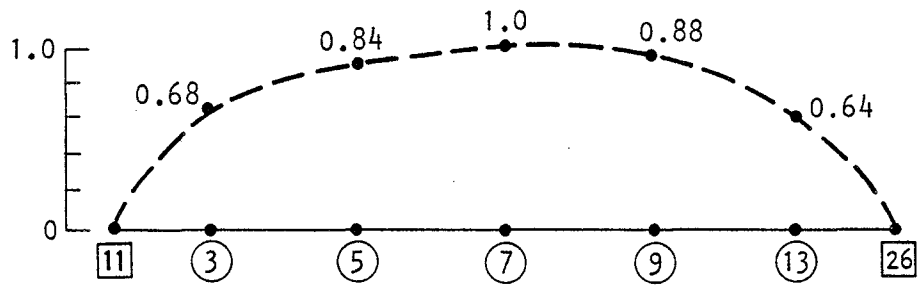


closely spaced modes. This could account for the high value of the modal damping ratio that was identified for the system transverse response mode during the Case 2 superrun ($\xi = 0.103$).

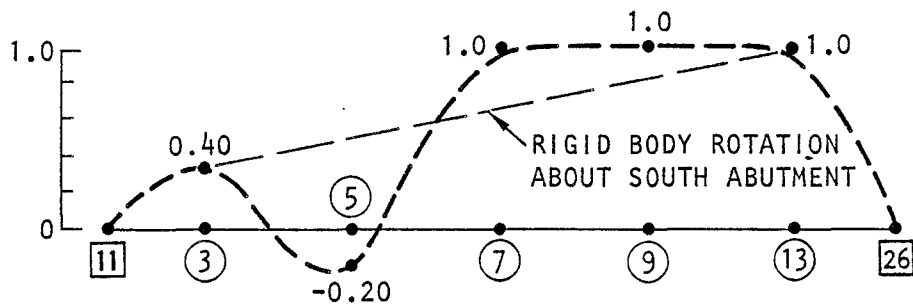
4.4.4.2 MODE-ID Calculations

To gain further insight into the possible existence of an antisymmetric mode of the type indicated above, additional MODE-ID calculations are implemented for the Case 2 subset of transverse-input/transverse-response channels. These differ from the earlier transverse-input/transverse-response calculations that confirm the normal modes of the Case 2 model (Sec. 4.4.1), in that now a 3-mode model (to accommodate the antisymmetric mode) rather than a 2-mode model is used.

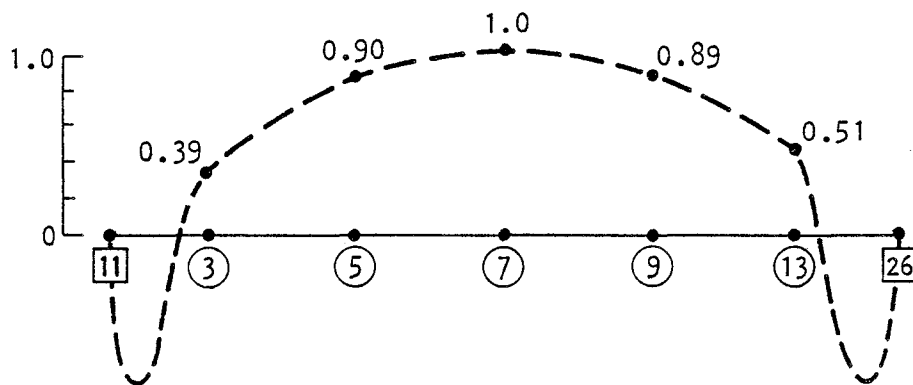
Two different MODE-ID calculations were carried out that incorporated different initial values of the various modal properties. However, in each calculation, the MODE-ID results converged to virtually identical parameters for the system's symmetric and antisymmetric modes. These results (Table 4-11 and Fig. 4-53) show that (1) the inclusion of the additional antisymmetric mode has removed the kink in the mode shape of the original system transverse response mode, which now has a more physically plausible symmetric mode shape; (2) this symmetric mode has a natural period that is only slightly longer than that identified from the Case 2 superrun for the equivalent system transverse response mode ($T = 0.405$ sec), but has a damping ratio that is markedly reduced to a more physically plausible value ($\xi = 0.078$); and (3) the antisymmetric mode has a slightly smaller natural period ($T = 0.356$ sec) and markedly smaller damping ratio ($\xi = 0.048$) relative to the symmetric mode, and a mode shape that resembles antisymmetric transverse motions of the deck superimposed onto a rigid body rotation of the deck about its south abutment (Fig. 4-53b). It is also noted that the value of J computed using this 3-mode model ($J = 0.041$) is



(a) System transverse response mode (symmetric)
 ($T = 0.405$ sec, $\zeta = 0.072$)




(b) System transverse response mode (antisymmetric)
 ($T = 0.356$ sec, $\zeta = 0.048$)



(c) Deck transverse response mode
 ($T = 0.309$ sec, $\zeta = 0.076$)

FIGURE 4-53. CASE 2 RESULTS: NORMALIZED MODE SHAPES FROM 3-MODE MODEL OF MRO TRANSVERSE INPUT/TRANSVERSE RESPONSE



only slightly smaller than that obtained from the 2-mode transverse-input/transverse-response model described in Section 4.4.1 ($J = 0.048$). This shows that the additional antisymmetric mode that has been identified here does not have a strong effect on the fit to the measured transverse motions.

4.4.5 DISCUSSION OF APPARENT PHYSICAL ANOMALIES

The normal modes that comprise the Case 2 superrun model have been shown to exhibit the following unusual phenomena: (1) the partial row-sums of the EPF matrix for the system transverse response mode exhibits noticeable vertical translational response components due to transverse input motions, and prominent transverse, vertical, and torsional components due to vertical input motions; and (2) the partial row-sums for the deck vertical response mode exhibits prominent vertical translational response components due to transverse input motions. Neither of these response components are consistent with the symmetry of the MRO's configuration and its measured MRO support and response motions. Therefore, where such components are computed to be large, they are most probably physical anomalies that are attributable to the same inherent shortcomings in the array of strong motion measurements and in classical mode modeling procedures that were discussed with regard to the Case 1 results (Sec. 4.3.4.1). The sensitivity of these apparent anomalies to the array of response measurements considered is clearly shown by comparisons of the Case 1 and Case 2 results for similar modes. For example, as noted in Sections 4.4.2.4 and 4.4.2.5, the anomalies exhibited by the Case 1 results for the deck transverse and vertical response modes are reduced substantially when a different subset of input and response channels (as represented by the Case 2 subset) is considered.



CHAPTER 5

CONCLUDING COMMENTS

This chapter provides concluding comments that summarize the overall results of this project (Sec. 5.1), provide recommendations for further work pertaining to evaluation of the MRO's seismic response characteristics (Sec. 5.2), and discuss the role of dynamic analysis and system identification in the planning of strong motion instrumentation of major bridge structures (Sec. 5.3).

5.1 SUMMARY OF PROJECT RESULTS

This project consisted of three main tasks that addressed the reprocessing of the strong motion data measured at the MRO during the Imperial Valley earthquake, the development and verification of a new modal identification methodology, and the application of this methodology to the MRO's strong motion measurements in order to assess its seismic response characteristics. Results from each task are briefly summarized in the sections that follow.

5.1.1 STRONG MOTION DATA REPROCESSING (CHAPTER 2)

The array of 26 strong motion records measured at the MRO during the Imperial Valley earthquake is the most extensive yet obtained for bridges in the United States. It therefore provides a key opportunity for gaining further insight into how bridge structures respond to strong seismic excitations. However, to study the MRO's seismic response in this manner, the strong motion measurements first required special reprocessing efforts in order to circumvent certain problems that arose because of a periodic stalling of one of the two central recorders at the bridge site during the ground shaking, and nonsynchronization of the motions from the two recorders.

The periodic stalling of one of the central recorders occurred at approximately 3 sec intervals, and was characterized by a distortion of the acceleration traces from the recorder and




a bulging and shortening of the time traces. To reconstruct the bridge response in these stalled regions, special digitization techniques were developed and implemented under this project. The techniques were carried out using the existing hardware and software facilities at the University of Southern California, together with new software that was specially developed to correct the acceleration and time coordinates of the traces. Following this, standard software was applied to the redigitized traces to obtain motion histories and spectra that incorporated corrections for instrument frequency response and baseline adjustment.

The nonsynchronization of the motions from the two recorders at the MRO appears to have occurred because of different start-up characteristics of their film transport mechanisms. This problem was identified by computing the cross correlation between several pairs of MRO acceleration records. The records that comprised each pair were chosen so that (1) they were each from a different recorder, and (2) they were measured at instruments whose locations were such that the two records should be well correlated except for nonsynchronization effects. Results of this assessment for each record pair consistently showed that the motions from the recorder for Channels 1 to 13 led the motions from the recorder for Channels 14 to 26, by about 60 msec. This significant nonsynchronization was corrected by an appropriate time shifting of the motions from the Channel 1-to-13 recorder.

5.1.2 MODAL IDENTIFICATION METHODOLOGY (CHAPTER 3)

Analysis of the extensive array of strong motion data obtained at the MRO required use of a new state-of-the-art system identification methodology that could accommodate the multiple input and response measurements that comprise this array. The methodology that we developed for this purpose is named MODE-ID. It is applicable to an elastic structure with any arbitrary configuration, classical normal modes, any number



of support and structural response measurements, and an initial at-rest position. It is an extension of a procedure originally developed by Beck (1978), for the case of a structure with a single base motion and response measurement. The methodology uses a computationally efficient iterative procedure to identify a model whose parameters minimize the mean square difference between the measured and model response. The model parameters identified in this way are the structure's pseudostatic influence matrix and the natural frequency, effective participation factor matrix, and damping ratio of its significant fixed-base normal modes. The pseudostatic influence matrix represents the "static" contributions of the multiple support motions to the overall structural response (neglecting inertial effects), whereas the structure's normal modes together characterize the "dynamic" contributions of its fixed-base vibratory response characteristics to its overall response.


The MODE-ID methodology was verified by applying it to an elastic beam model of an idealized three-dimensional simply-supported bridge structure, whose geometry and material properties were generally comparable to those of the MRO. Input motions that correspond to the MRO's measured response at its abutments and central-pier base were applied at the supports of the bridge model, and its dynamic response was computed. This computed dynamic response was then used as a set of simulated "measurements" to which MODE-ID was then applied. The results of this MODE-ID application produced pseudostatic and normal mode parameters that agreed very well with the actual parameters of the idealized bridge. Thus it was shown that, when applied to a linear elastic system with classical normal modes, well-defined boundary conditions, and virtually noise-free response measurements, MODE-ID produced excellent results. However because actual earthquake motions at real structures do not satisfy such ideal conditions, the application of MODE-ID to the measured MRO motions required certain practical considerations and judgement factors as described in Chapter 4.



5.1.3 SEISMIC RESPONSE CHARACTERISTICS OF MELOLAND ROAD OVERPASS (CHAPTER 4)

The seismic response characteristics of the MRO were evaluated in two ways. First, a preliminary evaluation was carried out that involved visual inspection of the time histories and Fourier amplitude spectra of the recorded motions at each MRO response channel. The preliminary evaluation also included initial estimation of potential normal modes of the MRO through use of (1) transfer functions derived from Fourier spectra of the recorded motions; (2) simplified mathematical models of the MRO; and (3) simplified system identification applications. This preliminary evaluation process served to indicate basic response characteristics and potential normal modes that were helpful in planning the subsequent MRO modal identification calculations and in interpreting their results.

The second and principal approach used to evaluate the MRO's seismic response characteristics involved the application of MODE-ID to its array of transverse and vertical strong motion records. Two different subsets of MRO records were considered in this MODE-ID application, in order to assess dynamic response characteristics of two alternative subsystems of the bridge. The first, termed Case 1, emphasized the dynamic response characteristics of a subsystem comprised of the road deck and the central pier. It consisted of (1) input records that corresponded to the motions measured at the two abutments and the central-pier base; and (2) response records that corresponded to the motions measured along the road deck. The second subset, termed Case 2, emphasized the dynamic response characteristics of a subsystem comprised of the abutments and part of the embankments, as well as the road deck and central pier. Accordingly, its subset of recorded motions differed from Case 1 in that (1) the abutment motions were included with the road deck motions to comprise a new array of response records; and (2) the embankment motions replaced the abutment motions in the array of input records.



The application of MODE-ID to the Case 1 and Case 2 subsets of strong motion records involved three main steps which were (1) confirmation of potential modes indicated by the prior preliminary evaluation, through separate applications of MODE-ID to the MRO's transverse input and response measurements and to its vertical input and response measurements; (2) final estimation of the pseudostatic and normal mode parameters that comprise the bridge model, by applying MODE-ID to the full array of coupled vertical and transverse motion measurements considered in Case 1 and Case 2; and (3) evaluation of the results of this application, through examination of measure-of-fit parameters and by visual comparison of measurement vs. model motion time-history plots at each channel location. Results of these steps are summarized as follows.

- The identified linear models from the Case 1 and Case 2 applications of MODE-ID both produced an excellent fit to the measured MRO motions at each response channel, despite the fact that the peak accelerations exceeded 0.50 g.
- The transverse response of the MRO was dominated by its abutment motions, with relatively little dynamic amplification in the deck. In the Case 1 application of MODE-ID, these dominant abutment response characteristics were primarily represented through the pseudostatic influence matrix whereas, in Case 2, they were primarily represented through a fundamental symmetric transverse mode (with a natural period of about 0.4 sec and a damping ratio of about 0.07) as well as the pseudostatic influence matrix. A second symmetric transverse mode was identified in Case 2 that was similar to the only transverse mode identified in Case 1. It had a mode shape in which the embankment and the deck translations are presumably 180 deg out of phase. This mode, which had a natural period of about 0.3 sec and a damping ratio of about




0.08, did not contribute substantially to the bridge's overall transverse response. Both transverse response modes included torsional rotations of the road deck that accompanied lateral bending of the central pier.

- The vertical response along the length of each span of the road deck was dominated by a single vertical response mode. This mode had a natural period of about 0.21 sec, and a symmetric mode shape with vertical translational components that were especially large near the midlength of each deck span and were small at the abutments and at the deck above the central pier. The damping ratio of this fundamental vertical mode was about 0.06.
- The vertical response of the MRO road deck near the abutments and the central pier supports was dominated by the support motions themselves and, at the central pier, by the torsional component of the transverse response modes as well. In Case 1, the support motion contributions were represented through the pseudo-static influence matrix, while the deck's torsional contributions to the vertical response near the central pier were incorporated through the single transverse mode identified from that case. In Case 2, the torsional component of the fundamental transverse mode also had a major effect on the vertical response measured along the faces of the road deck above the central pier.

5.2 RECOMMENDATIONS

Although this application of MODE-ID to the MRO strong motion records was quite successful, the basic modeling approach and the array of measured records have certain shortcomings. For example, the use of a classical normal mode model to represent



the behavior of a real structure subjected to strong seismic excitation does not directly account for either nonlinear response phenomena or for complex modes which may be present even under lower excitation levels. In addition, the array of strong motion measurements at the MRO was insufficient to separate the translational and rotational components of motion at the bridge supports (embankments, abutments, and central pier base) - which are necessary for defining a complete set of foundation/soil boundary constraints for the Case 1 and Case 2 models. These shortcomings not only affected assessment of the bridge's seismic response characteristics in some instances, but also led to certain anomalies in the identified bridge parameters that were not consistent with the MRO's simple symmetric configuration and its similar input motions at each support. Although these anomalies were readily identified and isolated for the simple bridge structure considered here, their very presence underscores the desirability of using more detailed bridge modeling procedures and of supplementing the existing array of strong motion instruments.

With this as background, it is recommended that the following additional efforts be implemented with regard to characterization of the MRO's seismic response characteristics:

- Extended Modeling Procedures. Although the classical mode modeling procedures used herein provided valuable insight into basic response characteristics of the MRO, they should be supplemented with extended modeling procedures that account for the possible presence of complex modes and of nonlinear response phenomena. Along these lines, an initial evaluation of the possible importance of nonlinear response phenomena at the MRO should be carried out by (1) applying MODE-ID to the array of less intense motions measured at the MRO during aftershocks of the Imperial Valley earthquake; and (2) comparing the resulting modal frequencies and damping ratios for a given mode as identified from the main shock and aftershock motions.



- Extended Strong Motion Instrumentation. The contributions of foundation/soil constraints to the bridge's overall seismic response are among the most difficult elements to model for seismic analysis purposes. Nevertheless, such constraints can have an extremely important effect, not only on the seismic response of the bridge foundations themselves, but also on the state of stress induced within the bridge superstructure by the earthquake. To assess such foundation/soil constraint effects on the response of the MRO, it is necessary to have instrumentation that is sufficient to (1) separate the bridge's translational and rotational response at its abutments and central-pier base; (2) represent the longitudinal motions at both abutments which, if out-of-phase, could influence the vertical response characteristics of the road deck; and (3) measure the spatial distribution of the embankment motions in the vicinity of the abutments. The current array of instruments at the MRO, which emphasizes the response characteristics only along its road deck, is insufficient for this purpose. Therefore, the above-indicated extension of this instrument array is recommended.
- Measurement of Soil Properties. In accordance with the above need to assess the foundation/soil constraint characteristics at the MRO, it is necessary to obtain dynamic properties of the soil materials in the vicinity of the bridge. Such dynamic soil properties, when used with earthquake motion measurements from the extended array of instruments recommended above, would provide a sound basis for assessing these potentially important foundation/soil characteristics. However, at present, the only known measurement of dynamic soil properties at the MRO site has consisted of small-strain shear wave velocity data measured in



the upper soil layers by Nazarian and Stokoe (1984). No such data are available for the embankment soils, and there is a complete lack of dynamic soil properties at strain levels representative of strong earthquakes. Therefore, it is recommended that a complete set of dynamic properties of the soil materials at the MRO be measured.

5.3 PLANNING OF STRONG MOTION INSTRUMENTATION AT MAJOR BRIDGE STRUCTURES

The planning of strong motion instrumentation at a major bridge structure entails many considerations such as (1) locations of elements of the bridge that would be particularly susceptible to effects of seismic excitation or vital to continued operation of the bridge during and after an earthquake; (2) the number and locations of instruments necessary to fully characterize the dynamic response of the bridge and its foundation during an earthquake; (3) the expected amplitude, frequency content, and duration of shaking of the bridge that might be expected due to possible earthquakes in the area; (4) the types of measurements most suitable for characterizing the bridge response at each instrument location (e.g., accelerations, pressures, etc); (5) requirements and procedures for processing and interpreting the measured motions after an earthquake event; (6) accessibility of the various instrument locations, with regard to installation, calibration, and maintenance requirements; and (7) cost considerations. Planning of bridge instrumentation in accordance with these various considerations should involve the joint efforts of the engineer and the bridge administrator, to assure that all technical, operational, and cost requirements are met.

State-of-the-art dynamic analysis and system identification techniques of the type used during this project can enhance virtually all of the above elements of a bridge instrumentation



plan. In this, dynamic analysis of the bridge response to anticipated seismic excitations would be carried out as an early step in this instrumentation planning process. This would serve to indicate the nature of the bridge response characteristics, critical elements of the structure, and those measurements that should be made to fully characterize the overall response of the bridge and its critical elements. Then, system identification techniques can be applied to these computed dynamic motions to further enhance this instrumentation planning effort. For example, such techniques can treat the dynamic analysis results as "measurements" in order to back-predict the bridge model parameters. This would indicate those parameters that can be well identified by the planned array of instruments, and those parameters for which identification is more difficult. For those important parameters for which identification is difficult, additional appropriately placed instruments can be deployed in order to improve the accuracy of the identified parameter values.

In summary, it is important to know when planning strong motion instrumentation of bridges (1) those bridge response characteristics that are most important to identify from the array of instruments; (2) how accurately the array can represent these parameters; and (3) how the array can be modified to enhance the accuracy within which the parameters can be identified. The application of dynamic analysis and system identification techniques during the instrumentation planning process can provide important guidance along these lines.




REFERENCES

- Abdel-Ghaffar, A.M. and Illiscu, S.D. (1982) *Analysis of Highway Bridge Response to Earthquakes*. Department of Civil Engineering, Princeton, NJ: Princeton University, Department of Civil Engineering, Oct.
- Abdel-Ghaffar, A.M. et al. (1983) *Analysis of the Dynamic Characteristics of the Golden Gate Bridge by Ambient Vibration Measurements*, Report No. SM-83-8. Princeton, NJ: Princeton Univ., Dept. of Civil Eng., Dec.
- American Association of State Highway and Transportation Officials (AASHTO). (1983) *Guide Specifications for Seismic Design of Highway Bridges - 1983*. Washington, DC: AASHTO, 106 pp.
- Applied Technology Council (ATC). (1981) "Seismic Design Guidelines for Highway Bridges," FHWA/RD-81/081. Palo Alto, CA: ATC, Oct, 195 pp.
- . (1983) "Seismic Retrofitting Guidelines for Highway Bridges," FHWA/RD-83/007. Palo Alto, CA: ATC, Dec, 205 pp.
- Beck, J.L. (1978) *Determining Models of Structures from Earthquake Records*, Report No. EERL 78-01. Pasadena: California Institute of Technology, Earthquake Engineering Research Laboratory, Jun.
- Beck, J.L. and Jennings, P.C. (1980) "Structural Identification Using Linear Models and Earthquake Records," *Earthq. Eng. and Struct. Dynamics*, 8:2, Mar-Apr, pp 145-160.
- Bendat J.S. and Piersol, A.G. (1971) *Measurement and Analysis of Random Data*. New York: Wiley.
- Brady, A.G. (1980) "Current Strong-Motion Ground Record Processing," *Proc. Workshop on Interpretation of Strong-Motion Earthquake Records Obtained In and/or Near Buildings*, UCLA Report No. 8015. Los Angeles: Univ. of California, Apr, pp 23-48.
- Brune, J.N. et al. (1982) "Strong Motion Data Recorded in Mexico During the Main Shock," *The Imperial Valley California Earthquake of October 15, 1979*, Geological Survey Professional Paper 1254, Washington, DC, pp 319-350.
- Chen, M. and Penzien, J. (1979) "Soil/Structure Interaction of Short Highway Bridges," *Proc. of Workshop on Earthquake Resistance of Highway Bridges*, San Diego, Jan 29-31.
- Clough, R.W. and Penzien, J. (1975) *Dynamics of Structures*. New York: McGraw-Hill.



- Degenkolb, O.H. and Jurach, P. (1980) "Highway and Bridge Damage, Imperial Valley Earthquake of October 15, 1979," *Reconnaissance Report, Imperial County, California Earthquake, October 15, 1979*, ed. D.J. Leeds. Berkeley, CA: Earthquake Engineering Research Institute, Feb, pp 85-96.
- Douglas, B.M. ed. (1984) *A National Bridge Engineering Laboratory - A Proposed Plan*, Report No. 84-4. Reno: Univ. of Nevada, Center for Civil Engineering Earthquake Research, Dec.
- Douglas, B.M. and Norris, G.M. (1983) "Bridge Dynamic Test Implications for Seismic Design," *J. of Tech. Topics in Civil Eng., ASCE*, 109:1, Apr, pp 1-22.
- Douglas, B.M. and Reid, W.H. (1982) "Dynamic Tests and System Identification of Bridges," *J of the Structural Div., ASCE*, 108:ST10, Oct, pp 2295-2312.
- Douglas, B.M. and Richardson, J.A. (1984) "Maximum Amplitude Dynamic Tests of a Highway Bridge," *Proc. of Eighth World Conference on Earthquake Engineering*, Vol. VI, San Francisco, Jul 21-28, pp 897-904.
- Gates, J.H. (1976) "California's Seismic Design Criteria for Bridges," *Jnl. Struct. Div., ASCE*, 102:12, Dec, pp 2301-2314.
- . (1979) "Factors Considered in the Development of the California Seismic Design Criteria for Bridges," *Proc. Workshop on Earthquake Resistance of Highway Bridges*, Applied Technology Council, Jan 29-31, pp 141-162.
- Gates, J.H. and Smith, M.J. (1982) *Verification of Dynamic Modeling Methods by Prototype Excitation*, Report No. FHWA/CA/SD-82/07. Sacramento: Calif. Dept. of Transportation, Office of Structures Design, Nov.
- Godden, W.C. (1979) "Seismic Model Studies of Long-Span Curved Bridges," *Proc. Workshop on Earthquake Resistance of Highway Bridges*, Applied Technology Council, Jan 29-31, pp 409-422.
- Hartzell, S. and Helmsberger, D.V. (1982) "Strong Motion Modeling of the Imperial Valley Earthquake of 1979," *Bull. Seismol. Soc. Amer.*, 72:2, Apr, pp 571-596.
- Hudson, D. (1979) *Reading and Interpreting Strong Motion Accelerograms*. Berkeley: Earthquake Engineering Research Institute.
- Imbsen, R.A. (1984) "Implementation of the Analytical Capabilities Required for the Aseismic Design of Bridges," *Proc. of US-Japan Bridge Workshop*, Tscuba, Japan, Feb.

- 
- Iwasaki, T. and Hagiwara, R. (1983) "Dynamic Response Analysis of Shizunai Bridge Damaged by the Urakawa-Oki Earthquake," *Proc. of 15th Joint Meeting of US-Japan Panel on Wind and Seismic Effects*, May 17-20, 34 pp.
- Iwasaki, T.; Penzien, J.; and Clough, R.W. (1972) *Literature Survey - Seismic Effects on Highway Bridges*, EERC-72-11. Berkeley, CA: Univ. of California, Earthquake Engineering Research Center, Nov.
- Jennings, P.C., ed. (1980) *Earthquake Engineering and Hazards Reduction in China*, SCSPRC Report No. 8. Washington, DC: National Academy of Sciences.
- Jennings, P.C. and Wood, J.H. (1971) "Earthquake Damage to Freeway Structures," Chapt. 6, *Engineering Features of the San Fernando Earthquake, February 9, 1971*, EERL-71-02. Pasadena, CA: California Institute of Technology, Jun, pp 366-433.
- Lee, V.W. and Trifunac, M.D. (1979) *Automatic Digitization and Processing of Strong Motion Accelerograms, Part 2: Computer Processing of Accelerograms*, Report No. 79-15 II, Los Angeles: Univ. of Southern California, Dec.
- Lew, H.S. (1984) "NBS Large Scale Seismic Testing Program," *Proc. of US-Japan Bridge Workshop*, Tscuba, Japan, Feb.
- Lisiecki, L.C.C. (1982) *Analysis of the Meloland Overcrossing Response to the October 15, 1979 Imperial Valley Earthquake*, Structural Mechanics Report 82-1. Irvine, CA: University of California, Irvine.
- McJunkin, R.D. and Ragsdale, J.T. (1980) *Compilation of Strong-Motion Records and Preliminary Data from the Imperial Valley Earthquake of October 15, 1979*, Preliminary Report 26. Sacramento: Calif. Div. Mines and Geology, Office of Strong-Motion Studies.
- McVerry, G.H. and Beck, J.L. (1983) *Structural Identification of the JPL Building 180 Using Optimally Synchronized Earthquake Records*, Record No. EERL 83-01. Pasadena: California Institute of Technology, Earthquake Engineering Research Laboratory, Aug.
- Miller, R.K. and Felszeghy, S.F. (1978) *Engineering Features of the Santa Barbara Earthquake of August 13, 1978*, UCSB-ME-78-2. Santa Barbara, CA: Univ. of California, Dec.
- Nazarian S. and Stokoe, K.H. (1984) "In Situ Shear Wave Velocities from Spectral Analysis of Surface Waves," *Proc. of Eighth World Conference on Earthquake Engineering*, Vol. III, San Francisco, Jul 21-28, pp 31-38.



- Park, R.J.T. et al. (1984) "The Seismic Performance of Steel-Encased Reinforced Concrete Bridge Piles," *Proc. of Eighth World Conference on Earthquake Engineering*, Vol. VI, San Francisco, Jul 21-28, pp 897-904.
- Porcella, R.L. et al. (1982) "Strong-Motion Data Recorded in the United States," *The Imperial Valley California Earthquake of October 15, 1979*, Geological Survey Professional Paper 1254, Washington, DC, pp 289-318.
- Public Works Research Institute (PWRI). (1984) "A Case History of Bridge Performance during Earthquakes in Japan," *Proc. of International Conference on Case Histories in Geotechnical Engineering*, St. Louis: PWRI, May 6-11.
- Raggett, J.D. and Rojahn, C. (1978) *Use and Interpretation of Strong Motion Records from Highway Bridges*, Report No. FHWA-RD-78-158. Menlo Park, CA: U.S. Geological Survey, Oct.
- Rojahn, C. and Raggett, J.D. (1981) *Guidelines for Strong-Motion Instrumentation of Highway Bridges*, Report No. FHWA-RD-78-158. Menlo Park: CA: U.S. Geological Survey, Dec.
- Rojahn C. et al. (1982) "Main-Shock Strong Motion Records from Meloland Road - Interstate 8 Highway Overcrossing," *The Imperial Valley California Earthquake of October 15, 1979*, Geological Survey Professional Paper 1254, Washington, DC, pp 377-384.
- Scott, R.F. (1983) Personal Communication to M.B. Levine, Oct.
- Selna, L.G. (1984) "Box Girder Bridge Hinge Restrainer Program," *Proc. of US-Japan Bridge Workshop*, Tscuba, Japan, Feb.
- Sturman, G.C. (1973a) "The Alaska Railroad," *The Great Alaska Earthquake of 1964, Engineering*. Washington, DC: National Academy of Sciences, pp 958-986.
- . (1973b) "The Alaska Highway System," *The Great Alaska Earthquake of 1964, Engineering*. Washington, DC: National Academy of Sciences, pp 987-1009.
- Trifunac, M.D. and Lee, V.W. (1979) *Automatic Digitization and Processing of Strong Motion Accelerograms, Part 1: Automatic Digitization*, Report No. 79-15 I. Los Angeles: Univ. of Southern California, Dec.
- Tseng, W.S. and Penzien, J. (1973) *Analytical Investigations of the Seismic Response of Long Multiple Span Highway Bridges*, EERC-73-12. Earthquake Engineering Research Center, Berkeley: University of California, Jun.



- Werner, S.D. et al. (1979) "Effects of Traveling Seismic Waves on the Response of Bridges," *Proc. of Workshop on Earthquake Resistance of Highway Bridges*, San Diego, Jan 29-31.
- Wilson, J.C. (1984) *Analysis of the Observed Earthquake Response of a Multiple Span Bridge*, Report No. EERL 84-01. Pasadena, CA: California Institute of Technology, Earthquake Engineering Research Laboratory, May.
- Yanev, P.I., ed. (1978) *Miyagi-Ken-Oki, Japan Earthquake, June 12, 1978*. Berkeley, CA: Earthquake Engineering Research Institute, Dec.



APPENDIX A

PLOTS AND AVAILABLE DATA TAPES FOR REPROCESSED
MOTIONS FROM MELOLAND ROAD OVERPASS

This appendix provides plots of motion time histories, Fourier amplitude spectra, and response spectra of the data from all 26 channels of the Meloland Road Overpass. These data incorporate the special corrections for recorder stall and nonsynchronization effects that have been described in Chapter 2, as well as standard corrections for baseline shift and instrument frequency response characteristics.

Data tapes containing all of these time-history and spectra results have been forwarded to the California Division of Mines and Geology in Sacramento, California. Copies of these tapes can be obtained by contacting:

Anthony F. Shakal
Office of Strong Motion Studies
California Division of Mines and Geology
2811 "O" Street
Sacramento, California 95816

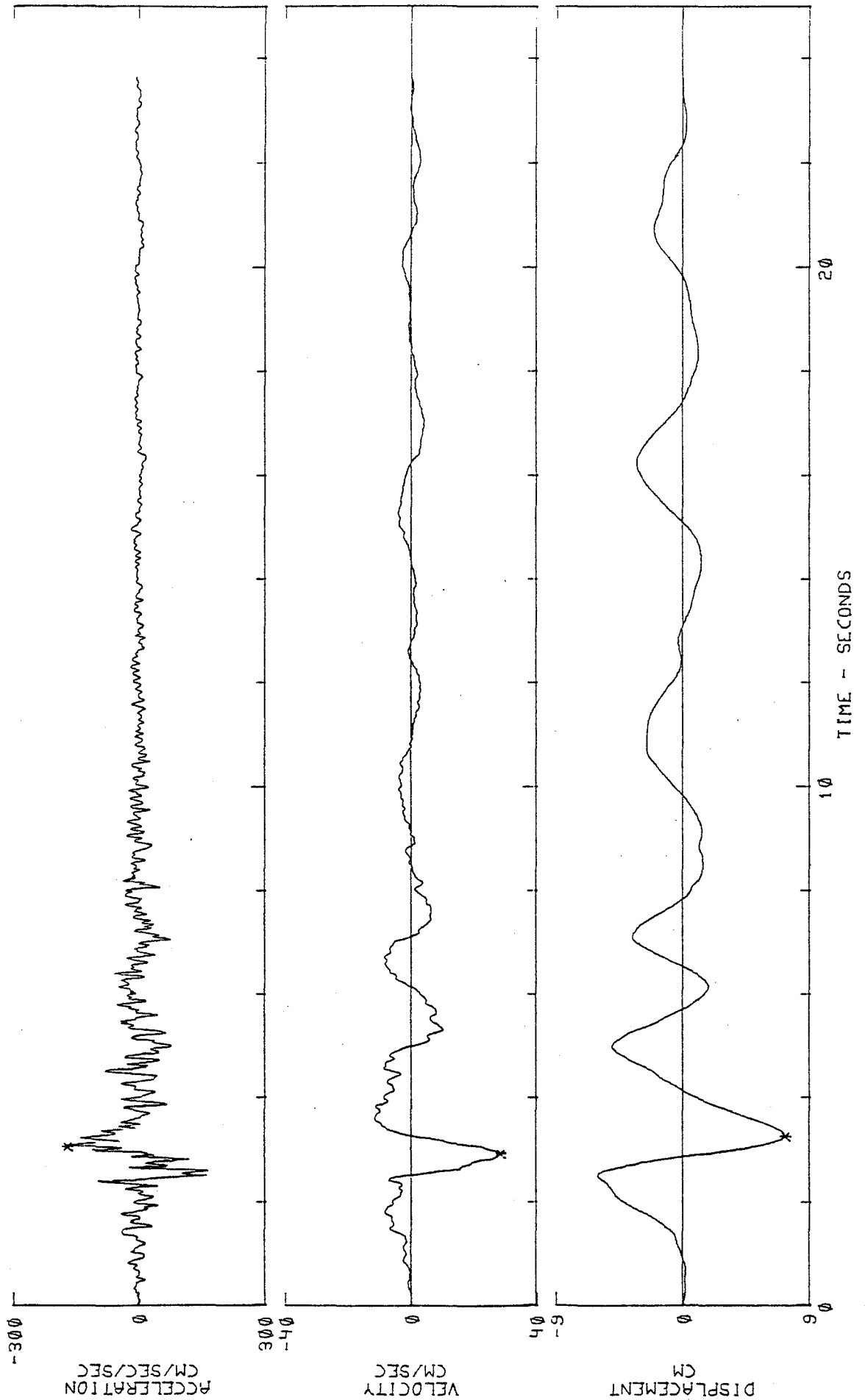


IMPERIAL VALLEY EARTHQUAKE OCT 15, 1979 -1616 PDT

1IMP201 79.201.0 ROUTE 8/MELOLAND OVERPASS, EL CENTRO, CA COMP TR 1

ACCELEROGRAM IS BAND-PASS FILTERED BETWEEN .145- .165 AND 25.00-27.00 CYC/SEC.

*PEAK VALUES : ACCELERATION = -171.6 CM/SEC/SEC VELOCITY = 28.5 CM/SEC DISPLACEMENT = 7.31 CM



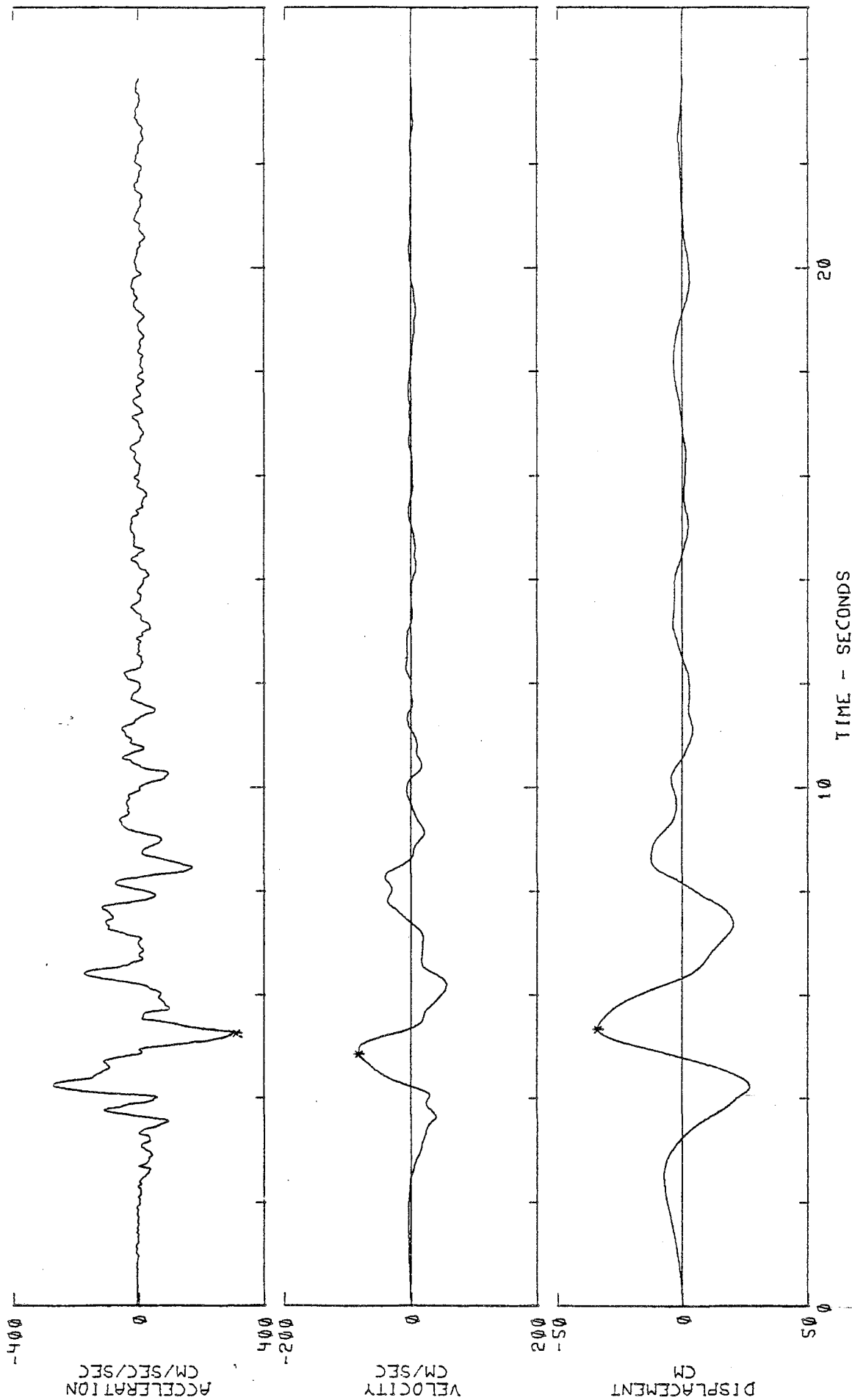


IMPERIAL VALLEY EARTHQUAKE OCT 15, 1979 -1616 PDT

IIMP201 79.201.0 ROUTE 8/MELOLAND OVERPASS, EL CENTRO, CA COMP TR 2

ACCELEROGRAM IS BAND-PASS FILTERED BETWEEN .145- .165 AND 25.00-27.00 CYC./SEC.

*PEAK VALUES : ACCELERATION = 311.4 CM/SEC/SEC VELOCITY = -83.1 CM/SEC DISPLACEMENT = -34.0 CM



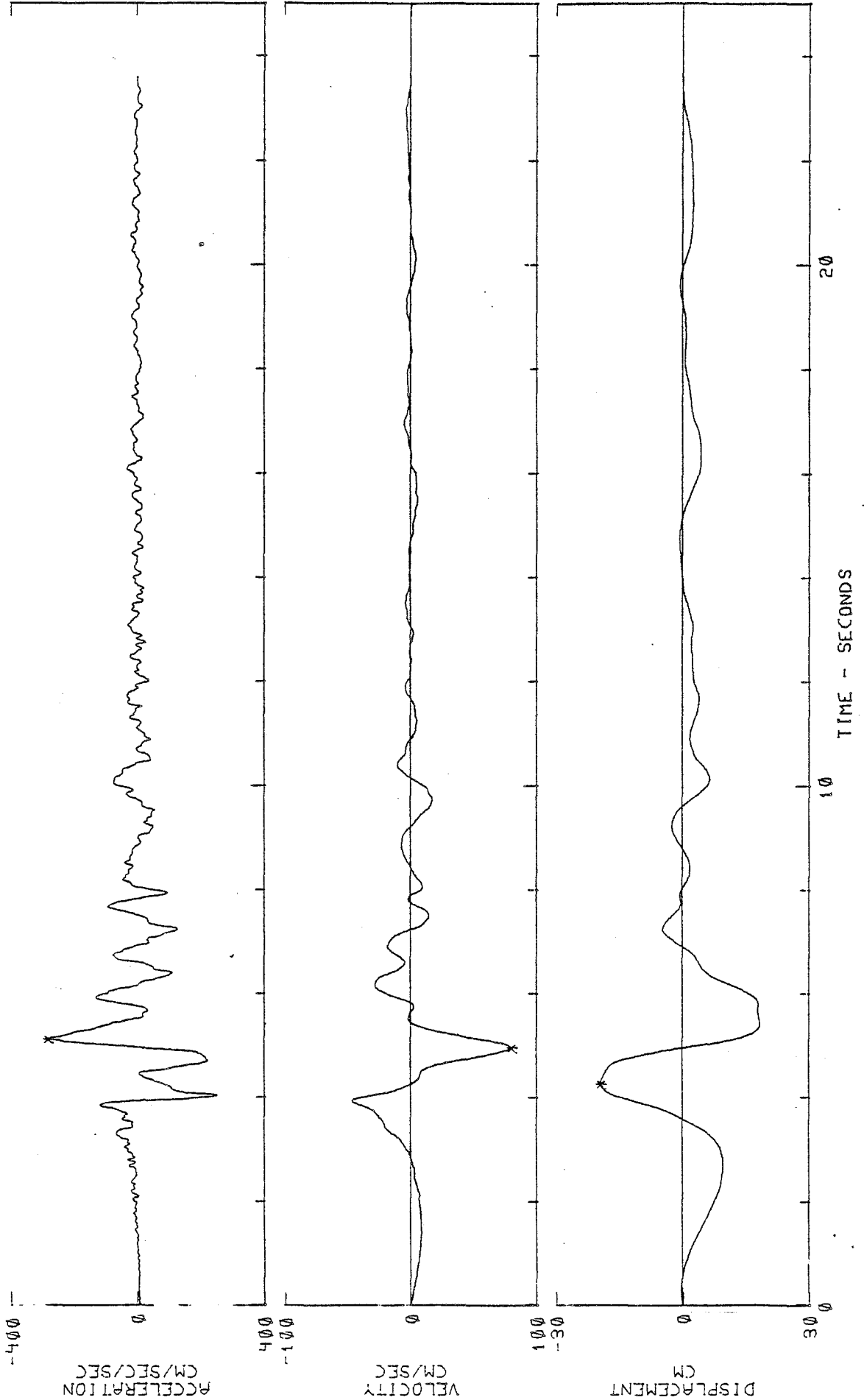


IMPERIAL VALLEY EARTHQUAKE OCT 15, 1979 -1616 PDT

IIMP201 79.201.0 ROUTE 8/MELOLAND OVERPASS, EL CENTRO, CA COMP TR 4

ACCELEROGRAM IS BAND-PASS FILTERED BETWEEN .145- .165 AND 25.00-27.00 CYC/SEC.

*PEAK VALUES : ACCELERATION = -281.1 CM/SEC/SEC VELOCITY = 79.9 CM/SEC DISPLACEMENT = -19.4 CM



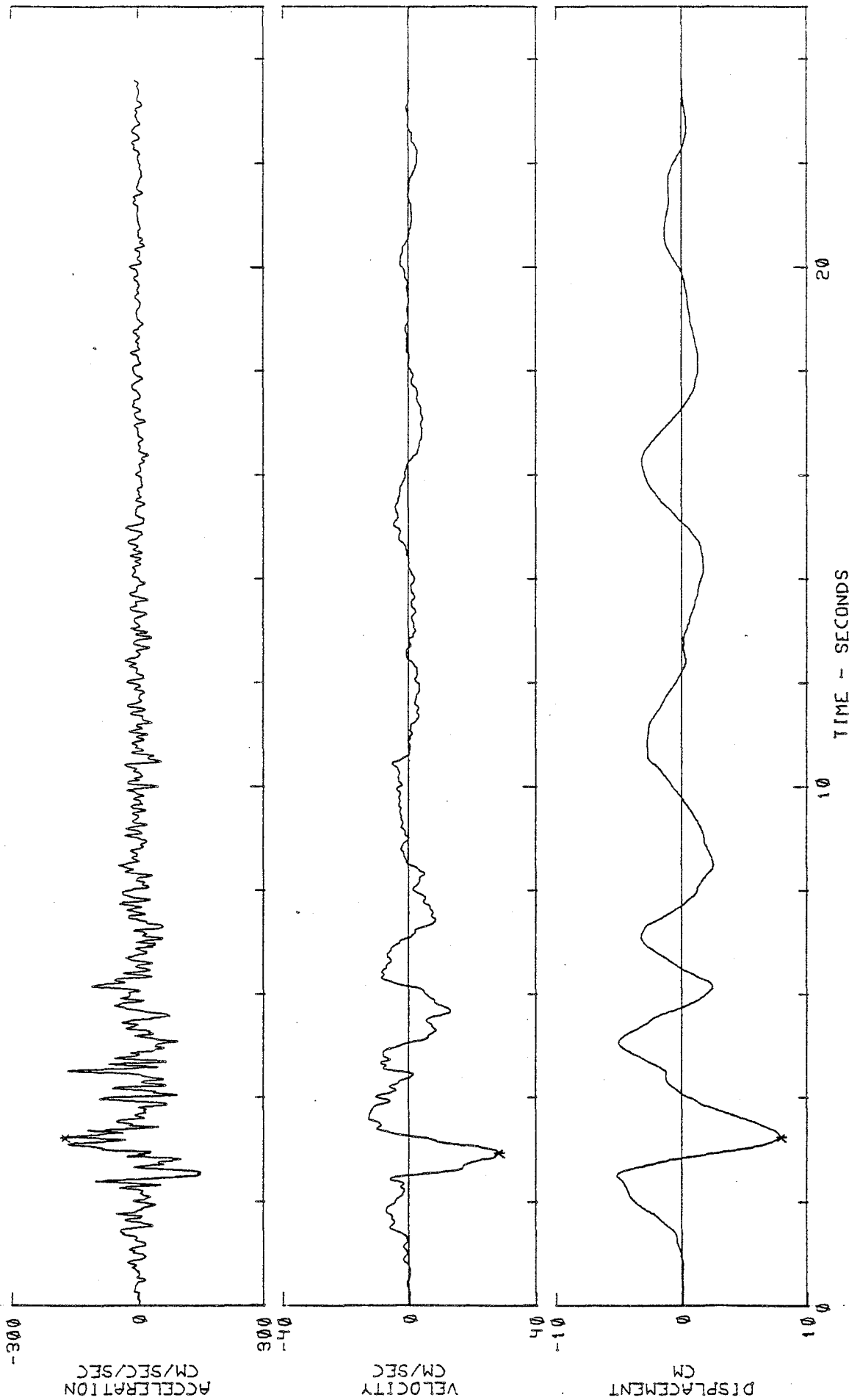


IMPERIAL VALLEY EARTHQUAKE OCT 15, 1979 -1616 PDT

IMP201 79.201.0 ROUTE 8/MELOLAND OVERPASS, EL CENTRO, CA COMP TR 6

ACCELEROGRAM IS BAND-PASS FILTERED BETWEEN .145- .165 AND 25.00-27.00 CYC/SEC.

*PEAK VALUES : ACCELERATION = -176.3 CM/SEC/SEC VELOCITY = 28.0 CM/SEC DISPLACEMENT = 7.92 CM



R-8222-5603



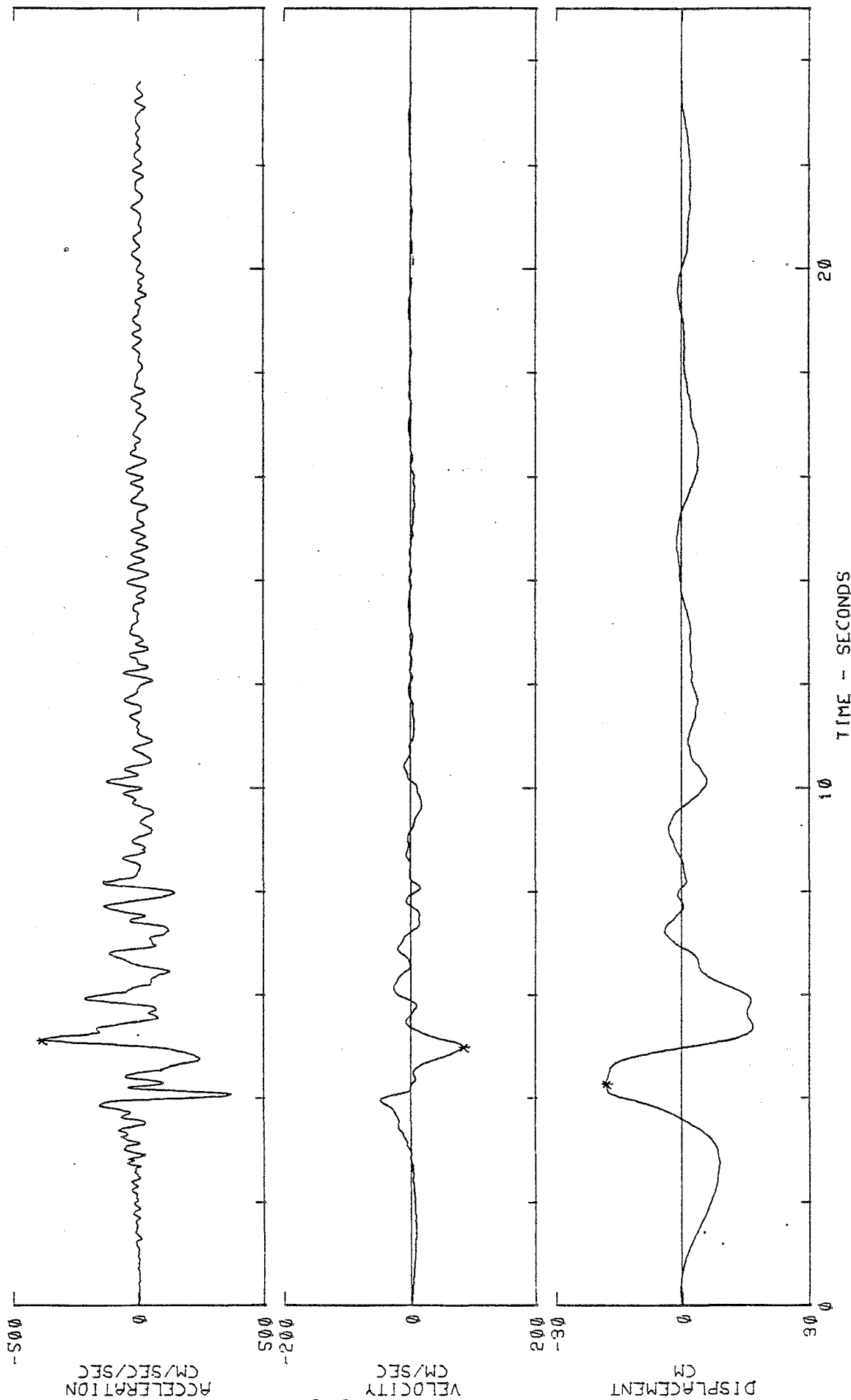
IMPERIAL VALLEY EARTHQUAKE OCT 15, 1979 -1616 PDT

IMP201 79.201.0 ROUTE 8/MELDLAND OVERPASS, EL CENTRO, CA COMP TR 8

ACCELEROGRAM IS BAND-PASS FILTERED BETWEEN .145- .165 AND 25.00-27.00 CYC/SEC.

*PEAK VALUES : ACCELERATION = -386.0 CM/SEC/SEC VELOCITY = 82.9 CM/SEC DISPLACEMENT = -18.0 CM

R-8222-5603





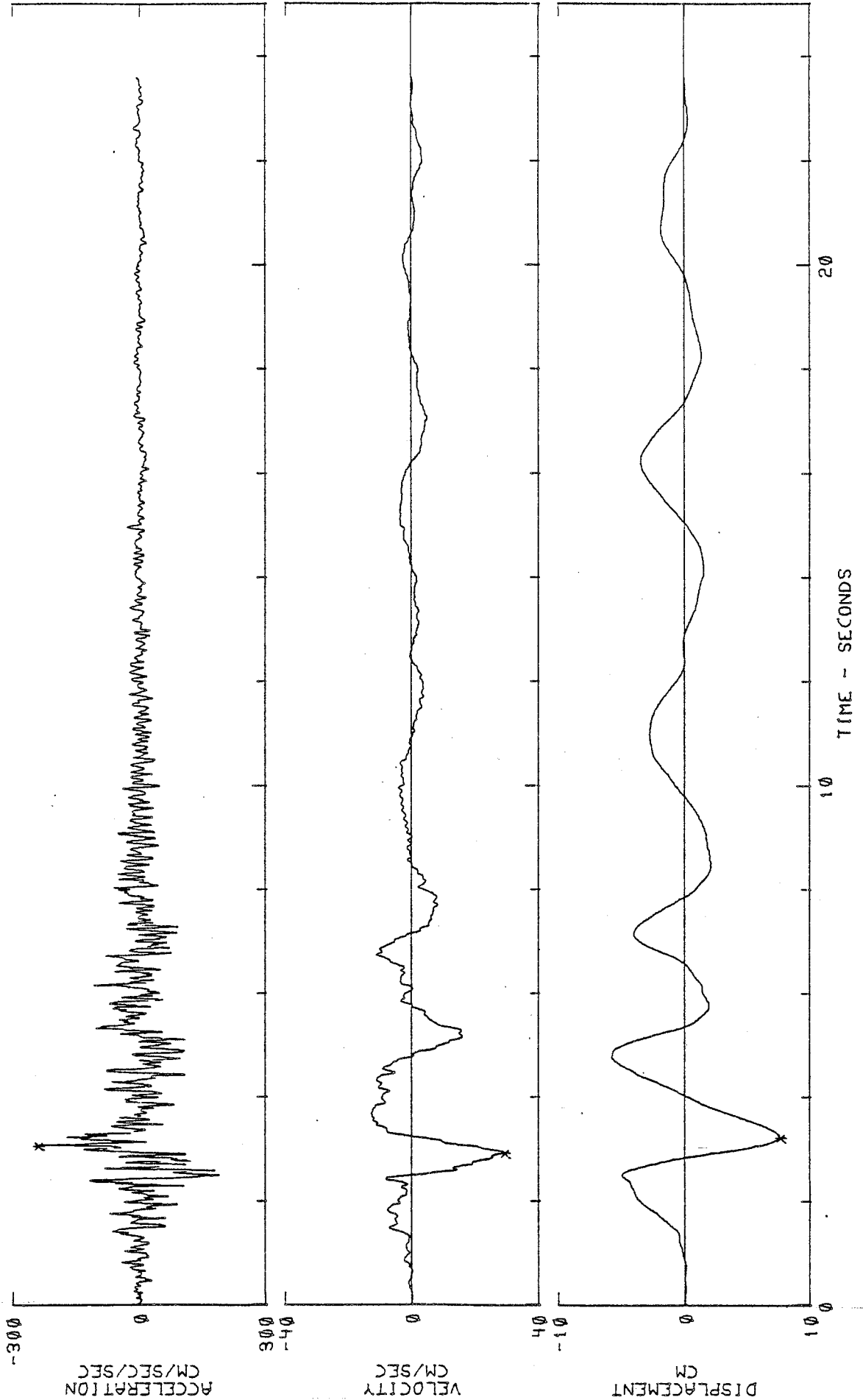
IMPERIAL VALLEY EARTHQUAKE OCT 15, 1979 -1616 PDT

IIMP201 79.201.0 ROUTE 8/MELDAND OVERPASS, EL CENTRO, CA COMP TR10

ACCELEROGRAM IS BAND-PASS FILTERED BETWEEN .145- .165 AND 25.00-27.00 CYC/SEC.

*PEAK VALUES : ACCELERATION = -240.5 CM/SEC/SEC VELOCITY = 29.1 CM/SEC DISPLACEMENT = 7.65 CM

R-8222-5603





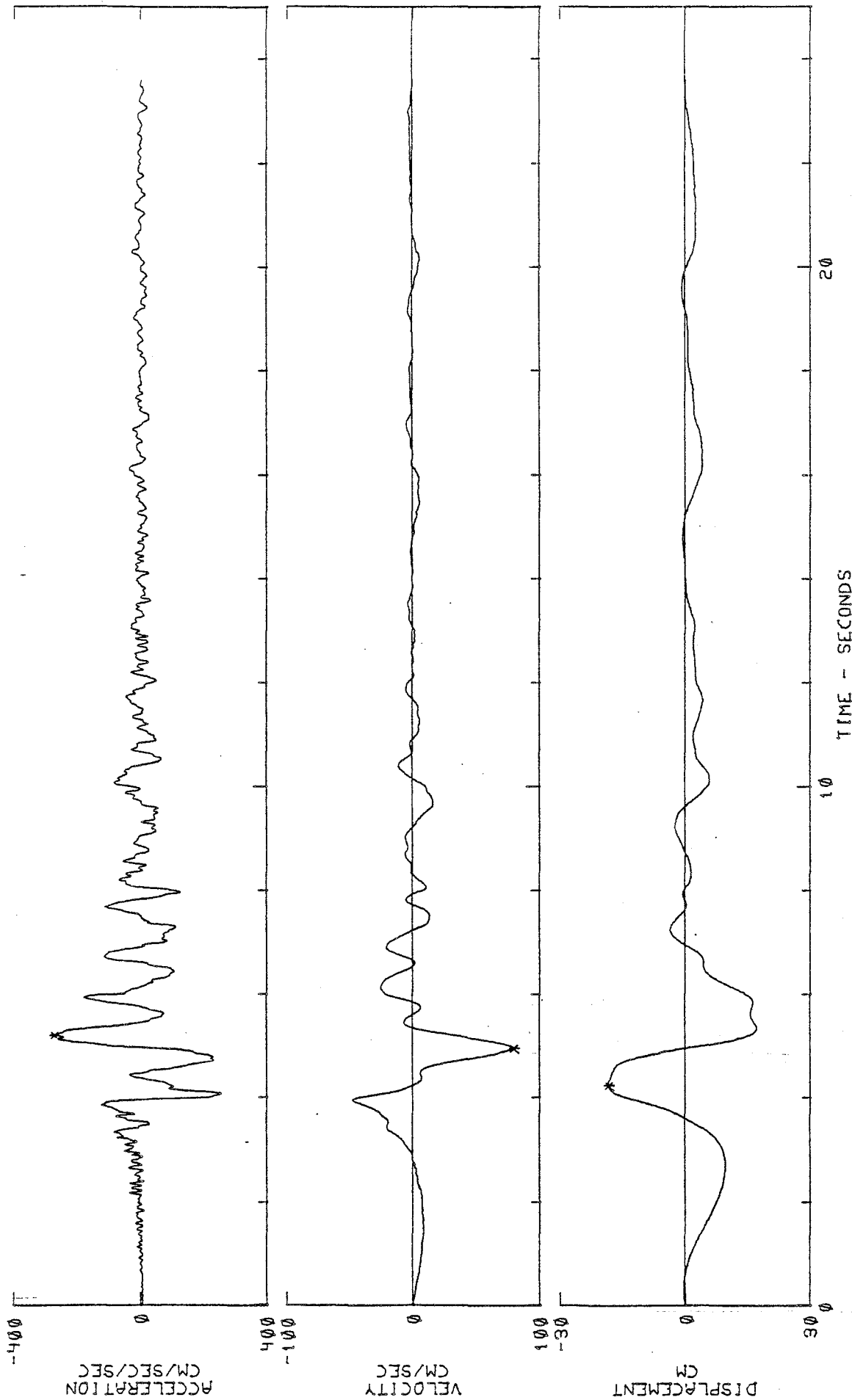
IMPERIAL VALLEY EARTHQUAKE OCT 15, 1979 -1616 PDT

IIMP201 79.201.0 ROUTE 8/MELOLAND OVERPASS, EL CENTRO, CA COMP TR12

ACCELEROGRAM IS BAND-PASS FILTERED BETWEEN .145- .165 AND 25.00-27.00 CYC/SEC.

*PEAK VALUES : ACCELERATION = -272.9 CM/SEC/SEC. VELOCITY = 79.2 CM/SEC DISPLACEMENT = -18.4 CM

R-8222-5603



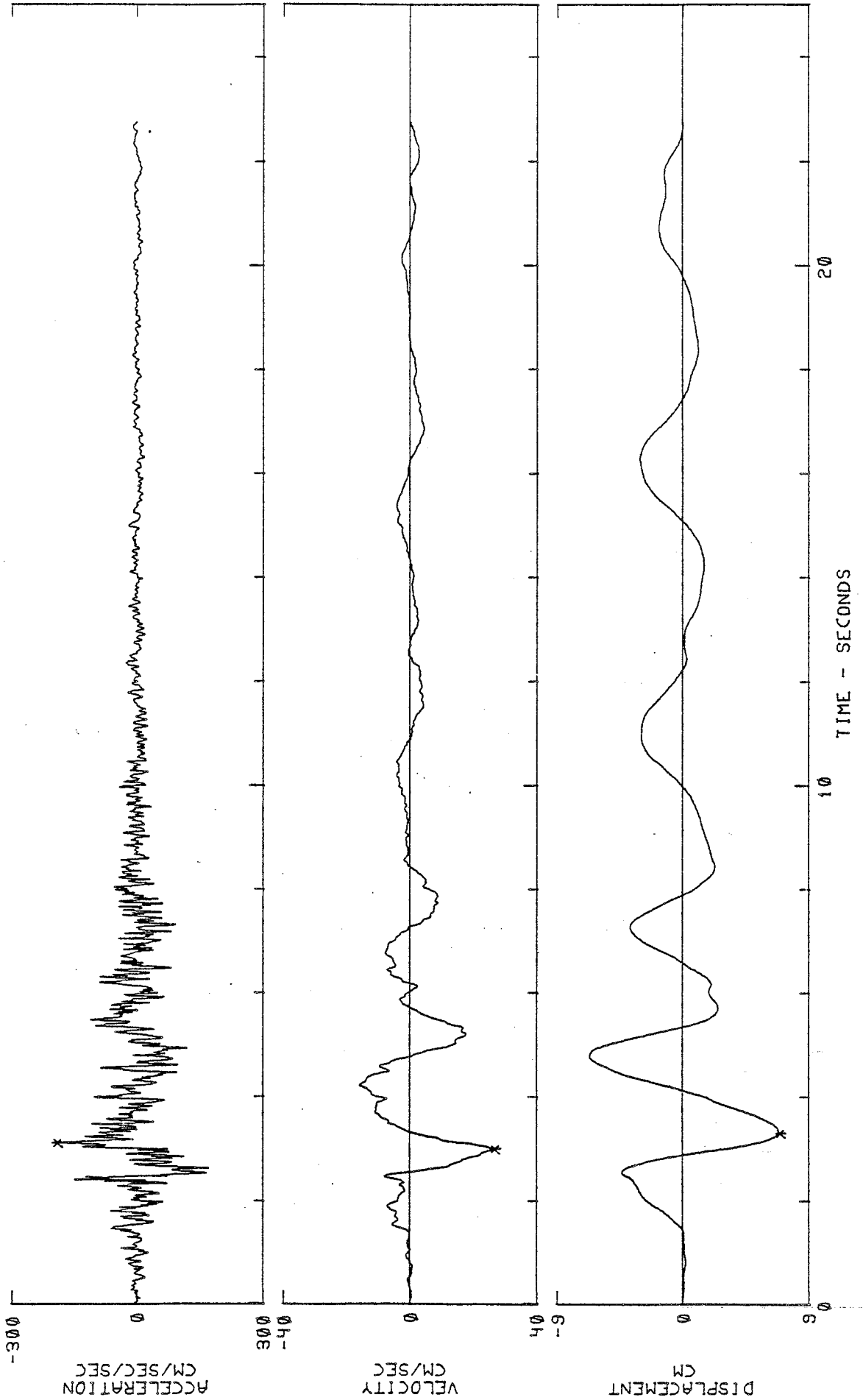


IMPERIAL VALLEY EARTHQUAKE OCT 15, 1979 -1616 PDT

IMP202 79.202.0 ROUTE 8/MELOLAND OVERPASS, EL CENTRO, CA COMP TR14

ACCELEROGRAM IS BAND-PASS FILTERED BETWEEN .145- .165 AND 25.00-27.00 CYC/SEC.

*PEAK VALUES : ACCELERATION = -190.7 CM/SEC/SEC VELOCITY = 26.7 CM/SEC DISPLACEMENT = 6.98 CM



R-8222-5603



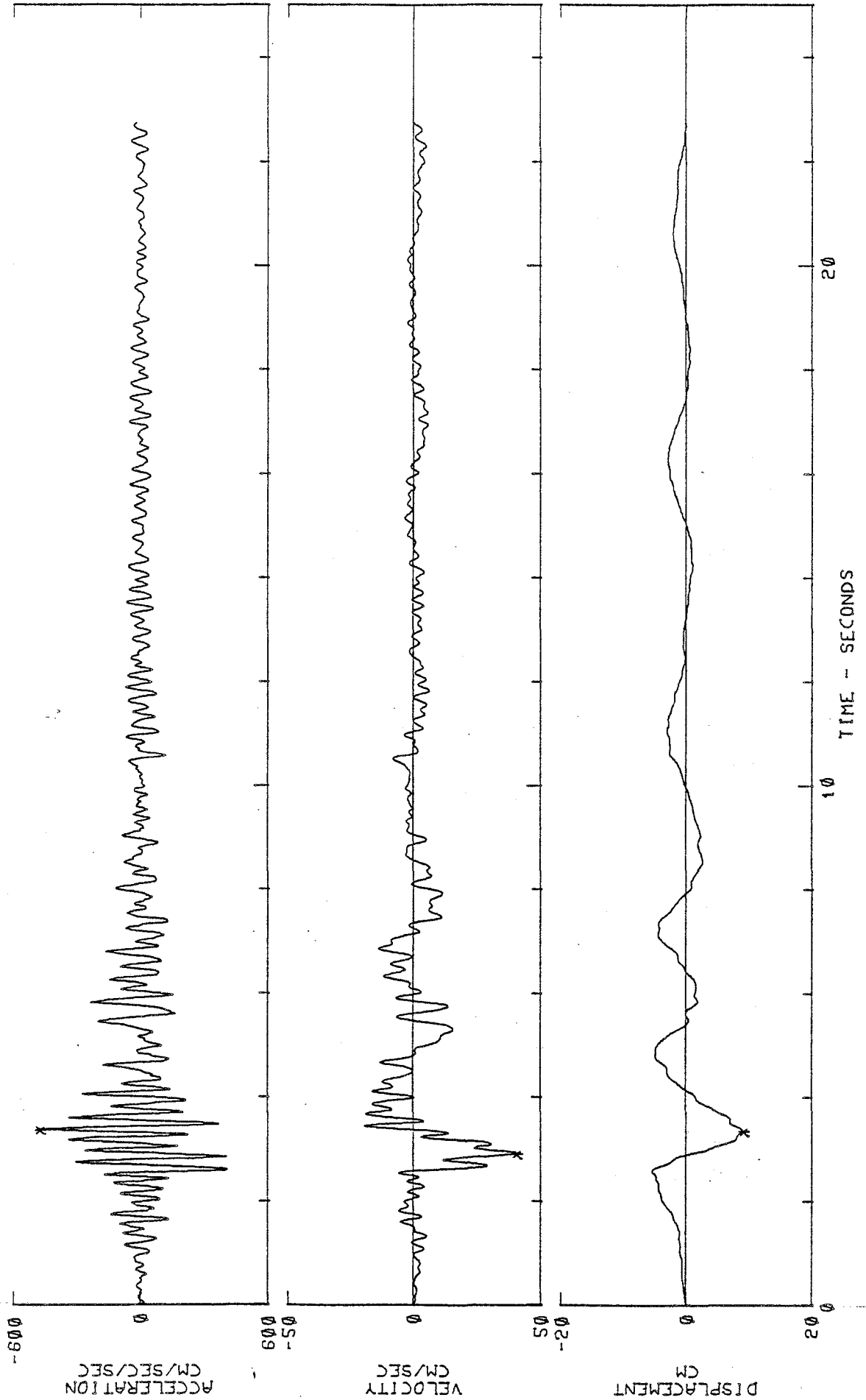
IMPERIAL VALLEY EARTHQUAKE OCT 15, 1979 -1616 PDT

IIMP202 79.202.0 ROUTE 8/MELOLAND OVERPASS, EL CENTRO, CA COMP TR16

ACCELEROGRAM IS BAND-PASS FILTERED BETWEEN .145-.16S AND 25.00-27.00 CYC/SEC.

*PEAK VALUES : ACCELERATION = -478.2 CM/SEC/SEC VELOCITY = 40.7 CM/SEC DISPLACEMENT = 9.03 CM

R-8222-5603



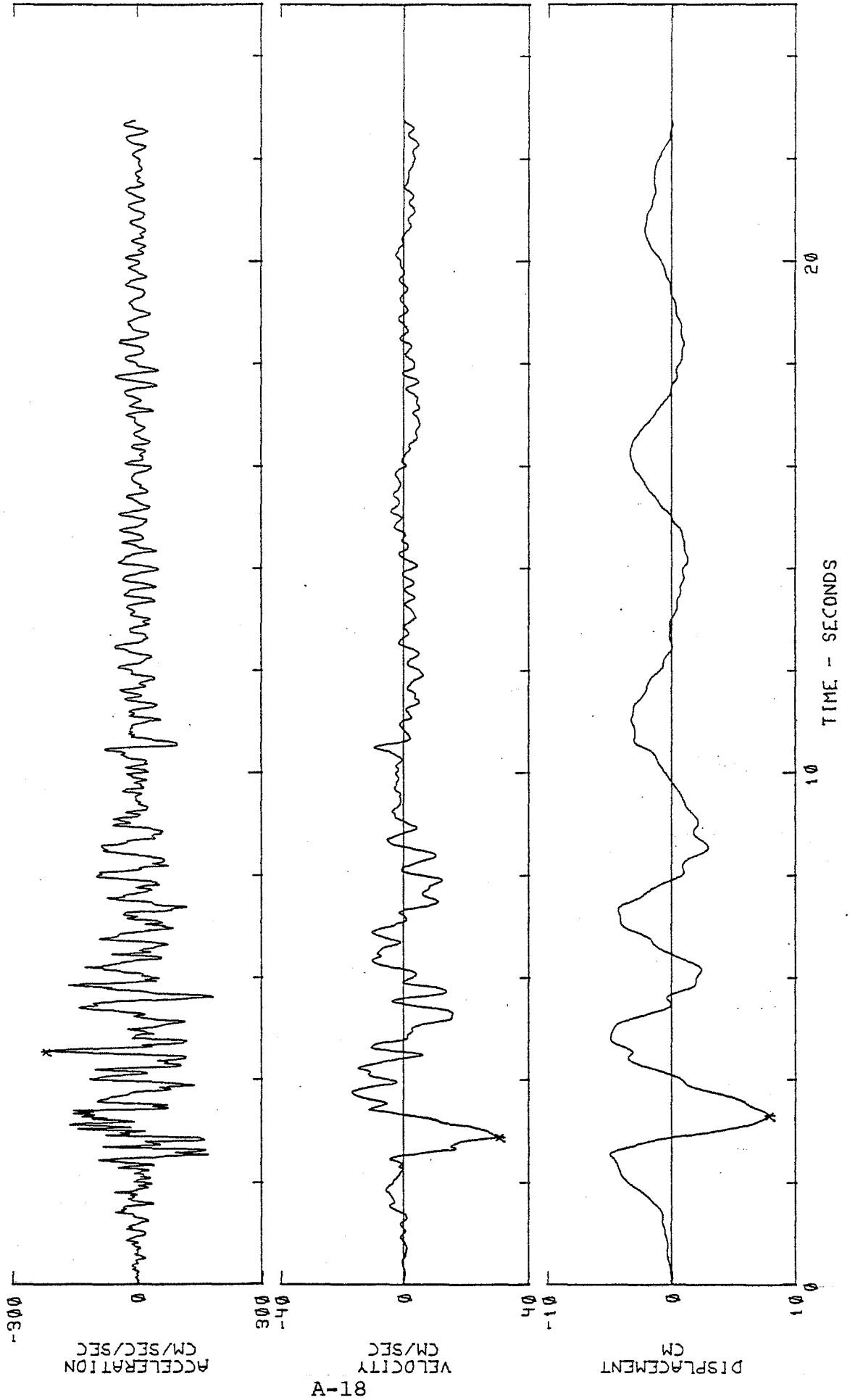


IMPERIAL VALLEY EARTHQUAKE OCT 15, 1979 -1616 PDT

IMP202 79.202.0 ROUTE 8/MELOLAND OVERPASS, EL CENTRO, CA COMP TR17

ACCELEROGRAM IS BAND-PASS FILTERED BETWEEN .145- .165 AND 25.00-27.00 CYC/SEC.

*PEAK VALUES : ACCELERATION = -222.9 CM/SEC/SEC VELOCITY = 30.6 CM/SEC DISPLACEMENT = 7.87 CM





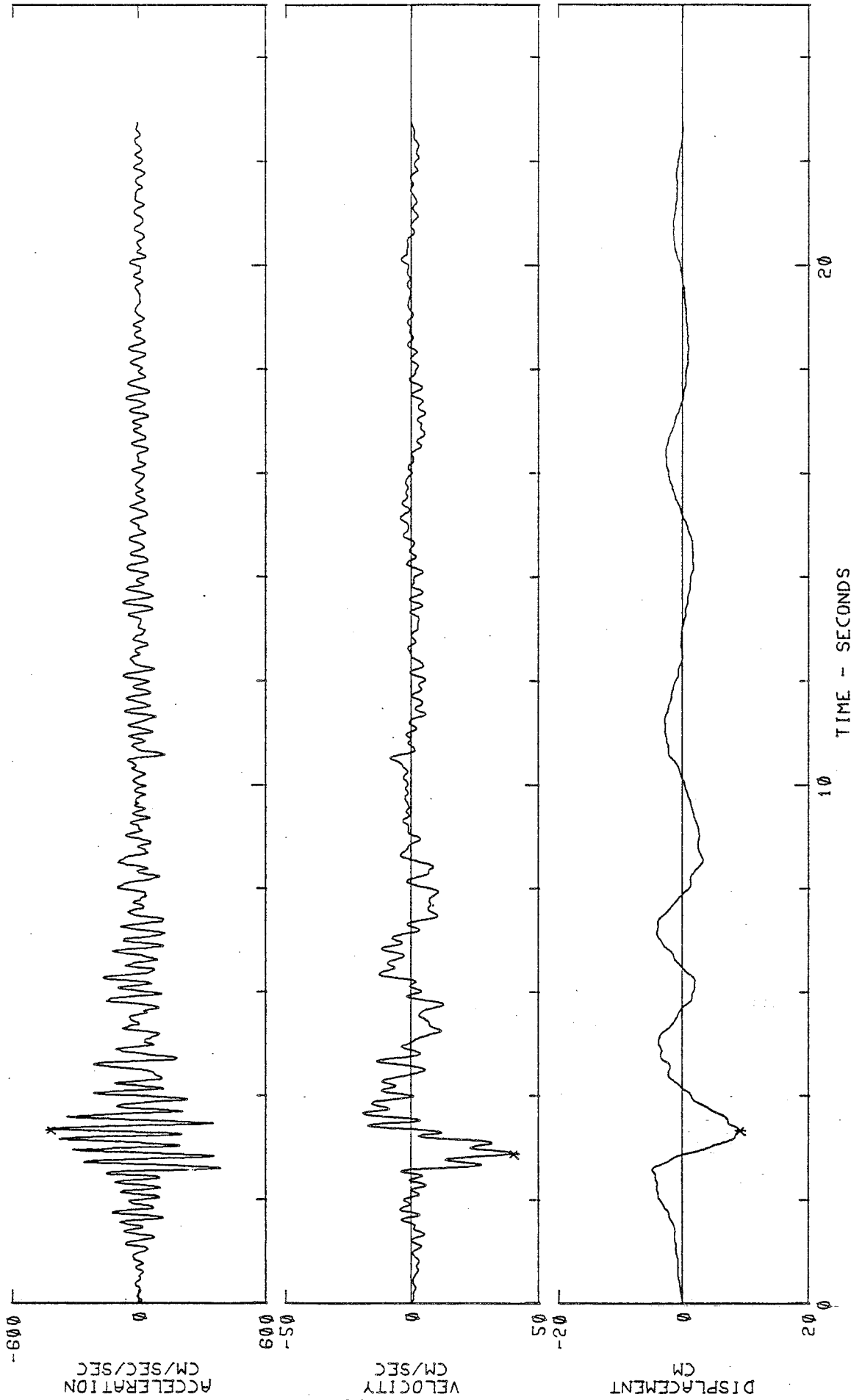
IMPERIAL VALLEY EARTHQUAKE OCT 15, 1979 -1616 PDT

IMP202 79.202.0 ROUTE 8/MELOLAND OVERPASS, EL CENTRO, CA COMP TR20

ACCELEROGRAM IS BAND-PASS FILTERED BETWEEN .145- .165 AND 25.00-27.00 CYC/SEC.

*PEAK VALUES : ACCELERATION = -423.0 CM/SEC/SEC VELOCITY = 40.2 CM/SEC DISPLACEMENT = 9.04 CM

R-8222-5603



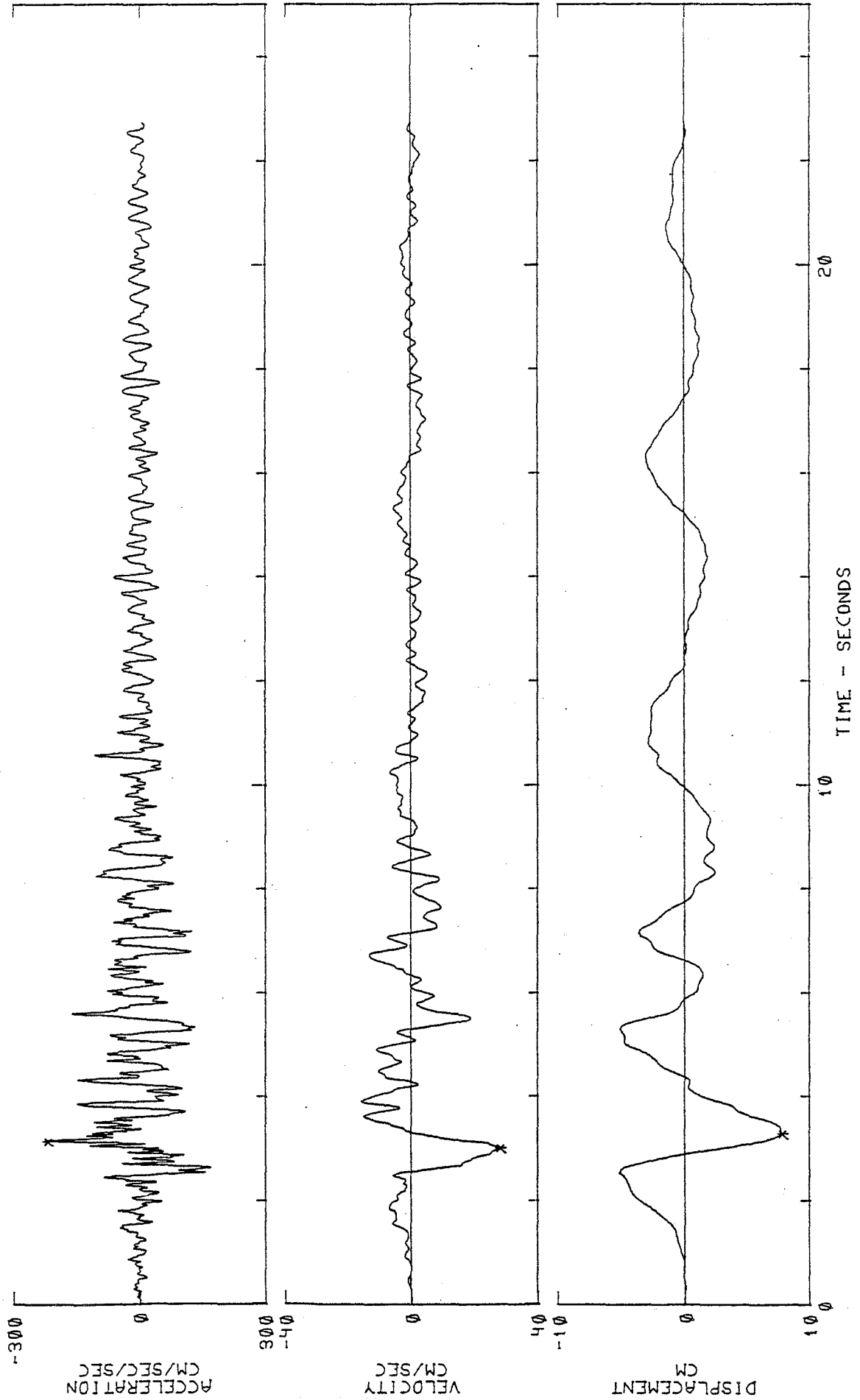


IMPERIAL VALLEY EARTHQUAKE OCT 15, 1979 -1616 PDT

IMP202 79.202.0 ROUTE 8/MELOLAND OVERPASS, EL CENTRO, CA COMP TR21

ACCELEROGRAM IS BAND-PASS FILTERED BETWEEN .145- .165 AND 25.00-27.00 CYC/SEC.

*PEAK VALUES : ACCELERATION = -221.0 CM/SEC/SEC VELOCITY = 28.1 CM/SEC DISPLACEMENT = 7.85 CM



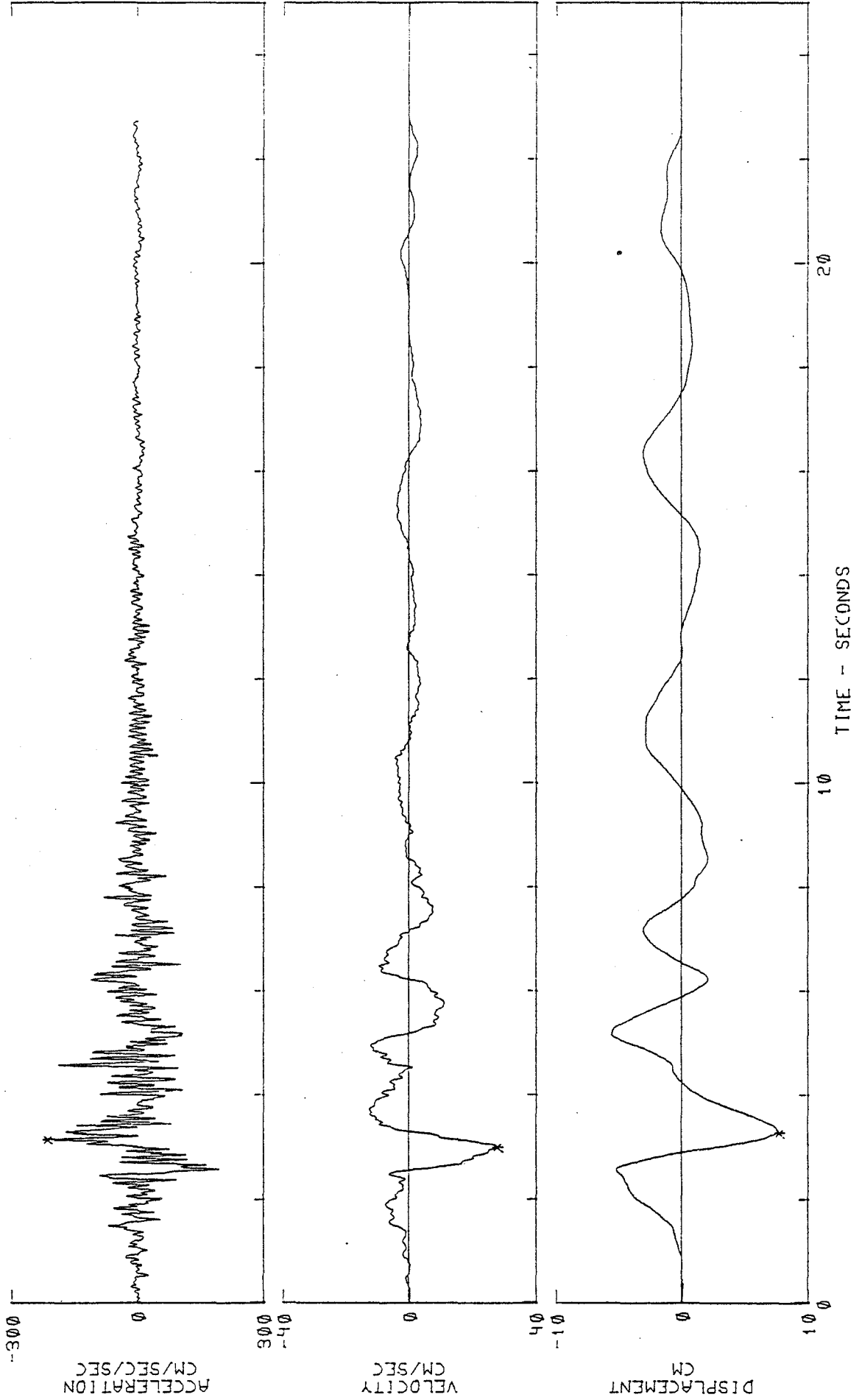


IMPERIAL VALLEY EARTHQUAKE OCT 15, 1979 -1616 PDT

IIMP202 79.202.0 ROUTE 8/MELOLAND OVERPASS, EL CENTRO, CA COMP TR23

ACCELEROGRAM IS BAND-PASS FILTERED BETWEEN .145-.165 AND 25.00-27.00 CYC/SEC.

*PEAK VALUES : ACCELERATION = -215.9 CM/SEC/SEC VELOCITY = 27.7 CM/SEC DISPLACEMENT = 7.71 CM



R-8222-5603

0 1 2 3 4 5 6 7 8 9 10 11 12 13 14 15 16 17 18 19 20

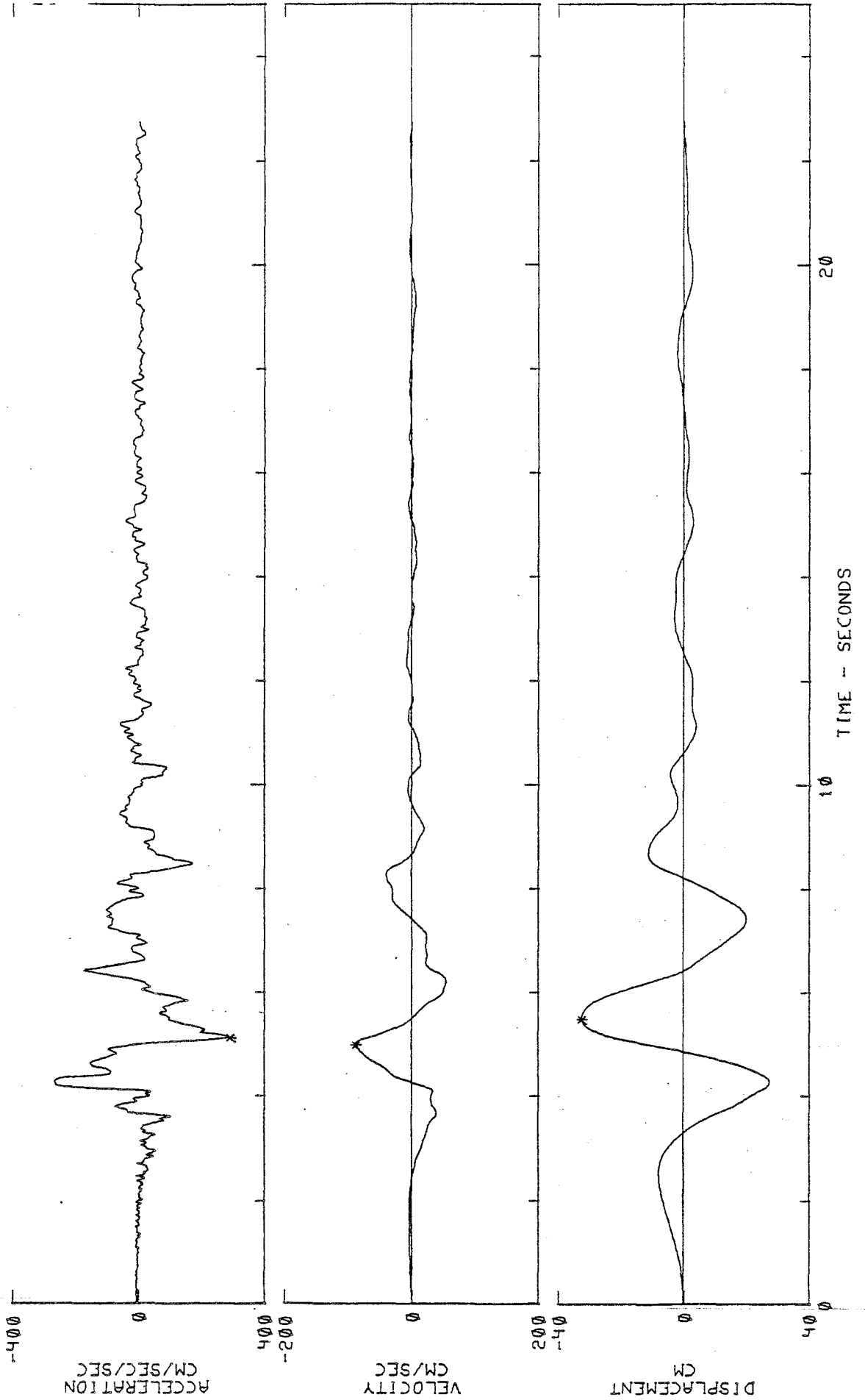


IMPERIAL VALLEY EARTHQUAKE OCT 15, 1979 -1616 PDT

IIMP202 79.202.0 ROUTE 8/MELOLAND OVERPASS, EL CENTRO, CA COMP TR24
ACCELEROGRAM IS BAND-PASS FILTERED BETWEEN .145-.165 AND 25.00-27.00 CYC/SEC.

*PEAK VALUES : ACCELERATION = 292.5 CM/SEC/SEC VELOCITY = -88.9 CM/SEC DISPLACEMENT = -32.6 CM

R-8222-5603





RESPONSE AND FOURIER SPECTRA

IMPERIAL VALLEY EARTHQUAKE OCT 15, 1979 -1616 PDT

IIIMP201 79.201.0 COMP TR 1

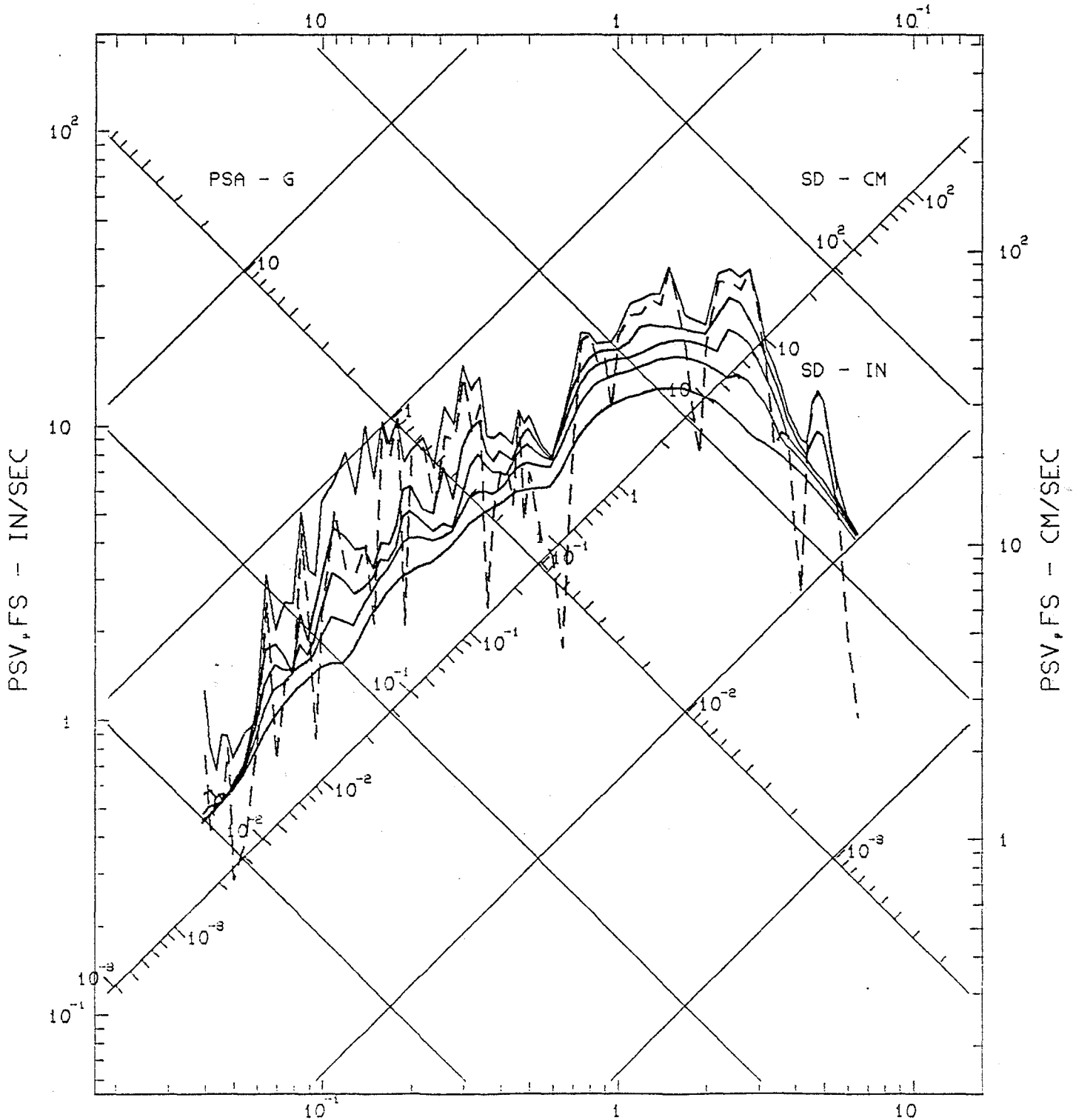
ROUTE 8/MELOLAND OVERPASS, EL CENTRO, CA

ACCELEROGRAM IS BAND-PASS FILTERED BETWEEN .145- .165 AND 25.00-27.00 CYC/SEC.

DAMPING VALUES ARE 0, 2, 5, 10 & 20 % OF CRITICAL

— RESPONSE SPECTRA: PSV, PSA & SD - - - FOURIER AMPLITUDE SPECTRUM: FS

FREQUENCY - HZ



PERIOD - SEC



RESPONSE AND FOURIER SPECTRA IMPERIAL VALLEY EARTHQUAKE OCT 15, 1979 -1616 PDT

IIIMP201 79.201.0 COMP TR 2

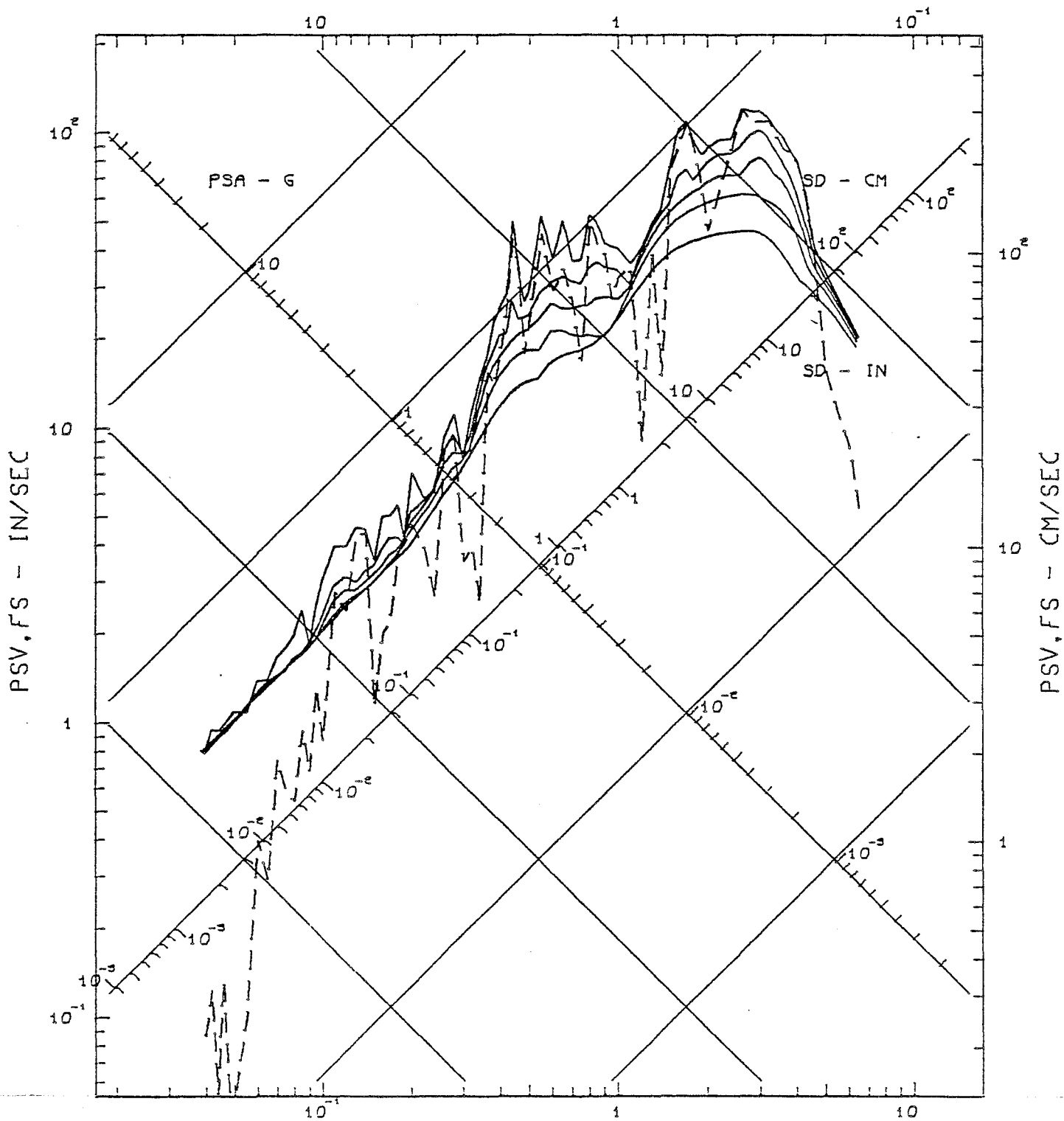
ROUTE 8/MELOLAND OVERPASS, EL CENTRO, CA

ACCELEROGRAM IS BAND-PASS FILTERED BETWEEN .145- .165 AND 25.00-27.00 CYC/SEC.

DAMPING VALUES ARE 0, 2, 5, 10 & 20 % OF CRITICAL

— RESPONSE SPECTRA: PSV, PSA & SD - - - FOURIER AMPLITUDE SPECTRUM: FS

FREQUENCY - HZ



PERIOD - SEC



RESPONSE AND FOURIER SPECTRA

IMPERIAL VALLEY EARTHQUAKE OCT 15, 1979 -1616 PDT

IIIMP201 79.201.0 COMP TR 3

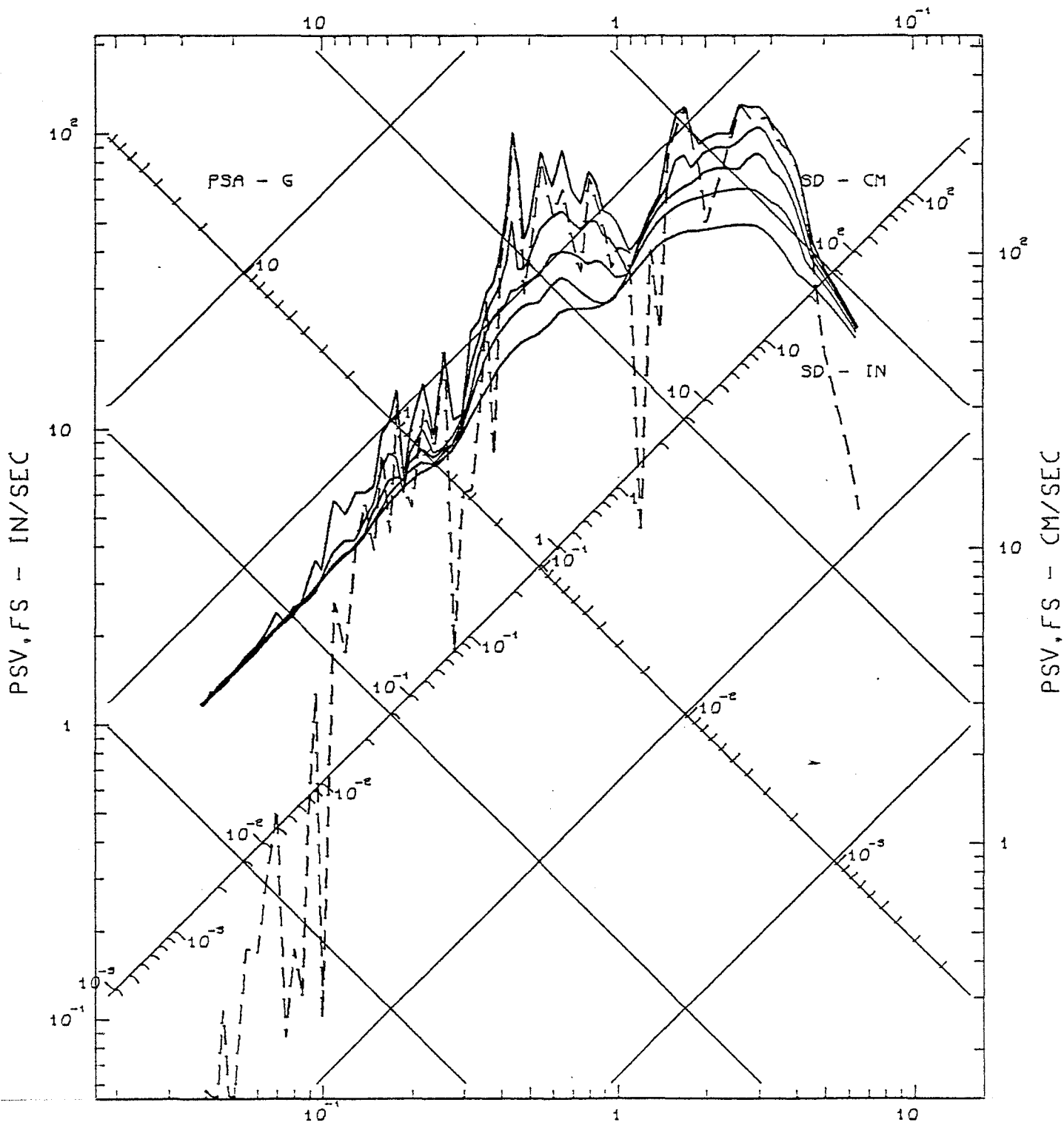
ROUTE 8/MELOLAND OVERPASS, EL CENTRO, CA

ACCELEROGRAM IS BAND-PASS FILTERED BETWEEN .145- .165 AND 25.00-27.00 CYC/SEC.

DAMPING VALUES ARE 0, 2, 5, 10 & 20 % OF CRITICAL

— RESPONSE SPECTRA: PSV, PSA & SD - - - FOURIER AMPLITUDE SPECTRUM: FS

FREQUENCY - HZ



PERIOD - SEC



RESPONSE AND FOURIER SPECTRA

IMPERIAL VALLEY EARTHQUAKE OCT 15, 1979 -1616 PDT

IIIMP201 79.201.0 COMP TR 4

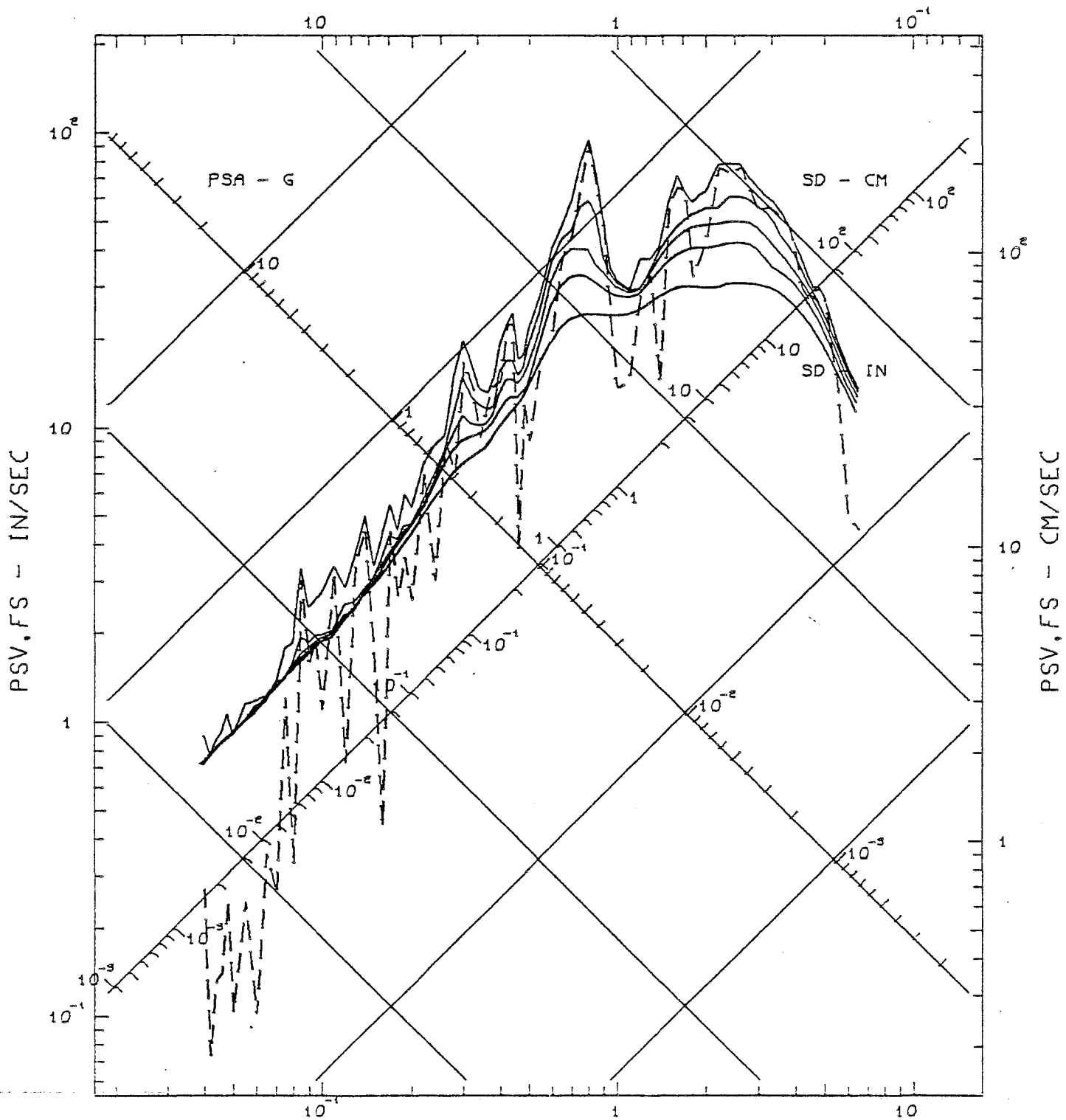
ROUTE 8/MELOLAND OVERPASS, EL CENTRO, CA

ACCELEROGRAM IS BAND-PASS FILTERED BETWEEN .145- .165 AND 25.00-27.00 CYC/SEC.

DAMPING VALUES ARE 0, 2, 5, 10 & 20 % OF CRITICAL

— RESPONSE SPECTRA: PSV, PSA & SD - - - FOURIER AMPLITUDE SPECTRUM: FS

FREQUENCY - HZ



PERIOD - SEC



RESPONSE AND FOURIER SPECTRA

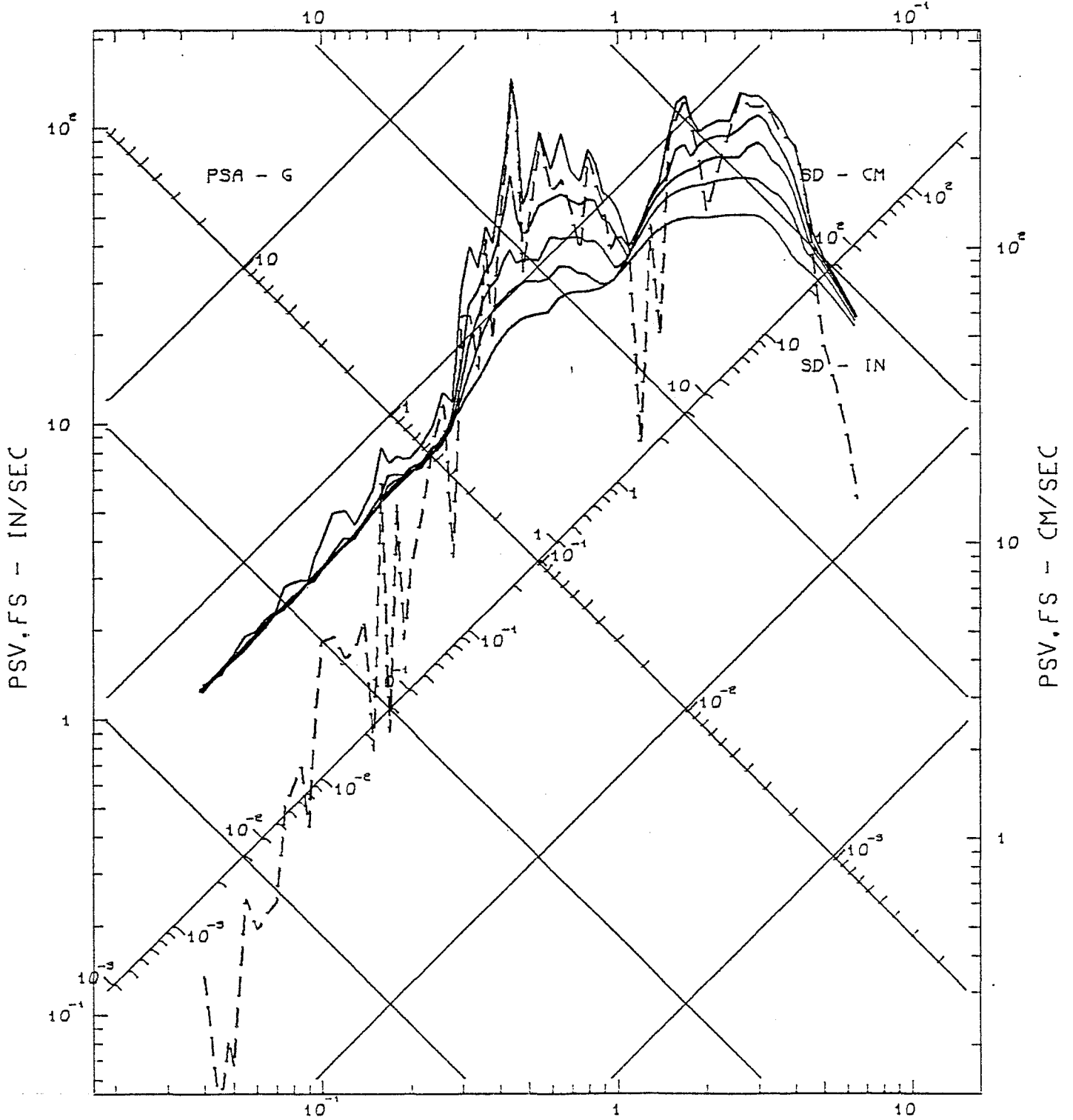
IMPERIAL VALLEY EARTHQUAKE OCT 15, 1979 -1616 PDT

IIIMP201 79.201.0 COMP TR 5
ROUTE 8/MELOLAND OVERPASS, EL CENTRO, CA

ACCELEROGRAM IS BAND-PASS FILTERED BETWEEN .145- .165 AND 25.00-27.00 CYC/SEC.
DAMPING VALUES ARE 0, 2, 5, 10 & 20 % OF CRITICAL

———— RESPONSE SPECTRA: PSV, PSA & SD - - - - - FOURIER AMPLITUDE SPECTRUM: FS

FREQUENCY - HZ



PERIOD - SEC



RESPONSE AND FOURIER SPECTRA IMPERIAL VALLEY EARTHQUAKE OCT 15, 1979 -1616 PDT

IIIMP201 79.201.0 COMP TR 6

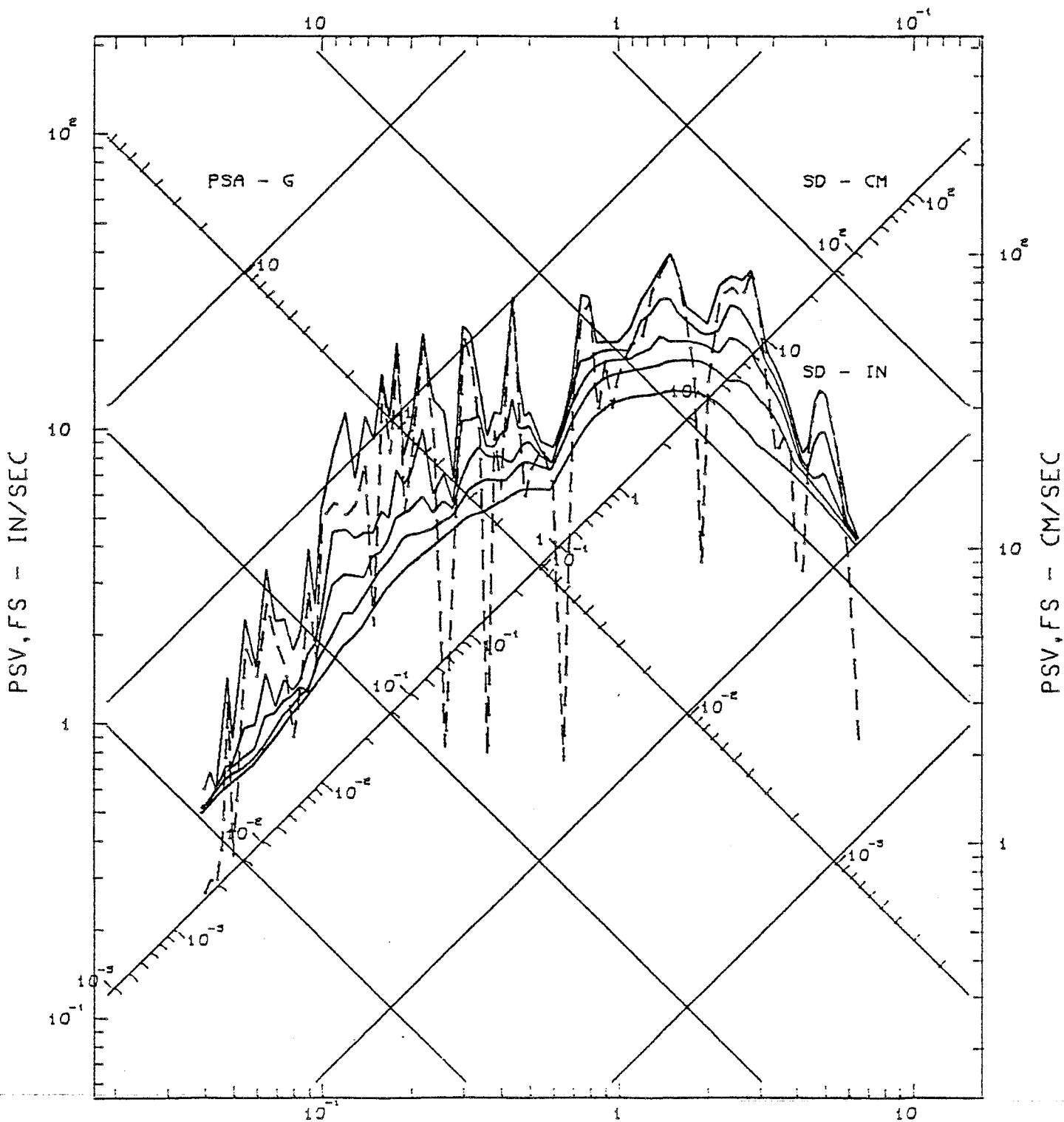
ROUTE 8/MELOLAND OVERPASS, EL CENTRO, CA

ACCELEROGRAM IS BAND-PASS FILTERED BETWEEN .145- .165 AND 25.00-27.00 CYC/SEC.

DAMPING VALUES ARE 0, 2, 5, 10 & 20 % OF CRITICAL

— RESPONSE SPECTRA: PSV, PSA & SD - - - FOURIER AMPLITUDE SPECTRUM: FS

FREQUENCY - HZ





RESPONSE AND FOURIER SPECTRA IMPERIAL VALLEY EARTHQUAKE OCT 15, 1979 -1616 PDT

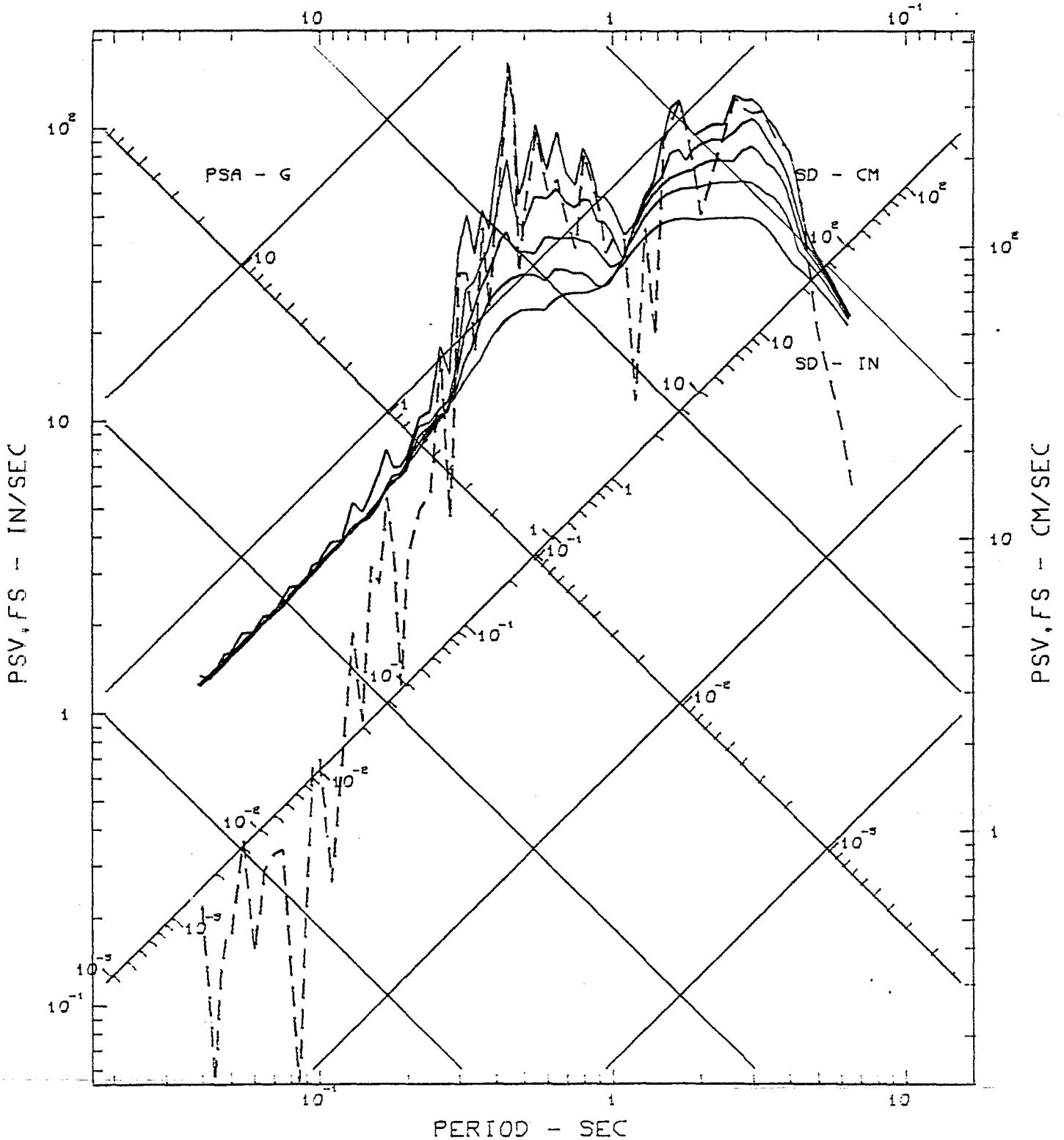
IIIMP201 79.201.0 COMP TR 7
ROUTE 8/MELOLAND OVERPASS, EL CENTRO, CA

ACCELEROGRAM IS BAND-PASS FILTERED BETWEEN .145- .165 AND 25.00-27.00 CYC/SEC.

DAMPING VALUES ARE 0, 2, 5, 10 & 20 % OF CRITICAL

— RESPONSE SPECTRA: PSV, PSA & SD - - - FOURIER AMPLITUDE SPECTRUM: FS

FREQUENCY - HZ





RESPONSE AND FOURIER SPECTRA

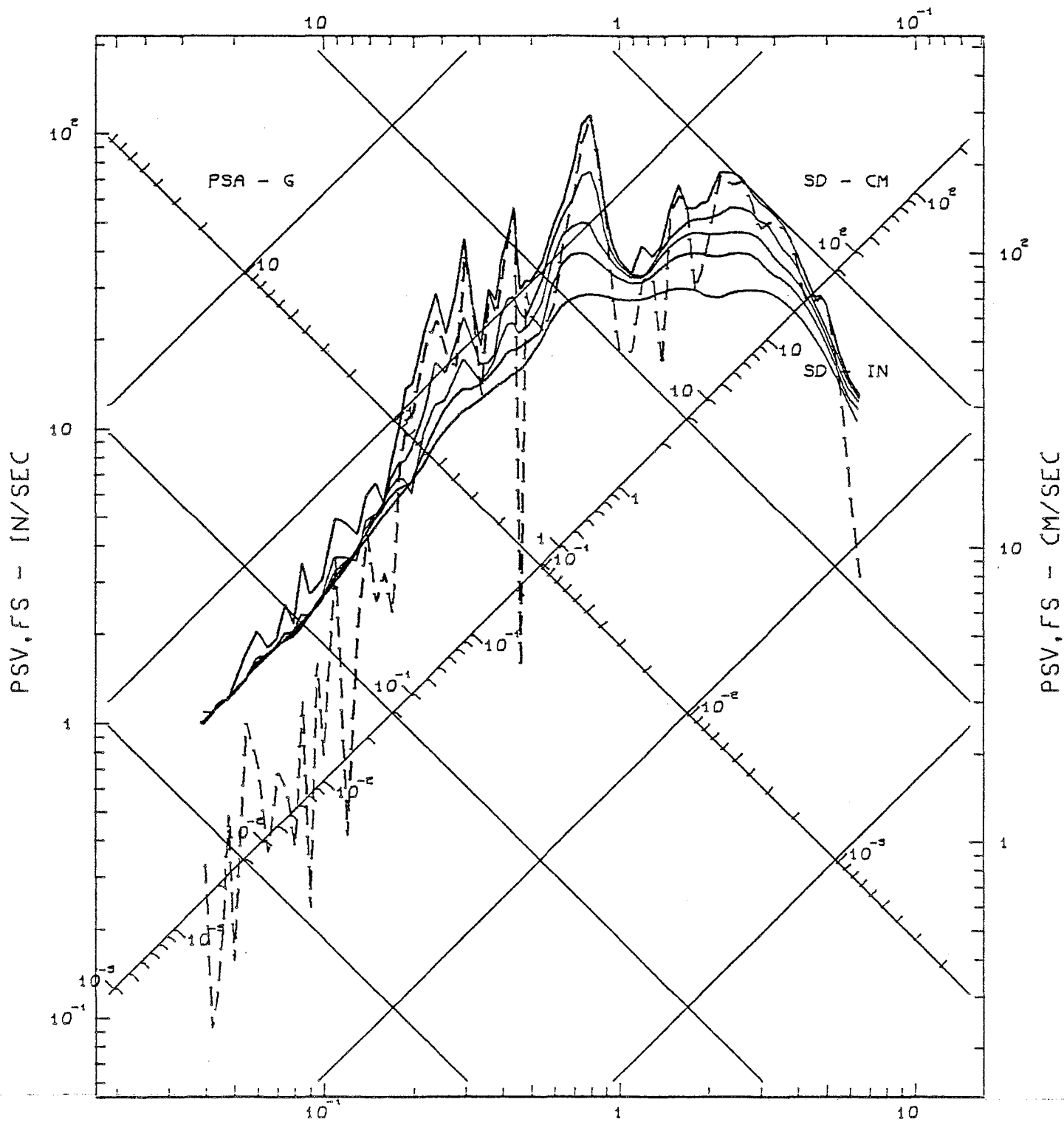
IMPERIAL VALLEY EARTHQUAKE OCT 15, 1979 -1616 PDT

IIIMP201 79.201.0 COMP TR 8
ROUTE 8/MELOLAND OVERPASS, EL CENTRO, CA

ACCELEROGRAM IS BAND-PASS FILTERED BETWEEN .145- .165 AND 25.00-27.00 CYC/SEC.
DAMPING VALUES ARE 0, 2, 5, 10 & 20 % OF CRITICAL

————— RESPONSE SPECTRA: PSV, PSA & SD - - - - - FOURIER AMPLITUDE SPECTRUM: FS

FREQUENCY - HZ



PERIOD - SEC



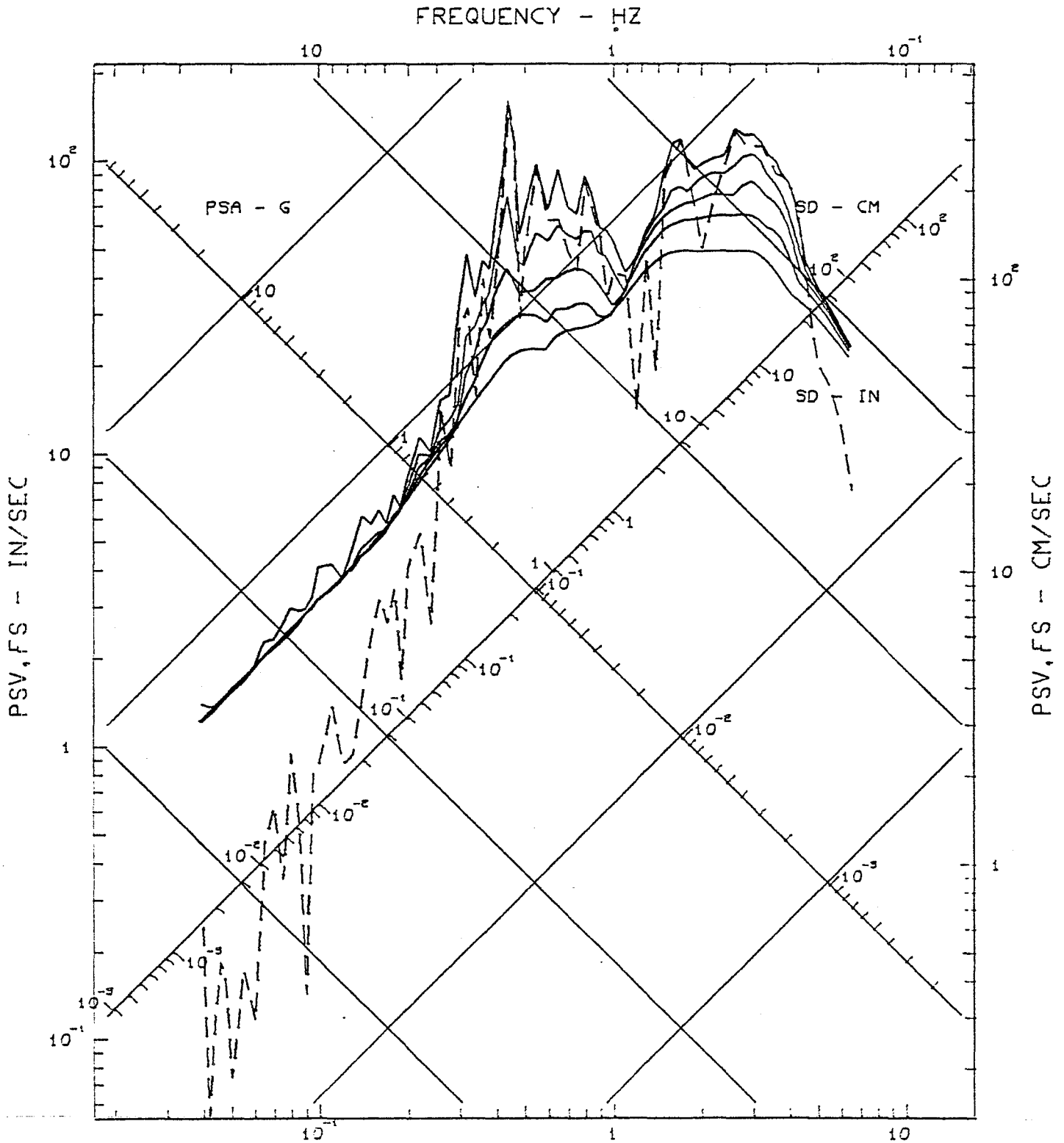
RESPONSE AND FOURIER SPECTRA IMPERIAL VALLEY EARTHQUAKE OCT 15, 1979 -1616 PDT

IIIMP201 79.201.0 COMP TR 9
ROUTE 8/MELOLAND OVERPASS, EL CENTRO, CA

ACCELEROGRAM IS BAND-PASS FILTERED BETWEEN .145- .165 AND 25.00-27.00 CYC/SEC.

DAMPING VALUES ARE 0, 2, 5, 10 & 20 % OF CRITICAL

————— RESPONSE SPECTRA: PSV, PSA & SD - - - - - FOURIER AMPLITUDE SPECTRUM: FS





RESPONSE AND FOURIER SPECTRA

IMPERIAL VALLEY EARTHQUAKE OCT 15, 1979 -1616 PDT

IIIMP201 79.201.0 COMP TR10

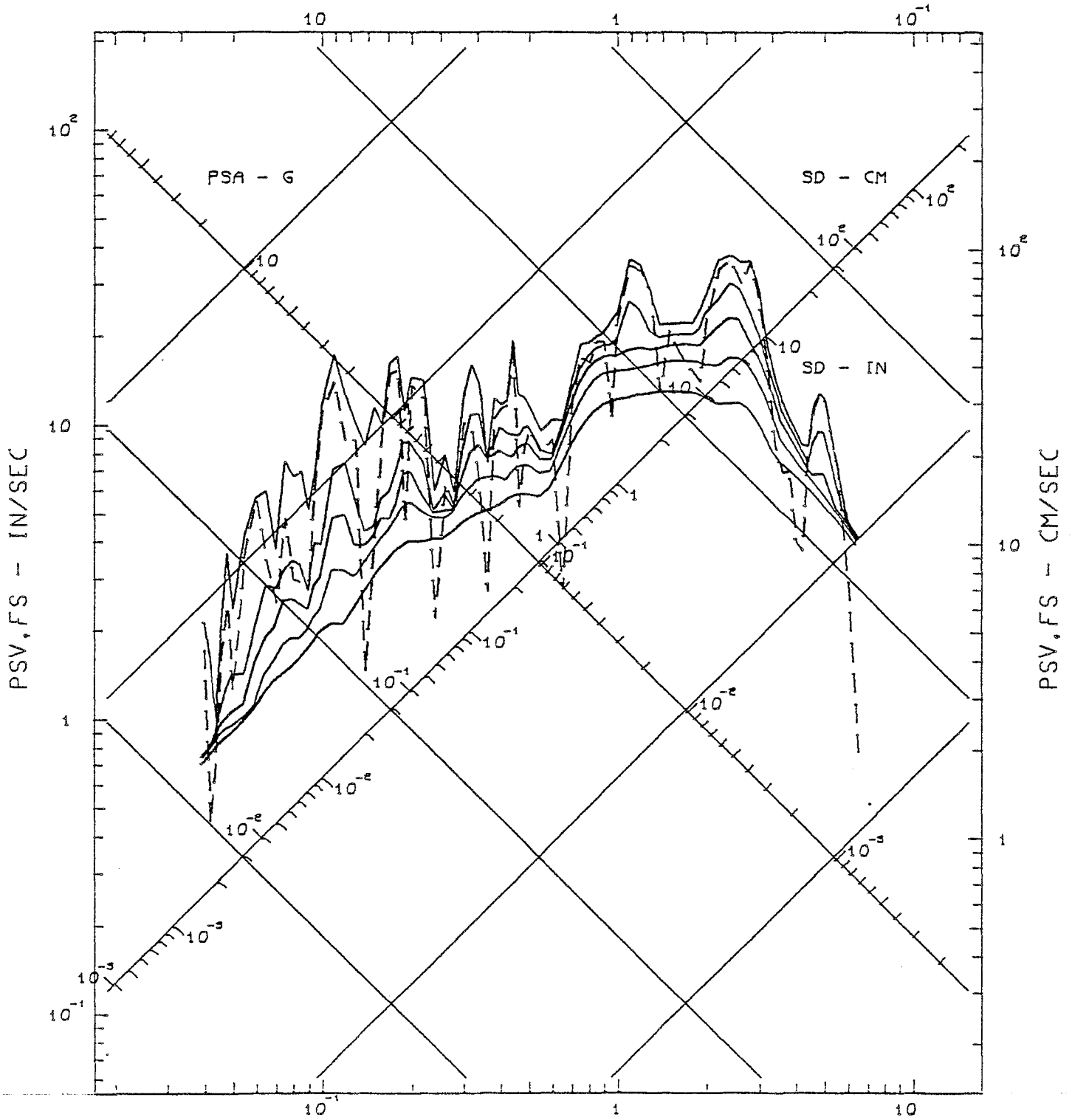
ROUTE 8/MELOLAND OVERPASS, EL CENTRO, CA

ACCELEROGRAM IS BAND-PASS FILTERED BETWEEN .145- .165 AND 25.00-27.00 CYC/SEC.

DAMPING VALUES ARE 0, 2, 5, 10 & 20 % OF CRITICAL

— RESPONSE SPECTRA: PSV, PSA & SD - - - FOURIER AMPLITUDE SPECTRUM: FS

FREQUENCY - HZ





RESPONSE AND FOURIER SPECTRA

IMPERIAL VALLEY EARTHQUAKE OCT 15, 1979 -1616 PDT

IIIMP201 79.201.0 COMP TR11

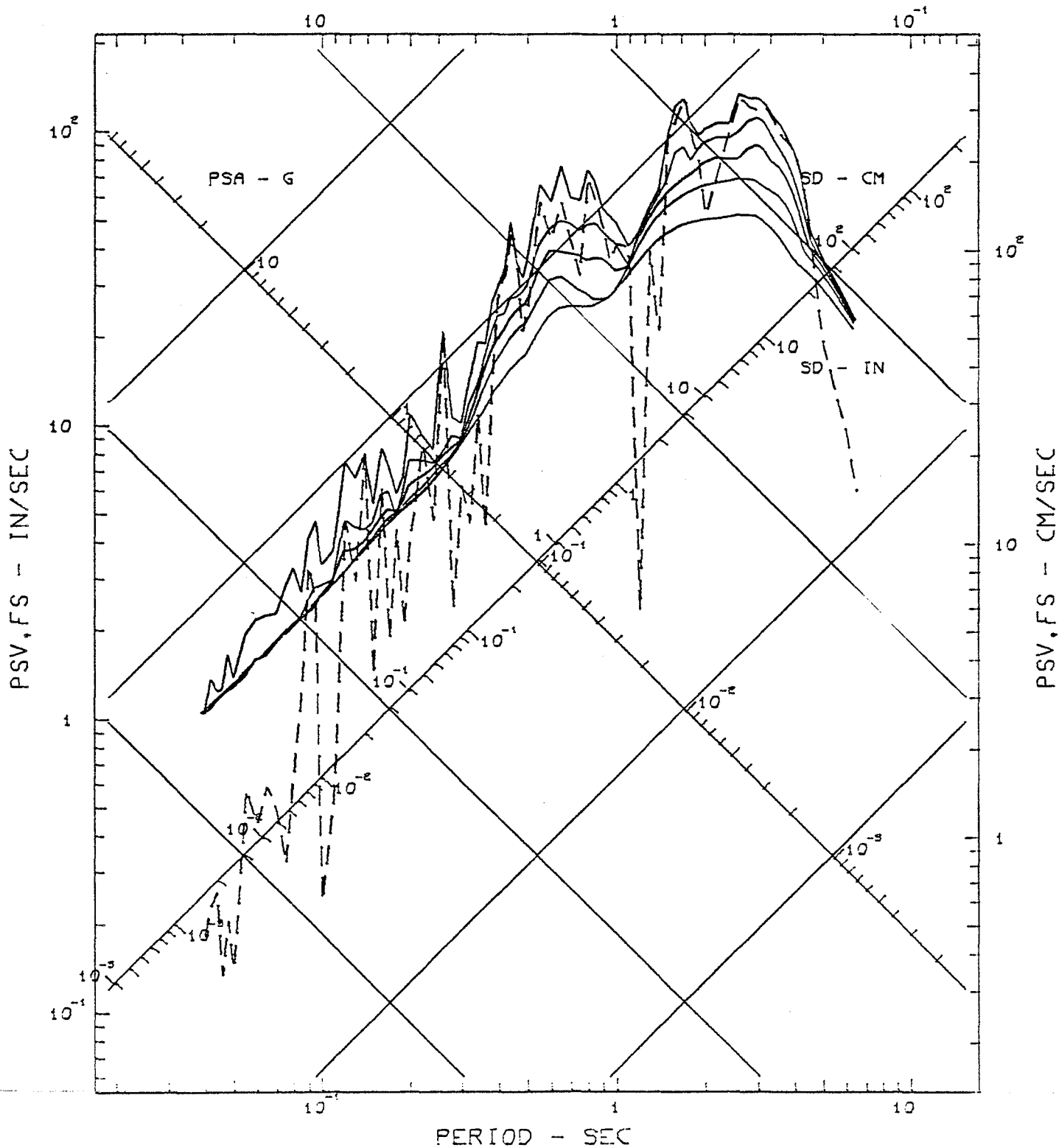
ROUTE 8/MELOLAND OVERPASS, EL CENTRO, CA

ACCELEROGRAM IS BAND-PASS FILTERED BETWEEN .145- .165 AND 25.00-27.00 CYC/SEC.

DAMPING VALUES ARE 0, 2, 5, 10 & 20 % OF CRITICAL

————— RESPONSE SPECTRA: PSV, PSA & SD - - - - - FOURIER AMPLITUDE SPECTRUM: FS

FREQUENCY - HZ





RESPONSE AND FOURIER SPECTRA

IMPERIAL VALLEY EARTHQUAKE OCT 15, 1979 -1616 PDT

IIIMP201 79.201.0 COMP TR12

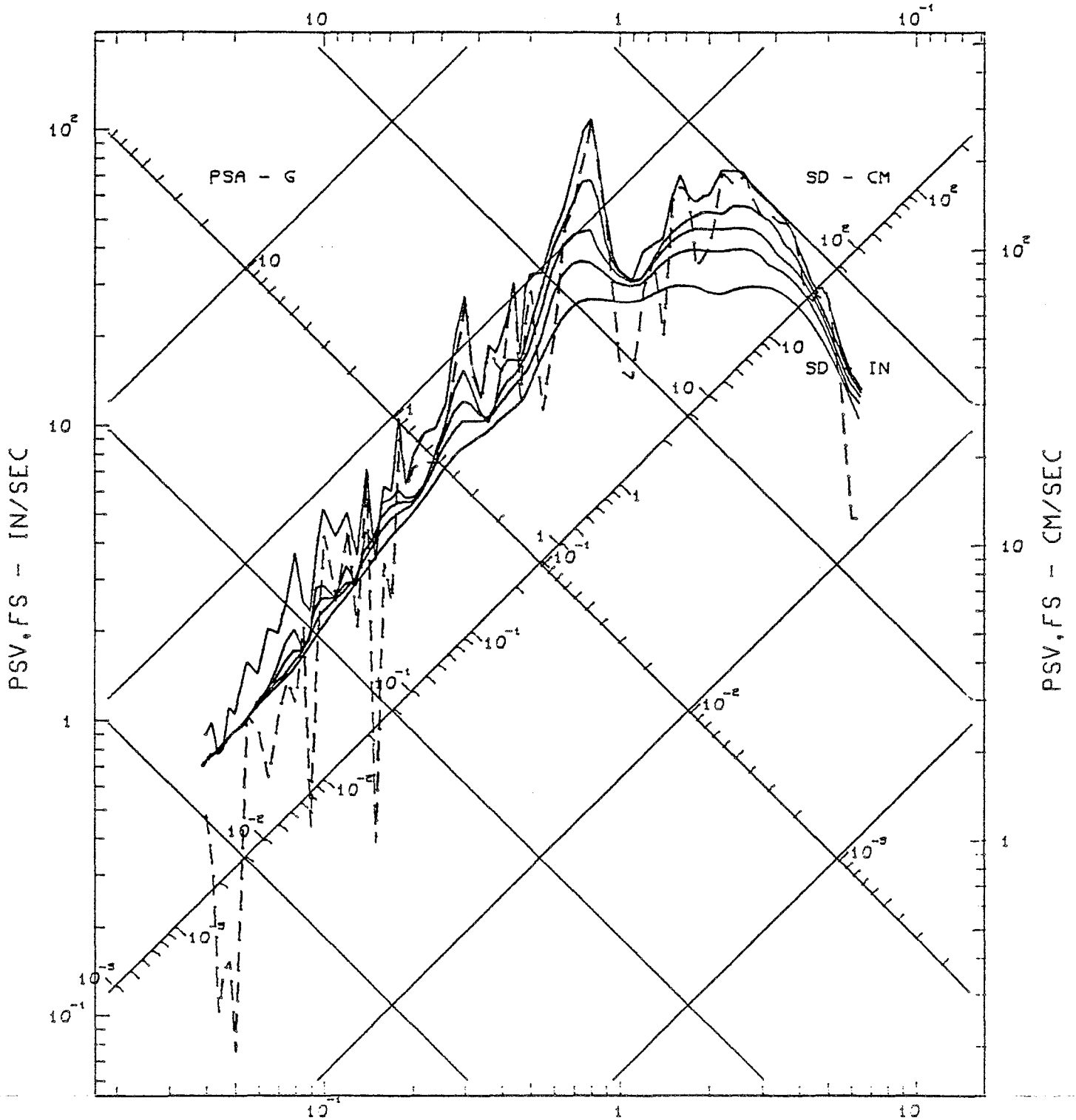
ROUTE 8/MELOLAND OVERPASS, EL CENTRO, CA

ACCELEROGRAM IS BAND-PASS FILTERED BETWEEN .145- .165 AND 25.00-27.00 CYC/SEC.

DAMPING VALUES ARE 0, 2, 5, 10 & 20 % OF CRITICAL

————— RESPONSE SPECTRA: PSV, PSA & SD - - - - - FOURIER AMPLITUDE SPECTRUM: FS

FREQUENCY - HZ



PERIOD - SEC



RESPONSE AND FOURIER SPECTRA

IMPERIAL VALLEY EARTHQUAKE OCT 15, 1979 -1616 PDT

IIIMP201 79.201.0 COMP TR13

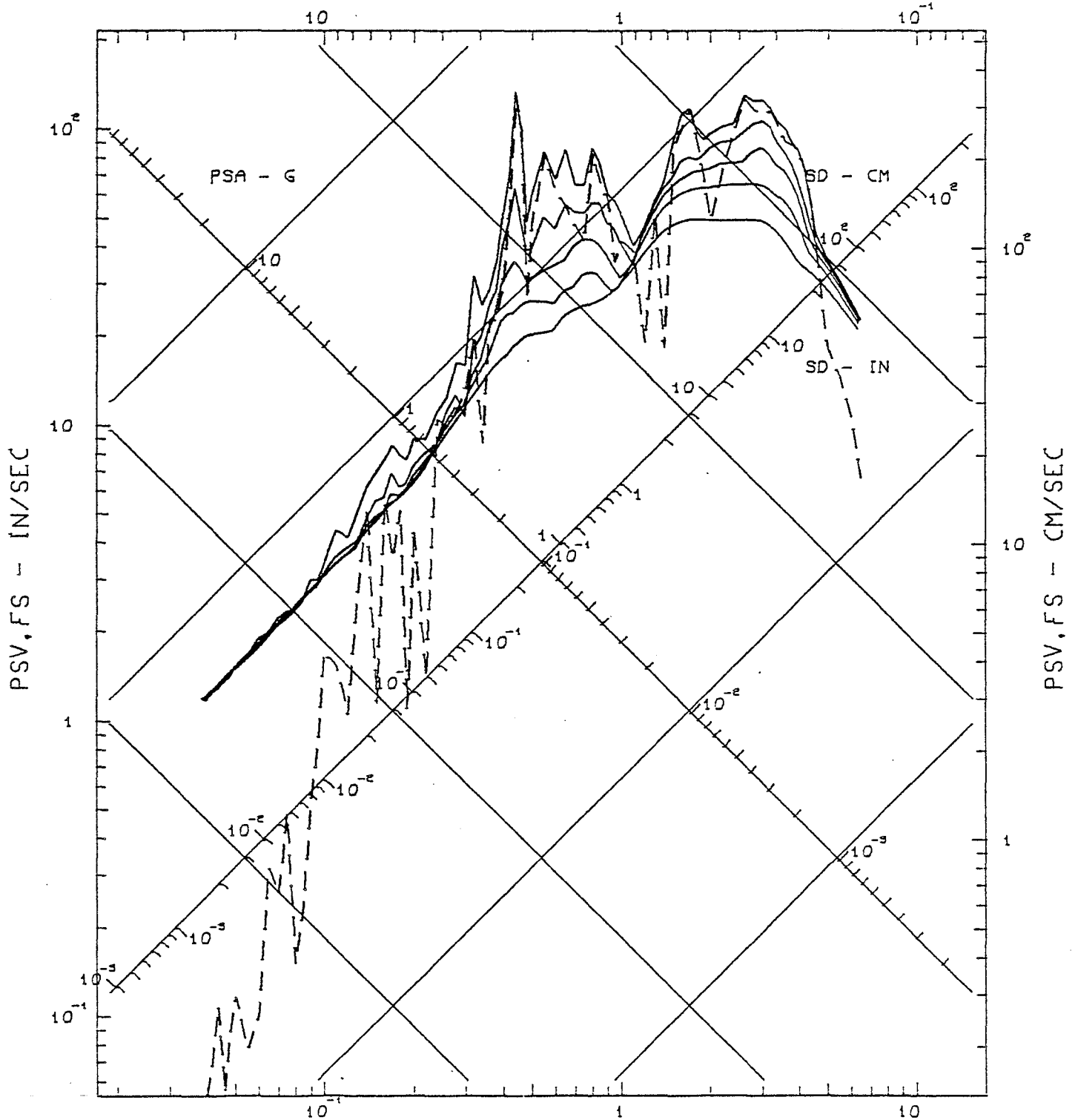
ROUTE 8/MELOLAND OVERPASS, EL CENTRO, CA

ACCELEROGRAM IS BAND-PASS FILTERED BETWEEN .145- .165 AND 25.00-27.00 CYC/SEC.

DAMPING VALUES ARE 0, 2, 5, 10 & 20 % OF CRITICAL

————— RESPONSE SPECTRA: PSV, PSA & SD - - - - - FOURIER AMPLITUDE SPECTRUM: FS

FREQUENCY - HZ



PERIOD - SEC



RESPONSE AND FOURIER SPECTRA

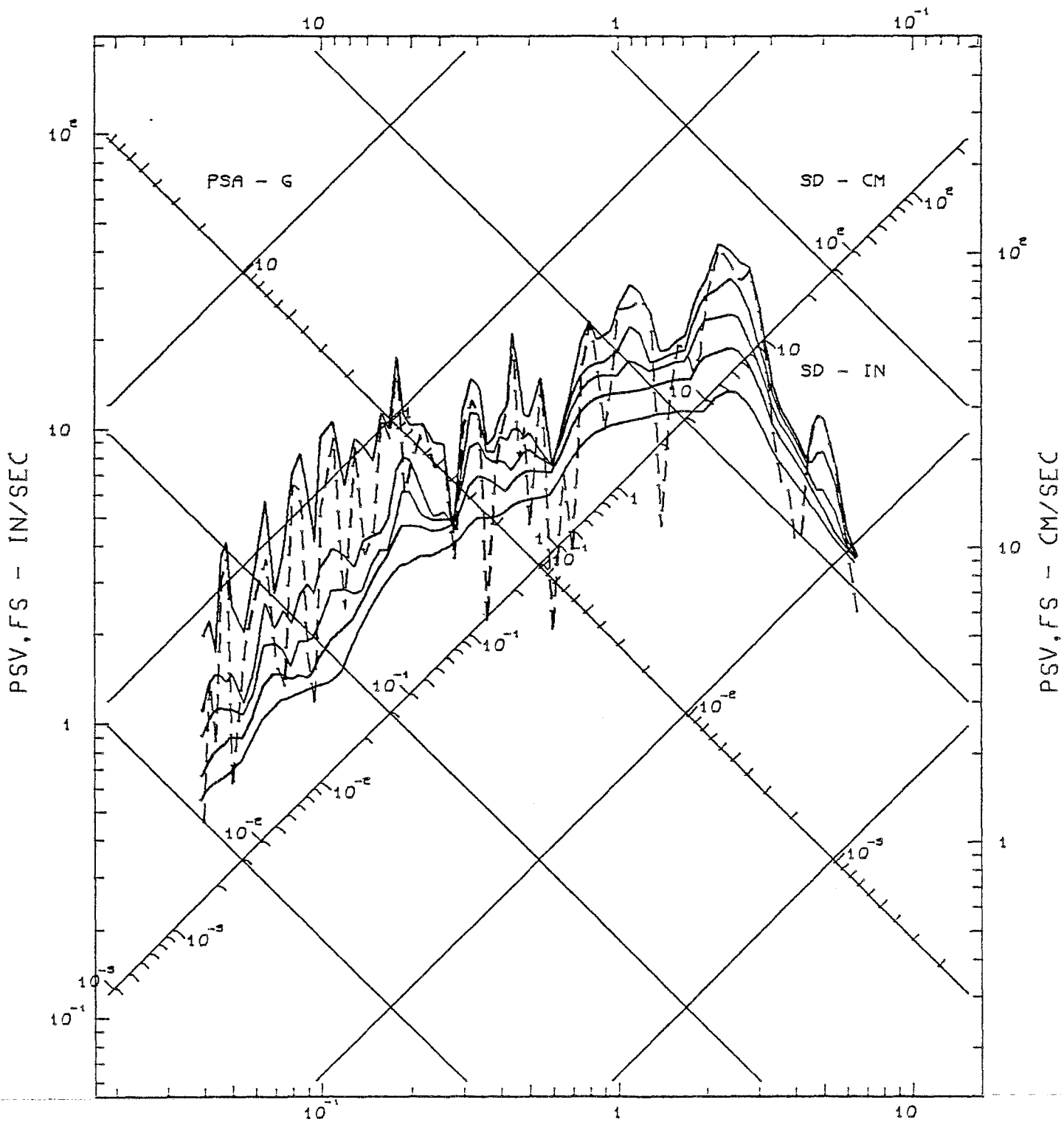
IMPERIAL VALLEY EARTHQUAKE OCT 15, 1979 -1616 PDT

IIIMP202 79.202.0 COMP TR14
 ROUTE 8/MELOLAND OVERPASS, EL CENTRO, CA

ACCELEROGRAM IS BAND-PASS FILTERED BETWEEN .145- .165 AND 25.00-27.00 CYC/SEC.
 DAMPING VALUES ARE 0, 2, 5, 10 & 20 % OF CRITICAL

————— RESPONSE SPECTRA: PSV, PSA & SD - - - - - FOURIER AMPLITUDE SPECTRUM: FS

FREQUENCY - HZ



PERIOD - SEC



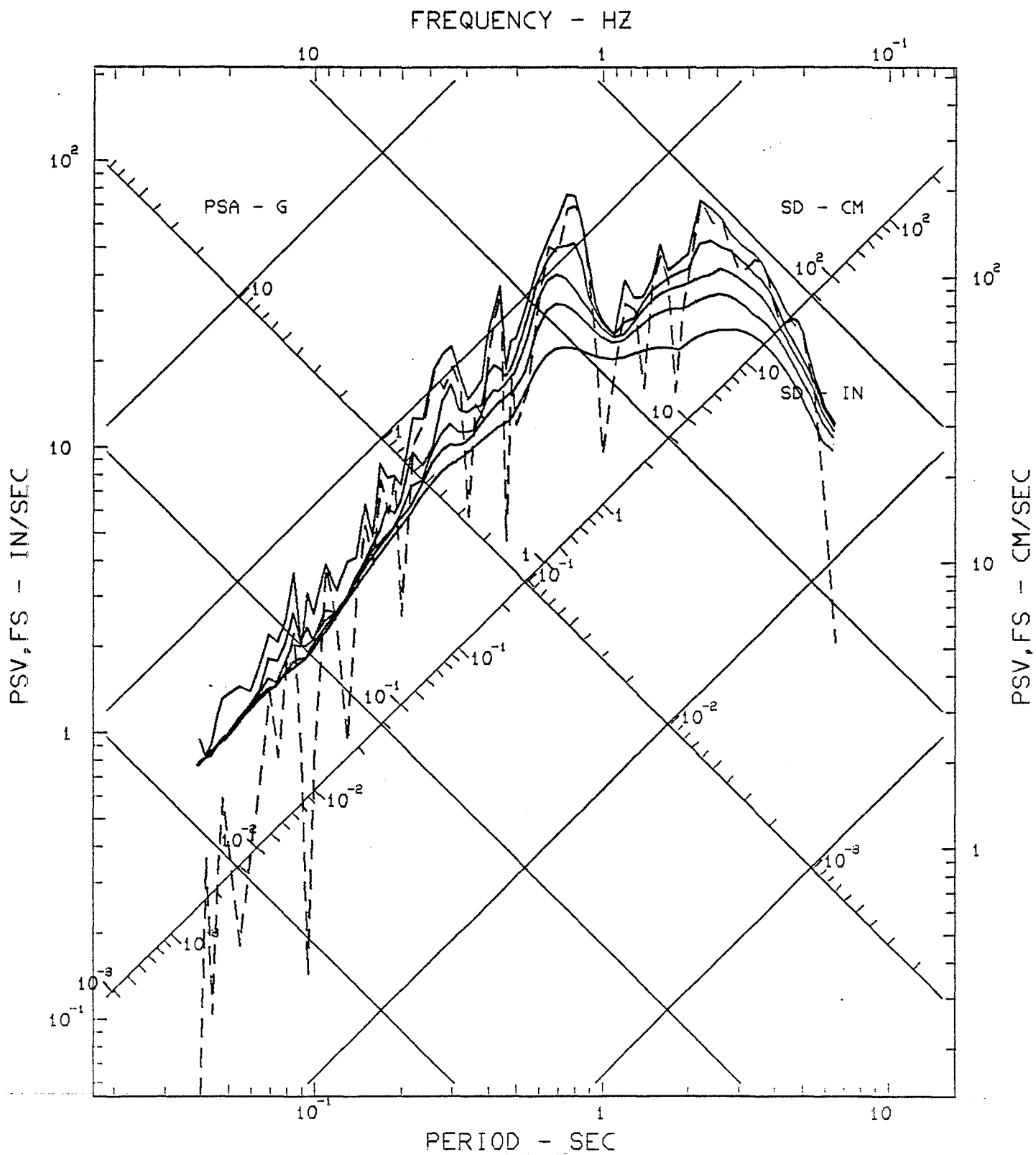
RESPONSE AND FOURIER SPECTRA

IMPERIAL VALLEY EARTHQUAKE OCT 15, 1979 -1616 PDT

IIIMP202 79.202.0 COMP TR15
 ROUTE 8/MELOLAND OVERPASS, EL CENTRO, CA

ACCELEROGRAM IS BAND-PASS FILTERED BETWEEN .145- .165 AND 25.00-27.00 CYC/SEC.
 DAMPING VALUES ARE 0, 2, 5, 10 & 20 % OF CRITICAL

———— RESPONSE SPECTRA: PSV, PSA & SD - - - - FOURIER AMPLITUDE SPECTRUM: FS





RESPONSE AND FOURIER SPECTRA

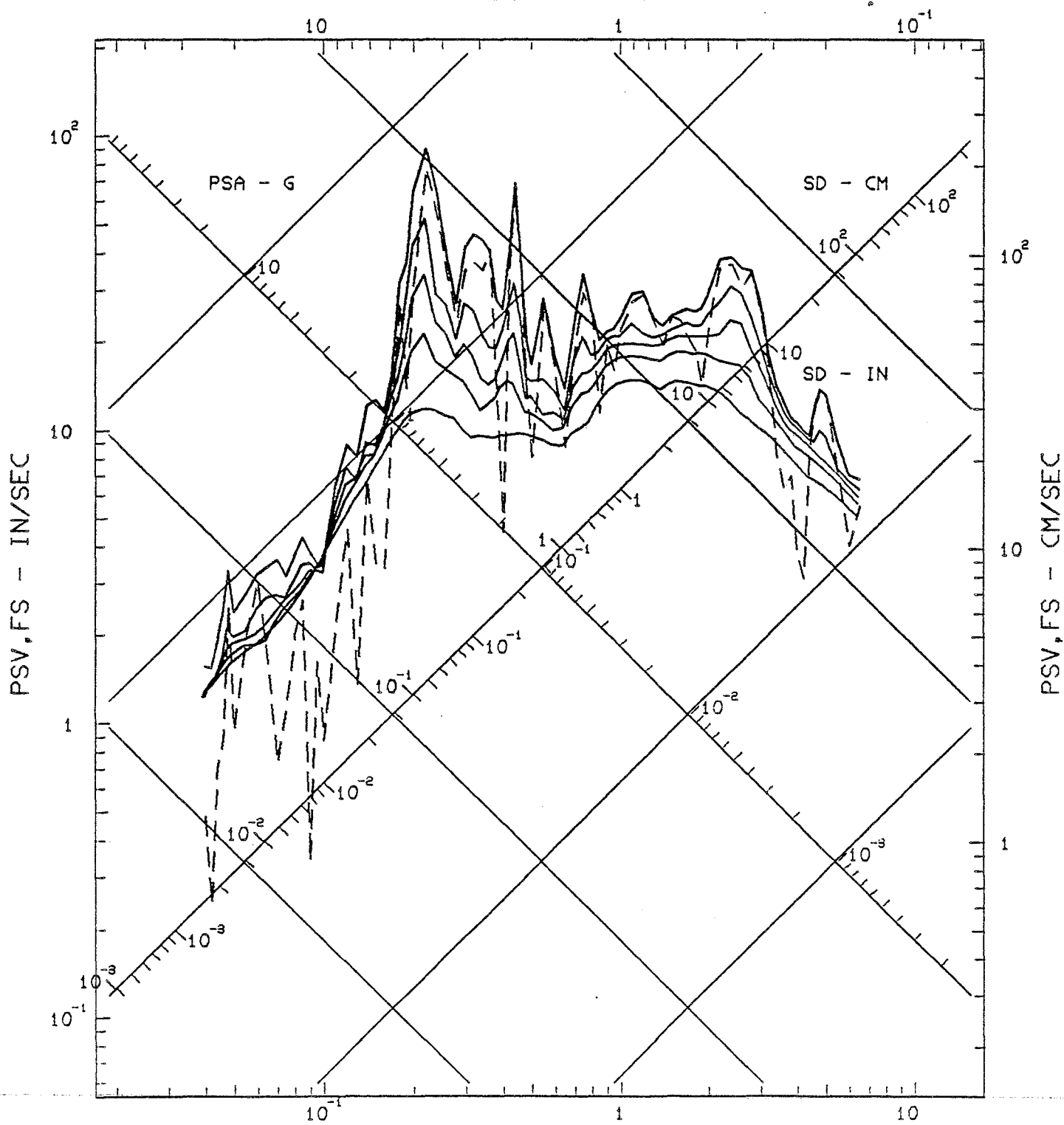
IMPERIAL VALLEY EARTHQUAKE OCT 15, 1979 -1616 PDT

IIIMP202 79.202.0 COMP TR16
ROUTE 8/MELOLAND OVERPASS, EL CENTRO, CA

ACCELEROGRAM IS BAND-PASS FILTERED BETWEEN .145- .165 AND 25.00-27.00 CYC/SEC.
DAMPING VALUES ARE 0, 2, 5, 10 & 20 % OF CRITICAL

———— RESPONSE SPECTRA: PSV, PSA & SD - - - - FOURIER AMPLITUDE SPECTRUM: FS

FREQUENCY - HZ





RESPONSE AND FOURIER SPECTRA

IMPERIAL VALLEY EARTHQUAKE OCT 15, 1979 -1616 PDT

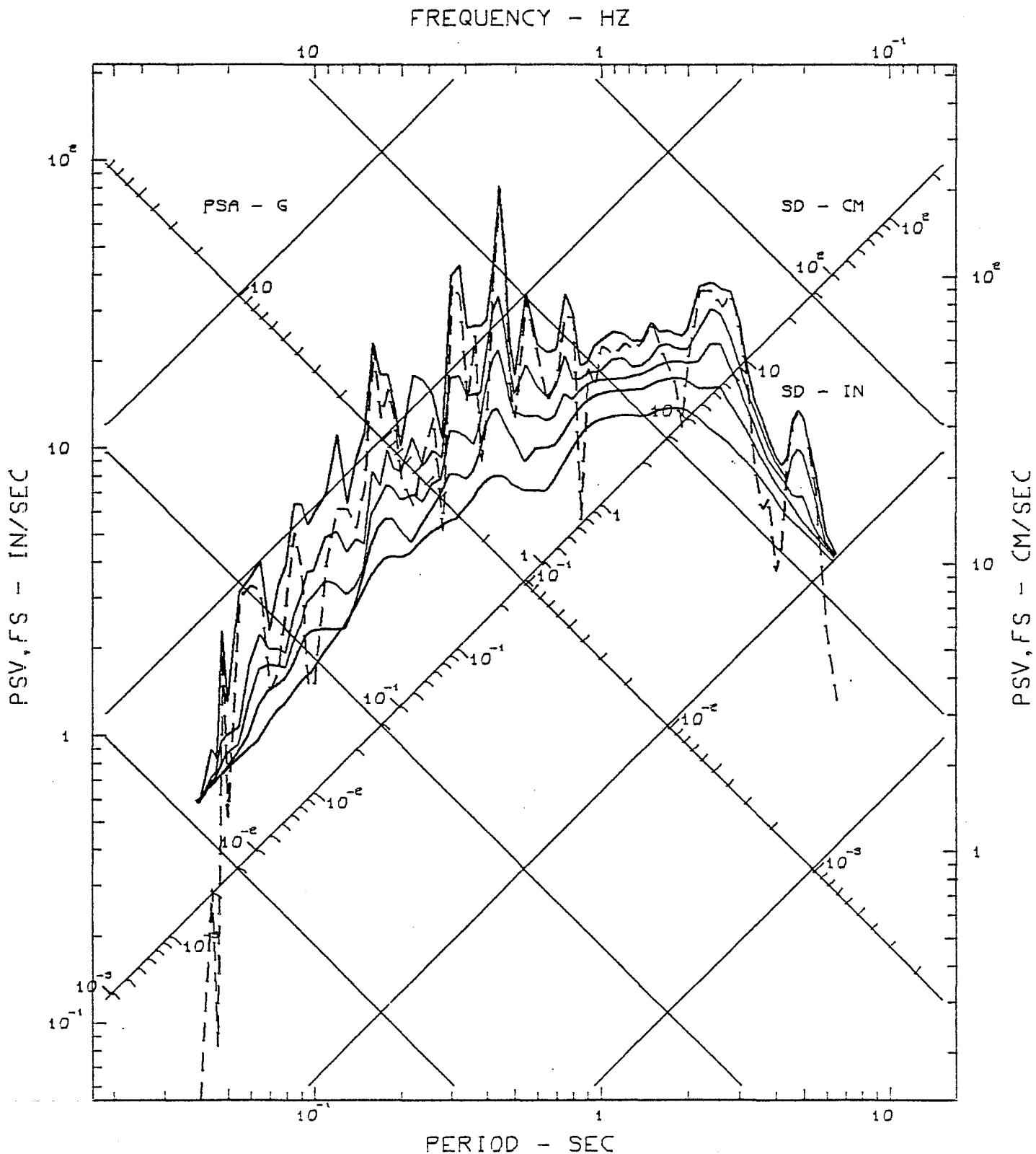
IIIMP202 79.202.0 COMP TR17

ROUTE 8/MELOLAND OVERPASS, EL CENTRO, CA

ACCELEROGRAM IS BAND-PASS FILTERED BETWEEN .145- .165 AND 25.00-27.00 CYC/SEC.

DAMPING VALUES ARE 0, 2, 5, 10 & 20 % OF CRITICAL

— RESPONSE SPECTRA: PSV, PSA & SD - - - FOURIER AMPLITUDE SPECTRUM: FS





RESPONSE AND FOURIER SPECTRA

IMPERIAL VALLEY EARTHQUAKE OCT 15, 1979 -1616 PDT

IIIMP202 79.202.0 COMP TR18

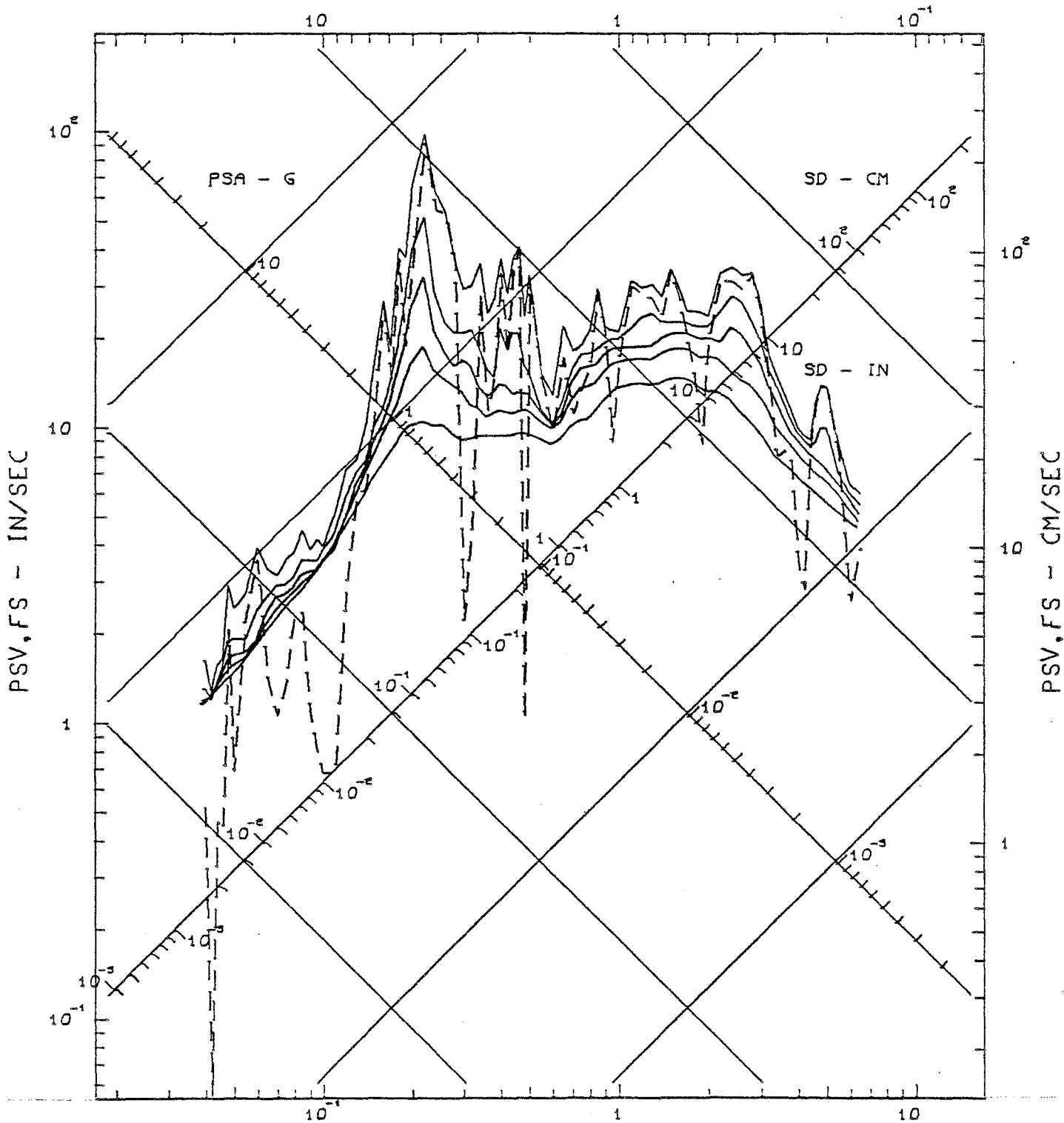
ROUTE 8/MELOLAND OVERPASS, EL CENTRO, CA

ACCELEROGRAM IS BAND-PASS FILTERED BETWEEN .145- .165 AND 25.00-27.00 CYC/SEC.

DAMPING VALUES ARE 0, 2, 5, 10 & 20 % OF CRITICAL

— RESPONSE SPECTRA: PSV, PSA & SD — — — FOURIER AMPLITUDE SPECTRUM: FS

FREQUENCY - HZ





RESPONSE AND FOURIER SPECTRA

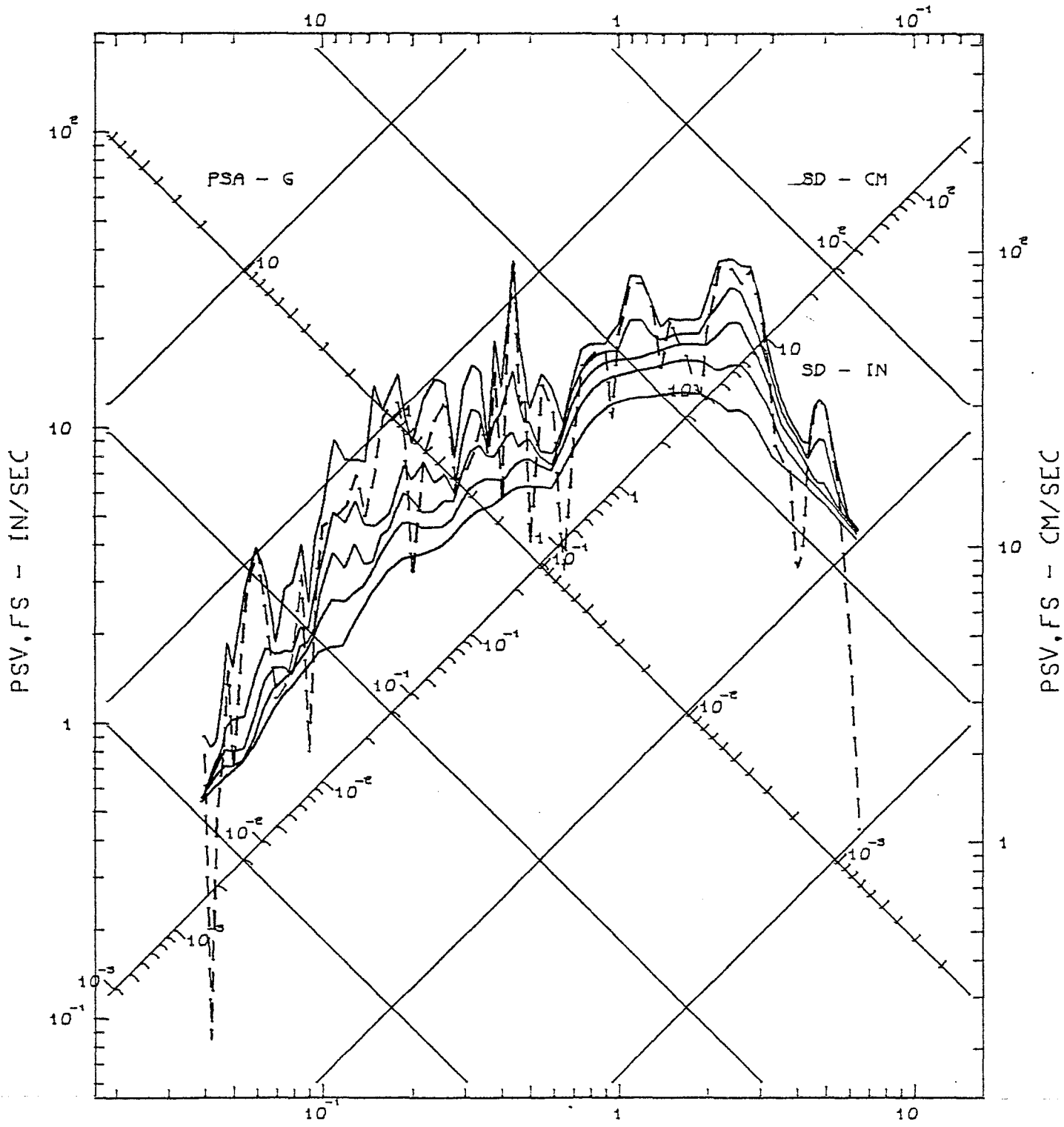
IMPERIAL VALLEY EARTHQUAKE OCT 15, 1979 -1616 PDT

IIIMP202 79.202.0 COMP TR19
ROUTE 8/MELOLAND OVERPASS, EL CENTRO, CA

ACCELEROGRAM IS BAND-PASS FILTERED BETWEEN .145- .165 AND 25.00-27.00 CYC/SEC.
DAMPING VALUES ARE 0. 2. 5. 10 & 20 % OF CRITICAL

— RESPONSE SPECTRA: PSV, PSA & SD — — — FOURIER AMPLITUDE SPECTRUM: FS

FREQUENCY - HZ



PERIOD - SEC



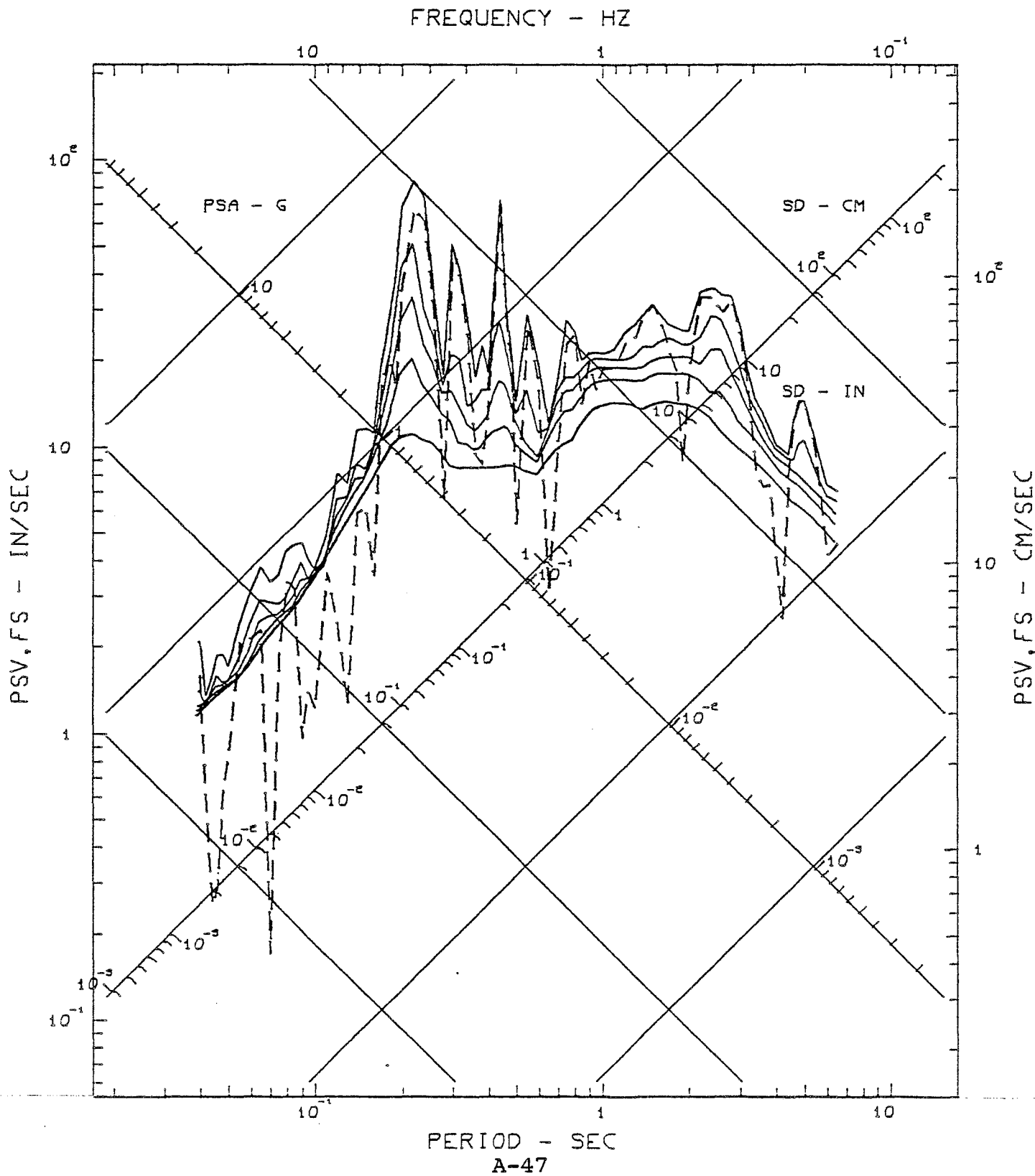
RESPONSE AND FOURIER SPECTRA

IMPERIAL VALLEY EARTHQUAKE OCT 15, 1979 -1616 PDT

IIIMP202 79.202.0 COMP TR20
ROUTE 8/MELOLAND OVERPASS, EL CENTRO, CA

ACCELEROGRAM IS BAND-PASS FILTERED BETWEEN .145- .165 AND 25.00-27.00 CYC/SEC.
DAMPING VALUES ARE 0, 2, 5, 10 & 20 % OF CRITICAL

— RESPONSE SPECTRA: PSV, PSA & SD — — — FOURIER AMPLITUDE SPECTRUM: FS





RESPONSE AND FOURIER SPECTRA

IMPERIAL VALLEY EARTHQUAKE OCT 15, 1979 -1616 PDT

IIIMP202 79.202.0 COMP TR21

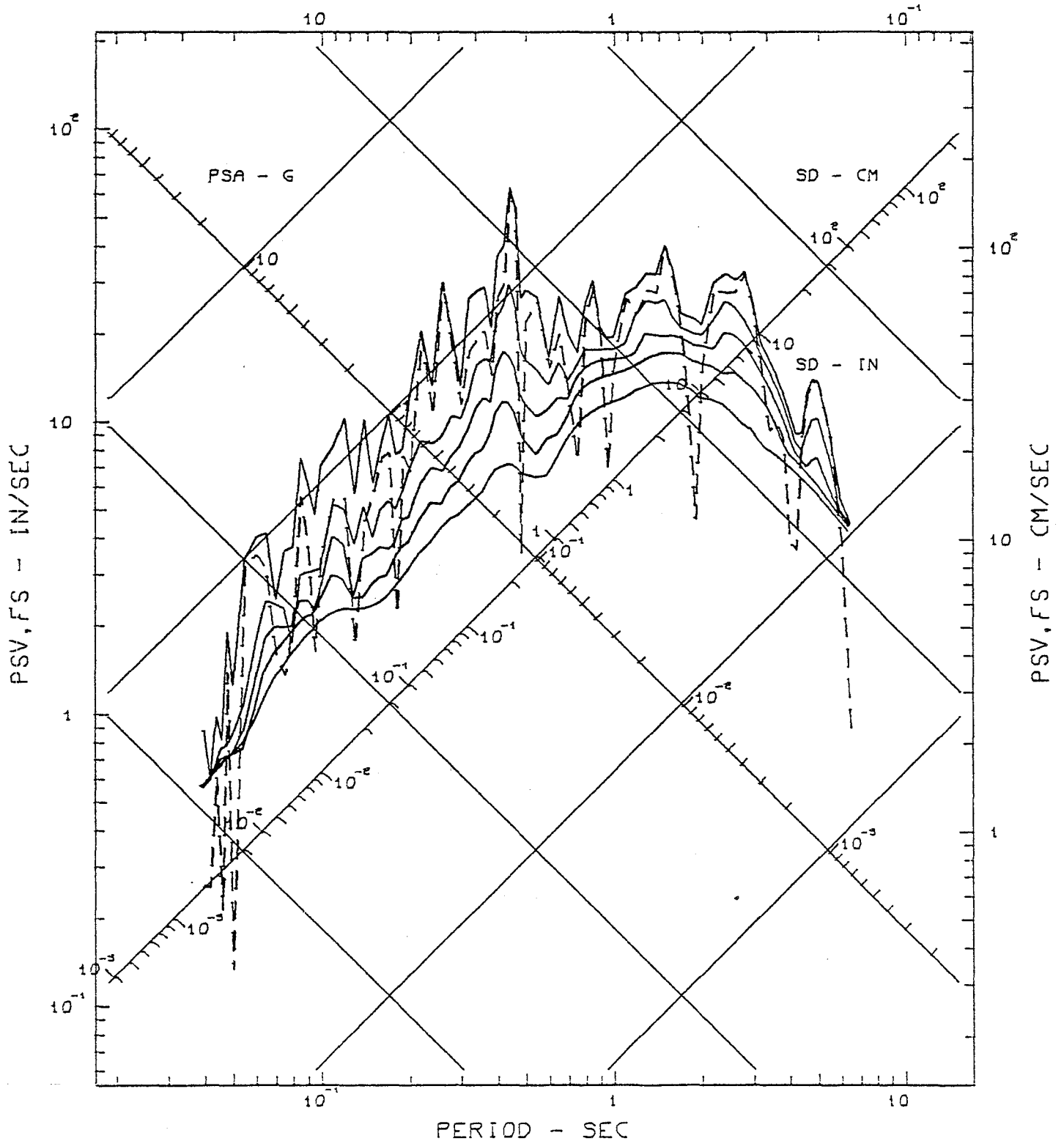
ROUTE 8/MELOLAND OVERPASS, EL CENTRO, CA

ACCELEROGRAM IS BAND-PASS FILTERED BETWEEN .145- .165 AND 25.00-27.00 CYC/SEC.

DAMPING VALUES ARE 0, 2, 5, 10 & 20 % OF CRITICAL

———— RESPONSE SPECTRA: PSV, PSA & SD - - - - FOURIER AMPLITUDE SPECTRUM: FS

FREQUENCY - HZ





RESPONSE AND FOURIER SPECTRA

IMPERIAL VALLEY EARTHQUAKE OCT 15, 1979 -1616 PDT

IIIMP202 79.202.0 COMP TR22

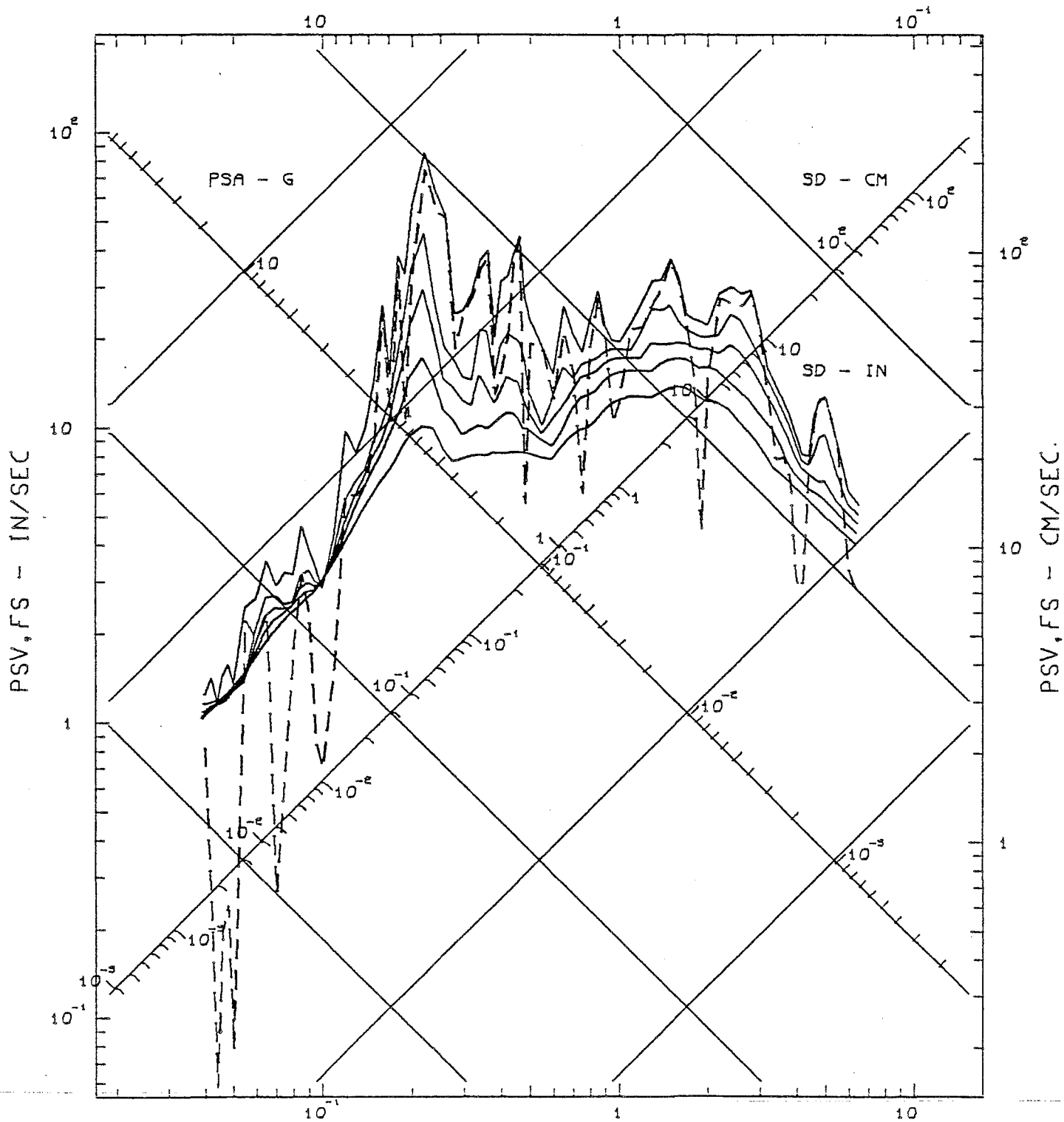
ROUTE 8/MELOLAND OVERPASS, EL CENTRO, CA

ACCELEROGRAM IS BAND-PASS FILTERED BETWEEN .145- .165 AND 25.00-27.00 CYC/SEC.

DAMPING VALUES ARE 0, 2, 5, 10 & 20 % OF CRITICAL

— RESPONSE SPECTRA: PSV, PSA & SD - - - FOURIER AMPLITUDE SPECTRUM: FS

FREQUENCY - HZ





RESPONSE AND FOURIER SPECTRA

IMPERIAL VALLEY EARTHQUAKE OCT 15, 1979 -1616 PDT

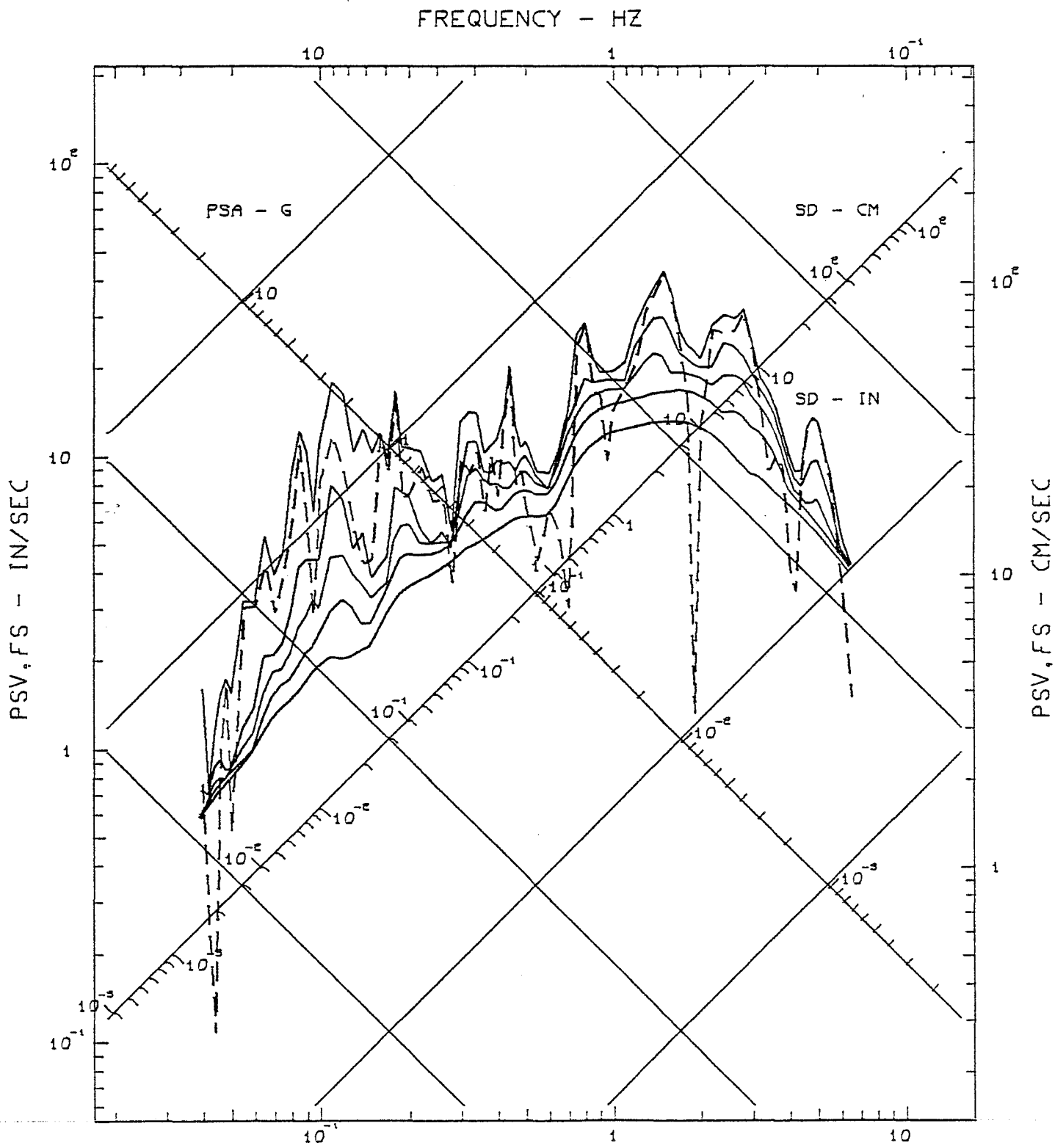
IIIMP202 79.202.0 COMP TR23

ROUTE 8/MELOLAND OVERPASS, EL CENTRO, CA

ACCELEROGRAM IS BAND-PASS FILTERED BETWEEN .145- .165 AND 25.00-27.00 CYC/SEC.

DAMPING VALUES ARE 0, 2, 5, 10 & 20 % OF CRITICAL

— RESPONSE SPECTRA: PSV, PSA & SD — — — FOURIER AMPLITUDE SPECTRUM: FS





RESPONSE AND FOURIER SPECTRA

IMPERIAL VALLEY EARTHQUAKE OCT 15, 1979 -1616 PDT

IIIMP202 79.202.0 COMP TR24

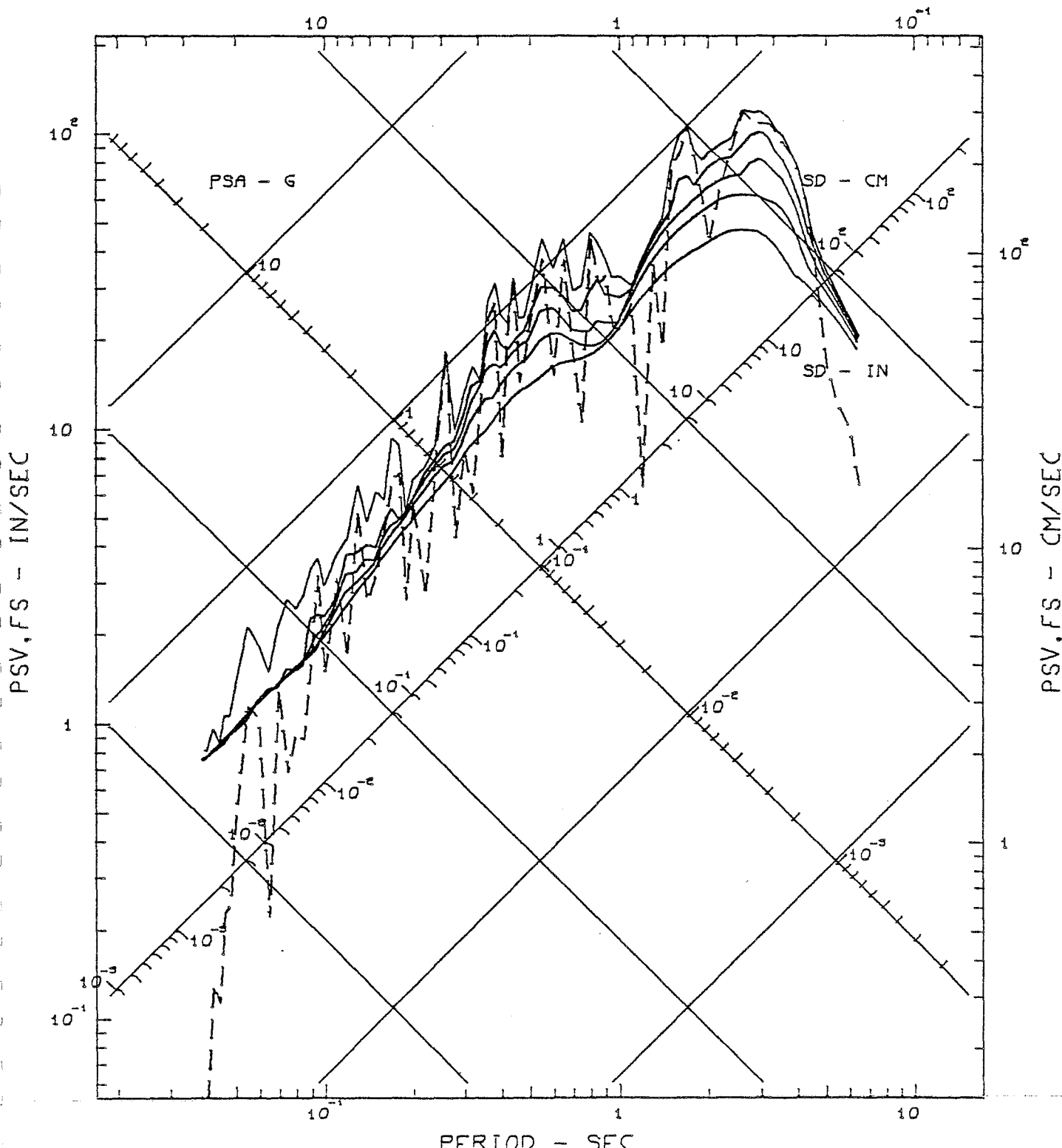
ROUTE 8/MELOLAND OVERPASS, EL CENTRO, CA

ACCELEROGRAM IS BAND-PASS FILTERED BETWEEN .145- .165 AND 25.00-27.00 CYC/SEC.

DAMPING VALUES ARE 0, 2, 5, 10 & 20 % OF CRITICAL

————— RESPONSE SPECTRA: PSV, PSA & SD - - - - - FOURIER AMPLITUDE SPECTRUM: FS

FREQUENCY - HZ



PERIOD - SEC



RESPONSE AND FOURIER SPECTRA

IMPERIAL VALLEY EARTHQUAKE OCT 15, 1979 -1616 PDT

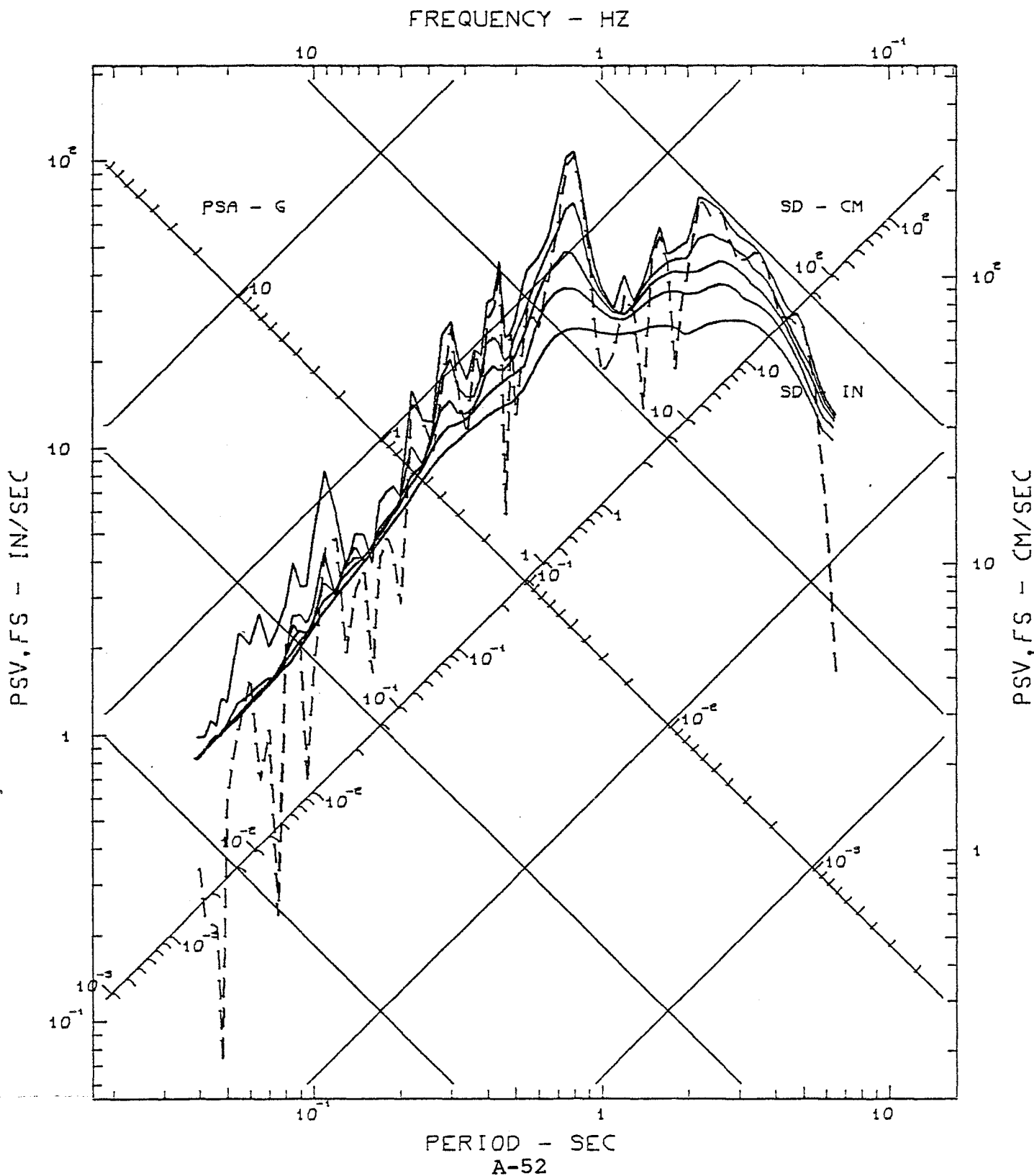
11IMP202 79.202.0 COMP TR25

ROUTE 8/MELOLAND OVERPASS, EL CENTRO, CA

ACCELEROGRAM IS BAND-PASS FILTERED BETWEEN .145- .165 AND 25.00-27.00 CYC/SEC.

DAMPING VALUES ARE 0, 2, 5, 10 & 20 % OF CRITICAL

————— RESPONSE SPECTRA: PSV, PSA & SD - - - - - FOURIER AMPLITUDE SPECTRUM: FS





RESPONSE AND FOURIER SPECTRA IMPERIAL VALLEY EARTHQUAKE OCT 15, 1979 -1616 PDT

IIIMP202 79.202.0 COMP TR26

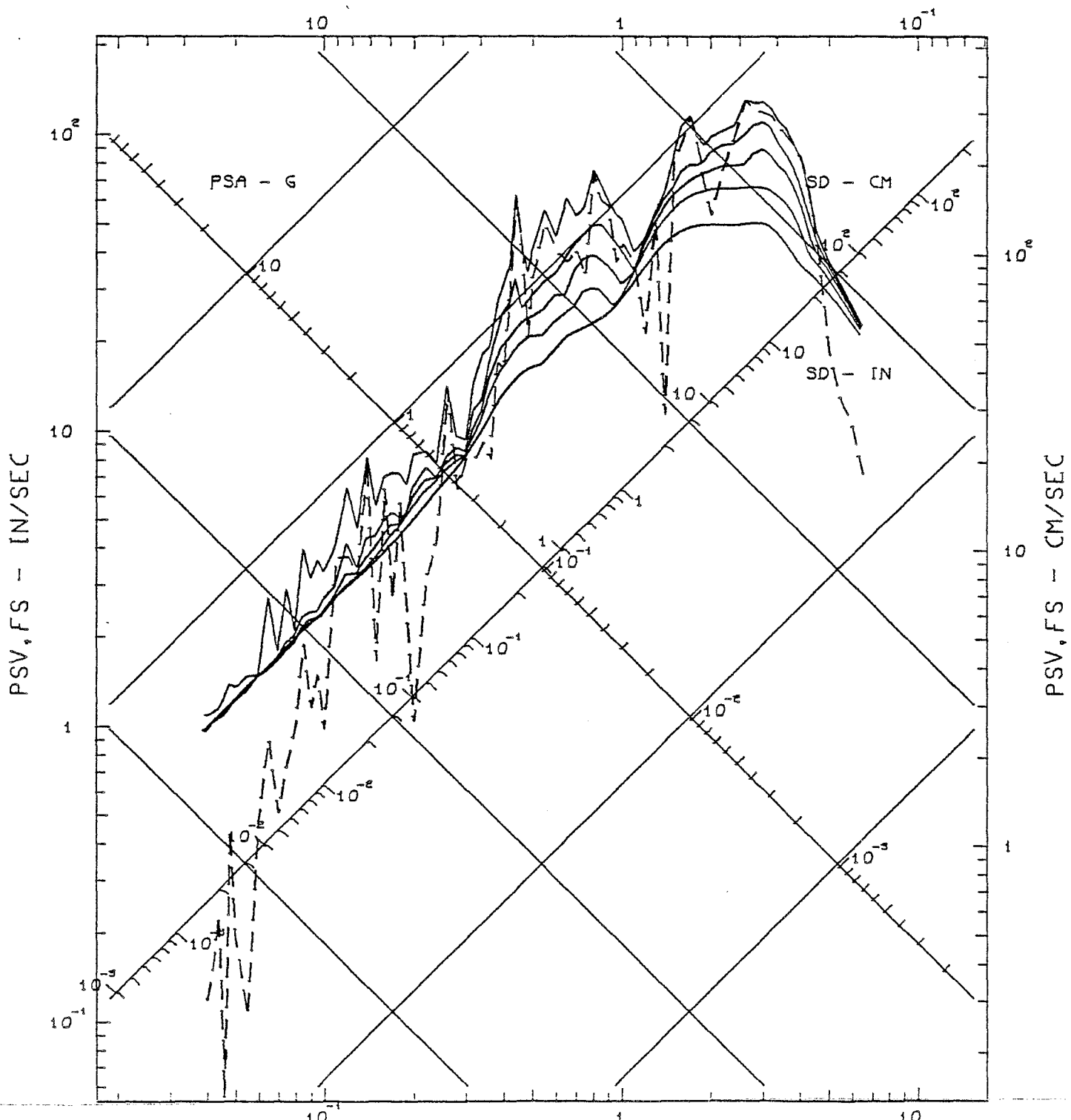
ROUTE 8/MELOLAND OVERPASS, EL CENTRO, CA

ACCELEROGRAM IS BAND-PASS FILTERED BETWEEN .145- .165 AND 25.00-27.00 CYC/SEC.

DAMPING VALUES ARE 0, 2, 5, 10 & 20 % OF CRITICAL

— RESPONSE SPECTRA: PSV, PSA & SD - - - FOURIER AMPLITUDE SPECTRUM: FS

FREQUENCY - HZ



PERIOD - SEC

